2006-01-01

Solubilisation, Purification and Processing of Single Walled Carbon Nanotubes Using Organic Molecules

Theresa Hedderman
Technological University Dublin, Theresa.Hedderman@tudublin.ie

Solubilisation, Purification and Processing of Single Walled Carbon Nanotubes Using Organic Molecules

By

Theresa Hedderman B.A. (mod.)

A thesis submitted to the Dublin Institute of Technology for the degree of Doctor of Philosophy (Ph.D.)

School of Physics,
Dublin Institute of Technology,
Kevin Street, Dublin 8.

Dr. Hugh Byrne and Dr. Gordon Chambers

August 2006

Abstract

The aims of this research are seven fold;

- To enhance the solubility of SWNTs in organic solvents.
- To purify an untreated sample of SWNTs that contains many side products.
- To gain a greater understanding of the interaction between the polycyclic aromatic hydrocarbons and SWNTs.
- To debundle and disperse SWNTs.
- To select SWNTs of a specific structure based on the structures of the polycyclic aromatic hydrocarbons used.
- To observe and compare the interaction of polycyclic aromatic hydrocarbons with SWNTs produced by different methods.
- To elucidate factors which contribute to different degrees of interaction between different SWNT samples and the hydrocarbon molecules.

In this research, the solubilisation, purification and debundling of single walled carbon nanotubes (SWNTs) on interaction with the polycyclic aromatic hydrocarbons (PAHs), anthracene and *p*-terphenyl are explored. The investigations were performed in toluene due to its poor affinity for the retention of SWNTs. Thus this solvent can act as a good indicator for improvements in the solubility of the SWNTs due to the presence of the PAHs. The hydrocarbons anthracene and *p*-terphenyl were chosen because of their high degree of solubility in toluene and their simple structure that is proposed in this research to exhibit molecular recognition of SWNTs with a similar backbone structure to that of the hydrocarbon.

The study begins with the exploration of the interaction between the SWNTs in an untreated sample and the PAHs, and results reveal an enhanced solubility of the SWNTs in toluene and subsequently the purification of the SWNT sample. Interaction between the PAHs and the SWNTs draws the SWNTs into solution allowing all side products to precipitate out. The composite solution is a stable suspension of finely dispersed SWNTs with no evidence of SWNT precipitation observed in over a five year period. This observation indicates an enhanced stability of the SWNTs in solutions due to an interaction

with the PAH molecules and this observation is supported by Raman and fluorescence spectroscopic studies which are presented in this thesis. Both anthracene and *p*-terphenyl map *via* a $\pi - \pi$ interaction to the SWNT backbone with strong indications of structural selectivity between the SWNT surfaces and PAHs.

The literature is scarce with regard to the interaction between organic molecules and SWNTs. In this research an investigation into the interaction that occurs between PAHs and SWNTs is conducted. The interactions and debundling of SWNTs over a broad concentration range are probed through spectroscopic methods including fluorescence and Raman. Fluorescence concentration dependence studies define the concentration range where aggregated PAHs and isolated PAHs exist. A fluorescence model based on the fraction of free hydrocarbons is used to indicate the concentration range where debundled and bundled SWNTs and PAHs are interacting with atomic force microscopic (AFM) studies supporting the results. AFM is used to obtain a surface profile of the SWNTs at a range of concentrations to image the debundling of SWNTs with decreasing concentration. The fluorescence model also allows the calculation of a binding energy between the SWNTs and PAHs at low concentrations. The binding energy determined is further supported by alternative theoretical models and the results obtained correlate well. Raman studies support fluorescence and AFM studies with regard to the interaction and debundling of SWNTs and the Raman radial breathing modes (RBMs) are probed to investigate selective interaction of the PAH molecules at low concentrations and results reveal a degree of selective interaction.

To conclude this work, a study using SWNTs produced by different methods is performed to investigate any changes which may occur to the SWNT/PAH/solvent system as a result of replacing one tube type for another. The study elucidates factors that are favourable for interaction with the hydrocarbon in the given solvent toluene. Spectroscopic methods such as fluorescence and microscopic studies such as AFM are used as the investigative tools. The studies reveal that large bundles with large diameter SWNTs are most favourable for interaction with *p*-terphenyl and debundling in toluene. Such a study is of interest for the development of a standardised purification and processing protocol.

DECLARATION

I certify that this thesis which I now submit for examination for the award of doctor of philosophy, is entirely my own work and has not been taken from the work of others save and to the extent that such work has been cited and acknowledged within the text of my work.

This thesis was prepared according to the regulations for postgraduate study by research of the Dublin Institute of Technology and has not been submitted in whole or in part for an award in any other Institute or University.

The work reported on in this thesis conforms to the principles and requirements of the Institute's guidelines for ethics in research.

The Institute has permission to keep, or lend or to copy this thesis in whole or in part, on condition that any such use of the material or the thesis be duly acknowledged.

Signature _____ Date 12/10/06.

Candidate

Particularly, I have urged them to learn what they can of chemistry, for I feel that chemistry is basic, ergo architecture.

Buckminster Fuller, The Comprehensive Man

ACKNOWLEDGEMENTS

There are many people who over the years have helped me through this thesis. Firstly I would like to thank Dr. Hugh Byrne for giving me the opportunity to do this degree. I would like to thank both my supervisors for all their advice and guidance through this project. A big thanks to Eoghan and Sinead who helped keep me sane. Thanks for all the laughs in the cottages and the wild nights in Kirchberg. A special thanks to Anika, I wouldn't have a thesis if it wasn't for your generosity and time with the AFM, I owe you big time. Thanks to Anne for your tireless hours doing TEM (I'm surprised you are not blind from staring at the screen) and all your support with my technical chores as a result of the newest addition to the Focas Institute. I would also like to mention Claire, my internal reader for all your help and comments. Thanks to you the thesis looks great. And finally a big huge thanks to Brian, for all your help with the thesis layout, all the feedback and of course for appealing to my stubborn nature by telling me I'd never make on time ☺. Ha Ha ...I did.

ABBREVIATIONS

AFM	Atomic Force Microscopy
Ant	Anthracene
AD-SWNT	Arc Discharge Single Walled carbon NanoTubes
APTES	3-Aminopropyltriethoxy silane
ATR	Attenuated Total Reflectance
C	Carbon or Graphite
C_{60}	Carbon Sixty Fullerene
C-C	Carbon to carbon single bond
C=C	Carbon to carbon double bond
CNI	Carbon Nanotechnology Incorporated
CO	Carbon Monoxide
CO_2	Carbon Dioxide
Co	Cobalt
CS_2	Carbon Disulphide
CVD	Chemical Vapour Deposition
DOS	Density of States
DFT	Density Functional Theory
Fe	Iron
$Fe(CO)_5$	Iron pentacarbonyl
HiPco	High Pressure carbon monoxide disproportionation
H-SWNT	HiPco Single Walled carbon NanoTubes
IR	InfraRed
LV-SWNT	Laser Vapourisation Single Walled carbon NanoTubes
Ni	Nickel
HNO_3	Nitric Acid
NMR	Nuclear Magnetic Resonance
P*m*NV	poly *m*-phenylenevinylene-*co*-(1,5-dioctyl-2,6-naphthlene vinylene)
PAH	Polycyclic Aromatic Hydrocarbons

P*m*PV-*co*-DOctOPV	poly*p*-phenylene vinylene-*co*-2,5-dioctyloxy-*m*-phenylenevinyl
p-ter	*p*-terphenyl
RBM	Radial Breathing Modes
RuO_4	Ruthenium Tetroxide
SWNT	Single Walled carbon NanoTubes
TEM	Transmission Electron Microscopy
UV-Vis-NIR	UltraViolet- Visible- Near InfraRed
w/w	weight/weight
Y	Yttrium

TABLE OF CONTENTS

TABLE OF ILLUSTRATIONS

CHAPTER 1 - INTRODUCTION

1.1 Research Objective

Single Walled carbon NanoTubes (SWNTs), have generated much interest due to their unique properties and potential applications (Baughman and Zakhidov 2002; Hamada *et al.*, 1992; Javey *et al.*, 2004; McEuen, 2000; Mintmire *et al.*, 1992; Saito *et al.*, 1992). There are, however, some fundamental problems which need to be addressed. As a result of the production process employed not only are SWNT samples impure, they are almost always present in the form of bundles and the properties of a bundle are inferior to those of an individual SWNTs (Cadek *et al.*, 2004, Coleman *et al.*, 2004, Strong *et al.*, 2003, Thess *et al.*, 1996, Tomanek and Enbody, 2000). Moreover, even purified SWNTs can have electronic properties that range from metallic to semiconducting depending on their structure and in their as produced state a sample of SWNTs can contain a broad range of structures. In order to understand their fundamental properties and to realise their potential applications, it is necessary to be able to purify, isolate and access SWNTs with particular properties and electronic characteristics. Hence it is the objective of this research to solubilise, purify and process SWNTs using organic molecules such as *p*-terphenyl and anthracene and to gain an understanding of the interaction that occurs between the organic molecules and SWNTs.

1.2 Context and Overview

Carbon nanotubes are graphene (a single layer of graphite) sheets rolled up to form a seamless cylinder that is closed at both ends by a bisected fullerene-like molecule as depicted in Figures 1.1 and 1.2 (Dresselhaus *et al.*, 1996; Rao *et al.*, 2001). Graphene is a planar hexagonal network of sp^2 hybridised carbon atoms while fullerene molecules are curved structures due to the mixture of both hexagon and pentagon carbon structures. Carbon nanotubes are classified into two types, Multi-Walled carbon NanoTubes (MWNTs) and SWNTs with the former being discovered in 1991 (Iijima, 1991) before the

latter in 1993 (Iijima and Ichihashi, 1993). During a routine production of C_{60}, Iijima found hollow tubes of carbon in the by-product that are commonly known today as carbon nanotubes. MWNTs are comprised of two to thirty concentric graphene sheets, diameters of which range from 10 – 50 nm that have lengths of up to millimeters (mm) while SWNTs consist of a single graphene sheet cylinder that is much thinner with diameters in the range of 0.7 – 2.0 nm and typical lengths of a few micrometers (μm). Techniques such as arc-discharge and laser vapourisation have been used to synthesise both MWNTs and SWNTs but the parameters used are specific to the tube type produced. For instance, MWNTs are readily prepared by arc-discharge by striking an arc between graphite electrodes in an atmosphere of ~500 Torr of helium. A current of 50-100 A across a potential drop of 20-25 V gives a high yield of MWNT (Harris, 1999; Rao *et al.*, 2001). To produce SWNTs, the same parameters as just described are used with the addition of a specific percentage of metal catalyst such as 2% cobalt (Co), (Harris, 1999; Rao *et al.*, 2001). The graphite anode is filled with metal powders such as iron, cobalt and nikel (Fe, Co and Ni) and the cathode is pure graphite.

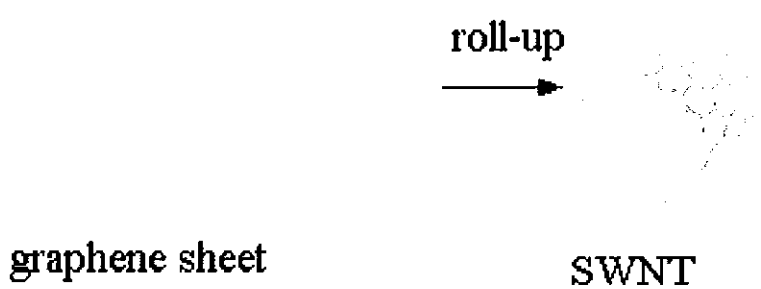

Figure 1.1 Rolling of graphene to form a SWNT (Odom *et al.*, 2002).

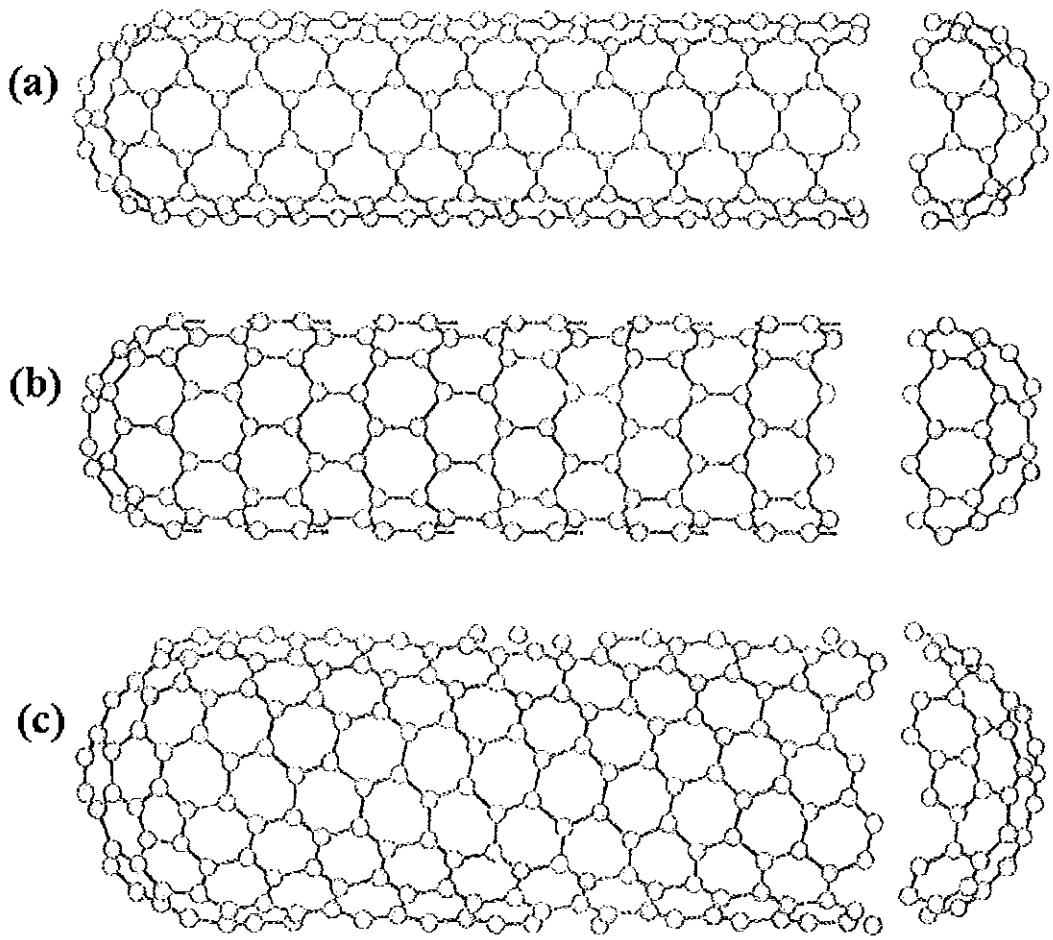

Figure 1.2 Classification of SWNTs, (a) represents an armchair SWNT, (b) zigzag SWNT, and (c) chiral SWNT (Saito *et al.*, 1998, Dresselhaus, *et al.*, 1996).

As is the case with graphene, both MWNT and SWNT contain C=C (double bonds) which are one of the strongest bonds in nature and therefore carbon nanotubes are regarded as the potential ultimate fibre with regards to their strength in the direction of the nanotube axis and flexibility in the direction normal to the nanotube surface. Carbon nanotubes have the ability to withstand cross sectional and twisting distortion and can be elongated by several percent and compressed without fracture (Saito *et al.*, 1998). The shear modulus was experimentally shown to be 1 GPa and the elastic modulus was shown to be 1 TPa (Reich *et al.*, 2004; Yu *et al.*, 2000). The Young's modulus for carbon nanotubes has been

calculated to be between 500 – 1500 GPa depending on the diameter of the nanotube. However Transmission Electron Microscopy (TEM) images show that MWNTs are very straight which indicates that they are very rigid and buckling has been observed on the inner radius of the bend compared to SWNTs which are more pliable and can have curvature bends without buckling. *Ab initio* calculations have been performed to support the above observations (Saito *et al.*, 1998, Reich *et al.*, 2004). It has been demonstrated that SWNTs are capable of bending around small circles or about sharp bends without breaking and these structures exhibit a radius of curvature as low as 20 nm (Endo *et al.*, 1993). Structurally, carbon nanotubes of small diameter (approximately 1 nm) are examples of one – dimensional periodic structures along the nanotube axis. In SWNTs, confinement of the structure in the radial direction is provided by the monolayer thickness of the nanotube in the radial direction. Large diameter MWNTs are found not to exhibit one – dimensional effects and it is found that the contributions from the inner constituent shells complicate the interpretation of transport experiments. For these reasons SWNTs have generated more interest than MWNTs as their unique properties are believed to have a greater potential for application (Collins and Avouris, 2000; Jarvey *et al.*, 2004).

1.3 An Overview of SWNT

There are two structural forms of SWNTs possible depending on the angle at which the graphene sheet is rolled. These are chiral and achiral. There are many different chiral tubes possible depending on how the graphene sheet is rolled but there are only two distinguishable achiral forms, 'zigzag' and 'armchair' (Figure 1.2). Further details on the structure of SWNTs may be found in Chapter 2 section 2.2.

In terms of molecular structure, carbon nanotubes and fullerenes are very similar, both structures containing hexagonal and pentagonal carbon rings. However, the fullerene C_{60} is a molecular insulator while carbon nanotubes exhibit metallic and semiconducting electronic properties depending on the angle at which the graphene is rolled and the resulting diameter. Theoretical studies indicate that the physical properties of carbon nanotubes are strongly dependent on the tube diameter and chiral angle (Saito *et al.*, 1998;

Reich *et al.*, 2004) (Chapter 2). Generally the different structures of SWNTs can be associated with distinct physical properties. Table 1.1 associates the chirality of the SWNTs with their electronic properties (Dresselhaus, *et al.*, 1995; Liz-Marzan and Kamat, 2003).

Table 1.1 Outline of the structure and the associated physical properties of SWNTs.

Structure	Physical properties
Armchair	metallic
Zigzag	~2/3 semiconducting and ~1/3 metallic
Chiral	semiconducting or metallic depending on the structure

SWNTs were predicted to be one-dimensional ballistic conductors and so far this has been observed at low bias only (Jarvey *et al.*, 2004; Saito *et al.*, 1998). Such properties are highly sought in the molecular electronics industry and their potential in molecular electronics as nanowires and even as molecular transistor candidates is currently under investigation (Fuhrer *et al.*, 2000; Javey *et al.*, 2004; Shea *et al.*, 1999). A fundamental problem for conventional semiconductors is the degradation of electrical properties due to carrier scattering mechanisms introduced at the high-k film-semiconductor interface (Fuhrer *et al.*, 2000; Javey *et al.*, 2004; Shea *et al.*, 1999). For example, silicon Metal-Oxide Semiconductor Field Effect Transistors (MOSFET) with deposited high-k dielectrics consistently display inferior properties compared to those with thermally grown SiO_2 gate insulators. Javey *et al.*, (2004) have developed a carbon nanotube field effect transistor with near ballistic conductance up to high biases at both room and low temperatures. Such a result opens the field to ultra fast electronics since both ballistic transport and high-k

dielectrics facilitate high on-current that is directly proportional to the speed of the transistor. At present, companies such as IBM and Lucent Bell are investing large sums of money into research of SWNT as candidates for commercial transistors (Shea *et al.,* 1999).

SWNT-tipped scanning probes that are used in microscopy techniques are currently on the market (Cheung *et al.*, 2000). It has been shown that SWNTs attached to the tip of the scanning probe, for techniques such as atomic force microscopy (AFM), have an enhanced lateral resolution of a factor of ten or more allowing clearer views of proteins and larger molecules. Imaging of deep pits in nanostructures that were previously hidden may now be explored (Cheung *et al.*, 2000; Collins and Avouris, 2000; Dai *et al.*, 1996). Also SWNT-tipped AFM can trace a strand of DNA and identify chemical markers that reveal which of the several possible variants of the gene is present in the strand (Collins and Avouris, 2000; Kong *et al.*, 2000).

It has also been theoretically proposed that SWNT can store hydrogen in their hollow centre with a potential application for a fuel-cell in electric vehicles (Lee *et al.*, 2001). Experimental data to date shows low levels of hydrogen absorption but recent improvements are attributed to the presence of metal particles (Dillon *et al.*, 1997; Dillon *et al.*, 2003).

Many thousands of papers in the field have been published since the discovery of carbon nanotubes indicating the great interest in their fundamental properties and applications potential. Research with a view to application is however hindered by the lack of readily available pure and isolated SWNT with specific physical characteristics. Current available techniques to purify samples are oxidation, size selection chromatography, filtration and organic processing (Ajayan *et al.*, 1993; Dalton *et al.*, 2000; Dalton *et al.*, 2001; Dillon *et al.,* 1999, Duesberg *et al.*, 1999; Niyogi, *et al.,* 2001; Rinzler *et al.*, 1998; Tsang *et al.,* 1993). Oxidation entails combustion of impurities and amorphous carbon in air or other oxidising agents at 600 K. This temperature is below that for the combustion of carbon nanotubes. Size selection chromatography offers selectivity with respect to length. A surfactant stablised solution of carbon nanotubes is passed through a column containing

glass beads of a specific pore size hence allowing the separation of carbon nanotubes of different lengths as they elute in different fractions. Filtration involves passing a solution of carbon nanotubes through filter paper of pore size 0.45 μm. This allows the carbon nanotubes to pass through the pores while the larger impurities remain on the filter paper surface. Organic processing using the conjugated polymer (*p*-phenylene vinylene-*co*-2,5-dioctyloxy-*m*-phenylenevinyl) P*m*PV-*co*-DOctOPV was shown to purify a sample of carbon nanotubes and exhibit a degree of diameter selectivity. The technique is based on the interaction of the organic polymer with the carbon nanotube backbone which draws the tubes into solution and allows the amorphous carbon and impurities to precipitate out (Figure 1.3). All of the above techniques have their advantages but there are also serious disadvantages which hinder any up-scaling of the processing methods. A detailed description of the pros and cons of each technique is given in Chapter 2.

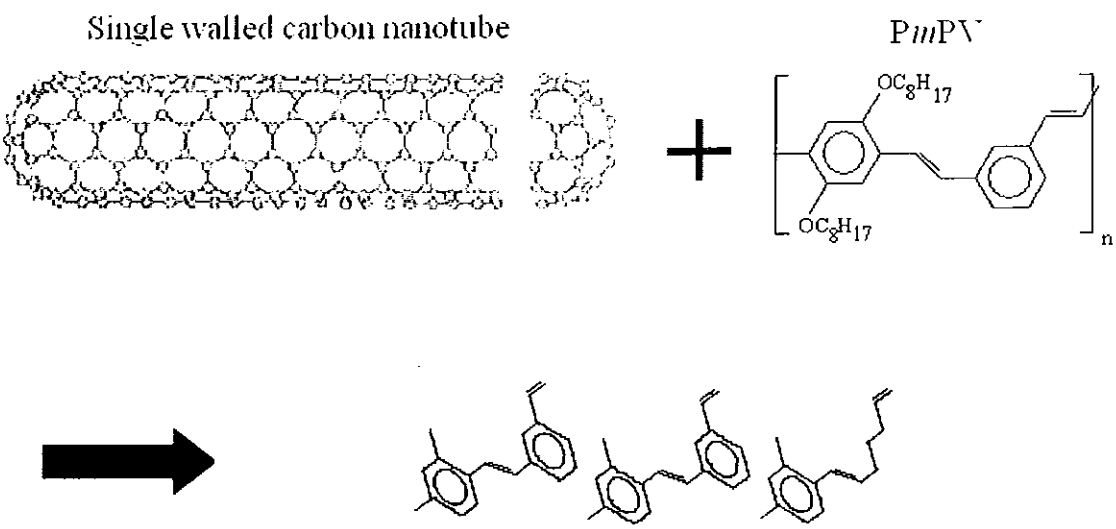

Figure 1.3 Proposed mapping of the polymer P*m*PV to SWNT (adapted from Keogh *et al.*, 2002).

1.4 Aims of Research

The aims of this research are seven fold;

- To enhance the solubility of SWNTs in organic solvents.
- To purify an untreated sample of SWNTs that contains many side products.
- To gain a greater understanding of the interaction between the polycyclic aromatic hydrocarbons and SWNTs.
- To debundle and disperse SWNTs.
- To select SWNTs of a specific structure based on the structures of the polycyclic aromatic hydrocarbons used.
- To observe and compare the interaction of polycyclic aromatic hydrocarbons with SWNTs produced by different methods.
- To elucidate factors that may disrupt universal behaviour between different SWNT samples.

It is proposed that the aims listed above may be achieved using two types of polycyclic aromatic hydrocarbons (PAHs), anthracene and *p*-terphenyl. Both *p*-terphenyl and anthracene each contain three phenyl rings. The rings are fused in the case of anthracene and are separated by a C-C (single bond) in the *p*-terphenyl structure. The two hydrocarbons were chosen because of their structure. The structure of anthracene is similar to the backbone structure of an armchair SWNT and the structure of *p*-terphenyl is like the backbone structure of a zigzag SWNT. It was hypothesised that the similar structures would interact resulting not only in solubilisation but also structurally selective solubilisation of SWNTs as depicted in Figure 1.4. Selecting SWNTs based on their structure would prove to be a novel processing technique and it would also inadvertently lead to a degree of electronic selectivity, with armchair SWNTs being metallic and zigzag SWNTs being mainly semiconducting. The solvent chosen for the studies was toluene as it exhibits a poor affinity for SWNT and therefore is an ideal candidate for monitoring the improvements in the solubility as a result of the SWNTs interacting with the PAHs (Bahr *et al.*, 2001). Given that most common SWNTs production methods result in a sample containing unwanted side products within the SWNT sample, the interaction between the SWNTs and PAHs

would result in the solubilisation of SWNTs and the precipitation of the side products thus providing a purification technique.

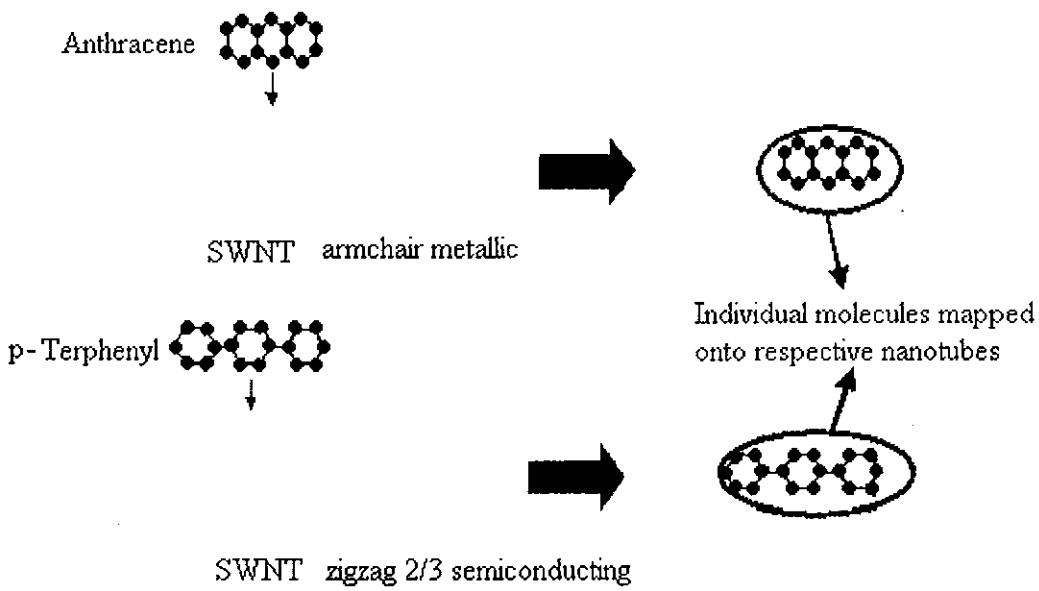

Figure 1.4 Proposed mapping of anthracene and *p*-terphenyl to armchair and zigzag SWNTs respectively.

Both hydrocarbons anthracene and *p*-terphenyl are chromophores, absorbing light at ~350 and ~295 nm and emitting it at ~405 and ~345 nm respectively. Both UV-Vis-NIR and fluorescence spectroscopy are thus used to characterise the PAHs in the absence and presence of SWNTs and changes to the spectroscopic properties are used to monitor the interaction of the chromophores with the nanotubes. Fluorescence concentration dependence studies of the chromophores in the absence and presence of SWNTs are conducted to gain a greater understanding of the interaction between the two components (PAHs and SWNTs). It is proposed that the study will divulge information as to the behaviour of the PAHs over a large concentration range and any effect the SWNTs exert on the PAHs. A model also based on a fluorescence study proposes to reveal concentration

ranges where bundled and debundled SWNTs exist. Within the model are equations which elucidate the binding energy between debundled SWNTs and PAHs.

SWNTs have a signature Raman spectrum which gives details of the vibrational energies within the SWNTs (Kuzmany *et al.*, 1998). The signature spectrum is examined for changes that may result from interaction with the hydrocarbons. It has been reported that an up-shift in the lower frequency Raman modes is a result of a change to the local environment of SWNTs but the up-shift may also be attributed to the debundling of SWNTs as a result of the addition of a third species to the solution such as a hydrocarbon (Dalton *et al.*, 2000; Fantini *et al.*, 2004; Rao *et al.*, 2001; Zhang *et al.*, 2002). Raman spectroscopy is used to probe the ability of anthracene and *p*-terphenyl to debundle SWNTs and add support to the results obtained from fluorescence spectroscopy. Raman spectroscopy is also used to probe for selective interaction between the PAHs and SWNTs. The concentration range where dispersed SWNTs and PAHs are interacting (as determined from the fluorescence model) is probed. Finally AFM and Transmission Electron Microscopy (TEM) are used to obtain a surface profile of the SWNTs before and after the interaction with the PAHs. AFM is used to support the effects of debundling that are exerted by the hydrocarbon on SWNTs.

To conclude the study, the interaction between PAHs and SWNTs produced by different methods are probed to investigate if the behaviour of SWNTs is universal irrespective of the production method. Spectroscopic analysis as described above is conducted and similarities and differences in the behaviour of the SWNT with the PAH are examined and factors which contribute to non-universal behaviour are explored. This study proposes to broaden the understanding of the behaviour of SWNT and is essential in the quest for a standardised processing and purification protocol.

1.5 Thesis Outline

In Chapter 2 an account of the structural, electronic and vibrational properties of SWNTs is provided and the proposed relationship between the structure and the electronic properties of the SWNTs is discussed. Past and present production methods as well as processing methods are described and related experimental and theoretical papers from the literature are reviewed. Chapter 3 explores the structure and photophysics of PAH molecules, specifically anthracene and *p*-terphenyl. This chapter also gives an overview of the physical properties of the two hydrocarbons as isolated molecules and also when stacked in molecular crystals, a differentiation which is relevant in the binary mixtures of PAHs and carbon nanotubes. Chapter 4 takes a look at the background of the various spectroscopic methods that were used in this research and the individual materials, namely the two hydrocarbons and SWNTs, are characterized using the methods discussed. Chapter 5 presents the examination of the composite solutions of PAHs and SWNTs, from the initial fluorescence spectroscopy results which point towards a mapping of the hydrocarbons onto the SWNTs surface to the Raman spectroscopy results which indicated that the hydrocarbons are interacting with, and debundling, the SWNTs. Conclusions are drawn from the results obtained as to what further experimental work is required to meet the objectives of the research. Chapter 6 describes this experimental work, which included the concentration dependent fluorescence studies to indicate the concentration range where debundled and bundled SWNTs and hydrocarbons exist and Raman analysis is used to explore the selective nature of the SWNTs. In Chapter 7, a comparison study of the interaction between the PAH, *p*-terphenyl and SWNTs produced by different methods is presented and arguments which obstruct universal behaviour between the different samples are made. Chapter 8 is a summation of the work conducted with a view to further work which may be carried out.

REFERENCES

Ajayan, P.M., Ebbesen, T.W., Ichihashi, T., Iijima, S., Tanigaki, K., Hiura, H., (1993), "Opening carbon nanotubes with oxygen and implications for filling", *Nature*, 362, 522-524.

Bahr J.L., Mickelson E.T., Bronikowski J., Smalley R.E., Tour J.M., (2001), "Dissolution of small diameter single walled carbon nanotubes in organic solvents", *Chem. Comm.*, 193 - 194.

Baughman, R.H., Zakhidov, A.A., (2002), "Carbon nanotubes, the route towards application", *Science*, 297, 787-792.

Cadek, M., Coleman, J.N., Ryan, K.P., Nicolosi, V., (2004), "Reinforcement of polymers with carbon nanotubes: the role of nanotube surface area", *Nanoletters*, 4, 353.

Cheung, C.L., Hafner, J.H., Odom, T.W., Kim, K., Lieber C.M., (2000), "Growth and fabrication with single wall carbon nanotube probe microscopy tips", *App. Phys. Lett.*, 76, 3136,-3138.

Coleman, J.N., Fleming, A., Maier, S., O'Flaherty, S., Minett, A.I., Ferreira, M.S., Hutzler, S., Blau, W.J., (2004), "Binding Kinetics and SWNT Bundle Dissociation in Low Concentration Polymer-Nanotube Dispersion", *J. Phys. Chem. B.*, 108, 3446-3450.

Collins, P.G., Avouris P., (2000), "Nanotubes for electronics", *Scientific American*, 62-69.

Dalton, A., Stephan, C., Coleman, J.N., McCarthy, B., Ajayan, P.M., Lefrant, S., Bernier, P., Blau, W.J., Byrne, H.J., (2000), "Selective interaction of a semi-conjugated organic polymer with single-wall nanotubes", *J. Phys. Chem. B.*, 104, 10012-10016.

Duesberg, G., Blau, W., Byrne, H.J., Muster, J., Burghard, M., Roth, S., (1999), "Chromatography of carbon nanotubes", *Synth. Metals*, 103, 2484-2485.

Dalton, A., Blau, W.J., Chambers, G., Coleman, J.N., Henderson, K., Lefrant, S., McCarthy, B., Stephan, C., Byrne, H.J., (2001), "A functional conjugated polymer to process, purify and selectively interact with single walled carbon nanotubes", *Synth. Metals*, 121, 1217-1218.

Dai, H., Hafner, J.H., Rinzler, A.G., Colbert D.T., Smalley, R.E., (1996) "Nanotube as nanoprobe in scanning probe microscopy", *Nature*, 384, 147-150.

Dillon, A., Gennett, T., Jones, K.M., Alleman, J.L., Parilla, P.A., Heben, M.J., (1999), "A simple and complete purification of single-walled carbon nanotube material", *Adv. Mater.*, 11, 1354-1356.

Dillon A.C., Jones, K.M., Bekkedahl, T.A., Kiang, C.H., Bethune, D.S., Heben, M.J. (1997), "Storage of hydrogen in single-walled carbon nanotubes", *Nature*, 386, 377-379.

Dillon A.C., Gilbert, K.E.H., Parilla, P.A., Horbacewicz, C., Alleman, J.L., Heben, M.J. (2003), "Hydrogen storage in carbon single-walled nanotubes", *Hydrogen, Fuel Cell and Infrastructure Technologies*, 1-7.

Dresselhaus, M.S., Dresselhaus, G., Eklund, P.C., (1996) *Science of Fullerenes and Carbon Nanotubes,* Academic Press, San Diego 756-864.

Dresselhaus, M.S., Dresselhaus, G., Saito, R., (1995), "Physics of carbon nanotubes", *Carbon*, 33, 883.

Endo, M., Takeuchi, K., Igarashi, S., Kobori, K., Shiraishi, M., Kroto, H.W., (1993), "Production and structure of pyrolytic carbon nanotubes", *J. Phys. Chem. Solids*, 54, 1841-1848.

Fantini, C., Jorio, A., Souza, M., Strano, M.S., Dresselhaus, M.S., Pimenta, M.A., (2004), "Optical transition energies for carbon nanotubes from resonant Raman spectroscopy: environment and temperature effects", *Phys. Rev. Lett.*, 93, 147404-1 – 147404-4.

Fuhrer, M.S., Nygard, J., Shih, L., Forero, M. Yoon, Y., Mazzoni, M.S.C., Choi, H.J., Ihm, J., Louie, S.G., Zettl, A., McEuen, P.L., (2000), "Crossed Nanotube Junctions", *Science*, 288, 494-497.

Hamada, N., Sawada, S, Oshiyama, S. (1992), "New one-dimensional conductors:graphitic microtubles" *Phys. Rev. Lett.* 68, 1579 - 1581.

Harris, P.J.; (1999), *Carbon Nanotubes and Related Structures,* Cambridge University Press, Cambridge.

Iijima, S., Ichihashi, T., (1993), "Single shell nanotubes of 1-nm diameter", *Nature*, 363, 603-605.

Iijima, S., (1991), "Helical microtubules of graphitic carbon", *Nature*, 354, 56-58.

Javey, A., Guo, J., Farmer, D.B., Wang, Q., Yenilmez, E., Gordon, R.G., Lundstrom, M., Dai, H., (2004), "Self aligned ballistic molecular transistors and electrically parallel nanotube arrays", *Nanoletters*, 4, 1319-1322.

Keogh, S.M., Maguire, A., Hedderman, T.G., Gregan, E., McCarthy, B., Dalton, A.B., Chambers, G., Byrne, H.J., (2002), "Physical interaction between HiPco SWNT's and semi-conjugated polymers", *Proceedings of the International Winterschool of the Electronic Properties of Novel Materials (IWEPNM),* 633, 570-573.

Kong, J., Franklin, N.R., Zhou, C., Chapline, M.G., Peng, S., Cho, K., Dai, H., (2000), "Nanotube molecular wires as chemical sensors", *Science*, 287, 622-625.

Kuzmany, H., Burger, B., Thess, A., Smalley, R.E., (1998), "Vibrational spectra of single wall carbon nanotubes", *Carbon*, 36, 709-712.

Lee, S.M., K.H., Kim, W.S., Lee, Y.H., Park, Y.S., Seifert, G., Frauenheim, T., (2001), "Hydrogen storage in carbon nanotubes", *Synth. Metals*, 121, 1189-1190.

Liz-Marzan, L.M., Kamat, P.V., (2003), *Nanoscale Materials*, Kluwer Academic publishers, Norwell, MA, 450-465.

McEuen, P.L., (2000), "Single walled carbon nanotubes", *Physics World*, 31-36.

Mintmire, J.W., Dunlap, B.I., White, C.T., (1992), "Are fullerene tubules metallic", *Phys. Rev. Lett.*, 68, 631-634.

Niyogi, S., Hu, H., Hamon, A., Bhowmik, P., Zhao, B., Rozenzhak, S.M., Chen, J., Itkis, M.E., Meier, S., Haddon R.C., (2001), "Chromatographic purification of soluble single-walled carbon nanotubes", *J. Am. Chem. Soc.*, 123, 733-734.

Odom, T.W., Huang, J.L., Lieber, C., (2002), "Single-walled carbon nanotubes: From fundemental studies to new device concepts" *Ann. N.Y. Acad. Sci.* 960, 203-215.

Rao, A.M., Chen, J., Richter, E., Schlect, U., Eklund, P.C., Haddon, R.C., Venkateswaran, U.D., Kwon, Y.K., Tomanek, D., (2001), "Effect of van der Waals interactions on the Raman modes in single walled carbon nanotubes", *Phys. Rev. Lett.*, 86, 3895-3898.

Rao, C.N.R., Satishkumar, B.C., Govindaraj, A., Nath, M., (2001), "Nanotubes", *ChemPhysChem*, 2, 78-105.

Reich. S., Thomsen, C., Maultzsch, J., (2004), *Carbon Nanotubes, Basic Concepts and Physical Properties,* Wiley-VCH, Weinheim.

Rinzler, A.G., Liu, J., Dai, H., Nikolaev, P., Huffman, C.B., Rodriguez-Macias, F.J., Boul, P.J., Lu, A.H., Heymann, D., Colbert, D.T., Lee, R.S., Fischer, J.E., Rao, A.M., Eklund, P.C., Smalley, R.E., (1998), "Large scale purification of single-wall carbon nanotubes:process, product, and characterisation", *App. Phy. A.*, 67, 29-37.

Saito, R., Fujita, F., Dresselhaus G., Dresselhaus, M.S., (1992), "Electronic structure of graphene tubules based on C_{60}", *Phys. Rev. B.*, 46, 1804-1811.

Saito, R., Dresselhaus, G., Dresselhaus, M.S., (1998), *Physical Properties of Carbon Nanotubes,* Imperial College Press, London.

Strong, K.L., Anderson, D.P., Lafdi, K., Kuhn, J.N., (2003), "Purification process for single walled carbon nanotubes", *Carbon*, 41, 1477 - 1488.

Shea, H.R., Martel, R., Hertel, T., Schmidt, T., Avouris, Ph., (1999), "Manipulation of carbon and properties of nanotube field effect transistors and rings", *Microelectronic Engineering*, 46, 101-104.

Tsang, S.C., Harris, P.J.F., Green, M.L.H., (1993), "Thinning and opening of carbon nanotubes by oxidation using carbon dioxide", *Nature,* 362, 520-522.

Thess, A.; Lee, R.; Nikolaev, P.; Dai, H.; Petit, P.; Robert, J.; Xu, C.; Lee, Y.H.; Kim, S.G.; Rinzler, A.G.; Colbert, D.T.; Scuseria, G.E.; Tomanek, D.; Fisher, J.E.; Smalley, R.E.; (1996), "Crystalline Bundles of Metallic Carbon Nanotubes", *Science*, 273, 483 -487.

Tomanek, D., Enbody, R.J., (2000), *Science and application of Nanotubes*, Kluwer Academic Publishers/Plenum Publishers, New York, 300-302.

Yu, M.F., Files, B.S., Arepalli, S., Ruoff, R.S., (2000), "Tensile loading of bundles of SWNT and their mechanical properties", *Phys. Rev. Lett.,* 84, 5552-5555.

Zhang, M., Yudasaka, M., Koshio, A., Jabs, C., Ichihashi, T., Iijima, S., (2002), "Structure of single-wall carbon nanotubes purified and cut using polymer" *Appl. Phys. A.,* 74, 7-10.

CHAPTER 2 -SINGLE WALLED CARBON NANOTUBES

2.1 Introduction to Single Walled Carbon Nanotubes

SWNTs were first synthesised *en masse* in an arc-discharge chamber using metal catalysts, such as iron (Fe) or cobalt (Co), during the synthesis process (Harris, 1999). Initial experiments showed a diameter range of 0.7–1.6 nm and lengths of 700 nm with low yield and purity (Bethune *et al.*, 1993; Iijima and Ichihashi, 1993; Saito *et al.*, 1998). The impurities were comprised of amorphous carbon and catalyst particles. However, in 1997 a French group showed that high yields of SWNTs could be achieved using the arc technique (Journet *et al.*, 1997). Yields of 70 % SWNTs, an average diameter of 1.4 nm and lengths of many micrometers were obtained in gram quantities. The diameter distribution as well as the structure of SWNTs is of interest, since theoretical studies indicate that the physical properties of carbon nanotubes are strongly dependent on these two factors (Reich *et al.*, 2004; Saito *et al.*, 1998). A breakthrough in the synthesis of SWNTs, making significant amounts of material available for experimental study, was the laser vapourisation method developed by Rice University in 1996 (Kroto *et al.*, 1985; Thess *et al.*, 1996). High yields with >70 % SWNTs and an average diameter of 1.4 nm were reported. The remaining 30 % consists of amorphous carbon and catalyst particles. The laser vapourisation technique was surpassed in 1999 by high pressure carbon monoxide disproportionation, commonly referred to as the HiPco method, which can produce >90 % pure SWNTs with an average diameter of 1.1 nm, the only impurity being iron catalyst particles (Nikolaev *et al.*, 1999). However mass production with a yield of 100 % SWNTs is yet to be achieved. In addition, irrespective of the production technique, SWNTs were found to form two-dimensional hexagonal-packed bundles during the growth process with the properties of the bundle inferior to that of individual SWNTs (Zhang, 2004). Processing techniques to purify and debundle SWNTs were devised and these included oxidation and filtration and the use of polymeric materials to name a few (Deusberg *et al.*, 1999; Rinzler *et al.*, 1998; Saito *et al.*, 1998). Although many of the processing techniques are effective they have been found to be destructive to the tube or offer a poor level of efficiency (Ajayan *et al.*, 1993; Tsang *et al.*, 1993).

2.2 Structure

As described in the overview in Chapter 1, a geometrically perfect carbon nanotube consists of an sp^2-hybridised graphene sheet rolled to form a cylinder which is capped on both ends with a bisected fullerene like structure. There are many ways to roll and seamlessly close a graphene sheet and thus there is a large variety of possible helical geometries for carbon nanotubes that provide a family of structures with different diameters and chiralities. How the geometries are defined and how the physical properties of carbon nanotubes depend on that geometry will be discussed in this chapter.

As discussed in Chapter 1, there are two primary classification of SWNTs, achiral and chiral (Wildoer *et al.*, 1998; Odom *et al.*, 1998). An achiral nanotube is defined as a carbon nanotube whose mirror image is superimposable on itself. There are only two cases of achiral nanotubes; armchair and zigzag, and they are depicted in Figures 1.2 (A) and 1.2 (B). Their names originate from the cross sectional ring of each tube. Bisecting the circumference of Figure 1.2 (A) shows a periodic armchair structure while Figure 1.2 (B), has a jagged zigzag structure. A chiral nanotube, shown in Figure 1.2 (C) has a twisted helical structure with no periodicity about the bisected circumference and exhibits a spiral symmetry whose mirror image is non-superimposable.

A more detailed description of the formation of different SWNT structures is given in Figure 2.1. It depicts the rolling of a graphene sheet along the line OA so that the origin O of the sheet overlaps with an arbitrary lattice point A and points B and B' coincide resulting in an uncapped carbon nanotube. The direction OA in Figure 2.1 determines the structure of the SWNT, and corresponds to a section perpendicular to the nanotube axis (equator). The vector OB corresponds to the direction of the nanotube axis. The vectors OA and OB define the chiral vector C_h and the translational vector T of a carbon nanotube respectively. The chiral vector C_h is expressed in real space by the unit vectors a_1 and a_2 of the hexagonal lattice (Equation 2.1) where n and m are integers, $n \geq |m| \geq 0$.

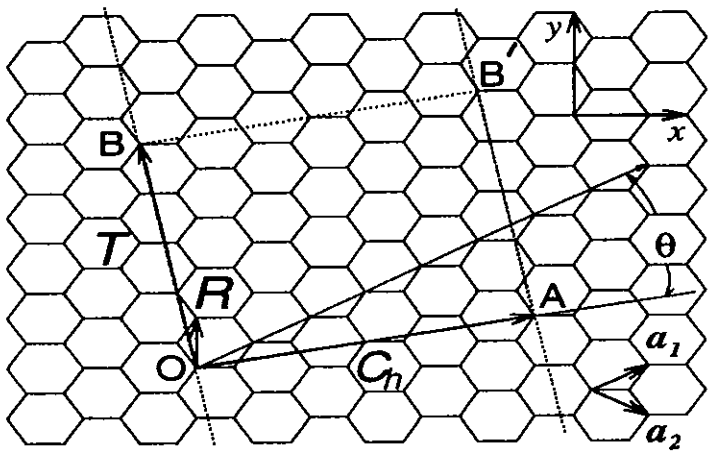

Figure 2.1 Unrolled honeycomb lattice of a nanotube. When the sites O and A coincide as well as B and B', a nanotube can be constructed. The rectangle OAB'B defines the unit cell for the nanotube. The vector R denotes a symmetry vector (Saito *et al.*, 1998).

$C_h = na_1 + ma_2 \equiv (n, m)$ Equation 2.1

Accordingly, any SWNT is characterised by two integers, n and m. For $n = m$ the tubes have an armchair-like (Figure 1.2 (A)) arrangement of carbon atoms at the circumference and when either n or m is equal to zero the arrangement is zigzag (Figure 1.2 (B)). For n not equal to m and neither equal to zero the tubes are said to be chiral (Figure 1.2 (C)). Note that θ is the chiral angle (Figure 2.1) and the value of θ determines the nanotube type (chiral, zigzag, and armchair) that is formed and also the electronic properties of the nanotube; whether the tube exhibits metallic or semiconducting behaviour (Saito *et al.*, 1998). Rolling the graphene sheet depicted in Figure 2.1 at an angle of 0° and 30°, results in the formation of zigzag and armchair SWNT respectively. Chiral SWNT are formed when the graphene sheet is rolled at an angle between 0° and 30°. Table 2.1 shows the correspondence between the chiral angle and the associated electronic properties.

Table 2.1 Classification of single walled carbon nanotubes.

Structure	electronic propreties	chiral angle (θ)	chiral vector C_h
Armchair	metallic	30°	(*n,n*)
Zigzag	2/3 semiconducting 1/3 metallic	0°	(*n,0*)
Chiral	semiconducting and metallic	$0° < \|\theta\| < 30°$	(*n,m*)

2.3 Electronic Properties

The ideal infinite graphene sheet is a semiconductor with a band-gap of 0 eV, and hence is usually observed to have metallic conduction properties (Reich *et al.*, 2004; Saito *et al.*, 1998). Due to the structure of graphene, electrons moving at the Fermi level are back-scattered by the atoms in the lattice, which give the material an energy gap, like that of a semiconductor. However in other directions, the electrons scatter from different atoms in the lattice and interfere destructively, which suppresses the back scattering leading to metallic behaviour. This suppression only occurs in certain directions and, for this reason, graphene can be described as a "semi-metal" since it is metallic in some directions and semiconducting in others (Harris, 1999; Reich *et al.*, 2004; Saito *et al.*, 1998).

The basic electronic structure of a SWNT can be derived from a graphene sheet while neglecting hybridisation effects due to the finite curvature of the tube structure. Graphene is a semi-metal which has valence and conduction bands that are degenerate at only six corners of the hexagonal first Brillouin zone (K_B) and so the Fermi surface of the graphene sheet is thus reduced to these six points as depicted in Figure 2.2 (a) and Figure 2.2 (b). In SWNT, the wave vector k is quantized along the circumferential direction due to periodic

boundary conditions known as the Born-von Karman boundary conditions given in equation 2.2 (Ouyang *et al.*, 2002).

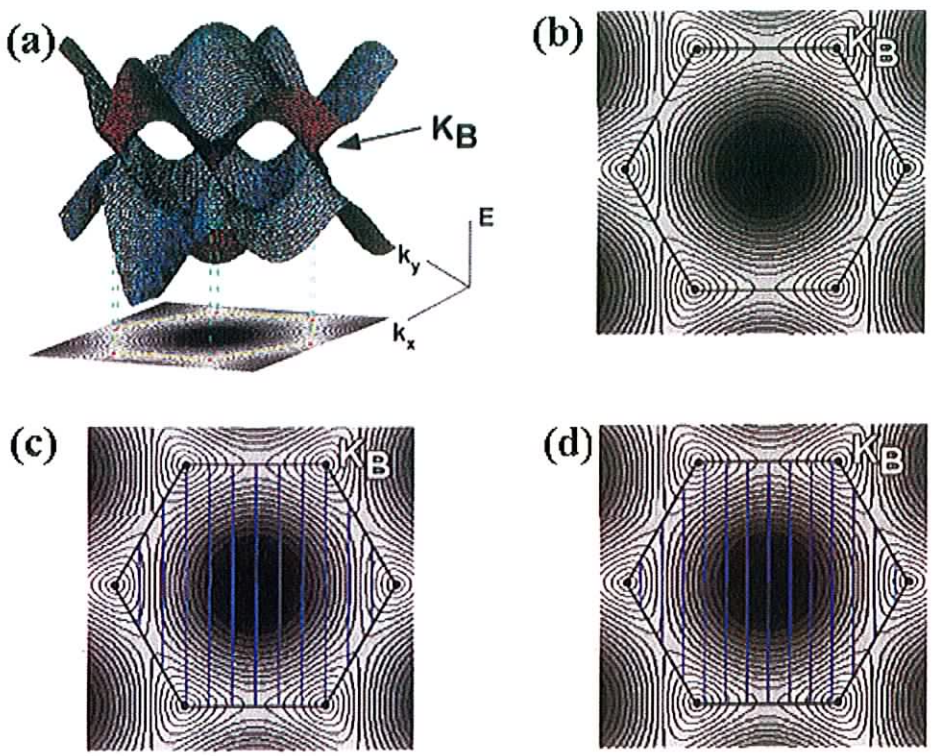

Figure 2.2 (a) Three-dimensional plot of the π and π^* graphene energy bands and (b) a two-dimensional projection. (c) Allowed one-dimensional wavevectors for a metallic (9,0) SWNT. (d) Allowed one-dimensional wavevectors for a semiconducting (10,0) tube. The black hexagons define the first Brillouin zone of a graphene sheet, and the black dots in the corners are the K_B points. Blue lines represent allowed wavevectors, k, within the first Brillouin zone (adapted from Ouyang *et al.*, 2002).

$k_n.C_h = 2\pi q$ Equation 2.2 (Joselevich, 2004)

In Equation 2.2, q is an integer, k_n is the quantised momentum vector and C_h is the circumference or chiral vector of the tube. The density of states (DOS) (Okahara *et al.*, 1994) of the carbon nanotube is restricted to states that have this periodicity. Therefore only

a particular set of states which are parallel to the corresponding tube axis with a spacing of $2/d_t$ (where d_t is the tube diameter) are allowed. On the basis of this simple scheme, if one of the allowed wavevectors passes through a Fermi K_B of the graphene sheet, the SWNT will be metallic. Otherwise the SWNTs will be semiconducting as depicted in Figure 2.2 (c) and Figure 2.2 (d).

2.4 Effect of Structure on Electronic Properties

Applying Equation 2.2 to model the electronic structure, it is found that nanotubes differ dramatically depending on the circumference of the carbon nanotube, and hence on the (*n*, *m*) values of the chiral vector. Depending on the length of periodicity, allowed states can exist at the Fermi energy ($\mathbf{E_f}$), and therefore the carbon nanotube will be metallic, or a band-gap can exist at the Fermi level ($\mathbf{E_f} = 0$), and the carbon nanotube will be semiconducting. At the Fermi energy, the density of states is finite for a metallic tube (though very small), and zero for semiconducting tubes. At higher energies, sharp peaks in the DOS, called van Hove singularities, appear at specified energy levels (Joselevich, 2004). Figure 2.3 below shows the DOS for both a metallic (a) and semiconducting (b) carbon nanotube where *vn* represents the valence bands and *cn*, the conduction bands for the first electronic transition (Yu *et al.*, 2001).

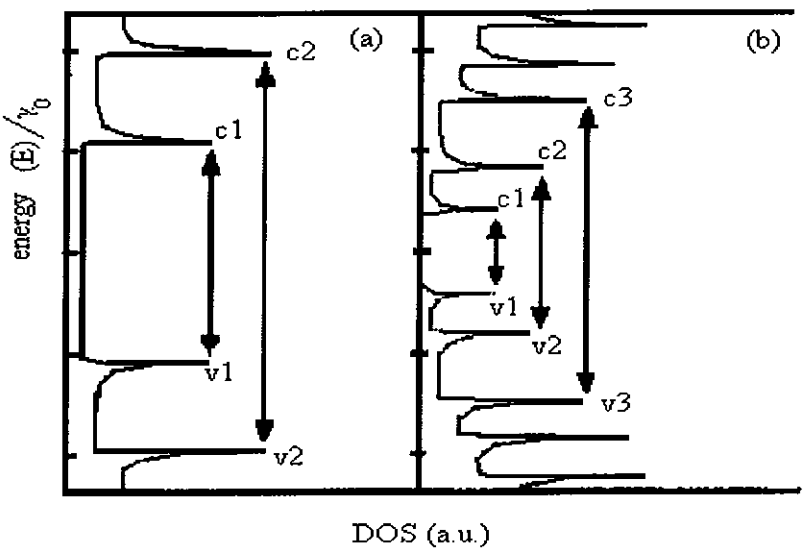

Figure 2.3 The density of states for carbon nanotubes. The van Hove singularities are apparent as sharp spikes in the density of states. The v1-c1 is the first electronic transition between van Hove singularities, corresponding to the band-gap in metallic (a) and semiconducting nanotubes (b) respectively (Yu *et al.*, 2001).

Figure 2.4 shows the energy band dispersion relations calculated for the three broad categories of electronic structures into which all carbon nanotubes fall (Dresselhaus *et al.*, 1996). Figure 2.4 (a) shows a metallic carbon nanotube with states existing at the Fermi level. Figure 2.4 (b) is a pseudo-metallic nanotube which similar to graphite is a semiconductor with a zero band-gap. This will be metallic at all temperatures above absolute zero, as thermal energy will ensure there are a large amount of occupied states in the conduction band. Figure 2.4 (c) is a semiconducting nanotube, with a finite band-gap. The relationship that determines which nanotubes will be metallic is relatively simple (Dresselhaus *et al.*, 1996) and is given in Equation 2.3 below.

$$(n-m)/3 = p \qquad \text{Equation 2.3}$$

With respect to Equation 2.3, if p is zero the nanotube is metallic, if p is an integer it is pseudo-metallic and if p equals anything else the nanotube is semiconducting. Immediately apparent from this is that one third of all nanotubes are metallic, and that all armchair nanotubes are metallic, i.e. nanotubes where $n = m$.

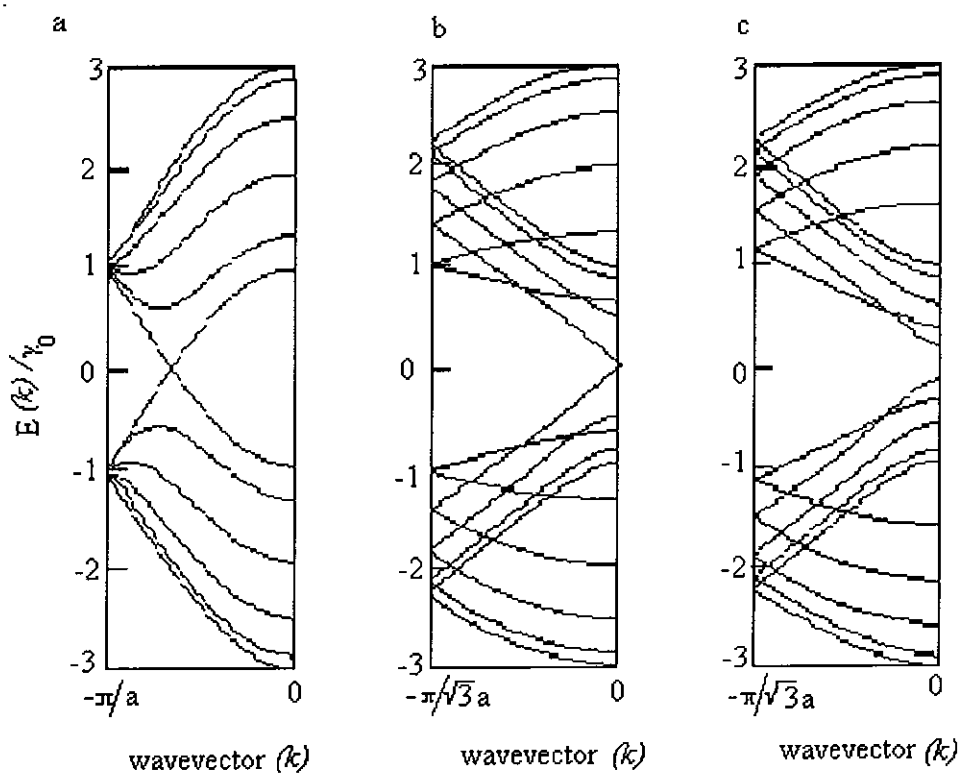

Figure 2.4 Energy dispersion relations based on structure calculations for single walled nanotubes where (a) is due to a truly metallic tube as there is a finite density of states at the Fermi energy, (b) is a semiconducting tube with zero band-gap and (c) is semiconducting (Dresselhaus *et al.*, 1996).

2.5 Effect of Tube Diameter and Chirality on Elelctronic Properties

It is a well established fact that tube diameter as well as chirality, determine whether tubes are semiconducting or metallic (Dresselhaus *et al.*, 1996; Rao *et al.*, 1997). The energy gap, E_{gap}, is related to the diameter of the tube as described by the following equation.

$E_{gap} = ka_{C\text{-}C}\gamma_0/d$ Equation 2.4

where E is the transition energy, $a_{C\text{-}C}$ is the distance between the carbon to carbon single (C-C) bonds, 0.144 nm, d is the diameter and γ_0 is the C-C tight binding overlap energy, experimentally determined to be 2.9 eV for carbon nanotubes, and k is a constant (Brown *et al.*, 2000). The value of k is 2, 4 and 8 for the 1st, 2nd and 3rd van Hove transitions in semiconducting tubes and 6, and 12 for 1st and 2nd van Hove transitions in metallic tubes, respectively (White and Mintmire, 1998).

Equation 2.4 determines the band-gap energy, being the energy difference between two mirroring van Hove singularities, between *cn* and *vn* in Figure 2.3, which is related to the diameter of the carbon nanotube (Yu and Brus, 2001). This occurs because the curvature of the lattice induces a strain (due to changes in the bond alternation/hybridisation) in the graphene sheet, manifesting itself in the band-gap (Okahara *et al.*, 1994). As the curvature decreases with increasing diameter, the band-gap will reduce. As the diameter goes to infinity, the band-gap goes to zero, and the result is a flat semiconducting graphene sheet with zero band-gap, as in graphene.

Figure 2.5 illustrates and also supports Table 2.1 by showing that the structure and electronic properties of the SWNTs are determined by the chiral angle of the graphene sheet. For metallic SWNTs, the condition is $(2n + m)$ or equivalently $(n\text{-}m)$ is a multiple of three. In particular the armchair SWNTs denoted by (n, n) are always metallic, and the zigzag $(n, 0)$ are only metallic when n is a multiple of three, otherwise they are semiconducting. Table 2.1 also shows that generally one third of SWNT are expected to be metallic while two thirds are semiconducting.

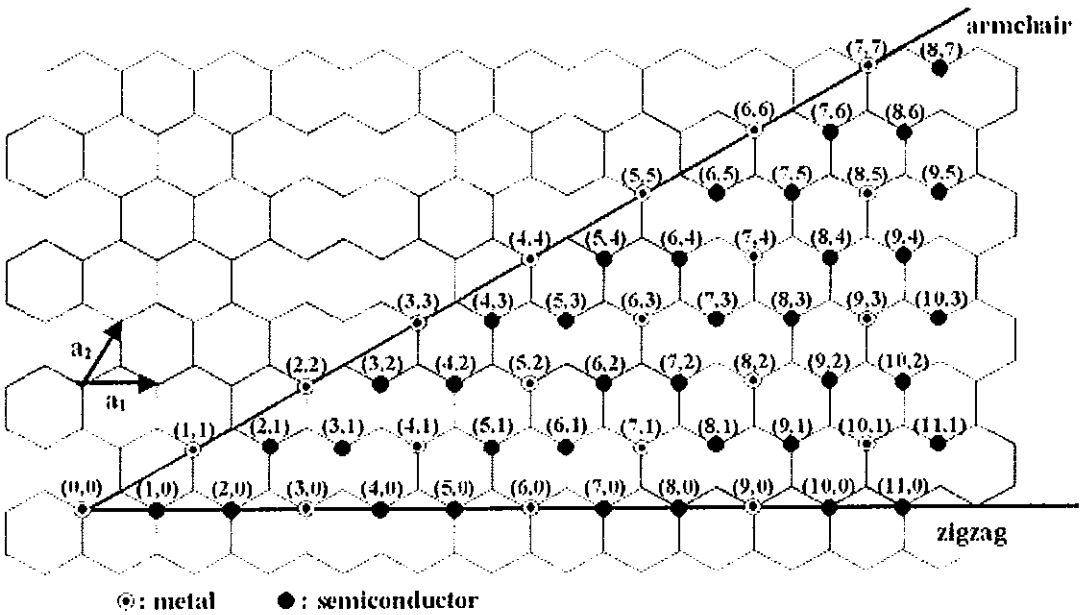

Figure 2.5 Carbon nanotubes (n, m) that are metallic and semiconducting, and are denoted by open and solid circles respectively on the map of chiral vectors (n, m) (Dresselhaus *et al.*, 2001).

Ideally, a carbon nanotube is a unique, quasi-one-dimensional conductor, which can have either metallic or semiconducting properties. Not all SWNTs produced are perfect, however, and nanotube structures with kinks and bends are also known to exist (Zhou *et al.*, 1994). These imperfections are as a result of defects. For example, pentagons, heptagons and sp^3 hybridised carbon are commonly found in the graphene sheet. Also, these hollow cylinders have a strong tendency to agglomerate as they form, resulting in bundles, or "ropes," of aligned SWNTs. The aggregates are complex composite conductors incorporating many weakly coupled nanotubes, each having a different electronic structure. The bundles are held together by weak van der Waals inter-nanotube bonds to form a two-dimensional triangular lattice with a lattice constant of 1.7 nm and an inter-tube separation of 0.315 nm at closest approach within a bundle as shown in Figures 2.6 and 2.7 (Kasuya *et al.*, 1998; Thess *et al.*, 1996). It is found that the spread in nanotube diameters within a single bundle is smaller than between bundles that are grown at the same time under the same conditions. Bundles of SWNTs have an added effect on the electronic properties

(Reich *et al.*, 2002) and they will also have an effect on the vibrational properties, which will be discussed later (Chapter 4).

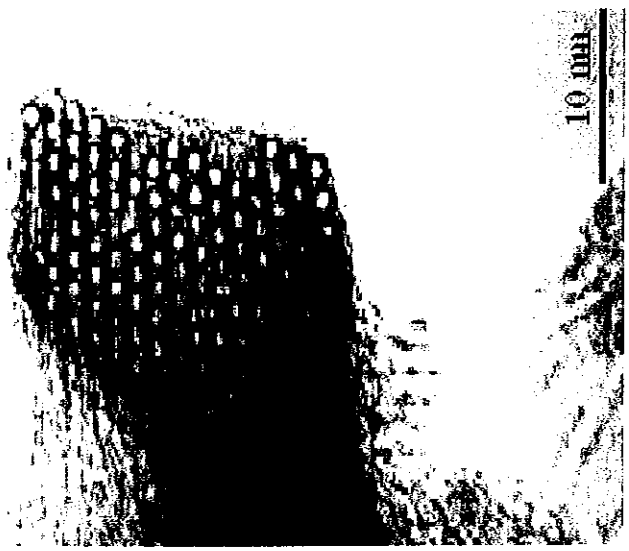

Figure 2.6 TEM image at high magnification shows that ropes comprise of bundles of SWNTs. This bundle is bent in such a way that it is seen edge-on (Thess *et al.*, 1996).

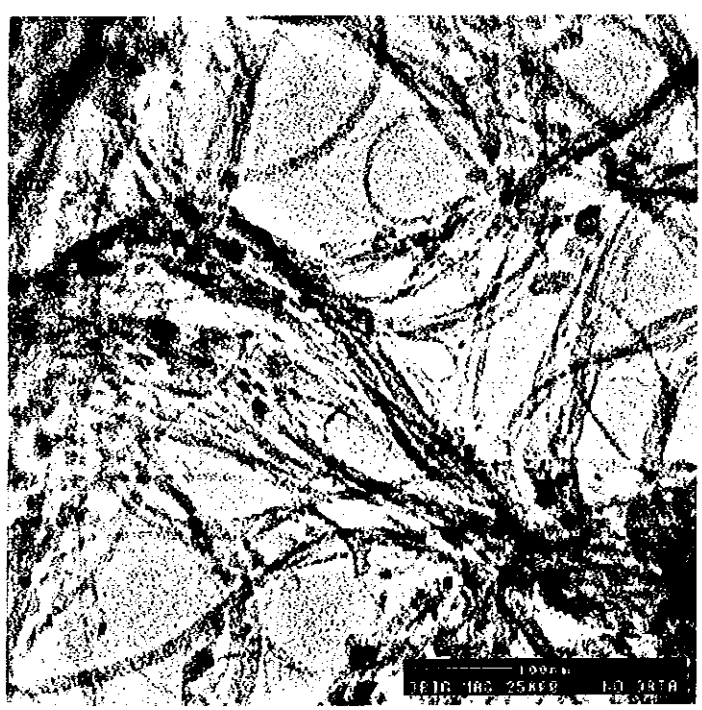

Figure 2.7 Bundles of SWNT observed by TEM. The bundles are 5-20 nm thick and up to several 100 μm long (Thess *et al.*, 1996).

2.6 Production Methods

Since the discovery of SWNTs there has been a considerable drive towards the bulk production of this material. Today, many different techniques exist and are used to produce them. This section gives a brief insight of a selected number of production methods. The methods discussed are electric arc-discharge (Hsu *et al.*, 1996; Iijima and Ichihashi 1993; Journet *et al.*, 1997), pulsed laser vapourisation (Puretzky *et al.*, 2000; Scott *et al.*, 2001; Thess *et al.*, 1996), and high pressure carbon monoxide disproportionation, also referred to as the HiPco process (Nikolaev *et al.*, 1999). The arc-discharge technique was the first technique by which SWNTs were produced and it was from a basic understanding of this technique that many other synthetic methods spawned. The laser ablation technique was the first technique to produce SWNTs *en masse* and it is these SWNTs that are used for the bulk of the experimental work in this thesis. Finally, the HiPco process is discussed as it is by far one of the most common techniques used to produce high purity SWNTs today. The description given below will show that the diameter, purity and bundle size of the SWNT sample is sensitive not only to the method used but also the parameters of the reaction chambers.

Arc-Discharge

The arc-discharge method was the first and is still one of the most widely used techniques for the production of SWNT (Bethune *et al.*, 1993; Iijima and Ichihashi 1993; Journet and Bernier, 1998). The carbon arc provides a simple traditional tool for generating the high temperatures needed for the vapourisation of carbon atoms into plasma (Ebbesen *et al.*, 1993; Seraphin *et al.*, 1993). Figure 2.8 is a schematic representation of the apparatus used in the University of Montpellier (France). The principle of this method is based on an electric arc-discharge generated between two graphite electrodes under an inert atmosphere of helium or argon. The high temperature occurring between the two rods allows the sublimation of carbon. The synthesis is performed in a water-cooled reaction chamber which is first evacuated and then filled with an inert gas atmosphere. Two graphite rods are used as electrodes: one is fixed while the other one can be moved by a translation mechanism. The mobile electrode (the anode) is moved towards the cathode until the

distance between them is so small (< 1 mm) that the current (60-100 A) passes through the electrodes and a plasma is created between them. The average temperature in the inter-electrode plasma region is extremely high (of the order of 4000 K) and therefore the carbon is sublimated and the positive electrode is consumed. In order to maintain the arc between the electrodes, the anode has to be continuously translated to keep a constant distance between the rods. Generally the anode is smaller than the cathode and both electrodes are water-cooled. By controlling the voltage (30 V) and the separation between the two rods, it is possible to reduce the fluctuations of the plasma. The technique first produced MWNTs in 1991 and it was later discovered that the addition of metal catalysts such as Co and Ni at specified ratios to the anode led to the production of SWNTs in 1993 (Harris, 1999; Iijima, 1991; Iijima and Ichihashi, 1993).

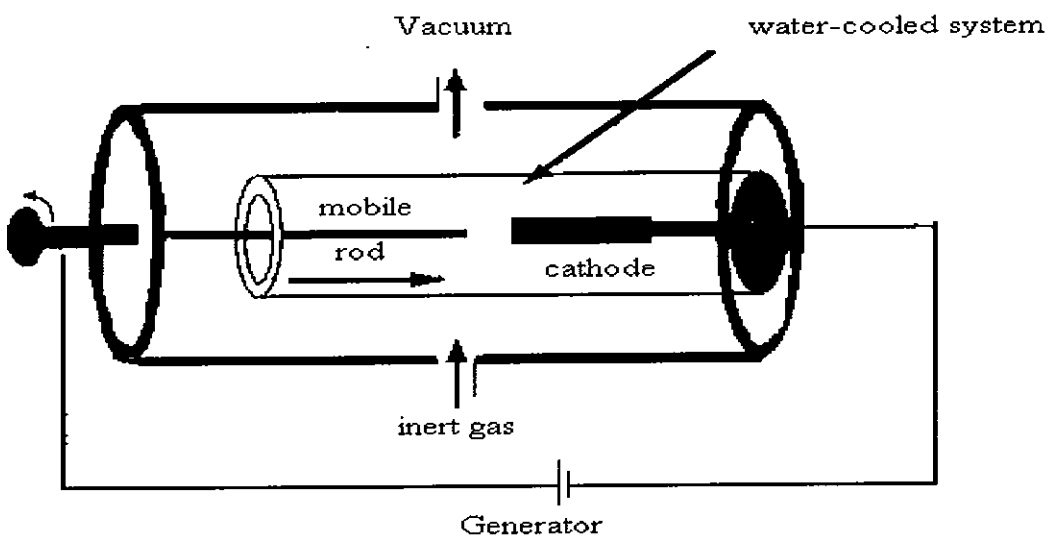

Figure 2.8 Schematic representation of electric-arc apparatus used at the University of Montpellier (France). The apparatus is also known as the Kraetschmer generator (Journet and Bernier, 1998).

SWNTs were produced by drilling a hole in the centre of the anode and filling it with a mixture of metal catalysts and graphite at specified ratios. Under the conditions stated above, the anode is consumed and a cylindrical deposit forms at the cathode which comprises of an exterior hard grey metallic shell and a soft interior belt. It is within the soft

belt that the amorphous carbon, spherical metallic nanoparticles, a few graphitic sheets and a high density of SWNT are found. Growing from the cathode to the reactor walls and decorating the chamber are "spider webs". These structures contain fullerenes and amorphous carbon and also a low density of SWNT. The purity and yield of the SWNTs sample using yttrium, nikel and graphite (Y/Ni/C) at 1 %/4 %/95 % was estimated at ~ 70 % with the majority of SWNTs having a diameter of 1.4 nm and gram quantity yields being achieved (Harris, 1999; Journet *et al.*, 1997). The number of tubes within the bundle was of the order of 20 and the bundle lengths were several micrometers. It is important to note that the quality and quantity of SWNTs produced mainly depend on the metal/carbon mixture as well as the pressure, temperature, current, and the geometry of the system.

Laser Ablation

The second technique for producing carbon nanotubes is laser ablation. A piece of graphite is vapourised by laser irradiation under an inert atmosphere, for example argon (Thess *et al.,* 1996). MWNTs are produced when a pure graphite target is used and the yields and quality are dependent on the temperature of the furnace. When a small amount of transition metal has been added to the carbon target, SWNTs are produced. Historically, laser ablation was the first technique used to generate fullerene clusters in the gas phase (Kroto *et al.*, 1985).

To produce SWNTs a carbon target containing 1 to 2 % Ni/Co catalyst is maintained at 1473 K in a tube furnace and is vapourised by a focused pulsed laser (Journet and Bernier, 1998). The laser beam scans across the target surface to maintain a smooth, uniform face for vapourisation. The vapourisation produces carbon species such as SWNTs, and to a lesser extent carbon nano-spheres (fullerenes) in the resultant plasma and both are swept down stream from the high temperature zone by the flowing argon gas where they are collected on a cold finger before they pass completely out of the furnace (for a schematic representation of the apparatus see Figure 2.9). The sample is removed and soaked in carbon disulphide (CS_2), to remove fullerenes and other soluble organics. Daily production of 1g of 70 % to 90 % pure SWNTs is achievable. The SWNT material is composed of

ropes (Figure 2.7) of 10-20 nm in diameter, with the bundles consisting of 100–500 SWNT, and 10-100 μm in length and gram quantity yields (Thess *et al.*, 1996). Transition electron microscopy (TEM) experiments on samples show that the average diameter is 1.4 nm for an isolated SWNT (Thess *et al.*, 1996).

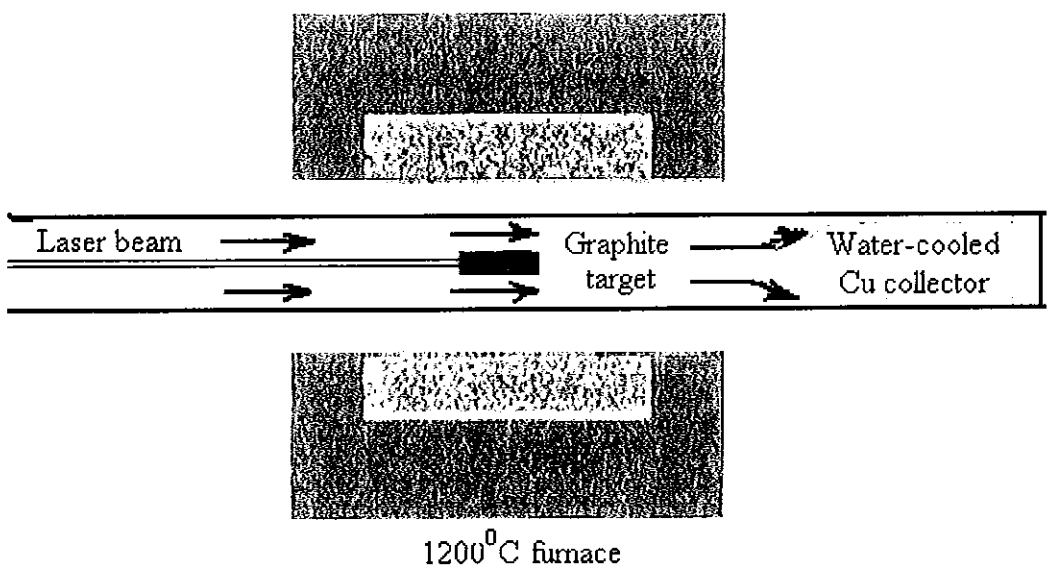

Figure 2.9 Schematic representation of oven laser-vapourisation apparatus used at Rice University (Houston, Texas, USA) (Journet and Bernier, 1998).

SWNTs were proposed to form through what is called the scooter mechanism, where atoms and catalysts Ni and Co are envisioned to attach to a fullerene or graphite sheet (Thess *et al.*, 1996). The catalyst atoms prevent the closing of the fullerene as additional carbons attach and lead to the formation of a tube. It was proposed that a single metal atom or a few metal atoms chemisorb to the open edge of a curving graphite sheet and circulate or scoot around the open end of the tube. They adsorb atoms of carbon and convert them into a tubular graphene sheet. Although only a single metal atom need be involved in the original nucleation and early growth of SWNT, other metal atoms congregate at the live end of the SWNT forming small metal clusters which then aggregate on the end of the nanotube. The

metal particles can then either detach or become over-coated with sufficient carbon to poison them hence allowing the tube to terminate with a fullerene like tip (Thess *et al.*, 1996).

Scott *et al.*, (2001), proposed an alternative mechanism for the growth of SWNTs. They proposed that the laser pulses heat the target surface containing graphite, Co and Ni and vapourise them. A very hot plume is formed that expands and cools rapidly. As the vapourised species cools, small carbon molecules and atoms quickly condense to form larger clusters, including possibly fullerenes. The catalyst also begins to condense but much more slowly than carbon and attaches to the carbon clusters preventing their closure. It was thought that the catalysts may also open closed cage structures when they attach to them. From the initial clusters, SWNTs grow until the catalyst particles become too large or until conditions have cooled sufficiently so that carbon can no longer diffuse through the catalyst particles. It is also possible that the catalyst becomes so over-coated with a carbon layer that it can longer absorb and nanotube growth ceases.

High Presure Carbon Monoxide Disproportionation (HiPco)

High pressure carbon monoxide (CO) disproportionation (HiPco) has been shown to produce SWNTs of high purity, with current purity of 90 % atomic percent SWNTs. The tubes are produced by a gas-phase catalytic process. Catalysts for SWNT growth form *in situ* by thermal decomposition of iron pentacarbonyl ($Fe(CO)_5$) in a heated flow of carbon monoxide (CO) at pressures of 1 to 10 atm and temperatures of 1100 to 1500 K (Chiang *et al.*, 2001; Nikolaev *et al.*, 1999). The tube diameter and yield can be varied by controlling the process parameters and SWNTs as small as 0.7nm in diameter, the same as that of a C_{60} molecule, can be generated. Previously, all investigations reporting gas-phase continuous flow production of SWNTs had relied on hydrocarbons as the carbon source molecule for tube growth. However, hydrocarbons pyrolise readily on most surfaces above 900 to 1000 K (temperature required for growth of SWNT) forming graphitic deposits or amorphous carbon. In this case CO is used as the carbon feed stock and $Fe(CO)_5$ as the iron containing

catalyst precursor. The Boudard reaction in Equation 2.5 shows how carbon soot is produced from reacting CO.

$$CO + CO \rightarrow C_{(s)} + CO_{2(g)} \qquad \text{Equation 2.5}$$

The model proposed for SWNT growth begins with the formation of metal clusters which nucleate and grow SWNTs. Metal clusters initially form by the aggregation of iron atoms from the decomposition of iron pentacarbonyl. The clusters grow by collision until they reach a size near that of C_{60} by which time CO can disproportionate on the surface of the metal cluster *via* Equation 2.5 and SWNTs nucleate and grow. The tubes continue to grow until the metal cluster, which is also growing, reaches a size that favours formation of a carbon shell around the cluster and this ends the growth of the SWNT. The average diameters and percentage of graphite converted to SWNTs are 1.1 nm and 90% respectively but the diameters can be enlarged to 1.47 nm by heat treatment. The conditions for achieving tubes with 0.7nm diameter are 10 atm of pressure and a temperature of 1500 K. The average lengths of the SWNTs produced are of the order of 1μm and yields obtained are gram quantities per day. The dominant impurity in the tubes are metal catalysts, which are encased in thin carbon shells and distributed throughout the sample as 3-5 nm size particles. Four to five percent of Fe is typical in raw HiPco material (Chiang *et al.*, 2001; Nikolaev *et al.*, 1999; Yudasaka *et al.*, 2001).

2.7 Processing of SWNT

All large scale production methods afford SWNT that contain side products and the presence of these hamper progression in SWNT applications. Some of the impurity species are C_{60}, carbon polyhedra, amorphous carbon and metal catalyst particles to name a few (Journet *et al.*, 1997; Nikolaev *et al.*, 1999; Thess *et al.*, 1996). Besides the impurities, SWNTs are not uniform in diameter, chirality or length (Saito et al., 1998). The different species are closely entangled as bundles in the raw soot and occasionally even *via* chemical

bonds. As a consequence, the raw material is difficult to process. A number of techniques have been devised to try and rid the sample of side products and this began with improving the production methods. The HiPco process (discussed above) and chemical vapour deposition (CVD) are currently the most successful production techniques with >90 % conversion of reactants to SWNTs. Hence these samples contain <10% impurities (Nikolaev *et al.*, 1999; Zheng *et al.*, 2002). A number of purification techniques have been developed. These include oxidation (Dillon *et al.*, 1999; Tsang *et al.*, 1993), size selection chromatography (Ajayan *et al.*, 1993; Duesberg *et al.*, 1999; Niyogi, *et al.*, 2001), filtration (Rinzler *et al.*, 1998) and organic purification (Dalton *et al.*, 2000; Dalton *et al.*, 2001).

Oxidation

Oxidation is a wide spread technique used to purify SWNTs. Oxidation involves burning off amorphous carbon by heating the carbon nanotubes in air or other oxidising agents at 600 K. This particular technique is known as gas-phase oxidation (Tsang *et al.*, 1993). When using the wet or liquid-phase approach, strong oxidising agents such as nitric acid (HNO_3) or ruthenium tetroxide (RuO_4) attack the raw material. The technique has been found to be destructive to SWNTs however as oxidation readily occurs in areas of high curvature therefore targeting SWNT tips as well as polyhedra and fullerenes (Ajayan *et al*, 1993, Tsang *et al.*, 1993). The process results in the consumption and opening of the SWNT at the tip thus destroying the integrity of the SWNT. It is believed that the SWNT tips are targeted because of the strain due to curvature and the presence of pentagons. Although the technique is very successful in the removal of side products, over all it is destructive to the integrity of the SWNT and therefore not ideal. It is of interest to note that open SWNTs have been put to use. SWNTs that are functionalised with halogens or amines, which makes them more soluble in organic solvents, have been reported (Bahr *et al.*, 2001; Chen *et al.*, 1998), but functionalising SWNTs also brings about the loss of metallic behaviour. It should be noted that this technique offers no degree of selectivity of the carbon nanotubes.

Size Selection Chromatography

Size selection chromatography is a powerful non-destructive tool. The technique offers selectivity with respect to the varying lengths of SWNTs (Duesberg *et al.*, 1999). The technique is applied to a surfactant stablised dispersion of the SWNT material. The solution is passed through a column containing porous glass, (CPG 3000 Å, Fluka) with a pore size of 300 nm. It works on the basis that the pores are large enough to trap the amorphous carbon in the cavity, but allow free passage of the SWNTs through the column. The SWNTs are too large for the cavity and are collected in the fraction taken from the column. Experimental results showed that the SWNTs taken from different fractions differ significantly in length. Histograms show that one fraction taken contains SWNTs with an average length of 1μm whilst in another fraction 0.6 μm is the average length (Duesberg *et al.*, 1999). These results would appear to suggest that longer SWNTs elute first followed by the shorter tubes. It has also been demonstrated that as the number of fractions increase the amount of SWNTs in each fraction decreases, hence adding support that SWNTs elute in the early stages of chromatography. AMF investigations confirm length separation but no diameter selectivity was inferred or observed.

Filtration

As with size selection chromatography, the filtration technique is non-destructive to SWNTs. This technique is often used in conjunction with oxidation. The acid decomposition products are highly soluble in basic solutions and SWNTs are not and they are separated using a basic solution of pH 11 and a filter with a pore size of 3-5 μm. With the standard filtration technique the efficiency is limited by SWNTs blocking the filter pores. As the SWNTs filter cake thickens, the permeation rate of the basic solution containing the impurities decreases dramatically. When the amount of material exceeds 3 mg/cm^2 of filter surface area this method of washing becomes prohibitively slow and a number of successive filtration steps are necessary to get satisfactory purity (Rinzler *et al.*, 1998). A method to overcome this problem was introduced. The technique is known as hollow-fibre, cross-flow filtration. In this technique the filtration membrane takes the form

of a hollow-fibre, the wall of which is permeable to the solution. The cartridge contains fibres of mixed cellulose ester having a diameter of 0.6 mm with a pore size of 200 nm and 0.56 m^2 of surface area. Triton X-100, a non-ionic surfactant was added to both the filtrate in the system reservoir and the buffer solution to prevent the SWNTs from clumping and blocking the pores. The filtrate is pumped down the bore of the fibre at head pressure from the reservoir and the major fraction of the fast flowing solution which does not permeate out from the sides of the fibre is fed back into the same reservoir to be cycled through the fibre repeatedly. The fast hydrodynamic flow down the fibre bore sweeps the membrane surface to prevent the build up of a filter cake. A second reservoir contains buffer solution which is used to make up the filtrate reservoir solution volume lost to permeation through the fibre wall. Despite the dramatic improvement in the SWNTs purity, high-resolution transmission electron microscopy (TEM) images show that the material still contains a significant amount of impurities (Rinzler *et al.*, 1998).

Organic Processing

SWNTs have been processed using organic polymers such as poly P*m*PV-*co*-DOctOPV (Dalton *et al.*, 2000; Dalton *et al.*, 2001). P*m*PV-*co*-DOctOPV is soluble in organic solvents such as toluene. As previously stated in Chapter 1, SWNTs show a varying degree of solubility in commonly used organic solvents. In particular, SWNTs show a negligible degree of solubility in toluene. However, solubility is greatly improved as a result of the interaction with P*m*PV-*co*-DOctOPV. The polymer works *via* π-π mapping to the SWNT backbone drawing them into solution while all unwanted side products and catalyst particles precipitate out (Figure 1.3). Studies report that the polymer is diameter selective, selecting SWNTs in the range of 1.35 nm to 1.55 nm (Dalton *et al.*, 2000; Dalton *et al.*, 2001; Keogh *et al.*, 2004). It was also reported that the polymer isolated SWNTs by separating bundles, acting as a nanospacer. Purified SWNTs were obtained by washing the polymer from the nanotube with excess toluene through a Buchner funnel and collecting the washed tubes on filter paper of pore size 0.45μm.

Objectives for this Study

This thesis proposes to use the hydrocarbon molecules *p*-terphenyl and anthracene, to purify and process SWNTs. It is proposed that the hydrocarbon molecules, like the polymer molecules, will map *via* π-π interaction onto the backbone of the SWNTs drawing them into solution and allowing all side products to precipitate out (Figure 1.4). It is also proposed that the differing structures of the two hydrocarbon molecules will interact with specific SWNTs whose backbone is similar to their structure thereby resulting in structural selectivity of the SWNTs as depicted in Figure 1.4. It is proposed that anthracene will preferentially map to armchair SWNT while *p*-terphenyl will preferentially map to zigzag SWNTs. Consequently a degree of electronic separation will be achieved as all armchair SWNTs are proposed to be metallic and two thirds of all zigzag SWNTs are semiconducting.

Fluorescence quenching, concentration dependent studies will be carried out to probe not only the optimum solubility conditions but also to identify concentration ranges where bundled and debundled SWNTs and PAHs exist thereby giving a greater understanding of the nature and delicate balance of the different systems at different concentrations.

Summary

This Chapter has dealt with the structural and physical properties of SWNTs. An overview of some of the major production and processing techniques was given. In the case of the processing methods, a new and novel technique, using PAHs, has been proposed that will not only purify the SWNT sample but also select SWNTs relative to their backbone structure. Chapter 3 looks at the structural and physical properties of polycyclic aromatic hydrocarbons.

REFERENCES

Ajayan, P.M., Ebbesen, T.W., Ichihashi, T., Iijima, S., Tanigaki, K., Hiura, H., (1993), "Opening carbon nanotubes with oxygen and implications for filling", *Nature*, 362, 522-524.

Bahr, J.L., Yang, J., Kosynkin, D.V., Bronikowski, M.J., Smalley, R.E., Tour, J.M., (2001), "Functionalisation of carbon nanotubes by electrochemical reduction of aryl diazonium salts: a bucky paper electrode", *J. Am. Chem. Soc.*, 123, 6536-6542.

Bethune, D.S., Kiang, C.H., de Vries, M.S., Gorman, G., Savoy, R., Vazquez, J., Beyers, R., (1993) "Cobalt-catalysed growth of carbon nanotubes with single-atomic-layer walls", *Nature*, 363, 605-607.

Brown, S.D.M., Corio, P., Marucci, A., Dresselhaus, M.S., Pimenta, M.A., Kneipp, K., (2000), "Anti-Stokes Raman spectra of single-walled carbon nanotubes", *Phys. Rev. B.*, 61, R5137 – R5140.

Chiang, I.W., Brinson, B.E., Huang, A.Y., Willis, P.A., Bronikowski, M.J., Margrave, J.L., Smalley, R.E., Hauge, R.H., (2001), "Purification and characterisation of single-wall carbon nanotubes (SWNT) obtained from gas-phase decomposition of CO (HiPco process)", *J. Phys. Chem. B.*, 105, 8297-8301.

Chen, J., Hamon, M.A., Hu, H., Chen, Y., Rao, A.M., Eklund, P.C., Haddon, R.C., (1998), "Solution properties of single-walled carbon nanotubes", *Science*, 282, 95-98.

Colomer, J.F., Benoit, J.M., Stephan, C., Lefrant, S., Van Tendeloo, G., Nagy, J.B., (2001), "Characterisation of single-wall carbon nanotubes produces by CCVD method", *Chem. Phys. Lett.*, 345, 11-17.

Dalton, A., Stephan, C., Coleman, J.N., McCarthy, B., Ajayan, P.M., Lefrant, S., Bernier, P., Blau, W.J., Byrne, H.J., (2000), "Selective interaction of a semi-conjugated organic polymer with single-wall nanotubes", *J. Phys. Chem. B.*, 104, 10012-10016.

Dalton, A., Blau, W.J., Chambers, G., Coleman, J.N., Henderson, K., Lefrant, S., McCarthy, B., Stephan, C., Byrne, H.J., (2001), "A functional conjugated polymer to process, purify and selectively interact with single walled carbon nanotubes", *Synth. Metals*, 121, 1217-1218.

Dillon, A., Gennett, T., Jones, K.M., Alleman, J.L., Parilla, P.A., Heben, M.J., (1999), "A simple and complete purification of single-walled carbon nanotube material", *Adv. Mater.*, 11, 1354-1356.

Dresselhaus, M.S., Dresselhaus, G., Eklund, P.C., (1996), *Science of Fullerenes and Carbon Nanotubes*, Academic Press, New York.

Dresselhaus, M.S., Dresselhaus, G., Avouris, Ph., (2001), *Carbon Nanotubes: Synthesis, Structure, Properties and Applications*, Springer-Verlag, Berlin Heidelberg.

Duesberg, G., Blau, W., Byrne, H.J., Muster, J., Burghard, M., Roth, S., (1999), "Chromatography of carbon nanotubes", *Synth. Metals*, 103, 2484-2485.

Duplock, E.J., Scheffler, M., Lindan, P.J.D., (2004), "Hallmark of prefect graphene", *Phys. Rev. Lett.*, 92, 225502-1 – 225502-4.

Ebbesen, T.W., Hiura, H., Fujita, J., Ochiai, Y., Matsui, S., Tanigaki, K., (1993), "Patterns in the bulk growth of carbon nanotubes", *Chem. Phys. Lett.*, 209, 83-90.

Endo, M., Iijima, S., Dresselhaus, M.S., (1998), *Carbon Nanotubes*, Pergamon, Exeter.

Harris, P.J.; (1999), *Carbon Nanotubes and Related Structures,* Cambridge University Press, Cambridge.

Hsu, W.K., Terrones, M., Hare, J.P., Terrones, H., Kroto, H.W., Walton, D.R.M., (1996), "Electrolytic formation of carbon nanostructures", *Chem. Phys. Letts.*, 262, 161-166.

Iijima, S., Ichihashi, T., (1993), "Single shell nanotubes of 1-nm diameter", *Nature*, 363, 603-605.

Iijima, S., (1991), "Helical microtubules of graphitic carbon", *Nature*, 354, 56-58.

Journet, C., Bernier, P., (1998), "Production of carbon nanotubes", *Appl. Phys. A.*, 67, 1-9.

Journet, C., Maser, W.K., Bernier, P., Loiseau, A., Lamy de la Chapelle, M., Lefrant, S., Deniard, P., Lee, R., Fisher, J.E., (1997), "Large-scale production of single-walled carbon nanotubes by the electric-arc technique", *Nature*, 388, 756-758.

Joselevich, E., (2004) "Electronic structure and chemical reactivity of carbon nanotubes: A chemist's view", *ChemPhysChem*, 5, 619-624.

Kasuya, A., Sugano, M., Maeda, T., Saito, Y., Tohji, K., Takaahashi, H., Sasaki, Y., Fukushima, M., Nishina, Y., Horie, C., (1998), "Resonant Raman scattering and the zone-folded electronic structure in single-wall nanotubes", *Phys. Rev. B.*, 57, 4999-5001.

Keogh, S.M., Hedderman, T.G., Greegan, E., Chambers, G., Byrne, H.J., (2004), "Spectroscopic analysis of single-walled carbon nanotubes and semiconjugated polymer composites", *J. Phys. Chem. B.*, 108, 6233 -6241.

Kroto, H.W., Heath, J.R., O'Brien, S.C., Curl, R.F., Smalley, R.E., (1985), "C_{60}: Buckminsterfullerene", *Nature*, 318, 162-163.

Nikolaev, P., Bronikowski, M.J., Bradely, R.K., Rohmund, F., Colbert, D.T., Smith, K.A., Smalley, R.E., (1999), "Gas-phase catalytic growth of single walled carbon nanotubes from carbon monoxide", *Chem. Phys. Lett.*, 313, 91-97.

Niyogi, S., Hu, H., Hamon, A., Bhowmik, P., Zhao, B., Rozenzhak, S.M., Chen, J., Itkis, M.E., Meier, S., Haddon R.C., (2001), "Chromatographic purification of soluble single-walled carbon nanotubes", *J. Am. Chem. Soc.*, 123, 733-734.

Odom, T.W., Huang, J.L., Kim, P., Lieber, C.M., (1998), "Atomic structure and electronic properties of single-walled carbon nanotubes", *Nature*, 391, 62-64.

Ouyang, M., Huang, J.L., Lieber, C.M., (2002), "Fundamental electronic properties and applications of single-walled carbon nanotubes", *Acc. Chem. Res.*, 35, 1018-1025.

Okahara, K., Tanaka, K., Aoki, H., Sato, and T., Yamabe T., (1994), "Band structure of carbon nanotubes with bond alternation", *Chem. Phys. Lett.*, 219, 462-468.

Puretzky, A.A., Geohegan, D.B., Fan, X., Pennycook, S.J., (2000), "Dynamics of single-wall carbon nanotube synthesis by laser vapourisation", *Appl. Phys. A.*, 70, 153-160.

Rao, M.A., Richter, E., Bandow, S., Chase, B., Eklund, P.C., Williams, K.A., Fang, S., Subbaswamy, K.R., Menon, M., Smalley, R.E., Thess, A., Dresselhaus, G., Dresselhaus, M.S., (1997), "Diameter selective Raman scattering from vibrational modes in carbon nanotubes", *Science*, 275, 187-191.

Rinzler, A.G., Liu, J., Dai, H., Nikolaev, P., Huffman, C.B., Rodriguez-Macias, F.J., Boul, P.J., Lu, A.H., Heymann, D., Colbert, D.T., Lee, R.S., Fischer, J.E., Rao, A.M., Eklund, P.C., Smalley, R.E., (1998), "Large scale purification of single-wall carbon nanotubes:process, product, and characterisation", *App. Phy. A.*, 67, 29-37.

Reich, S., Thomsen, C., Maultzsch, J., (2004), *Carbon Nanotubes, Basic Concepts and Physical Properties*, Wiley-VCH Verlag, GmbH and Co. KGaA, Weinheim.

Reich, S., Thomsen, C., Ordejon, P., (2002), "Electronic band structure of isolated and bundled carbon nanotubes", *Phys. Rev. B.*, 65, 155411 – 155422.

Saito, R., Dresselhaus, G., Dresselhaus, M.S., (1998), *Physical Properties of Carbon Nanotubes,* Imperial College Press, London.

Scott, C.D., Arepalli, S., Nikolaev, P., Smalley R.E., (2001), "Growth mechanism for single-wall carbon nanotubes in a laser-ablation process", *Appl. Phys. A.*, 72, 573-580.

Seraphin, S., Zhou, D., Jiao, J., Withers, J.C., Loufty, R., (1993), "Effect of processing conditions on the morphology of carbon nanotubes", *Carbon*, 31, 685-689.

Smalley, R.E., (1992), "Self assembly of fullerenes", *Acc. Chem. Res.*, 25, 98 - 105.

Thess, A., Lee, R., Nikolaev, P., Dai, H., Petit, P., Robert, J., Xu, C., Lee, Y.H., Kim, S.G., Rinzler, A.G., Colbert, D.T., Scuseria, G.E., Tomanek, D., Fisher, J.E., Smalley, R.E., (1996), "Crystalline bundles of metallic carbon nanotubes", *Science*, 273, 483- 487.

Tsang, S.C., Harris, P.J.F., Green, M.L.H., (1993), "Thinning and opening of carbon nanotubes by oxidation using carbon dioxide", *Nature,* 362, 520-522.

White, C.T., Mintmire, J.W., (1998), "Density of states reflects diameter in nanotubes", *Nature*, 394, 29- 2509.

Wildoer, J.W.G., Venema, L.C., Rinzler, A.G., Smalley, R.E., Dekker, C., (1998), "Electronic structure of atomically resolved carbon nanotubes", *Nature*, 391, 59-61.

Yu, Z.,. Brus, L., (2001), "Rayleigh and Raman scattering from individual carbon nanotube bundles", *J. Phys. Chem. B.*, 105, 1123 – 1134.

Yudasaka, M., Kataura, H., Ichihashi, T., Qin, L.C., Kar, S., Iijima S., (2001), "Diameter enlargement of HiPco single-wall carbon nanotubes by heat treatment", *Nanoletters*, 1, 487- 489.

Zhang, M., Yudasaka, M., Koshio, A., Jabs, C., Ichihashi, T., Iijima, S., (2002), "Structure of single-wall carbon nanotubes purified and cut using polymer" *Appl. Phys. A.*, 74, 7-10.

Zheng, B., Li, Y., Liu, J., (2002), "CVD synthesis and purification of single-walled carbon nanotubes on aerogel-supported catalyst", *Appl. Phys. A.*, 74, 345-348.

Zhou, O., Fleming, R.M., Murphy, D.W., Chen, C.H., Haddon, R.C., Ramirez, A.P., Glarum, S.H., (1994), "Defects in carbon nanostructures", *Science*, 263, 1744-1747.

CHAPTER 3 - POLYCYCLIC AROMATIC HYDROCARBONS

3.1 Introduction to Polycyclic Aromatic Hydrocarbons

This chapter gives a brief introduction to the physical and electronic properties of the polycyclic aromatic hydrocarbon (PAH) molecules *p*-terphenyl and anthracene mentioned in Chapter 1. The purpose of this chapter is to give some background information as to the structure and behaviour of both molecules. This knowledge will then be applied in the experimental section to explain and account for results obtained. Both molecules were chosen for this research because of structural characteristics that gave them the potential to selectively interact with SWNTs. In addition, as they are non polar molecules and toluene is a non polar solvent, both molecules exhibit a high level of solubility in the chosen solvent toluene.

An aromatic hydrocarbon is a molecular structure which incorporates one or more planar ring structures consisting of six carbon atoms of alternating single and double covalent bonds. Benzene (depicted in Figure 3.1) is the simplest of the aromatic hydrocarbons. It has a configuration of six carbon atoms and when it is present in larger structures it is often referred to as a phenyl group or an aromatic ring. The structure of benzene consists of an sp^2 hybridised sigma (σ) framework which is responsible for the steric configuration observed (Figure 3.1(b)) and delocalised pi (π) electrons. Sp^2 hybridised carbons typically have a planar geometry and bond angles of 120^o. One large group of aromatic hydrocarbons is the polycyclic aromatic hydrocarbons (PAHs), which consist of two or more aromatic rings made up of only carbon and hydrogen atoms only. When discussing the structure of PAHs it is convenient to divide them into two separate categories, constrained and unconstrained, with the molecules anthracene (Figure 3.2(a)) and *p*-terphenyl (Figure 3.2(b)) discussed as specific examples from each category respectively. Anthracene consists of three side by side fused phenyl rings whereas *p*-terphenyl consists of three phenyl rings each connected through a C-C single bond.

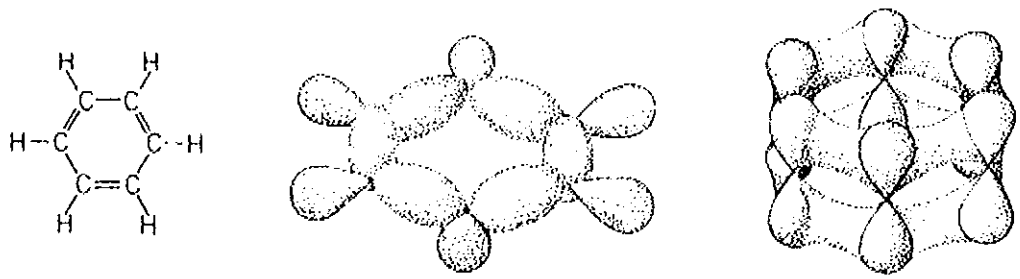

(a) (b) (c)

Figure 3.1 C_6H_6 (benzene): (a) chemical structure formula, (b) spatial distribution of the sp^2 hybridised σ-orbitals which is responsible for the steric configuration, (c) spatial distribution of the π-orbitals forming a delocalized π-system (Haken and Wolf, 1998).

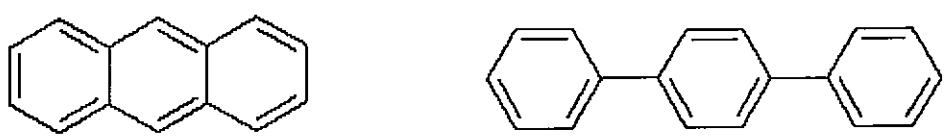

(a) (b)

Figure 3.2 (a) Structure of anthracene and (b) *p*-terphenyl showing the alternating single and double bond structure.

3.2 Physical Properties of Anthracene and *p*-Terphenyl

As depicted in Figure 3.2 (a) anthracene is a planar conjugated structure with a linear fusion of three phenyl rings which has the molecular formula $C_{14}H_{10}$. Valence bond theory considers that anthracene is best regarded as a resonance hybrid of structures and examination of the canonical forms indicates that the three rings cannot all be phenyl in character at the same time (Hepworth *et al.*, 2002). There is only one true phenyl ring in anthracene and in the case of Figure 3.3 the resonance structure shows the phenyl ring is positioned to the far left. The numbering system for anthracene shown in Figure 3.3 is a little unusual and was introduced during early chemical studies to indicate the special character associated with the 9- and 10- positions. The molecule is known to be stable in

the absence of light but when irradiated, anthracene can form a reversible photodimer through the 9-,10- positions as depicted in Figure 3.4.

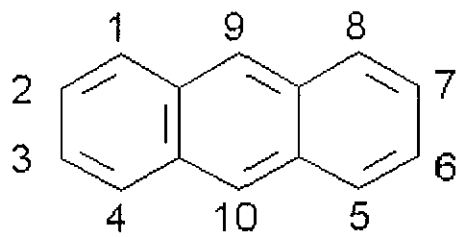

Figure 3.3 Numbering system for anthracene ring system.

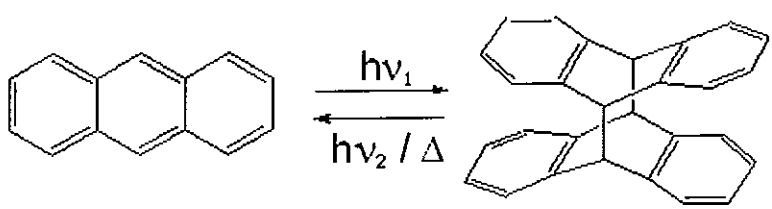

Figure 3.4 Depiction of the reversible photodimer of anthracene formed in the presence of light (http://en.wikipedia.org/wiki/Anthracene).

The structure of *p*-terphenyl (Figure 3.2 (b)) is viewed as three phenyl rings connected to a neighbouring ring by a single carbon bond. It has the molecular formula $C_{18}H_{14}$. Unlike anthracene the phenyl rings are not constrained as they are not fused and the single carbon bonds linking the rings can rotate. Therefore the structure is not planar. The resulting torsion angle of the phenyl rings is a direct result of the effect of their hydrogen atoms. The hydrogen atoms in *p*-terphenyl play a role in the electronic properties although they are not involved in states near the Fermi level (Cote, 2003). Due to the fact that the electronegativity of the hydrogen is less than that of carbon there is a significant charge transfer (~0.3 eV) from the hydrogen atom to the carbon ring and this means that the hydrogen is positively charged and the ring is negatively charged. The hydrogen atoms repel each other as they possess like charges but remain tightly bound to their carbon atom. The steric constraint between the hydrogen atoms can be overcome if the phenyl rings

rotate with respect to each other thus developing a torsion angle between the phenyl rings located on the C-C single bond. Figure 3.2 (b) shows *p*-terphenyl in the planar structure (torsion angle of 0°) but the hydrogen atoms prefer to be at a maximum separation, a torsion angle of 90° that minimizes the electrostatic energy of the system. The C-C single bond of the molecule is not completely free to rotate, however, and tight binding calculations show that the π electrons on each carbon atom across the bond are interacting (Cote, 2003). This implies that the torsion angle is not as severe as 90° (Cote, 2003). It is also worth bearing in mind that the torsion angle affects the electronic structure. With a greater degree of π interaction, i.e. as the torsion angle approaches 0°, the valence and conduction bands broaden and the band gap is reduced resulting in a red shift of the absorption spectrum (Heimel *et al.*, 2003a; Puschnig *et al.*, 2001; Puschnig, *et al.*, 2003). Calculations by Cote reveal the torsion angle is ~25° and this value is in good agreement with experimental values obtained by Ambrosch-Draxl *et al.*, (1995) (Cote, 2003, Heimel *et al.*, 2001). Figure 3.5 shows the relative energy of *p*-terphenyl with respect to the torsion angle as calculated by Cote and it is evident that the torsion angle with the lowest energy difference is ~25°.

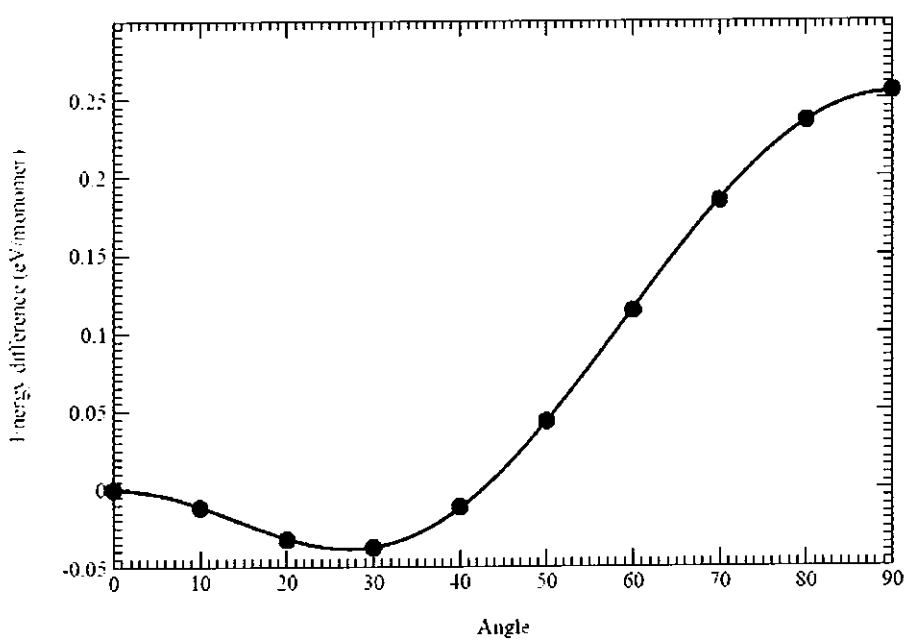

Figure 3.5 Relative energy of *p*-terphenyl as a function of the torsion angle (Cote, 2003).

3.3 The Electronic Structure of Anthracene and *p*-Terphenyl

The electronic structure of PAHs such as anthracene and *p*-terphenyl are based on the presence of delocalised π electrons. In both anthracene and *p*-terphenyl, each carbon atom provides four valence electrons, three of which form bonds termed σ bonds by end on overlap of orbitals with neighbouring carbon or hydrogen atoms, thus defining the geometry of the respective molecules (see Figure 3.1 (b)). The remaining valence electrons on each of the carbon atoms occupy p_z orbitals, which are aligned perpendicular to the plane of the σ bonds. The p_z electrons from two neighbouring carbons form an additional bond by lateral overlap of their orbitals (see Figure 3.1 (c)), known as a π bond, so that the molecules consists of several alternating single and double bonds termed conjugated double bonds. In this conjugated π system, π electrons can no longer be attributed to one specific C-C bond. Instead, their wavefunction is delocalised over the entire conjugated ring system (Haken and Wolf, 1998). These delocalised π electrons are relatively weakly bound and are responsible for the electron transport properties of anthracene and *p*-terphenyl. The extent of the conjugation length together with the bond alternation determines the highest occupied molecular orbital (HOMO) and the lowest unoccupied molecular orbital (LUMO) band-gap and the gap decreases as the aromatic hydrocarbon chain length increases. Experimentally, the band-gap follows the 1/n law (n denotes the number of phenyl rings per molecule) where the position of the first absorption peak shows a linear dependence as a function of the inverse of the PAHs length (Cote, 2003; Puschnig, 1999). The band-gaps for anthracene and p-terphenyl are 3.9 eV and 4.3 eV respectively. The following paragraph gives the first principle approach that describes the intrinsic electronic properties of PAHs.

Density functional theory (DFT) is an *ab initio* method since it does not rely on any experimental parameters and the calculations for crystalline PAHs have been proven to be in accordance with experimental data (Cote, 2003; Puschnig, 1999; Tobik *et al.*, 2004). However even the most sophisticated approximations of DFT when applied to molecular crystals show intrinsic limitations in that the band-gap is severely underestimated but results obtained can be used to predict trends within a single family of compounds. In PAHs there are two distinct bonds: strong covalent bonds within a single molecule and weak molecule – molecule bonds responsible for the cohesion of the molecular solid.

Within DFT, the van der Waals forces which are an important part of the molecule-molecule interaction cannot be accounted for. However, once the crystal geometry is chosen the DFT description is reasonable for molecular crystals.

The energy dispersion bands are shown in Figure 3.6 for anthracene between -2.0 and 3.5 eV. In the energy window the HOMO-1, HOMO and LUMO derived bands which represent the π orbitals are visible in Figure 3.6. The band structure of the molecular crystal shows a small dispersion which reflects the weak chemical interactions of the molecules with each other. The bandwidths of the HOMO and LUMO derived bands for anthracene are 0.3 and 0.4 eV respectively with the splitting of the bands being a measure of the intermolecular interaction. The band-gap for anthracene is calculated to be 2.1 eV but it is known that DFT underestimates the band-gap and experimentally it was measured to be 3.9 eV. In a pure π electron picture the unoccupied π conduction bands would mirror the occupied π valence bands. In Figure 3.6 this is not the case due to intermolecular interaction. As a result of the interaction the valence bands no longer have pure π character and the mirror relation is destroyed. A detailed description of DFT is given by Puschnig (1999).

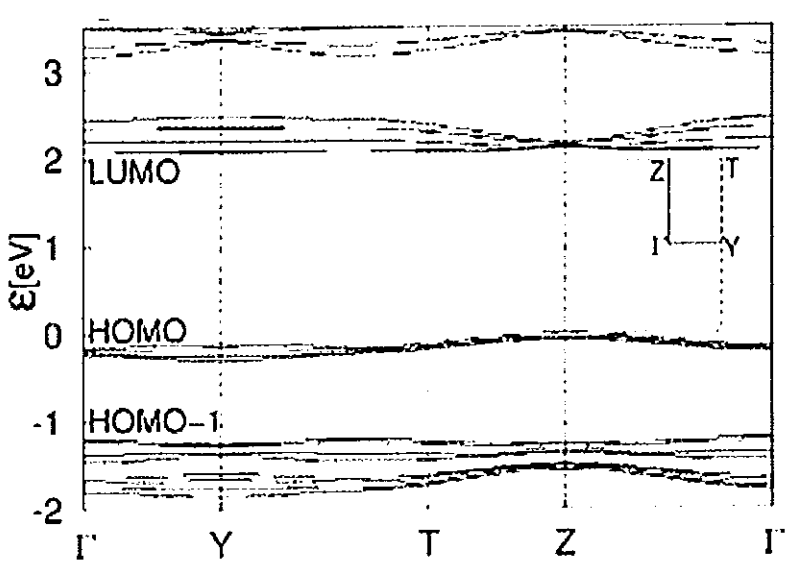

Figure 3.6 Electronic structure of anthracene as calculated by density functional theory (Tobik *et al.*, 2004).

p-Terphenyl shows similar energy dispersion bands to anthracene. Again, the HOMO-1, HOMO and LUMO lie between -2.0 and 3.5 eV. The bandwidth splitting of the HOMO derived bands is 0.45 eV due to intermolecular interactions. A band-gap of 2.71 eV was calculated by DFT but experimentally the value was found to be 4.3 eV for the same reasons discussed for anthracene.

3.4 The Crystal Structure of Anthracene and *p*-Terphenyl

The following section examines the behaviour of both molecules within a crystal. In particular, the stacking arrangement and interaction between the individual molecules are of interest. Both anthracene and *p*-terphenyl form monoclinic crystals (Hiemel *et al.*, 2003a; Hiemel *et al.*, 2003b; Oehzelt *et al.*, 2002), and this structure is recognisable by the 'herringbone' arrangement which is depicted in Figure 3.7. In a crystal, the molecules form layers which are aligned parallel to the *ab* plane as depicted in Figure 3.8 and 3.9 with the long molecular axes almost perpendicular to the plane. The distinctive 'herringbone' pattern is determined by the unit cell axis a and b and the herringbone angle θ which is the angle between the planes of translationally inequivalent molecules. The arrangement of two layers of molecules as shown in Figure 3.8 has the long molecular axes within the *ac* plane (Hegmann, 2003; Oehzelt *et al.*, 2001), and the molecules are tilted with respect to this plane by the setting angle χ with δ representing the angle between the long molecular axes of two inequivalent molecules. The setting angle, χ, not only represents the topology of the surfaces but also describes the 'linear slip' between two adjacent molecules within a layer as hydrocarbons, like graphite, tend not to stack directly in a coplanar fashion but in a commensurate fashion (Heimel *et al.*, 2003a).

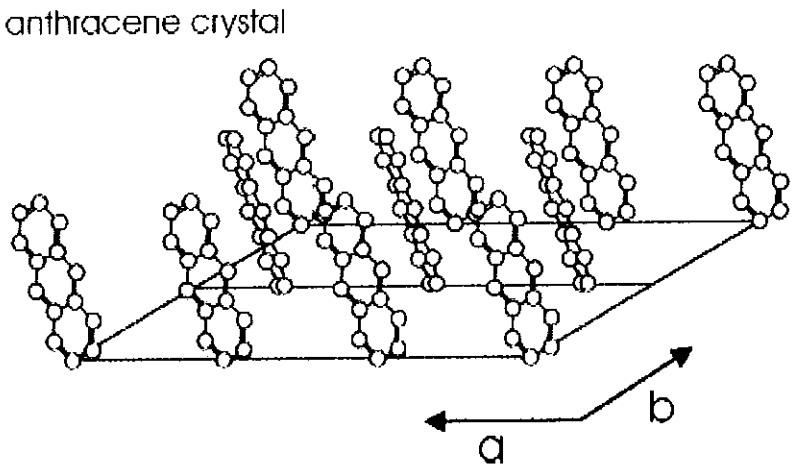

Figure 3.7 "Herringbone" stacking arrangement of anthracene in the *ab* plane of crystralline anthracene which is a typical polyacene molecular structure (Hegmann, 2003).

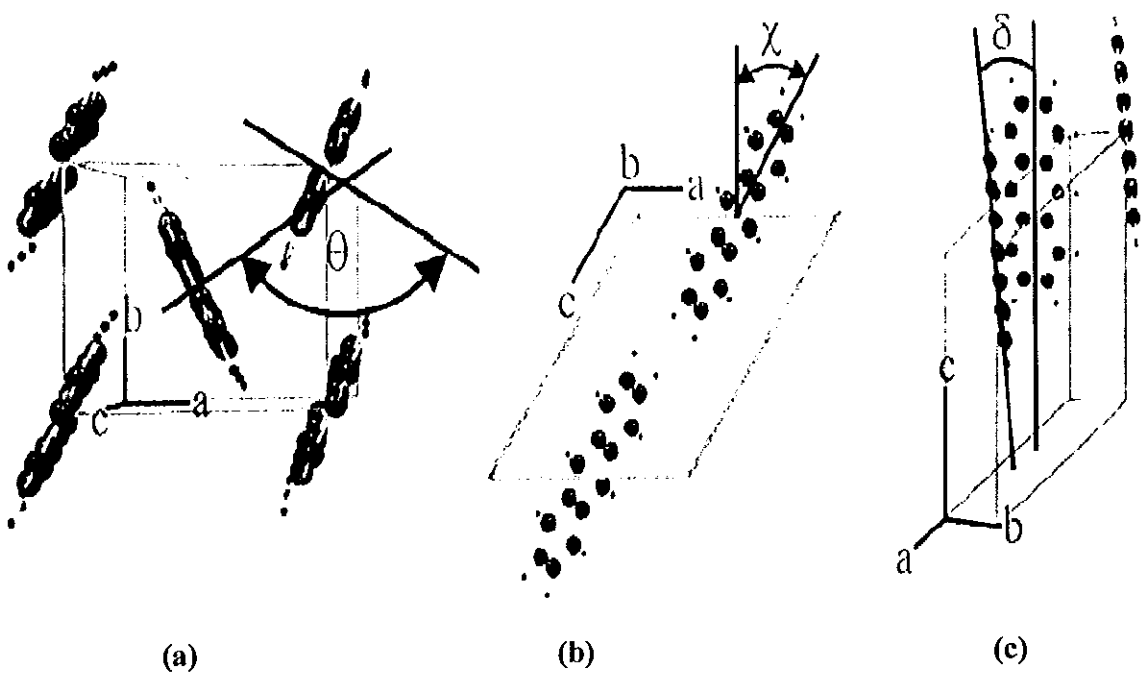

(a) **(b)** **(c)**

Figure 3.8 Different views of the anthracene unit cell to describe the definition of the three characteristic angles: (a) depicting the herringbone angle θ, (b) the tilting angle χ and (c) the angle between two inequivalent molecules δ (Oehzelt, 2001).

The interactions that take place between anthracene or *p*-terphenyl molecules within the crystal are two fold as mentioned in section 3.3. There are the strong covalent intra-molecular bonds and weak inter-molecular van der Waals forces acting between separate molecules. The weak nature of the bonds between molecules in the crystal results in the retention of the properties of the individual molecule. An isolated anthracene molecule, as discussed in section 3.2, is a planar molecule and no structural deviations are observed within the crystal (Figure 3.7). However, *p*-terphenyl in its isolated state is not planar and has a torsion angle of ~25° about the C-C bond. In the crystal structure, the inter-chain interactions (packing forces) result in a more planar arrangement of the molecules. X-ray and neutron diffraction experiments at room temperature reveal a planar configuration of *p*-terphenyl within the monoclinic crystal. As will be discussed in Chapter 4, the transition of *p*-terphenyl in its isolated state to a crystal structure is easily detected *via* spectroscopic methods. The planarisation of the three phenyl groups increases the π conjugation across the molecule and this is expressed by an increase in the fluorescence emission maximum from 345 nm in the isolated state to 365 nm in the crystal state. Figure 3.9 shows a side view of a *p*-terphenyl unit cell.

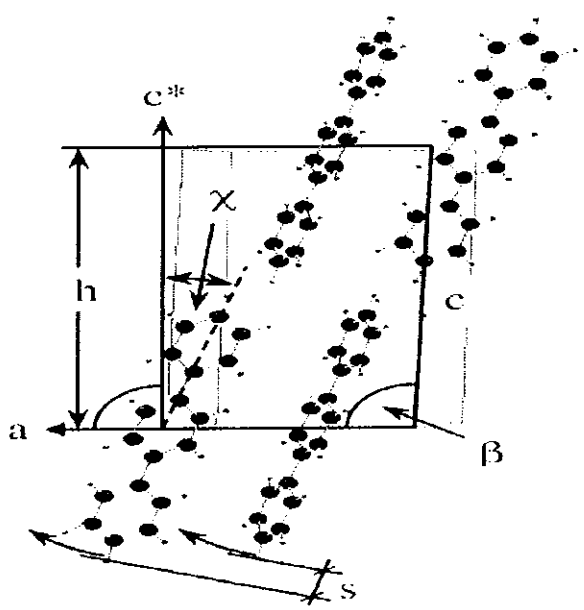

Figure 3.9 Side view of the unit cell of *p*-terphenyl. The unit cell depicts the tilting angle χ with respect to *c** (perpendicular to the *ab* plane) and the linear slip s between two adjacent molecules along the *a* direction. It also indicates that the unit cell height h to the lattice parameter *c* and β is the angle between two inequivalent molecules (Heimel *et al.*, 2003b).

Summary

Anthracene and *p*-terphenyl represent constrained and unconstrained PAHs. Anthracene has a naturally occurring planar structure however *p*-terphenyl does not. The phenyl rings of *p*-terphenyl have been shown to have a torsion angle of 25° relative to each other about the C-C single bonds linking them. The electronic structure of anthracene and *p*-terphenyl was discussed with relation to experimental data and the DFT model. Experimental data reveals that the π electrons are responsible for the electronic behaviour of the molecules and the DFT model puts the π orbitals in the HOMO-1, HOMO and LUMO energy states. The DFT model also accounts for the interaction between the molecules and the energy gap between the HOMO and LUMO can be calculated. One of the draw backs of the DFT model is that it severely underestimates the energy gap however it can predict trends within a single family of compounds. In a molecular crystal, both PAH molecules were found to stack in the herringbone arrangement showing strong covalent intra-molecular and weak inter-molecular interactions. It was also shown that as a result of packing forces *p*-terphenyl altered its conformation from a non-planar arrangement to a planar arrangement. Such a change in conformation may be detected spectroscopically as the more planar conformation increases the effective conjugation of the molecule. Knowledge of the interaction that occurs between individual PAHs is important as it potentially competes with the interaction of the PAHs with SWNTs. It is proposed however that the PAHs will stack *via* a face-face interaction as depicted in Figure 1.4. If this is the case, significant spectroscopic changes are expected for p-terphenyl on interaction because a face-face interaction requires a torsion angle of 0° but in its isolated state the torsion angle is 25°. Such spectroscopic changes are not expected for anthracene as its isolated conformation is ideal for face-face interaction.

This chapter provided a description of the physical and electronic properties of both anthracene and *p*-terphenyl. The next chapter looks at a number of spectroscopic and microscopic techniques which were used in this research to characterise both the SWNTs and PAH materials.

REFERENCES

Ambrosch-Draxl, C., Majewski, J.A., Vogl, P., Liesing, G., (1995), "First-principles studies of the structural and optical properties of crystalline poly(*para*-phenylene)" *Phys. Rev. B.*, 9668-9676.

Cote, M., (2003), "Electronic properties of polymers", *Physics in Canada*, 59, 1-15.

Haken, H., and Wolf, H.C.,(1998), *Molecular Physics and Quantum Chemistry*, Springer, Berlin.

Hegman, F, (2003), "Ultrafast carrier dynamics in conjugated polymers and organic molecular crystals", *Physics in Canada*, 59, 127-138.

Hepworth, J.D., Waring, D.R., Waring, M., (2002), *Aromatic Chemistry*, Published by the Royal Society of Chemistry, Cambridge.

(a) Heimel, G., Puschnig, P., Oehzelt, M., Hummer, K., Koppelhuber-Bitschnau, B., Porsch, F., Ambrosch-Draxl, C., Resel, R., (2003), "Chain-length-dependent intermolecular packing in polyphenylenes: a high pressure study", *J. Phys. Cond. Mat.*, 15, 3375-3389.

(b) Heimel, G., Puschnig, P., Oehzelt, M., Hummer, K., Koppelhuber-Bitschnau, B., Porsch, F., Ambrosch-Draxl, C., Resel, R., (2003), "High pressure studies on the packing forces and intermolecular interaction in polymers", *Mat. Res. Symp. Proc.*, 771, L7.22.1 – L7.22.6

Heimel, G., Puschnig, P., Cai, Q., Martin, C., Zojer, E., Graupner, W., Chandrasekhar, M., Chandrasekhar, H.R., Ambrosch-Draxl, C., Leising, G., (2001), "High pressure Raman studies on the structural conformation of oligophenyls", *Synth. Metals*, 116, 163-166.

Johnston, M.B., Herz, L.M., Kahn, A.L.T., Kohler, A., Davies, A.G., Linfield, E.H., (2003), "Low-energy vibrational modes in phenylene oligomers by THz time domain spectroscopy", *Chem. Phys. Lett.*, 377, 259-262.

Oehzelt, M., Weinmeier, K., Heimel, G., Puschnig, P., Resel, R., Ambrosch-Draxl, C., Porsch, F., Nakayama, A., (2002), "Structural properties of anthracene", *High Pressure Research*, 22, 343-347.

Puschnig, P., (1999), First-Principles Investigation of Poly(*para*-phenylene) and its Oligomers: Electronic, Optical and Structural, Masters Thesis http://physik.uni-graz.at/~pep/research4.html.

Puschnig, P., Ambrosch-Draxl, C., Heimel, G., Zojer, E., Resel, R., Liesing, G., Kriechbaum, M., Graupner, W., (2001), "Pressure studies on the intermolecular interactions in biphenyl", *Synth. Metals*, 116, 327-331.

Puschnig, P., Hummer, K., Ambrosch-Draxl, C., (2003), "Electronic, optical and structural properties of oligo-phenylene molecular crystals under high pressure: *ab initio* investigation", *Phys. Rev. B.*, 67, 235321-1 – 235321-6.

Tobik, J., Corso, A.D., Scandolo, S., Tosatti, E., (2004), "Organic molecular crystals in electric fields" *Surface Science*, 566-568, 644-649.

http://en.wikipedia.org/wiki/Anthracene, acessed 22 March 2006.

CHAPTER 4 - CHARACTERISATION OF MATERIAL PROPERTIES

4.1 Spectroscopic and Microscopic Techniques

Characterisation of the materials used in this research involved using well-established techniques to probe the electronic properties and the materials morphology. Two approaches were taken: the first was to use spectroscopic techniques to gather information on the electronic, molecular and physical structure of the material by measuring parameters such as absorption, emission, and chemical bond vibrations; the second was to use microscopic techniques to directly image the material structure on the micrometer and nanometer scale.

Both electronic and vibration spectroscopic techniques were employed. Electronic spectroscopy is defined in this thesis as methods that probe the electronic transitions of the material as a result of the interactions with photons whereas vibrational spectroscopy is defined as methods which give information concerning molecular vibrations.

4.2 Electronic Spectroscopy

The two principle electronic spectroscopic techniques used in this research are the complementary techniques of absorption and fluorescence spectroscopy. These two techniques examine the electronic transitions within a molecule, and hence provide information about the electronic structure of a material and its local environment.

In an organic system, the ground and excited states have many vibrational and rotational degrees of freedom. When Born-Oppenheimer separability conditions are assumed valid (Wayne, 1970), the total wave function of the molecule may be written as the product of the separated wavefunctions and the total energy E_t can be written as:

$$E_t = E_e + E_v + E_r \qquad \text{Equation 4.1}$$

where e,v and r in Equation 4.1 are the electronic, vibrational and rotational components respectively.

The absorption and emission of an organic molecule is depicted in the Jablonski diagram in Figure 4.1. The act of absorption involves the interaction of electromagnetic radiation with the components of a molecule. The initial absorption step takes the molecule to an excited electronic state. Since electronic transitions take place on a much faster time scale than nuclear motion, most electronic transitions are completed before the nuclei can alter their spatial relationships. Such a transition is denoted as a Franck-Condon transition and is indicated in Figure 4.1 by the solid vertical lines. The Franck-Condon principle states that an electronic transition occurs so rapidly in comparison with vibration frequencies that no change occurs in inter-nuclear separation during the course of the transition. After excitation of the molecule to an upper vibronic state, the nuclear coordinates are not in their equilibrium configuration for the new electronic state and hence non-radiative relaxation between the vibrational states occurs. Generally, after relaxing to the lowest vibrational state, the electron can return to the ground state by emitting the excess energy as a photon or by other radiationless channels of decay. The emitted photon is characteristically of longer wavelength than that of the exciting light. The wavy lines in Figure 4.1 represent radiationless energy conversion. The vertical wavy lines within a particular electronic state indicate degradation of vibrational excitation, while the horizontal wavy lines indicate changes of state. The term "internal conversion" is applied to radiationless transitions between states of the same spin multiplicity, while "intersystem crossing" refers to transitions between states belonging to different spin systems.

Deactivation through emission of radiation can happen in one of two ways. These two processes were originally distinguished in terms of whether or not there was an observable afterglow. In 1935, Jablonski interpreted phosphorescence as being emission from some long lived metastable electronic state lying lower in energy than the state populated by the absorption of radiation (Wayne, 1970). This was in fact a triplet state of a species. The long lifetime of the emission is a direct consequence of the forbidden nature of a transition from an excited triplet to the ground state singlet. Hence, phosphorescence can be described as a

radiative transition between states of different multiplicity. Fluorescence is then understood to be a radiative transition between states of the same multiplicity (Wayne, 1970).

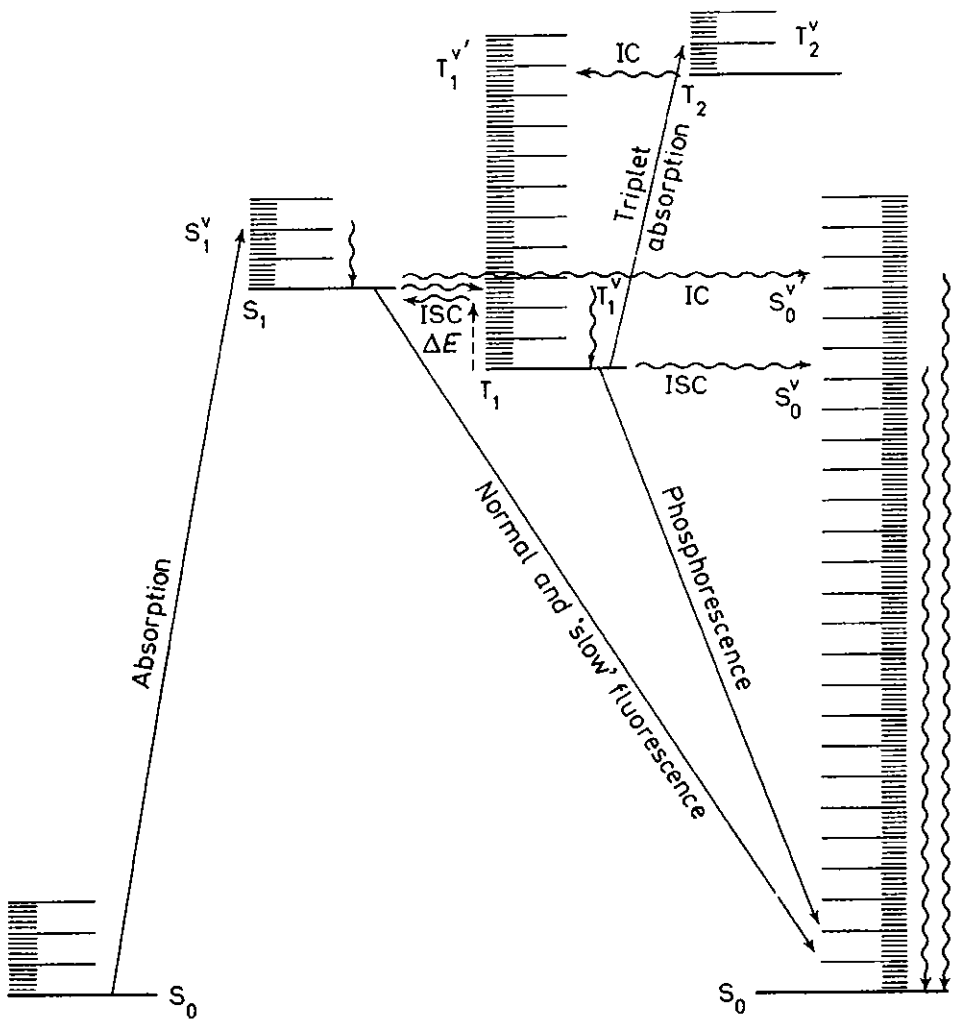

Figure 4.1 Jablonski diagram showing the sequence of steps leading to radiative decay. After initial absorption the upper excited vibrational states undergo non radiative decay by giving up energy to the surroundings. A radiative transition then occurs from the lowest vibrational level of the excited electronic state (Wayne, 1970). S_0 is the singlet ground electronic state and S_1 is the singlet excited electronic state; with T_1 representing the triplet state. ISC and IC represent intersystem crossing of an electron from the S_1 to T_1 excited states or vice versa and internal conversion where the electron orients itself so that it may return from T_1 to S_0 respectively.

4.2.1 Absorption Spectroscopy of Materials

The three materials used in this research are anthracene, *p*-terphenyl and SWNTs. Their structure consists of a conjugated system of atoms covalently bonded with alternating single and double bonds. Such a system results in a general delocalisation of the π electrons as described in Chapters 2 and 3. UV-Vis-NIR spectroscopy is based on exciting the electronic levels in these conjugated molecules and the wavelength at which the conjugated systems absorb is determined by the conjugated length. The absorption spectra of the materials are presented and discussed in the following section.

The spectrometer used to probe the materials in this research was the Perkin Elmer Lambda 900 UV-Vis-NIR spectrometer. The spectrometer is a double-beam, double monochromator ratio recording system with pre-aligned tungsten-halogen and deuterium lamps as sources. The wavelength range is from 175 to 3,300 nm with an accuracy of 0.08 nm in the UV-Vis region and 0.3 nm in the NIR region. It has a photometric range of ± 6 in absorbance. For all of the experimental studies, the absorption was measured at all times with a reference sample in a double beam arrangement; for example a solution of anthracene in toluene would have a reference sample of just toluene. The purpose of this was to eliminate variations caused by the difference in lamp intensities at different frequencies.

Sample Preparation

Solutions containing concentrations of 1×10^{-9} M of *p*-terphenyl in toluene and 3×10^{-3} M of anthracene in toluene were prepared for UV-Vis-NIR analysis as these were determined to be the optimum concentrations for this study. It was necessary to use a very dilute concentration of *p*-terphenyl compared with anthracene as saturation at higher concentrations was an issue. In the case of SWNTs a mass of 5.6 mg was added to 10 ml of toluene as it had been established by trial and error to be the optimum mass of SWNTs to work with. The SWNT solution was then spin-coated onto a spectrosil B disc in order to obtain a thin uniform film as solution samples resulted in a background with a large degree of scattering.

Results and Discussion

Figures 4.2 and 4.3 depict the absorbance spectra of anthracene and *p*-terphenyl respectively, the spectral profiles being similar to those reported in the literature (Berlman, 1971; Wayne, 1970). The absorbance spectrum of anthracene in Figure 4.2 shows the electronic and vibrational structure of the molecule. The electronic absorption corresponds to an electronic transition involving the lowest excited electronic state, S_1. The individual absorption bands at ~330 nm, ~345 nm, ~360 nm and ~380 nm correspond to the excitation of a series of vibrational states within this electronic transition. The absorption of anthracene between 330 and 380 nm indicates that a minimum energy of 3.9 eV is required to excite an electron from the ground electronic state to the excited electronic state. The vibrational energy spacing is approximately 1400 cm^{-1} coresponding to an aromatic ring stretching mode which is influenced by the promotion of a π electron from the bonding orbitals to the anti-bonding orbitals (Mullins and Sheu, 1999). The vibrational levels of the ground electronic state will overlap with several of the vibrational levels in the excited electronic state and they are identified in Figure 4.2 as (0,0), (1,0), (2,0), (3,0). By convention, the first figure in the parentheses represents the vibrational levels of the excited electronic state and the second figure in the parentheses represents the vibrational levels of the ground electronic state.

The absorbance spectrum of *p*-terphenyl in Figure 4.3 is broad and featureless with the absorbance maximum at approximately ~300 nm indicating that a minimum energy of 4.3 eV is required to excite an electron from the ground electronic state to the excited electronic state (Malkin, 1992; Wayne, 1970). The absence of a vibrational structure in the absorbance spectrum is due to rotation of the phenyl groups about the C-C single bond. The molecule *p*-terphenyl was found to absorb at a lower wavelength than anthracene because the degree of effective conjugation of *p*-terphenyl was less, again due to the rotation of the rings about the connecting C-C single bonds (Chapter 3).

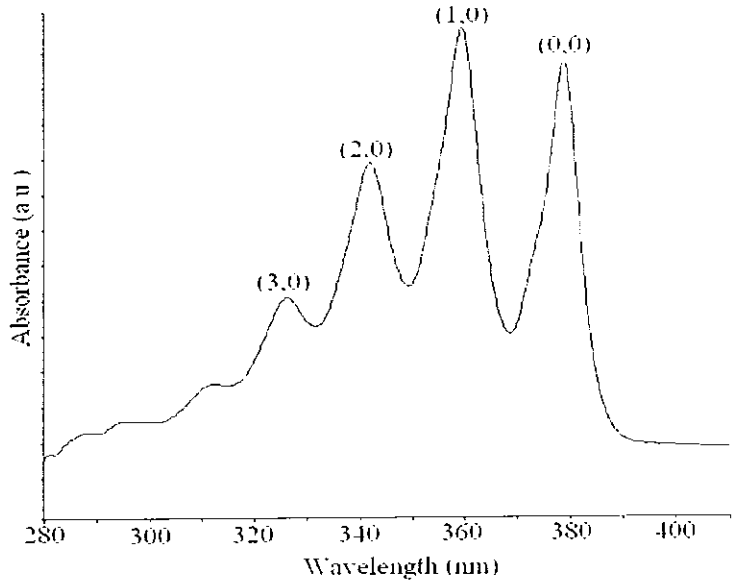

Figure 4.2 UV-Vis absorbance spectrum of anthracene in toluene at a concentration of 3 x 10^{-3} M at room temperature. The figures within the parentheses represent the vibrational levels of the molecule with the figure on the left in the parentheses representing the vibrational levels in the excited electronic state and the figure to the right representing the vibrational levels in the ground electronic state.

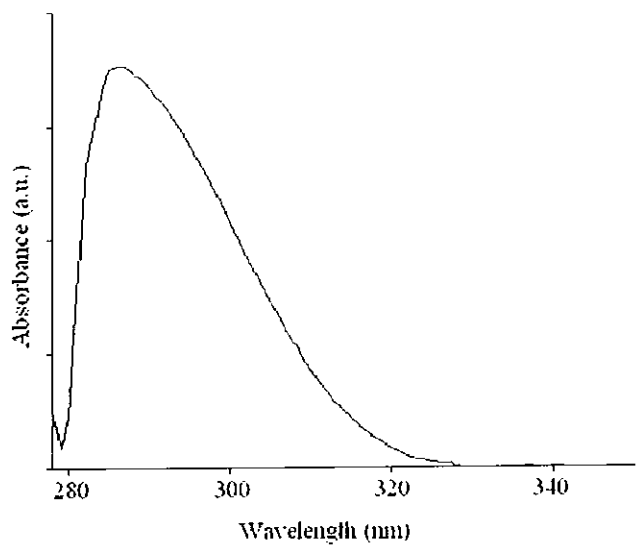

Figure 4.3 UV-Vis absorbance spectrum of *p*-terphenyl in toluene at a concentration of 1 x 10^{-9} M at room temperature. The absorbance is featureless because of the rotation of phenyl rings about the C-C bond. The resulting variety of structures within the sample leads to an unresolved vibrational spectrum.

The absorbance spectra of three different samples of SWNTs precipitated from solutions of 5.6 mg of substance in 10 ml of toluene were investigated. The sample weight of 5.6 mg was chosen as it was found to give the optimum concentration to work with in 10 ml of toluene. The three SWNT samples probed were produced by high pressure carbon monoxide disproportionation (HiPco) (H–SWNT), laser vapourisation (LV–SWNT) and arc–discharge (AD–SWNT) (see Chapter 2). Each of the samples was sonicated for 15 s using a sonic tip (ultrasonic processor VCX, 750 Watts) and the samples were then spin coated onto spectrosil B discs to obtain a uniform distribution before characterisation. Figure 4.4 shows the absorbance spectra of LV–SWNT, AD–SWNT and H–SWNT. The features observed have origin in the singularities in the density of states (DOS) as discussed in Chapter 2. It is immediately obvious that the absorption spectra of the three SWNT samples differ. Therefore it may be concluded that the UV-Vis-NIR spectral profiles of SWNTs are to a degree dependent on the production process. Literature reports predict that the absorbance profile may also differ from batch to batch for SWNTs produced by the same process (Ausman *et al.*, 2000; Cai *et al.*, 2002; Chiang *et al.*, 2001; Hagen and Hertel, 2003). Therefore the only information that can be taken from the UV-Vis-NIR spectra is the range of diameters of SWNTs present in that sample and the ratio of metallic to semiconducting SWNTs.

Theoretical predictions suggest that the absorbance bands of SWNTs can be ascribed to the inter-band transitions between the mirror image spikes in the DOS of SWNTs (Chapter 2). From electronic band theory, absorbances between 1400 – 1900 nm are assigned to the first inter-band transition v1 → c1 in semiconducting SWNTs , whereas the bands between 800 – 1100 nm are assigned to the second inter-band transitions v2 → c2 again in semiconducting SWNTs (Yu and Brus, 2001). The predicted absorbance at 650 nm is believed to be the v1 → c1 of metallic SWNTs and weak bands at 550 nm and 300 nm are due to v3 → c3 in semiconducting SWNTs and v2 → c2 in metallic tubes respectively (Ryabenko *et al.*, 2004). The absorbance at 270 nm is the π plasmon frequency of carbon material such as C_{60}, SWNTs, and graphite. The precise position of the SWNT absorption bands has been shown to be roughly described by the following equations;

$E^{S}_{11} = 2k/d$ Equation 4.2

$E^{S}_{22} = 4k/d$ Equation 4.3

$E^{M}_{11} = 6k/d$ Equation 4.4

where k is a constant, d is the diameter, E is the energy transition and the superscripts S and M represent semiconducting and metallic SWNTs respectively whereas the subscripts 11 and 22 represent the first and second electronic transition between mirror spikes in the DOS (Hamon *et al.*, 2001). However it has since been shown experimentally that the relationship between E^{S} and d is more complex than originally thought as described by more current calculations by Bachilo *et al.*(2002) (Bachilo *et al.*, 2002; Ryabenko *et al.*, 2004). The width of the van Hove bands are determined by the overlapping transitions from all different diameters and chiral indices.

Comparing the spectra in Figure 4.4, it is evident that both AD–SWNT and LV–SWNT have a strong absorbance centred at ~1700 nm and ~950 nm which correspond to the first and second inter-band transitions for semiconducting SWNTs. H–SWNT has absorbances centred at ~1400 and ~800 nm which also fall under the first and second inter-band transitions for semiconducting SWNTs. The fact that H–SWNT are centred at ~1400 nm compared to ~1700 nm indicates a different diameter distribution for the H–SWNT sample compared with AD–SWNT and LV–SWNT samples in that range. AD–SWNT and H–SWNT have a strong absorbance at ~650 nm compared to LV–SWNT and absorbance in this region corresponds to the first inter-band transition for metallic SWNTs. This would indicate the presence of more metallic SWNTs in the H–SWNT and AD–SWNT samples compared to the LV–SWNT sample. Absorbance at ~550 nm corresponds to the third inter-band transition for semiconducting SWNTs and it is evident in the AD–SWNT and H-SWNT samples and negligible for LV–SWNT. Finally, the π plasmon band at ~270 nm is present for all three SWNT samples. It is of interest to note that the H–SWNT spectrum exhibits more structure in this region than that of either of the other two samples and this is believed to be due to a smaller average tube diameter of about 1.0 nm resulting in a higher

degree of structural information (Chiang *et al.*, 2001; Hagen and Hertel, 2003; Kataura *et al.*, 1999).

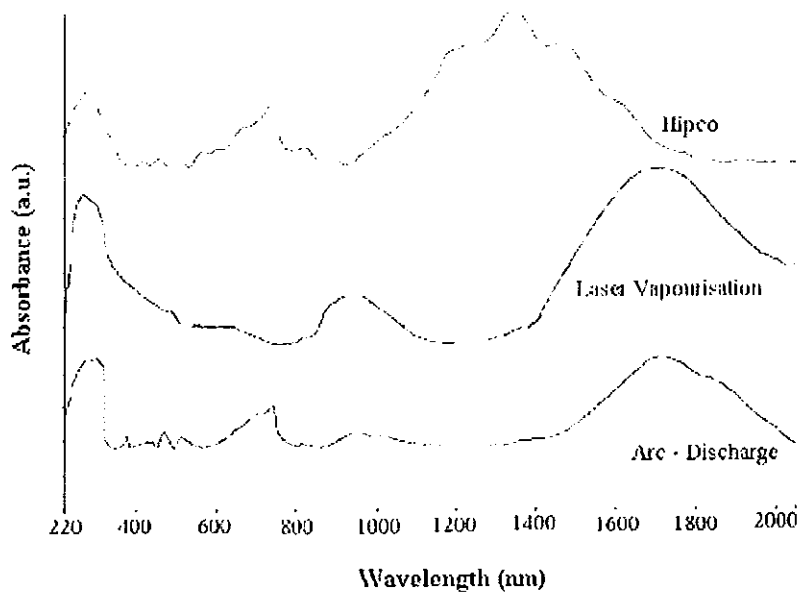

Figure 4.4 UV-Vis-NIR absorbance spectra of arc-discharge, laser vapourisation and HiPco SWNT.

4.2.2 Fluorescence Spectroscopy

A molecule that has absorbed a photon can discard its excess energy *via* radiative decay, in which an electron relaxes back into the lower energy levels of the ground electronic state and in the process generates a photon and yields information with regards to the electronic and vibrational levels of the ground electronic state. The three materials used in this research undergo fluorescent radiative decay. However, only anthracene and *p*-terphenyl are discussed as the fluorescence of the SWNTs was beyond the range of the fluorimeter used (O'Connell *et al.*, 2002).

The Perkin Elmer LS55 luminescence spectrometer used throughout this research was computer controlled. Excitation is provided by a pulsed Xenon discharge lamp with a pulse width at half peak height of < 10 μs and pulse power 20 kW. The source is monochromated using a Monk-Gillieson type monochromator and can be scanned over the range of 200-800

nm. The luminescence is passed through a similar monochromator, which can be scanned over the range of 200-900 nm.

Sample Preparation

The solutions prepared for fluorescence spectroscopy were of concentrations in toluene of 1 x 10^{-4} M for *p*-terphenyl and 3 x 10^{-3} M for anthracene.

Results and Discussion

Figure 4.5 depicts the emission spectral profile of anthracene and it is evident that it is a mirror image of the absorbance spectrum. It is often found that the emission spectrum is a mirror image of the absorption spectrum for a S_0-S_1 transition but is shifted to a higher wavelength (Wayne, 1970). The similarity occurs because the same electronic transitions are involved in both absorption and emission spectroscopy and because of similarities of the vibrational energy levels of S_0 and S_1. In many molecules the vibrational energy levels are not significantly altered by the different electronic distributions of S_0 and S_1. The vibrational levels are identified in Figure 4.5 as (0,0), (0,1), (0,2), (0,3). The (0,0) band is of slightly longer wavelength in the emission spectrum than the absorption spectrum and this is due to the Stokes shift. The emission spectrum of anthracene is independent of which vibrational band is excited as emission will occur only from the lowest vibrational energy level in the excited electronic state (Mullins and Sheu, 1999).

In Figure 4.6 it can be seen that the emission spectral profile of *p*-terphenyl was found not to mirror the absorption spectrum. While the absorption spectrum is devoid of vibrational structure the emission spectrum shows a degree of structure. This deviation from the mirror image rule usually indicates a different geometric arrangement of the nuclei in the excited state and ground state. For *p*-terphenyl, the individual phenyl rings that make up the structure become more co-planar in the excited state and as a result the emission spectrum becomes more structured than the absorption spectrum (Ajayaghosh, 2004). The vibrational levels of *p*-terphenyl are identified in Figure 4.6.

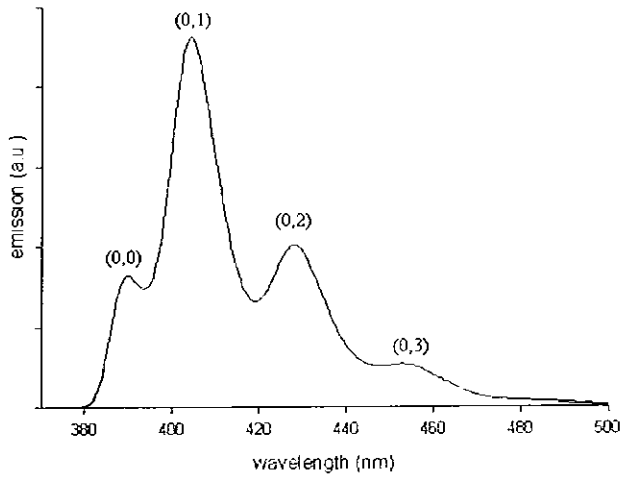

Figure 4.5 Fluorescence of anthracene at a concentration in toluene of ~3 x 10^{-3} M with an excitation wavelength of 350 nm. The figures within the parentheses represent the vibrational levels with the figure on the left in the parentheses representing the vibrational levels of the excited electronic state and the figure to the right representing the vibrational levels of the ground electronic state.

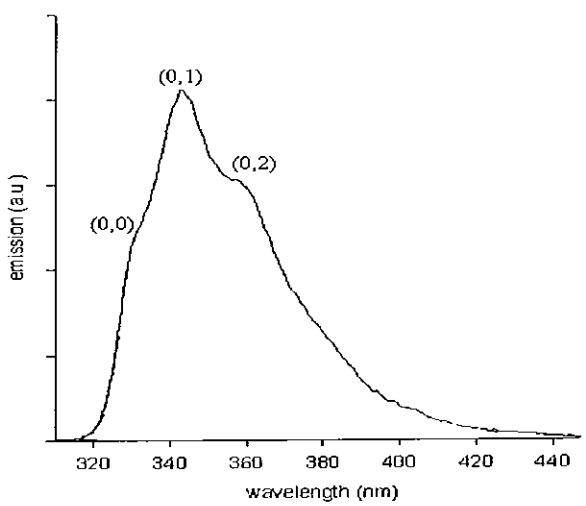

Figure 4.6 Fluorescence of *p*-terphenyl at a concentration in toluene of ~1 x 10^{-4} M with an excitation wavelength of 300 nm. The figures within the parentheses represent the vibrational levels with the figure on the left in the parentheses representing the vibrational levels of the excited electronic state and the figure to the right representing the vibrational levels of the ground electronic state.

4.3 Vibrational Spectroscopy

Vibrations can be excited by the absorption of electromagnetic radiation at an appropriate frequency and analysis of the frequencies where absorption is observed yields information about the identity of the molecule and the flexibility of its bonds. Molecules absorb radiation of frequencies which exactly match the frequencies of vibrations within the molecule. The frequencies at which the molecules vibrate depend on the forces between the atoms, the mass of the atoms and the geometry of the molecule. The stronger the forces between the atoms in the molecule, the higher the vibrational frequency while heavier atoms display lower vibrational frequencies. Traditionally, there are two techniques used to obtain a vibrational spectrum; infrared absorption (IR) and Raman spectroscopy (Atkins, 2001).

The energies associated with the vibrations in a molecule with respect to one another are quantised and absorption of electromagnetic radiation in the infrared region gives rise to transitions between these different vibrational states. Absorption results from the coupling of a vibration with the oscillating electric field of the IR radiation and this interaction can only occur when the electric dipole moment of the molecule changes during the vibration. Since vibrating atoms are linked together by chemical bonds it is usual to refer to the vibration as a bond deformation. The simplest bond deformations are bending and stretching. Usually, the only significant absorptions correspond to promotion of the bond deformation from their ground state to the next highest energy level. IR spectroscopy is based on bond deformation and hence the vibration which is related to the atoms involved. Thus by measuring the IR absorption spectrum over a range of energies, a series of absorptions corresponding to characteristic vibrations of particular bonds is obtained. Analysis of the location of the frequencies of these absorptions can aid in the identification of the material composition (Atkins, 2001).

Transitions between vibrational states can result from the scattering of radiation from molecules. In such scattering processes, the incident oscillating electric field of the incident optical wave should be of an energy that is greater than the energy difference between the vibrational states, for example UV or visible radiation. The oscillating electric field of the incident optical wave can be scattered off the molecule in two different ways. If the

scattered light induces an oscillating polarisation in the scattering molecule and when the oscillating electric field exchanges energy with the molecule, then the scattered radiation may have a higher (anti-Stoke) or lower (Stoke) frequency than the incident electric field. The difference in frequency corresponds to vibrational modes of the molecular structure and is referred to as Raman scattering. When the incident frequency equals the scattered light, the scattering is referred to as Rayleigh scattering. In Stokes Raman scattering, the molecule starts out in a lower vibrational energy state and after the scattering process ends up in a higher energy state. Thus the interaction of the incident light with the molecule creates a vibration in the material. In anti-Stokes scattering, the molecule begins in a higher vibrational energy state and after the scattering process ends up in a lower vibrational state. Thus the vibration in the material is lost as a result of the interaction. The frequency difference between Raman lines and the exciting lines are characteristic of the scattering molecule and are independent of the excitation frequency. Whereas in IR a change in dipole moment is required, in Raman a change in polarisability is required. As polar bonds are not often very polarisable, and vice versa, the two techniques are mutually complementary (Atkins, 2001).

4.3.1 Infrared Spectroscopy of Materials

When dealing with polyatomic molecules such as anthracene and *p*-terphenyl, normal modes are used to describe molecular vibrations and they are IR active if they give rise to a change in dipole moment on interaction with IR electromagnetic radiation. The IR spectra of anthracene and p-terphenyl are depicted in Figures 4.7 and 4.8 respectively and some of the normal modes which include stretching and bending are displayed. Figure 4.9 depicts the IR active phonon modes of SWNTs.

The spectrometer used in this research to carry out experimental work was the Perkin Elmer Spectrum GX. It is a single-beam, Michelson interferometer based, Fourier transform infrared spectrometer. It has a dual level optical module that is sealed and desiccated. The system is configured with a mid-infrared (MIR) single source. MIR and far infrared (FIR), beam splitters allow the range 7000 to 50 cm^{-1} to be covered with a maximum resolution of

0.3 cm^{-1}. The spectrometer is configured with the AutoIMAGE microscope system which can operate in transmittance and reflectance modes. All manual microscope operations including adjustments to aperture, focus and illumination are fully automated and collected from the PC. It includes a built-in 35W tungsten halogen illuminator, a motorised stage and a CCD video camera. The medium beam MCT detector covers the range from 5500 to 550 cm^{-1}. An ATR attachment with a micro germanium crystal with a range from 5500 to 600 cm^{-1} can be used for micro samples and ATR mapping for surface studies.

Sample Preparation

Solutions containing a concentration of 2.5 x 10^{-3} M of *p*-terphenyl in toluene, 3 x 10^{-3} M of anthracene in toluene and a mass of 5.6 mg of SWNTs in 10 ml of toluene were each dropcast from solution onto silver oxide coated glass surfaces (mirrIR reflectance plates, Kevley Technology, OH, USA). The three samples were then allowed to dry for 24 hours before characterisation.

Results and Discussion

Both anthracene and *p*-terphenyl show intense vibrational modes between 900-650 cm^{-1} which are attributed to the out-of-plane C-H vibrations of the aromatic rings. Between 1290 -900 cm^{-1} both PAHs exhibit in-plane C-H deformation vibrations which have a weak to medium intensity. The modes at 1625 - 1430 cm^{-1} are due to C-C ring stretching and C-H ring stretching vibrational modes are found between 3080 - 3010 cm^{-1} with vibrations that are strong to medium in intensity for both anthracene and p-terphenyl. Anthracene alone has a strong vibrational mode at 474 cm^{-1} due to the out-of-plane C-H ring vibrations and also modes at 726 and 884 cm^{-1} with the higher frequency modes attributed to the atoms at positions 9 and 10 (see Figure 3.3). IR vibrational modes unique to *p*-terphenyl are the intense modes at 746 and 688 cm^{-1} which are attributed to mono-substituted benzene of which there are two in the molecule, one at each end. The second of the modes is characteristically not as intense as the first. The molecule *p*-terphenyl also has an intense

mode at 838 cm^{-1} and according to the literature this is attributed to *para*- substituted benzene, the central benzene ring in the structure (Socrates, 2001).

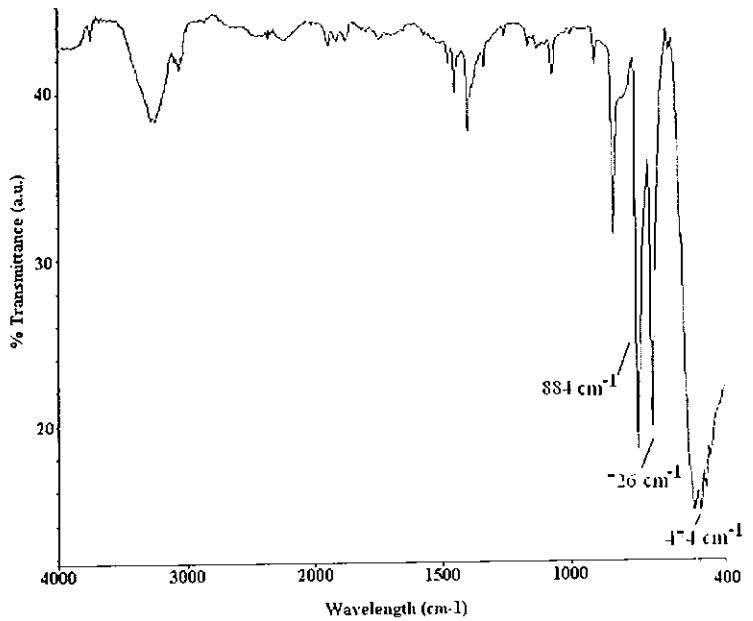

Figure 4.7 Infrared transmittance spectrum of p-terphenyl.

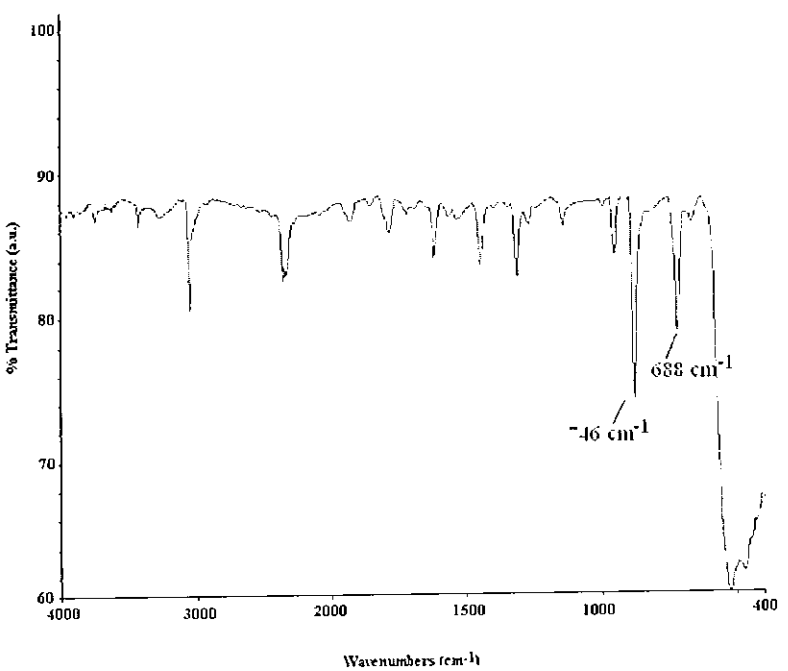

Figure 4.8 Infrared transmittance spectrum of anthracene.

In comparison to anthracene and *p*-terphenyl, SWNTs are reported to display a very weak IR spectrum (Kuhlmann *et al.*, 1998). Theory predicts that there are seven to nine IR active modes depending on their symmetry (Harris, 1999). The modes are predicted to be largely independent of the SWNTs diameter with only the position of the lowest frequency mode at 400 cm^{-1} reported to be highly diameter dependent although the frequencies have been found to vary. Literature is scarce with regard to the experimental observation of IR modes of untreated SWNTs. Kuhlmann *et al.*, reported that the spectrum of SWNTs is similar to that of graphite; however the IR active phonon modes in SWNTs have been shown to be shifted towards higher frequencies. To date the experimental observation of SWNT phonon modes have been reported at ~1590 and ~850 cm^{-1} (Kuhlmann *et al.*, 1998). Branca *et al.*, also reported the observation of SWNT modes with three main features at 1600 cm^{-1}, 1400 cm^{-1} and 1180 cm^{-1} which have been attributed to the C-C and C=C stretching along the hexagonal array of the nanotube backbone (Branca *et al.*, 2004). An IR transmittance reflection spectrum taken on mirrIR reflectance surfaces of LV-SWNT is presented in Figure 4.9. Here the features reported by Kuhlmann *et al.*, can clearly be identified with the profile shown below matching those reported in the literature (Kuhlmann *et al.*, 1998).

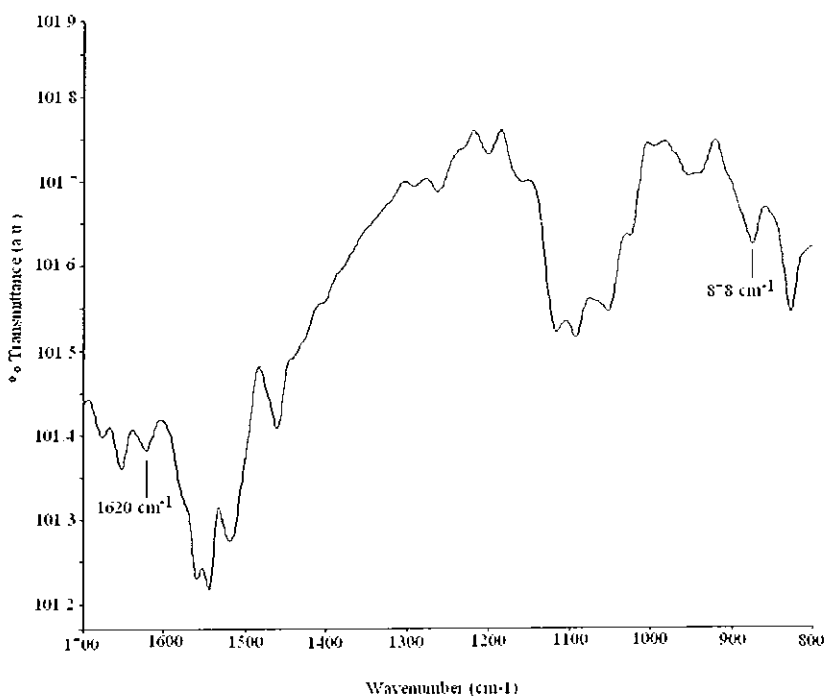

Figure 4.9 Infrared transmittance spectrum of laser vapourisation SWNT.

4.3.2 Raman Spectroscopy

As with IR spectroscopy, Raman spectroscopy also has a selection rule. It states that the normal modes of vibration of polyatomic molecules must undergo a change in their polarisability as a result of the interaction with electromagnetic radiation. If the polarisability changes the vibrational mode is then considered Raman active. There have been reports on the dramatic effect the Raman excitation frequency has on the distribution of the intensity and peak positions in the Raman spectrum. When the excitation frequency is close to the optical absorption, the Raman intensity is enhanced, and this effect is known as the resonant Raman effect and will be discussed in more detail below. The Raman active phonon modes for each of the three materials, anthracene, *p*-terphenyl and SWNTs are depicted and discussed below.

The Raman instrument used in this research to characterise the materials was the Instruments SA LabRam 1B with a confocal Raman imaging microscope system. Both Helium-Neon (632.8 nm/11 mW) and Argon ion (514.5 nm/130 mW, 488 nm/130 mW, 457 nm/20 mW) were available as sources. Both sources are polarized, enabling measurement of depolarisation ratios and studies of orientation in materials. The light is imaged to a diffraction limited spot (typically 1 μm) *via* the objective of an Olympus BX40 microscope. The scattered light is collected by the objective in a confocal geometry, and is dispersed onto an air cooled CCD array by one of two interchangeable gratings, 1800 lines/mm or 600 lines/nm, allowing the range from 150 cm^{-1} to 4000 cm^{-1} to be covered in a single image, or with greater resolution in a combination of images. With the former, a spectral resolution of 1 cm^{-1} per pixel is achievable. The system is furthermore equipped with a remote head, which is coupled to the spectrometer.

Sample Preparation

The concentration of solutions used for IR measurements were also used for Raman measurements but solutions were dropcast onto a glass surface. The three samples were then allowed to dry for 24 hours before characterisation.

Results and Discussion

Figure 4.10 depicts the Raman spectrum of anthracene taken at a laser excitation of 632.8 nm. The vibrational modes at 1554 cm^{-1} and 1400 cm^{-1} are attributed to the C=C stretch and the ring stretching mode respectively. At 1004 cm^{-1} the ring breathing mode is observed and the ring vibrational modes are observed at 750 cm^{-1} and 726 cm^{-1}. The characterisation of *p*-terphenyl depicted in Figure 4.11 was obtained using the 514.5 nm laser excitation line. Although off resonance, the spectrum should be independent of laser frequency. The moodes at 1603 cm^{-1} and 1592 cm^{-1} may be attributed to the C=C stretches in *p*-terphenyl with the vibrational mode at 1271 cm^{-1} representing a ring stretch. The vibrational modes at 1003 cm^{-1} and 988 cm^{-1} are due to ring breathing modes and at 770 cm^{-1} a ring vibrational mode is observed. The spectra in Figures 4.10 and 4.11 agree well with those reported in the literature (Socrates, 2001).

As discussed above resonance Raman scattering is a technique which allows one to selectively enhance different species by matching the laser line with the energy of the species absorption. By exciting in the UV-Vis region a strong photoluminescence signal may be observed for some conjugated molecules as a result of exciting the $\pi - \pi^*$ electron transitions.

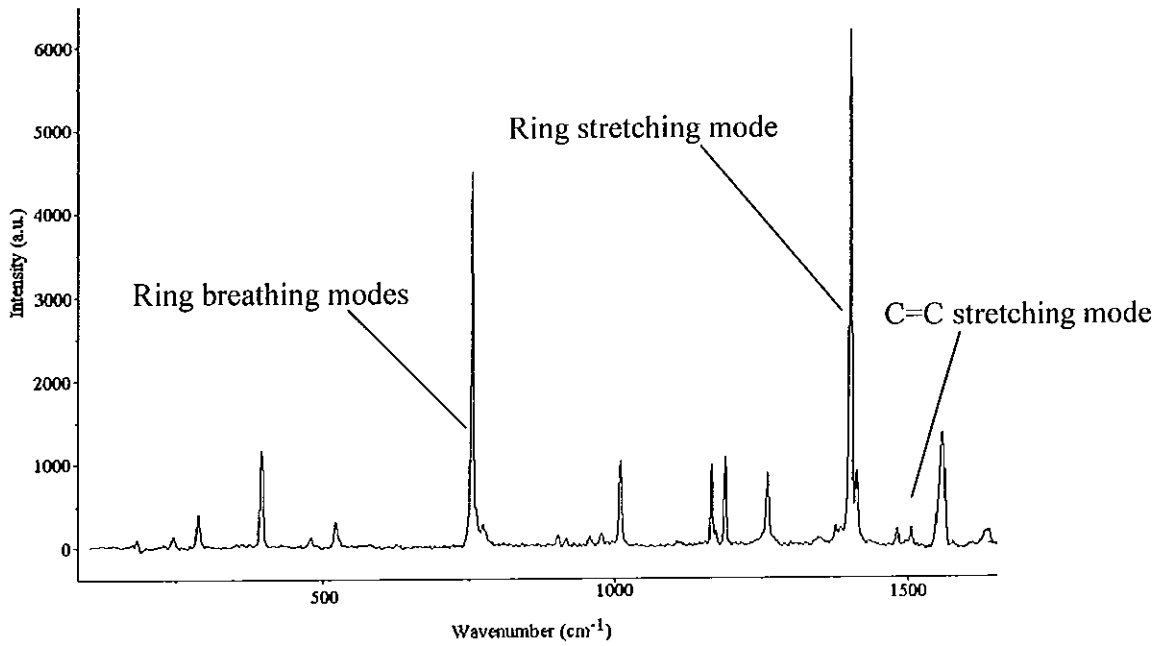

Figure 4.10 Raman spectrum of anthracene at a laser excitation wavelength of 632.8 nm.

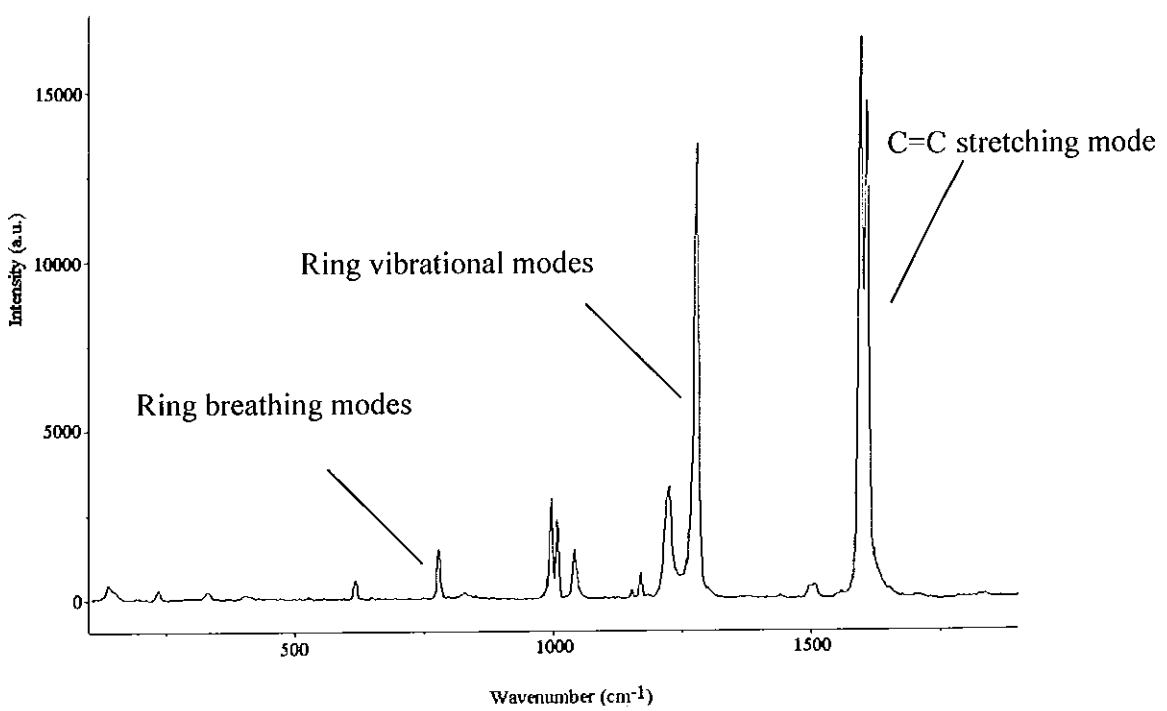

Figure 4.11 Raman spectrum of *p*-terphenyl at a laser excitation wavelength of 514.5 nm.

The vibrational modes in carbon nanotubes consist of optical and acustic modes, such as of out-of–plane, in-plane and in-plane radial modes. Three phonon modes dominate the Raman spectrum of SWNTs. In the low frequency region, the phonon modes are dominated by the radial out-of-plane modes whose frequency is diameter-related often referred to as the radial breathing modes (RBMs). In the medium frequency region, both radial and tangential modes (stretching and bending modes) are present, and the detailed structure of the spectrum depends not only on the diameter but also on the helicity. In the high frequency region, the phonon modes are dominated by the tangential modes (G-line). Figure 4.12 below depicts the Raman spectrum for an as produced sample of LV-SWNT with an excitation wavelength of 514.5 nm. Although theory predicts that SWNTs have 15 or 16 Raman allowed vibrational modes, experimental evidence shows only a few intense and several weaker modes (Holden *et al.*, 1994; Journet *et al.*, 1997). The intensity of the Raman modes not only depends on parameters such as the SWNT process method and the geometry of the SWNT but also on the bundle thickness (Alvarez *et al.*, 2000).

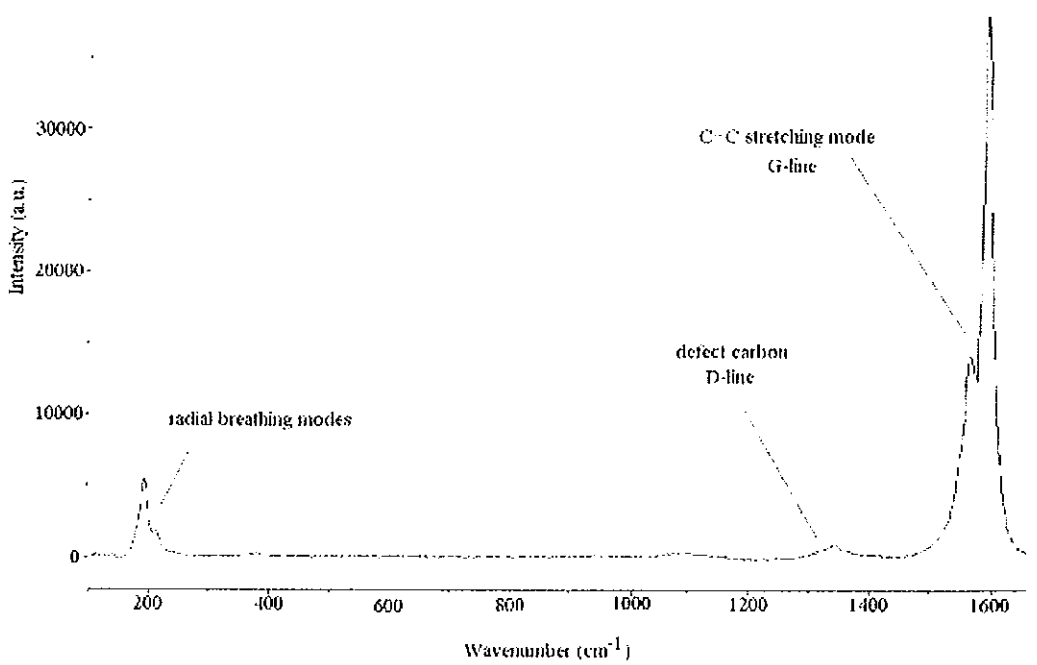

Figure 4.12 Raman spectrum of an untreated laser vapourisation SWNT bundle at an excitation wavelength of 514.5 nm. The spectrum shows the three main peaks which dominate the SWNT Raman spectrum, the RBM, the D-line and the G-line which are marked in the spectrum.

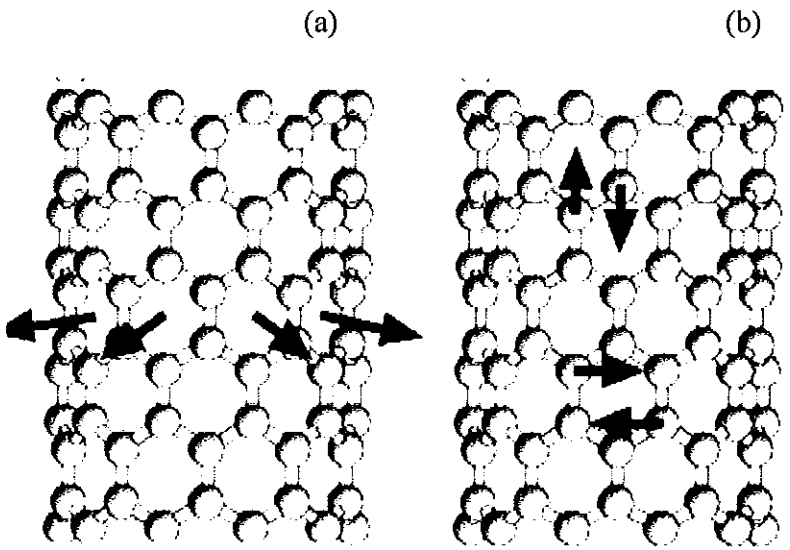

Figure 4.13 Schematic representation of the atomic vibrations for SWNTs for (a) RBM and (b) G-line (Jorio *et al.*, 2003).

The Raman spectrum of a graphene sheet exhibits an intense Raman active mode at ~1580 cm^{-1} (Chapter 1, Figure 1.1). When the graphene sheet is rolled to form a tube, the optical vibrational mode at ~1580 is split into higher (longitudinal) and lower (transverse) energies (Figure 4.13 (b)). Thus, the allowed Raman lines appear as a series of doubly split modes on the higher and lower energy sides of 1580 cm^{-1} termed the G-line (Pimenta *et al.*, 1998). The splitting increases as the diameter of the tubes decreases. The G-line is attributed to the C=C stretch within the SWNT and is the strongest vibrational mode in the spectrum of bundled SWNTs. It is believed that the profile of the G-line can be used to distinguish between metallic and semiconducting SWNTs with metallic SWNTs exhibiting a broad G-line with a the Breit-Wigner-Fano (BWF) line shape compared to the characteristic narrow G-line for semiconducting SWNTs (Bendiab, *et al.*, 2003; Jorio *et al.*, 2002; Jorio *et al.*, 2001). As well as the G-line, additional vibrational modes appear which are subject to cyclic boundary conditions such as the RBMs and the D-line (Chapter 2, Equation 2). The RBMs are observed in the lower frequency region, centred at approximately ~200 cm^{-1} and are usually the second strongest vibrational mode next to the G-line for a sample of SWNT bundles. These vibrational modes are attributed to the radial displacement of the carbon

atoms in the SWNT perpendicular to the axis of the SWNTs (Figure 4.13 (a)). The RBM distribution is normally broad due to the poly-diversity of diameters within a typical sample of bundled SWNTs. These vibrations are of particular interest as theory predicts a strong dependence of this frequency on SWNT diameter as stated in Equation 4.5 below (Jorio *et al.*, 2001; Pimenta *et al.*, 2001). The parameters within the equation are ω_{RBM} which denotes the RBM frequency, d_t which is the SWNT diameter and Γ which is the damping factor which accounts for a frequency shift resulting from changes in the SWNT bundle size and (or) the solvent used and (or) any other parameter that results in a change in the local environment of the SWNTs (Kuzmany *et al.*, 2001). With respect to Equation 4.5 there are many RBM constants of proportionality reported with values ranging from 223.5 – 248 cm^{-1} (Alvarez *et al.*, 2000; Hartschuh, *et al.*, 2003; Jorio *et al.*, 2001; Kuzmany *et al.*, 2001; Pimenta *et al.*, 1998; Wang *et al.*, 2001). Some of these constants have been theoretically determined while others were empirically derived from a variety of SWNT samples (Alvarez *et al.*, 2000; Hartschuh, *et al.*, 2003; Jorio *et al.*, 2001; Kuzmany *et al.*, 2001; Pimenta *et al.*, 1998; Wang *et al.*, 2001). In this thesis the value 248 cm^{-1} was chosen as the constant for determining the diameter of debundled SWNTs because this value was not only determined experimentally, it was also determined using isolated LV-SWNT obtained from Rice University which is the same method and origin of the SWNTs used primarily in this study (Jorio *et al.*, 2001).

$$\omega_{RBM} = (248\ cm^{-1} / d_t) + \Gamma \qquad \text{Equation 4.5}$$

The third most intense mode in a bundled SWNT spectrum is the D-line and it is observed at 1350 cm^{-1}. The origin of the mode is currently under dispute as some authors are of the opinion that the D-line results from the presence of defective carbon material in the sample (Kukovecz *et al.*, 2002; Pimenta *et al.*, 2001; Reich *et al.*, 2004). Other authors argue its presence as due to impurities in the sample such as amorphous carbon, carbon onions and non-graphitised sheets on the lattice of tubes within the SWNT sample (Duesberg *et al.*, 1999; Yu, *et al.*, 2001). It has also been argued that the D-line is diameter dependent and

the intensity of the D-line is greater for metallic SWNTs than for semiconducting SWNTs at the same laser energy (Brown *et al.*, 2001). Figure 4.12 depicts the G-line, D-line, and RBM and the profile of the G-line in this instance is characteristic of semiconducting SWNTs.

There have been many reports on the dramatic effect of the Raman excitation frequency on the distribution of the intensity and mode positions in the Raman spectrum. Figure 4.14 (a) and (b) shows the Raman spectra of the RBMs and G-line for SWNTs at a number of different excitation wavelengths respectively. The wavelengths span from the visible to the near infrared. It should be noted that for even a small change in excitation wavelength a marked change in the spectrum is observed. As the wavelength increases towards the infrared, the modes near 1580 and 180 cm^{-1} may be enhanced by an order of magnitude and many other modes are known to become observable. This redistribution in spectral intensity signifies resonant Raman scattering.

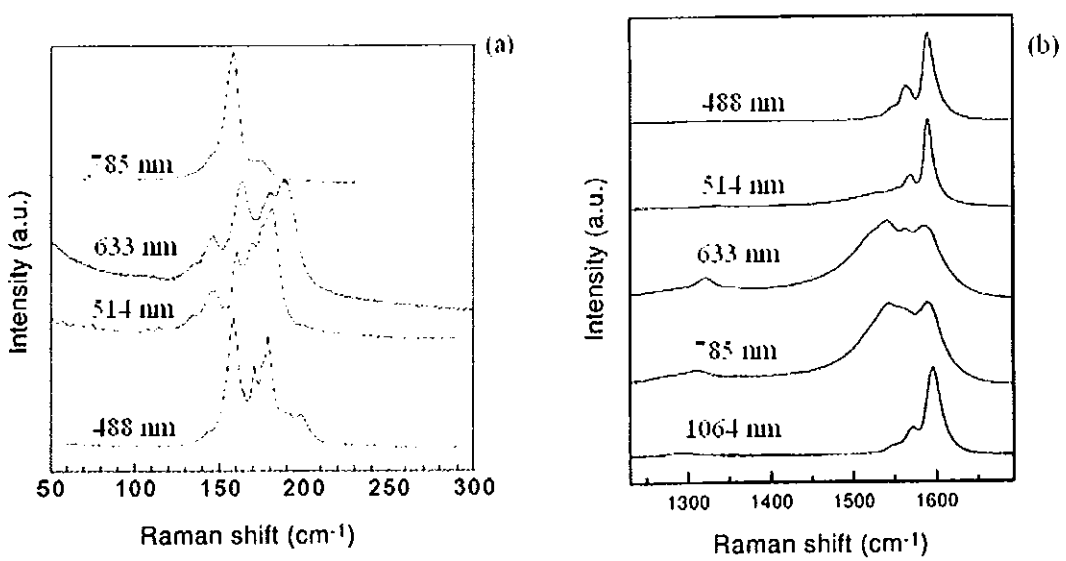

Figure 4.14 (a) RBMs and (b) G-line of the same SWNT at different laser excitation lines. It is clear from the resonance effect that different SWNT are excited at different laser energies (adapted from Alvarez *et al.*, 2000; Pimenta *et al.*, 1998).

Usually Raman spectra only involve phonons explicitly, being independent of the electronic structure of the material and the laser energy used to excite the Raman spectra. Furthermore, the usual Raman scattering is weak. However, the scattering efficiency gets larger when the laser energy matches the energy between optically allowed electronic transitions in the material, and this intensity enhancement process is termed resonance Raman scattering. The resonance Raman intensity depends on the DOS available for optical transitions, and this property is very important for one-dimensional systems. Figure 4.15 (a)-(c) shows the DOS for three different SWNTs, and since SWNTs are quasi-one-dimensional systems, their DOS is characterized by van Hove singularities (Chapter 2). The three DOS curves in Figure 4.15 (a)-(c) come from different SWNTs as described in the figure caption. An observable Raman signal from the SWNTs can be obtained when the laser excitation energy level is equal to the energy separation between the van Hove singularities in the valence and conduction bands. The resonance process allows simultaneous study of the electronic and phonon structure of the SWNTs.

Figure 4.15 (d) is a plot of energy (E_{ii}) versus diameter (d_t) where each point represents one optically allowed electronic transition energy (E_{ii}) for a given (n,m) SWNT. The crosses and circles represent semiconducting and metallic SWNT respectively. The plot provides a guide to the type of SWNT that will be in resonance at a certain laser line.

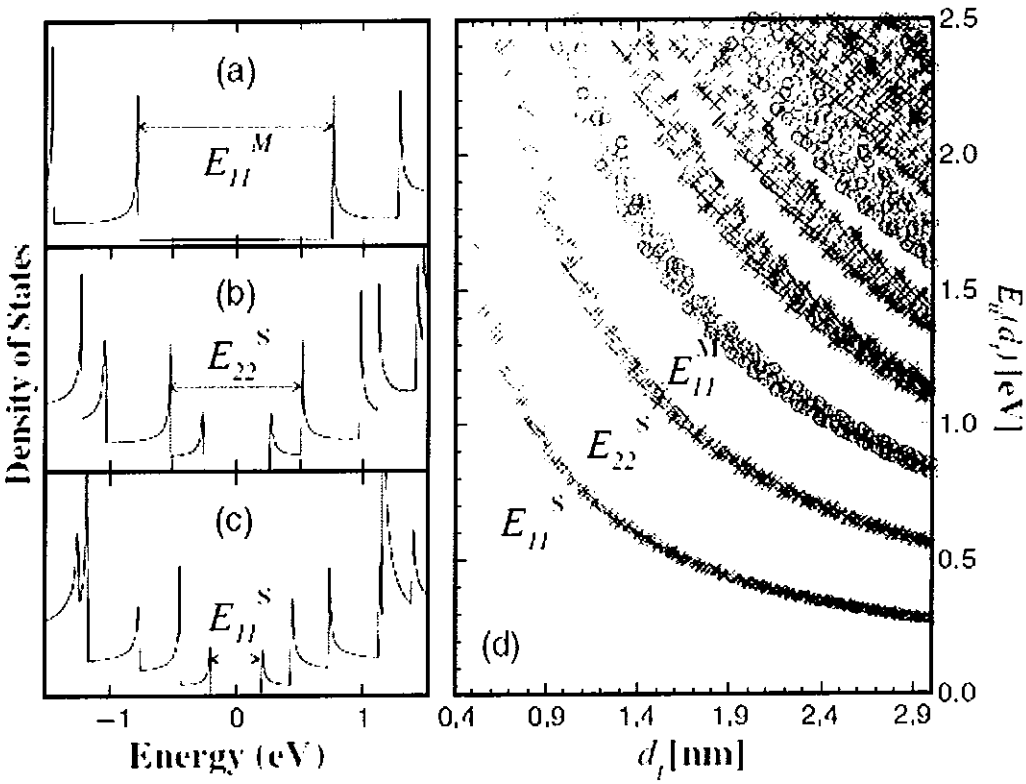

Figure 4.15 Density of states for (a) armchair (10,10) SWNT, (b) chiral (11,9) SWNT and (c) zigzag (22,0) SWNT obtained with the tight binding model (Reich *et al.*, 2002). (d) Shows the electronic transition energies E_{ii} for all the (n,m) SWNT with diameters from 0.4 to 3.0 nm using simple first-neighbour tight binding model (Saito *et al.*, 1998). Distortion from this simple one electron model is expected for the lower energy transitions E^{S}_{11} and for SWNTs with $d_t < 1$ nm.

4.4 Microscopy Techniques

Scanning probe microscopy (SPM) refers to techniques that use the interaction of a microscopic probe (usually on a sharp tip) with the surface of a sample to measure the characteristics of the sample at localised points. To measure a certain property locally, the probe is scanned relative to the sample surface in a two-dimensional pattern by applying voltages to the x and y electrodes of a piezoelectric scan unit. It is either possible to directly record the signal due to the probe-sample interaction at each position, or to use electronic feedback. In the latter case an appropriate voltage is applied to the z-electrode so that the probe-sample interaction is kept constant. Such piezoelectric scan units can achieve

picometer resolution in all three dimensions (Magonov and Whangbo, 1996). The probe-sample interaction may be the tunnel current, all types of long and short range forces.

Atomic force microscopy (AFM) operates by measuring attractive or repulsive forces between a tip and the sample (Binnig *et al.,* 1986). In its repulsive 'contact' mode, the instrument lightly touches a tip at the end of a cantilever to the sample. As a raster-scan drags the tip over the sample, the detection apparatus measures the vertical deflection of the cantilever, which indicates the local sample height. According to Hooke's law, the magnitude of the tip-sample force is proportional to the cantilever deflection (Atkins, 2001). Thus, in contact mode the AFM measures hard-sphere repulsion forces between the tip and sample. In non-contact mode, the AFM derives topographic images from the measurements of attractive forces; the tip does not touch the sample (Albrecht *et al.,* 1990). In the non-contact mode the cantilever is oscillated at or near its resonance frequency and depending on the excitation the cantilever is externally driven or self oscillating. Any tip-sample interaction influences amplitude, phase or frequency of the cantilever (Magonov and Whangbo, 1996).

Transmission electron microscopy (TEM) works by focusing a beam of electrons into a tight spot on the surface of a sample. The electrons are either absorbed or scattered at different rates depending on the local structure. The transmitted electrons are projected onto a phosphor screen and light is generated, allowing the user to see the image. The darker areas of the image represent those areas of the sample that fewer electrons were transmitted through (they are thicker or denser). The lighter areas of the image represent those areas of the sample that more electrons were transmitted through (they are thinner or less dense) (Fultz and Howe, 2002).

4.4.1 Transmission Electron Microscopy (TEM) of Materials

The TEM is a useful instrument for imaging materials on a nanometer scale. Due to the imaging capabilities and the size limitations of the PAHs, TEM images could be obtained only for SWNTs.

The TEM used to image the materials in this research was a Jeol 100 CX TEM, with an accelerating voltage of typically 100 keV applied. The substrates consisted of copper grids covered with an electron transparent polymer, 3 % formvar resin in 1,2-dichloroethane. Formvar resin is a synthetic film containing polyvinyl acetal and phenol resins.

Sample Preparation

To prepare the samples for imaging 2 mg of untreated SWNT was added to 10 ml of ethanol and sonicated in the sonic bath (ULTRA sonick 57x, 230 V), for 30 mins at medium power. The solution was then dropcast onto a copper grid with a 3% chloroform formvar polymer coating after which the samples were allowed to dry for approximately 24 hours.

Results and Discussion

Figure 4.16 depicts the TEM images of LV-SWNT, with the long bundle-like images representing the SWNT bundles and the dark amorphous structures representing the catalyst particles and amorphous carbon within the sample. It is clear from the image that the untreated SWNT samples exist in bundles and the bundle sizes were estimated on average to be approximately 50 nm. TEM images of both H-SWNT and AD-SWNT were also obtained with average bundle sizes estimated at 30 nm for each (Appendix B, Figure 1 and Appendix C Figures 1 and 2). The results conclude that LV-SWNT are the largest bundles of the three samples with AD-SWNT displaying the highest amount of amorphous carbon; similar results are reported in the literature (Chiang *et al.*, 2001; Coleman *et al.*,

2003; Iijima and Ichihashi, 1993; Journet *et al.,* 1997; Nikolaev *et al.*, 1999; Rao *et al.*, 2001; Saito *et al.*, 1998).

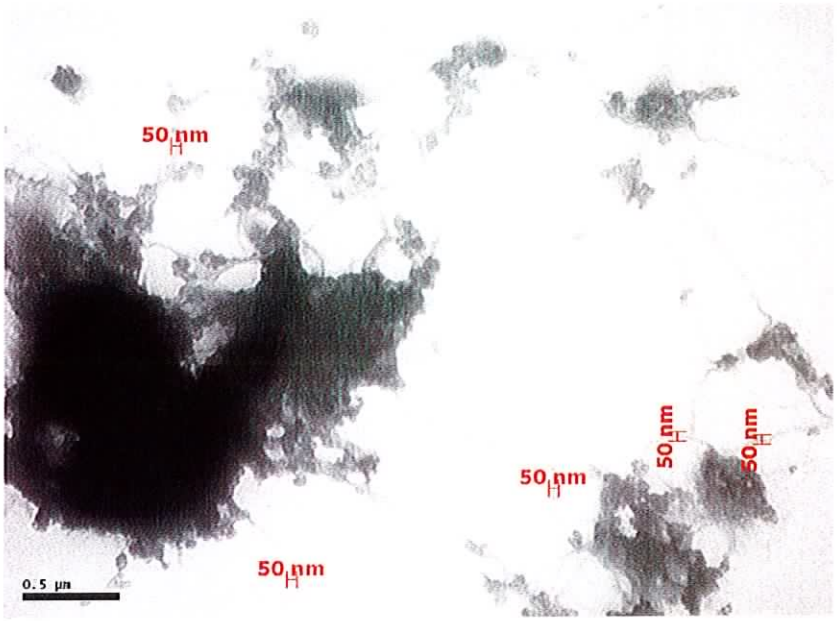

Figure 4.16 TEM images of untreated LV–SWNT at a magnification of 40,000X. The bundle-like structures represent the SWNT bundles and the amorphous structures represent the catalyst particles and amorphous carbon.

4.4.2 Atomic Force Microscopy (AFM) of Materials

The imaging technique AFM has the ability to image SWNT that are at the nanometer scale and below.

The AFM used in this research was the Asylum MFP 3D (Asylum Research, Santa Barbara, http://www.asylumresearch.com/Products/Mfp3DIO/Mfp3DIO.shtml). The MFP-3D base and scanner have three configurations for illuminating and viewing the sample. The system uses a flexured scanner and patent-pending sensors which measure the exact position of each axis (x and y). They correct for hysteresis and creep, providing flat scans and the ability to accurately zoom and offset. The MFP-3D head has a sensored optical lever with diffraction limited optics and a low coherence light source virtually eliminates interference artifacts. The sensored z axis provides precise measurements of the cantilever

position for accurate force and topography measurements. An optional extended head allows for a 28 μm z range. In this research only the dynamic tapping method was used with the appropriate tips which were NSC 36/ No AL and had a spring constant of 5 N/M (see www.spmtips.com). Due to the shape and size of the AFM tip (10nm apex ratio) compared to the SWNT which may be less than 10nm, AFM measurements typically result in broadened widths. To reduce the error incurred by the large tip size with respect to the smaller SWNTs the same tip was used to measure all LV-SWNT samples to prevent variation in the estimated SWNT width. However the shape of the tip does not affect the z-axis measurements. Therefore accurate heights of SWNTs can be determined from AFM measurements. The resolution of the height measurement is mainly limited by the z-axis noise, which is normally a few tenths of a nanometer under standard imaging conditions. The accuracy of the height measurements is limited by the tip sample interaction which is a function of imaging conditions.

Sample Preparation

The sample preparation for AFM studies involved dispersing untreated SWNT on an activated silicon surface. The silicon wafer was first activated by covering the surface in a layer of 3-aminopropyl tri-ethoxysilane (APTES) for 10 minutes after which the surface was rinsed with deionised water and then dried at room temperature. The activated surface was immersed in a solution containing 5.6 mg of LV-SWNT in toluene for approximately three weeks after which the surface was rinsed with deionised water and allowed to dry at room temperature before imaging.

Results and Discussion

Figure 4.17 shows the AFM of an untreated sample of LV-SWNT with the amorphous structures representing the presence of amorphous carbon and catalyst particles and the bundle-like images representing the bundles of LV-SWNT within the sample. The average parameters measured by AFM for LV-SWNT were a length of 5,000 nm, width of 33 nm and height of 4 nm. Width measurements were taken using the full width half maximum to

reduce the error incurred from using a tip with a 10 nm apex ratio. The bundle surface area was measured for a number of bundles within the sample using the formula for an elongated box and found to be approximately 3.7 x 10^{-13} m^2. Images of H-SWNT (Chapter 7, Figure 7.5a) and AD-SWNT (Chapter 7, Figure 7.7a) were also obtained and provided images similar to that depicted in Figure 4.17.

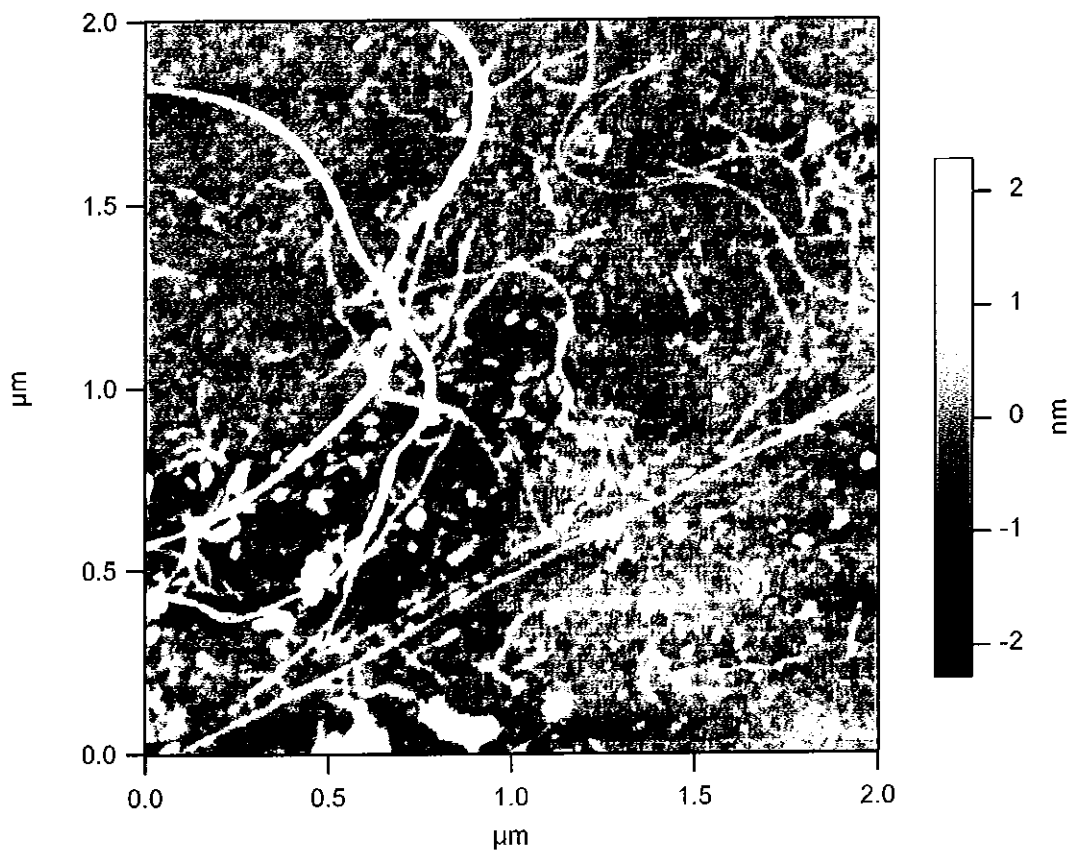

Figure 4.17 AFM of an untreated sample of LV–SWNT. The amorphous structures are due to the presence of amorphous carbon and catalyst particles within the sample. The bundle like-image represents the bundle of LV–SWNT with a bundle surface area of approximately 5.51 x 10^{-13} m^2.

Summary

Spectroscopy is a useful tool for characterising materials and providing information on their molecular structure. A variety of spectroscopic techniques were employed to characterise

anthracene, *p*-terphenyl and SWNTs. Absorption spectra provided information on the electronic and vibrational structure of the three different materials investigated. The UV-Vis-NIR spectra were especially useful when probing SWNT as the regions in which the SWNT absorbed electromagnetic radiation was related to the diameter and chiralities of the SWNT within the sample. Vibrational techniques such as Raman and IR probed the polarisability and dipole moment changes within the material as a result of the interaction with electromagnetic radiation and the spectra obtained provided information as to the vibrational structure of the molecules. Microscopy techniques such as AFM and TEM were used to image the SWNT structures and measure the SWNT bundle size in their untreated (as produced) state. It was observed that SWNTs produced by different methods had bundles of different sizes with LV-SWNT having the largest bundles and AD-SWNT having the least pure sample. Chapter 5 continues with the experimental studies of these materials and investigates the interactions that occur between anthracene and SWNTs and *p*-terphenyl and SWNTs.

REFERENCES

Ajayaghosh , A., (2004), "*A short term course on chemistry, light and materials*" Available at: www.iitk.ac.in/samtel_center/doc/course123.pdf, accessed 26 march 2006.

Alvarez, L., Righi, A., Rols, S., Anglaret, E., Sauvajol, A.L., (2000), "On the Raman spectrum of nanobundles of single wall nanotubes", *Amorphous and Nanostructures of Carbon,* 53, 107 – 112, Material Research Society, Boston.
Available at: http://www.geocities.com/CollegePark/3972/MRS_99.pdf, accessed 26 March 2006.

Alvarez, L., Righi, A., Guillard, T., Rols, S., Anglaret, E., Laplaze, D., Sauvajol, J.-L., (2000), "Resonant Raman study of the structure and electronic properties of single-wall carbon nanotubes", *Chem. Phys. Lett.*, 316, 186-190.

Albrecht, T.R., Akamine, S., Carver, T.E., and Quate, C.F., (1990), "Microfabrication of cantilever style for the atomic force microscope", *J. Vac. Sci. Technol.* A, 8(4), 3386-3396.

Atkins, P., (2001), *Elements of Physical Chemistry*, third edition, Oxford University Press, Oxford.

Ausman, K.D., Piner, R., Lourie, O., Ruoff, R.S., Korobov, M., (2000), "Organic solvent dispersions of single-walled carbon nanotubes: towards solutions of pristine nanotubes", *J. Phys. Chem. B.*, 104, 8911-8915.

Bachilo, S.M., Strano, M.S., Kittrell, C., Hauge, R.H., Smalley, R.E., Weisman, R.B., (2002), "Structure assigned optical spectra of single-walled carbon nanotubes", *Science*, 298, 2361 – 2366.

Bendiab, N., Almairac, R., Paillet, M., Sauvajol, J.-L., (2003), "About the profile of the tangential modes in single-wall carbon nanotubes bundles", *Chem. Phys. Lett.*, 372, 210-215.

Berlman, I.B., (1971), *Handbook of Fluorescence Spectra of Aromatic Molecules*, Academic Press, second edt., New York. (http://omlc.ogi.edu/spectra/PhotochemCAD/html/p-terphenyl.html) accessed on 7 March 2006.

Binnig, G., Quate, C.F., and Gerber, Ch., (1986), "Atomic force microscope", *Phys. Rev. Lett.*, 56(9), 930-933.

Branca, C., Corsaro, F., Frusteri, F., Mangione, A., Migliardo, F., Wanderlingh, U., (2004), "Structural and vibrational properties of carbon nanotubes by TEM and infrared spectroscopy", *Diamond and Related Materials*, 13, 1249-1253.

Brown, S.D.M., Jorio, A., Dresselhaus, M.S., Desselhaus, G., (2001), "Observations of the D-band feature in the Raman spectra of carbon nanotubes", *Phys. Rev. B.*, 64, 073403 -1 – 073403-4.

Cai, L., Bahr, J.L., Yao, Y., Tour, J.M., (2002), "Ozonation of single-walled carbon nanotubes and their assemblies on rigid self assembled monolayers", *Chem. Mater.*, 14, 4235-4241.

Chiang, I.W., Brinson, B.E., Huang, A.Y., Willis, P.A., Bronikowski, M.J., Margrave, J.L., Smalley, R.E., Hauge, R.H., (2001), "Purification and characterisation of single-wall carbon nanotubes (SWNT) obtained from gas-phase decomposition of CO (HiPco process)", *J. Phys. Chem. B.*, 105, 8297-8301.

Coleman, J.N., Blau, W.J., Dalton, A.B., Munoz, E., Collins, S., Kim, B.G., Razal, J., Selvidge, M., Vieiro, G., Baughman, R.H., (2003), "Improving the mechanical properties of

single-walled carbon nanotube sheets by intercalation of polymeric adhesives", *App. Phys. Lett.*, 82, 1682-1664.

Duesberg, G.S., Blau, W.J., Byrne, H.J., Muster, J., Burghard, M., Roth, S., (1999), "Experimental observation of individual single-wall nanotubes species by Raman microscopy", *Chem. Phys. Lett.*, 310, 8-14.

Fultz, B., Howe, J., (2002), *Transmission electron microscopy and diffractometry of material*, Springer, New York.

Hagen, A., Hertel, T., (2003), "Quantitative analysis of optical spectra from individual single-wall carbon nanotubes", *Nanoletters*, 3, 383-388.

Harris, P.J.; (1999), Carbon Nanotubes and Related Structures, Cambridge University Press, Cambridge.

Hamon, M.A., Itkis, M.E., Niyogi, S., Alvaraez, T., Kuper, C., Menon, M., (2001), "Effect of rehybridization on the electronic structure of single-walled carbon nanotubes", *J. Am. Chem. Soc.*, 123, 11292 – 11293.

Hartschuh, A., Pedrosa, H.N., Novotny, L., Krauss, T.D., (2003), "Simultaneous fluorescence and Raman scattering from single carbon nanotubes", *Science*, 301, 1354-1356.

Holden, J.M., Zhou, P., Bi, X., Eklund, P.C., Bandow, S., Jishi, R.A., Chowdhury, K.D., Dresselhaus, G., Dresselhaus, M.S., (1994), "Raman scattering from nanoscale carbons generated in a cobalt-catalysed carbon plasma", *Chem. Phys. Lett.*, 220, 186-191.

Iijima, S., Ichihashi, T., (1993), "Single shell nanotubes of 1-nm diameter", *Nature*, 363, 603-605.

Jorio, A., Saito, R., Hafner, J.H., Lieber, C.M., Hunter, M., McClure, T., Dresselhaus, G., Dresselhaus, M.S., (2001), "Structural (n,m) determination of isolated single-wall carbon nanotubes by resonant Raman scattering", *Phys. Rev. Lett.*, 86, 1118-1121.

Jorio, A., Filho, A.G.S., Dresselhaus, G., Dresselhaus, M.S., Swan, A.K., Unlu, M.S., Goldberg, B.B., Pimenta, M.A., Hafner, J.H., Lieber, C.M., Saito, R., (2002), "G-band resonant Raman study of 62 isolated single-wall carbon nanotubes", *Phys. Rev. B.*, 65, 155412-1 – 155412-9.

Jorio, A., Pimenta, M.A., Filho, A.G.S., Saito, R., Dresselhaus, G., Dresselhaus, M.S., (2003), "Characterising carbon nanotube samples with resonance Raman scattering", *New Journal of Physics*, 5, 139.1 – 139.17.

Journet, C., Maser, W.K., Bernier, P., Loiseau, A., Lamy de la Chapelle, M., Lefrant, S., Deniard, P., Lee, R., Fisher, J.E., (1997), "Large-scale production of single-walled carbon nanotubes by the electric-arc technique", *Nature*, 388, 756-758.

Kataura, H., Kumazawa, Y., Maniwa, Y., Umezu, I., Suzuki, S., Ohtsuka, Y., Achiba, Y., (1999), "Optical properties of Single-Wall Carbon Nanotubes", *Synthetic Metals*, 103, 2555-2558.

Kuhlmann, U., Jantoljak, H., Pfander, N., Bernier, P., Journet, C., Thomsen, C., (1998), "Infrared active phonons in single-walled carbon nanotubes", *Chem. Phys. Lett.*, 294, 237-240.

Kukovecz, A., Kramberger, Ch., Georgakilas, V., Prato, M., Kuzmany, H., (2002), "A detailed Raman study on thin single-wall carbon nanotubes prepared by the HiPco sample", *Eur. Phys. J. B.*, 28, 223-230.

Kuzmany, H., Plank, W., Hulman, M., Kramberger, Ch., Gruneis, A., Pichler, Th., Peterlik, H., Kataura, H., Achiba, Y., (2001), "Determination of SWCNT diameters from the Raman response of the radial breathing mode", *The Euro. Phys. J. B.*, 32, 307-320.

Magonov, S.N., Whangbo, M.H., (1996), *Surface Analysis with STM and AFM; Experimental and Theoretical Aspects of Image Analysis*, VCH Publishers, Inc., New York, USA.

Malkin, J., (1992), Photophysical and Photochemical Properties of Aromatic Compounds, Boca Raton CRC Press, Florida, 60-100.

Mullin, O.C., Sheu, E.Y., (1998), *Structure and Dynamics of Asphaltenes*, Plenum Press, New York.

Nikolaev, P., Bronikowski, M.J., Kelley Bradley, R., Rohmund, F., Colbert D.T., Smith, K.A., Smalley, R.E., (1999), "Gas-phase catalytic growth of single-walled carbon nanotubes from carbon monoxide", *Chem. Phys. Letts.*, 313, 91-97.

O'Connell M.J., Bachilo S.M., Huffman C.B., Moore V.C.; Strano M.S., Haroz E.H., Rialon, K.L., Boul P.J., Noon W.H., Kittrell C., Ma, J., Hauge, R.H., Weiseman R.B., Smalley R.E., (2002), "Bandgap fluorescence from individual single-walled carbon nanotubes" *Science*, 297, 593.

Pimenta, M.A., Jorio, A., Brown, S.D.M., Filho, A.G.S., Dresselhaus, G., Hafner, J.H., Lieber, C.M., Saito, R., Dresselhaus, M.S., (2001), "Diameter dependence of the Raman D-band in isolated single-wall carbon nanotubes", *Phys. Rev. B.*, 64, 041401-1 – 041401-4.

Pimenta, M.A., Marucci, A., Brown, S.D.M., Matthews, M.J., Rao, A.M., Eklund, P.C., Smalley, R.E., Dresselhaus, G., Dresselhaus, M.S., (1998), "Resonant Raman effect in single-wall carbon nanotubes", *J. Mater. Res.*, 13, 2396-2404.

Pimenta, M.A., Hanlon, E.B., Marucci, A., Corio, P., Brown, S.D.M., Empedocles, S.A., Bawendi, M.G., Dresselhaus, G., Dresselhaus, M.S., (2000), "The anomalous dispersion of

the disorder-induced and second-order Raman bands in carbon nanotubes", *The Brazilian Journal of Physics*, 30, 423-427.

Reich, S., Thomsen, C., Maultzsch, J., (2004), *Carbon Nanotubes, Basic Concepts and Physical Properties*, Wiley-VCH Verlag, GmbH and Co. KGaA, Weinheim.

Reich, S., Maultzsch, J., Thomsen, C., Ordejon, P., (2002), "Tight-binding description of graphene" *Phys. Rev. B.*, 66, 035412 – 035417.

Rao, C.N.R.; Satishkumar, B.C.; Govindaraj, A.; Nath, M., (2001), "Nanotubes", *Chemphyschem*, 2, 78-105.

Ryabenko, A.G., Dorofeeva, T.V., Zvereva, G.I., (2004), "UV-Vis-NIR spectroscopy study of sensitivity of single-wall carbon nanotubes to chemical processing and Van-der-Waals SWNT/SWMT interaction. Verification of the SWNT content measurements by absorption spectroscopy", *Carbon*, 42, 1523-1535.

Saito, R., Dresselhaus, G., Dresselhaus, M.S., (1998), *Physical Properties of Carbon Nanotubes.* Imperial College Press, London.

Socrates, G., (2001), *Infrared and Raman Characteristic Group Frequencies, Tables and Charts*, John Wiley and Sons, Ltd., third edition, New York, 157-170.

Wang, Y.F., Cao, X.W., Hu, S.F., Liu, Y.Y., Lan, G.X., (2001), "Graphical method for assigning Raman peaks of radial breathing modes of single-wall carbon nanotubes", *Chem. Phys. Lett.*, 336, 47-52.

Wayne, R.P., (1970), *Photochemistry*, Butterworth and Co. Ltd., London, 59-100.

Yu, Z., Brus, L., (2001), "Rayleigh and Raman scattering from individual carbon nanotubes bundles", *J. Phys. Chem. B.*, 105, 1123-1134.

Yu, H.Y., Jhang, S.H., Park, Y.W., Bittar, A., Trodahl, H.J., Kaiser, A.B., (2001), "Properties of single-wall carbon nanotubes", *Synth. Metals,* 121, 1223-1224.

http://www.asylumresearch.com/Products/Mfp3DIO/Mfp3DIO.shtml, accessed 2 April 2006.

CHAPTER 5 - THE SOLUBILISATION AND PURIFICATION OF SWNT USING SIMPLE ORGANIC MOLECULES

5.1 Introduction

Most of the common techniques used to produce SWNTs result in an impure sample (Chapter 2). Furthermore, SWNTs show a varying degree of solubility in commonly used organic solvents and it has been observed that the majority of the SWNT sample dissolved in toluene precipitates out within 24 hours (Bahr *et al.*, 2001; Niyogi *et al.*, 2001; Rao *et al.*, 1997). Several methods for enhancing the purity and solubility of SWNTs have been reported which entail functionalising the SWNTs with surfactants and the use of large polymer systems (Chen *et al.*, 1998; Dalton *et al.*, 2000; Dalton *et al.*, 2001; Duesberg *et al.*, 1999; Niyogi *et al.*, 2001). This study proposes to purify and solubilise SWNTs using commercially available, simple organic structures such as anthracene and *p*-terphenyl. A degree of structural selectivity is also anticipated due to similarities in the backbone structure of each PAH and particular types of SWNTs as discussed previously in Chapter 1. This chapter will show that the organic molecules, anthracene and *p*-terphenyl, interact with LV-SWNT *via* a π - π interaction between the PAHs and the SWNT backbone structure, thereby resulting in the purification of the LV-SWNT sample and an improved degree of SWNT solubility in toluene.

The work presented in this chapter is based on the observation that the solubility of LV-SWNT in toluene is substantially enhanced upon addition of the PAH molecules *p*-terphenyl and anthracene (Hedderman *et al.*, 2002 was the first publication of this observation, see publication list). It was observed that after initial preparation, the solutions were stable for indefinite periods (now greater than 5 years) and the SWNTs were finely dispersed in the solution. These observations indicate an enhanced stability of the SWNT solutions due to an interaction with the PAH molecules, and it is supported by the spectroscopic studies presented in this chapter. All studies were performed in toluene due to its poor affinity for the retention of SWNTs and thus it acted a good indicator for

improvements in the solubility due to the presence of the PAH. LV-SWNT are chosen because they have a large diameter range and therefore a significant mixture of both armchair and zigzag tubes.

5.2 Sample Preparation

Solutions of *p*-terphenyl and anthracene in toluene were prepared at concentrations between 4.0×10^{-4} and 2.5×10^{-3} M for *p*-terphenyl and 5.5×10^{-4} and 3.0×10^{-3} M for anthracene. Experimentally it was found that these concentrations were the highest workable concentrations. The PAH solutions were characterized using fluorescence (Perkin-Elmer LS55) and Raman spectroscopy (Instruments SA LabRam 1B). LV-SWNT were a gift from Rice University (Tubes@rice.edu, Houston, TX) and were added to the PAH solutions in a 1:1 by weight ratio (w/w) SWNT/PAH. A 1:1 w/w ratio was chosen because it was found experimentally to yield a workable amount of composite solution.

Both the PAH solutions and the composite solutions were sonicated using a sonic tip (ultrasonic processor VCX, 750 W) for 30 s and were then allowed to settle for 24 hours, after which the supernatant liquid from the composite samples was carefully withdrawn. The suspensions were allowed to settle for a further 24 hours before being characterised by the various spectroscopic methods mentioned above. It was noted in these studies that the precipitate was found to be relatively rich in SWNTs, so the solubilisation is only partial. Throughout this chapter all the dispersion concentrations quoted are as prepared. For Raman measurements at 632.8 and 514.5 nm, samples were drop-cast onto glass surfaces from suspension and allowed to dry for 24 hours under ambient conditions. The absence of any characteristic toluene features in the Raman spectra indicates that all of the toluene has been removed. Removal of the PAH molecules from the composite samples was achieved using filtration and subsequent flushing with toluene. The procedure entailed pouring the composite solution into a 10 ml syringe lined with a Millipore HV filter disc with a pore size of 0.45 μm and purging the solution. The composite collected on the Millipore disc was then flushed with excess toluene. The Millipore disc containing the SWNTs was allowed to dry, and then it was removed from the syringe and placed in a sample bottle

containing 10 ml of toluene. The contents of the sample bottle were placed in the sonic bath (ULTRA Sonick 57X, 230 W) at medium power for 2 hours, after which the Millipore disc was removed. The solution containing the washed SWNTs was then drop-cast onto a glass surface and allowed to dry under ambient conditions for 24 hours.

5.3 Results and Discussion

Fluorescence Spectroscopy

Moving from right to left across Figure 5.1, the first sample shown contains the solvent, toluene, only. The second sample contains LV-SWNT in toluene allowed to settle for a period of less than 24 hours, whereupon the LV-SWNT were found to precipitate out of solution. The third contains LV-SWNT and *p*-terphenyl in toluene. The presence of *p*-terphenyl in a solution clearly enhances the solubility of LV-SWNT in the solvent. The composite solution is black and translucent and exhibits a good degree of stability as there has been no indication of the LV-SWNT precipitating out of solution over the past five years. Similar results were observed when anthracene was added to a solution of LV-SWNT in toluene with the stability of the suspension again exceeding five years.

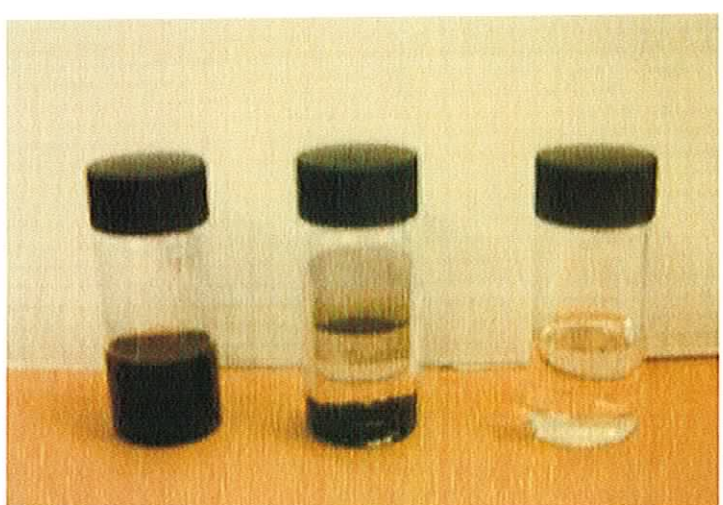

Figure 5.1 Moving from right to left the first sample bottle contains the solvent toluene (far right), the second sample bottle contains LV-SWNT in toluene (middle) and finally the third sample bottle contains the composite solution (far left) which is composed of the solvent toluene, LV-SWNT and *p*-terphenyl.

The formation of a stable suspension in the composite solution as indicated in Figure 5.1 was attributed to the interaction between the PAHs and LV-SWNT. This observation was investigated further and additional samples were prepared where one contained toluene, another contained a 2.5 x 10^{-3} M solution of *p*-terphenyl in toluene and a third contained a composite solution of 2.5 x 10^{-3} M *p*-terphenyl in toluene with LV-SWNT added at a 1:1 w/w ratio, as shown in Figure 5.2. The samples were simultaneously exposed to ultraviolet light and the following was observed: No visible fluorescence was observed for toluene or the composite sample while fluorescence was observed for the 2.5 x 10^{-3} M *p*-terphenyl solution. The above experiment was repeated for anthracene and similar results were obtained (see Figure 5.3). The observation was investigated spectroscopically and the results are depicted in Figures 5.4 and 5.5 and are discussed below.

Figure 5.2 Fluorescence of a sample of toluene (far right), 2.5 x 10^{-3} M of *p*-terphenyl in toluene (middle) and the composite solution containing a composite solution of 2.5 x 10^{-3} M *p*-terphenyl in toluene with LV-SWNT added at a 1:1 w/w ratio (left). It is clear that the interaction between the LV-SWNT and *p*-terphenyl in solution results in the quenching of the fluorescence of *p*-terphenyl.

Toluene Anthracene Composite

Figure 5.3 Fluorescence of a sample of toluene, 3.0 x 10^{-3} M of anthracene in toluene and the composite solution containing a composite solution of 3 x 10^{-3} M anthracene in toluene with LV-SWNT added at a 1:1 w/w ratio. It is clear from the composite sample that the interaction between the LV-SWNT and anthracene in solution results in the quenching of the fluorescence of anthracene.

The fluorescence of *p*-terphenyl before and after the addition of LV-SWNT in a 1:1 w/w ratio is depicted in Figure 5.4. In the absence of LV-SWNT, *p*-terphenyl exhibits an emission maximum at 345 nm, but the addition of LV-SWNT to the solution of *p*-terphenyl results in an emission red-shift of the emission maximum of *p*-terphenyl of approximately 20 nm. No emission red-shift in the fluorescence of *p*-terphenyl was observed up to concentrations of ~1 x 10^{-2} M in the absence of LV-SWNT so the fluorescence red-shift of *p*-terphenyl may be attributed to an increase in the effective conjugation of the molecule on interaction with LV-SWNT.

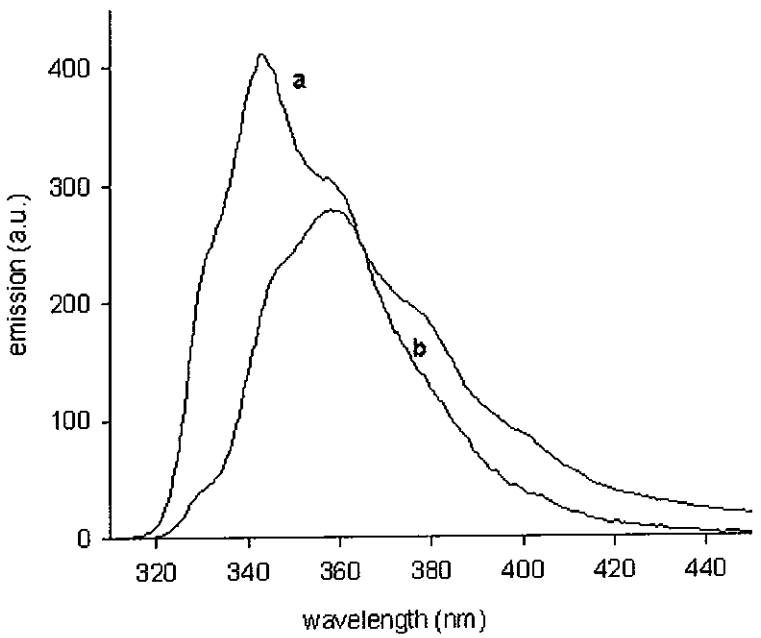

Figure 5.4 Fluorescence of *p*-terphenyl in the absence (a) and presence (b) of LV-SWNT at a concentration of 2.5 x 10^{-3} M in toluene. The intensity of spectrum (b) has been increased by a factor of ten to emphasise the fluorescence red-shift of *p*-terphenyl as a result of the interaction with LV-SWNT.

As described in Chapter 3, *p*-terphenyl is classed as an unconstrained PAH with three phenyl rings connected by C-C single bonds. When *p*-terphenyl is dissolved in toluene at the appropriate concentrations, the phenyl rings possess a torsion angle of ~25° with respect to each other and, as described in Chapter 3, the torsion angle affects the delocalisation of the π electrons. If *p*-terphenyl were to map *via* a face-face interaction with the LV-SWNT, the phenyl rings would align themselves so that the torsion angle across the C-C bond becomes 0° resulting in the molecule adapting a planar conformation (Cote *et al.*, 2001; Cote, 2003). The structural change would induce an increase in the effective conjugation which is then expressed in the fluorescence spectrum of *p*-terphenyl as an emission red-shift. The absence of an emission red-shift in solutions containing only *p*-terphenyl at these concentrations implies that the observed shift is a result of planarisation of *p*-terphenyl upon interaction with LV-SWNTs.

In addition to the emission red-shift, the fluorescent emission from the *p*-terphenyl of the composite solution is significantly quenched. The quenching in fluorescence of *p*-terphenyl resulting from the interaction with LV-SWNT at a 1:1 w/w ratio was investigated over a concentration range of 4.0×10^{-4} and 2.5×10^{-3} M and it was found that the fluorescence was quenched by ~90% within this range.

Figure 5.5 shows the fluorescence of anthracene in toluene in the absence and presence of LV-SWNT at a concentration of 3.0×10^{-4} M. The fluorescence of anthracene exhibits a quenching behaviour similar to *p*-terphenyl, but there is no significant spectral red-shift observed. The slight fluorescence shifting of the blue edge was found to be concentration dependent and is attributable to the re-absorption of the fluorescence emission. The spectral profile and wavelengths at ~405 and ~428 nm appear unaffected by concentration or the addition of LV-SWNT. In Chapter 3, it was described how anthracene like *p*-terphenyl, is comprised of three phenyl rings. However anthracene unlike *p*-terphenyl is classed as a constrained PAH as the rings are fused (share a C-C bond). Therefore it does not have the ability to adapt additional conformations. The natural structure of anthracene is planar and therefore the π electrons are already delocalised to a maximum so it is not possible to increase the effective conjugation of the molecule further. With this in mind no fluorescence red-shift for anthracene was to be expected on interaction with LV-SWNT.

Similar to *p*-terphenyl, the quenching of fluorescence of anthracene as a result of the interaction with LV-SWNT at a 1:1 w/w ratio was investigated for concentrations in the range from 5×10^{-4} to 3×10^{-3} M. It was found that the fluorescence was quenched by an average of ~20% within the range studied.

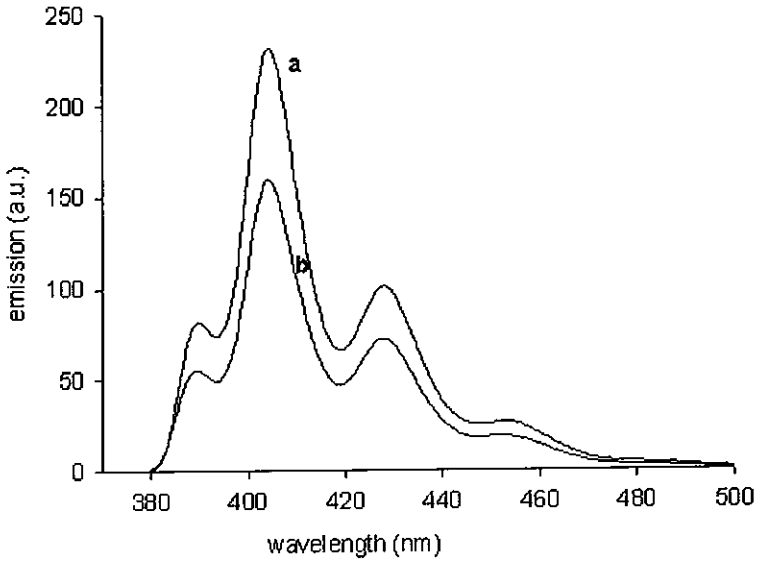

Figure 5.5 Fluorescence of anthracene in the absence (a) and presence (b) of SWNT at a concentration of 3 x 10^{-4} M in toluene. The spectrum (b) intensity has been increased by a factor of ten to emphasise that unlike p-terphenyl no fluorescence red-shift of anthracene was observed as a result of the interaction with SWNT.

The fluorescence studies point strongly to a mapping of the PAH molecules onto the SWNT surface *via* π -π stacking. There is so far no evidence of charge transfer between the PAHs and the SWNTs and the quenching of the fluorescence is most likely due to an energy transfer to the SWNTs *via* vibrational coupling (Henderson *et al.*, 2000).

Raman Spectroscopy

Raman scattering is a valuable tool to investigate the vibrational properties of, and thus characterise, a sample of SWNTs. Figure 4.12 in Chapter 4 shows a typical Raman spectrum for a SWNT bundle in the range 100 -1800 cm^{-1} taken with a 514.5 nm laser excitation line. Both the RBM centered at ~200 cm^{-1}, and the G-line centered at ~1580 cm^{-1} were discussed as well as the Raman spectra of anthracene and *p*-terphenyl (Figures 4.10 and 4.11 respectively) (Jorio *et al.*, 2002; Kuzmany *et al.*, 2001; Rao *et al.*, 1997). Figure 5.6 compares the Raman spectra of the untreated LV-SWNT (Figure 5.6 (a)), pristine *p*-

terphenyl powder (Figure 5.6 (b)), and a composite sample derived from a 1:1 w/w ratio of SWNT/*p*-terphenyl at a concentration of 2.5 x 10^{-3} M solution (Figure 5.6 (c)) taken at a laser excitation of 514.5 nm. The composite spectrum in Figure 5.6 (c) is in some ways a combination of the untreated LV-SWNT and the PAH material but unique modes not accounted for in either the LV-SWNT or the PAH spectra are present. Therefore the composite spectrum maybe considered to be a unique compound. Comparing Figure 5.6 (a) and (c), the characteristic SWNT modes such as the G-line centered at ~1591 cm^{-1} and the RBMs centered at ~200 cm^{-1} are present in the composite spectrum and these Raman modes do not appear to be enhanced or damped due to interaction with *p*-terphenyl. In Figure 5.6 (b) and Figure 5.6 (c), a number of the pristine *p*-terphenyl Raman modes are significantly damped, and these modes are assigned to the ring vibrations and ring stretches at ~770 and ~1271 cm^{-1} respectively. The damped vibrational modes are attributed to the restriction of the vibrations when the π electrons of the *p*-terphenyl molecule interact with the LV-SWNT. The mode at approximately 1600 cm^{-1} in Figure 5.6 (b), represents the conjugated carbons in *p*-terphenyl and this vibrational mode is damped by the tangential stretching of the LV-SWNT in the composite spectrum of Figure 5.6 (c). Most interesting of all in the composite spectrum is the number of new modes evident that are not present in the spectra of Figure 5.6 (a) or Figure 5.6 (b). These new modes are centered at 750, 1092, and 1440.9 cm^{-1} and are indicated by the arrows in Figure 5.6. To account for the origin of the new modes it is suggested that the modes are IR active modes which become Raman active as a result of the interaction that takes place between the LV-SWNT and PAHs. There are IR active modes at 750, 1092, and 1440.9 cm^{-1} for the PAHs (Chapter 4). The molecule *p*-terphenyl is known to have an intense IR peak at approximately 750 cm^{-1} which is due to C-H out-of-plane deformation of the aromatic ring, an in-plane C-H deformation at 1092 cm^{-1} and a C-C aromatic ring stretch at 1440 cm^{-1}. The unique Raman modes in the composite spectrum may thus be explained by IR modes that become Raman active when both the PAHs and the SWNTs interact as a result of the relaxation of selection rules due to changes in local symmetry and (or) environment which is consistent with the interaction with tubes. Similar finding were previously reported (Dalton, 1999). Figure 5.6 (d) is discussed later in the chapter.

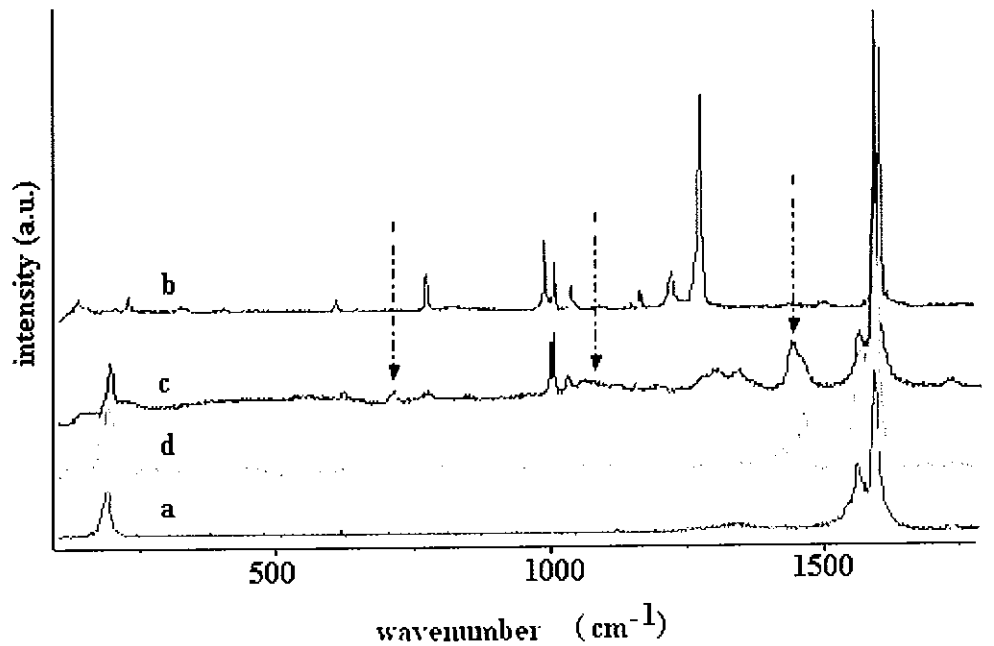

Figure 5.6 Raman spectra of (a) untreated SWNT, (b) pristine *p*-terphenyl, (c) composite spectrum of SWNT and p-terphenyl at 2.5 x 10^{-3} M at a 1:1 w/w ratio and (d) the washed composite sample at laser excitation 514.5 nm.

Similar behaviour is observed for the anthracene composite at a concentration of 3.0 x 10^{-4} M, as shown in Figure 5.7. The composite spectrum in Figure 5.7 (c) again shows the characteristic SWNT modes as well as some features attributable to anthracene. However, as before there are features of the anthacene composite spectrum that do not appear in the Raman spectra of either the pristine LV-SWNT (Figure 5.7 (a)) or anthracene (Figure 5.7 (c)). As before, it is proposed that these unique modes at 450, 1120, and 1440 cm^{-1} are attributed to anthracene IR modes that become Raman active upon interaction. The modes at 450, 1120, and 1440 cm^{-1} may be assigned to anthracene IR C-H out-of-plane ring vibrations, an in-plane C-H deformation and a C-C aromatic ring stretch respectively (Chapter 4).

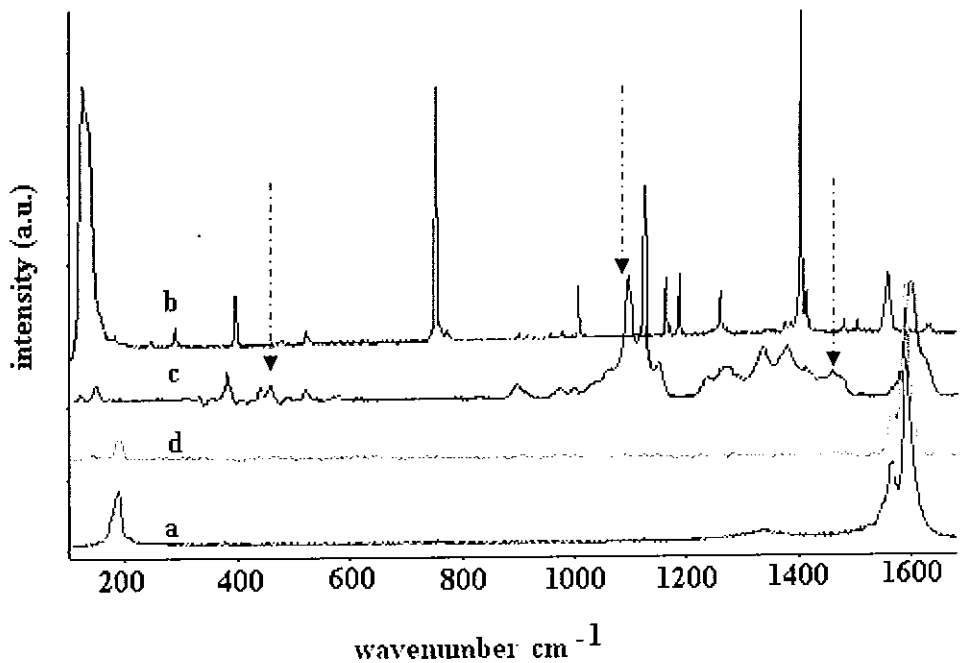

Figure 5.7 Raman spectra of (a) untreated SWNT, (b) pristine anthracene, (c) composite spectrum of SWNT and anthracene at 3 x 10^{-3} M at a 1:1 w/w ratio and (d) washed composite sample at laser excitation 514.5 nm.

Figures 5.6 (d) and 5.7 (d), show the Raman spectra of the residual as a result of washing the respective composite samples with excess toluene. In both cases, the spectra of the washed LV-SWNT samples were found to be similar to the untreated LV-SWNT spectra, indicating that the LV-SWNT can be recovered from the composites and that the PAHs are indeed interacting with SWNTs *via* adsorption. In the case of anthracene, the process appears fully reversible, whereas in the *p*-terphenyl there is a remnant mode at 1440 cm^{-1}. Such a feature has been observed for other systems although its presence to date has not been explained (Keogh *et al.*, 2004).

Although no structural selectivity has been demonstrated, the process may be looked upon as a possible purification technique for SWNTs as results show that the PAHs interact and solubilise SWNTs within the impure sample allowing side products to precipitate out. Once in solution the purified SWNTs may be retrieved by subsequent washing. The consideration of the procedure as a purification technique is further supported by the decrease in the D-

line in the wash composite samples. The D-line as stated in Chapter 4 is attributed to amorphous carbon and defective carbon. In the washed composite samples in Figures 5.6 (d) and 5.7 (d), the D-line is notably reduced compared with the untreated LV-SWNT in Figures 5.6 (a) and 5.7 (a).

A similar study to that discussed for Figure 5.6 and 5.7 was conducted using 632.8 nm as a laser excitation line as a source. The spectra are depicted in Figures 5.8 and 5.9. Figures 5.8 and 5.9 compare the Raman spectra of the untreated LV-SWNT (Figures 5.8 (a) and 5.9 (a)), pristine PAH powder (Figure 5.8 (b) Figure 5.9 (b)), and a composite sample derived from a 1:1 w/w ratio of SWNT/*p*-terphenyl at a concentration of 2.5 x 10^{-3} M (Figure 5.8 (c)) and SWNT/anthracene at a concentration of 3 x 10^{-3} M (Figure 5.9 (c)). The composite spectrum in Figure 5.8 (c) does not exhibit any obvious unique modes. The composite spectrum in Figure 5.9 (c) is in some ways a combination of the untreated LV-SWNT and the PAH material but unique modes not accounted for in either the LV-SWNT or the PAH spectra are also observed as marked in the figure. Therefore the composite spectrum in Figure 5.9 (c) may be considered to be a unique compound. The composite spectra are not as clearly defined for excitation line 632.8 nm as they are at 514.5 nm and appear considerably damped when Figures 5.6 and 5.7 are compared with Figures 5.8 and 5.9. Therefore this damped effect may explain why no unique modes for the composite spectrum in Figure 5.8 (c) were observed.

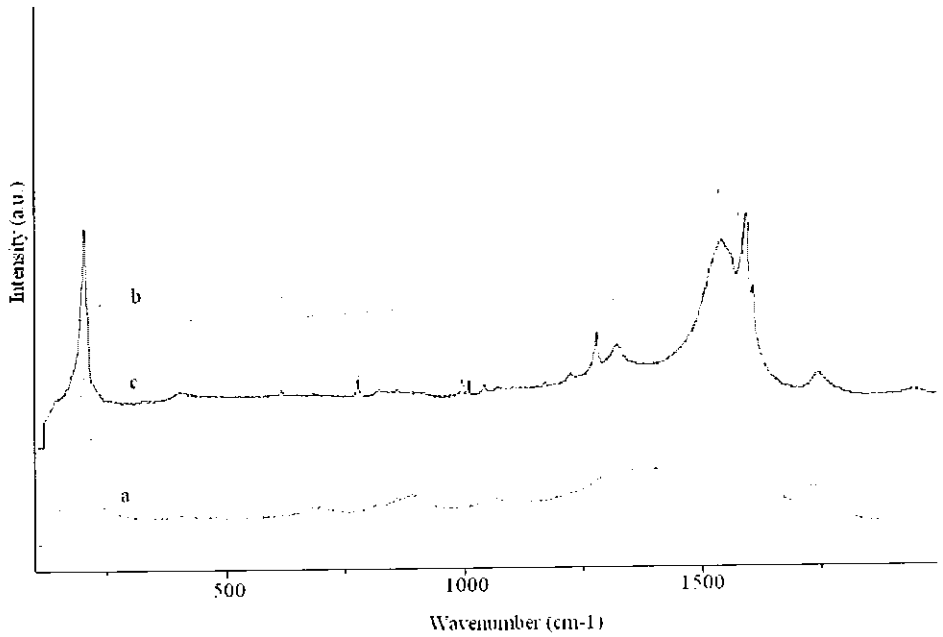

Figure 5.8 Raman spectra of (a) the untreated LV-SWNT, (b) the pristine *p*-terphenyl powder and (c) the composite sample at 2.5 x 10^{-3} M a 1:1 w/w ratio of *p*-terphenyl/SWNT at laser excitation 632.8 nm.

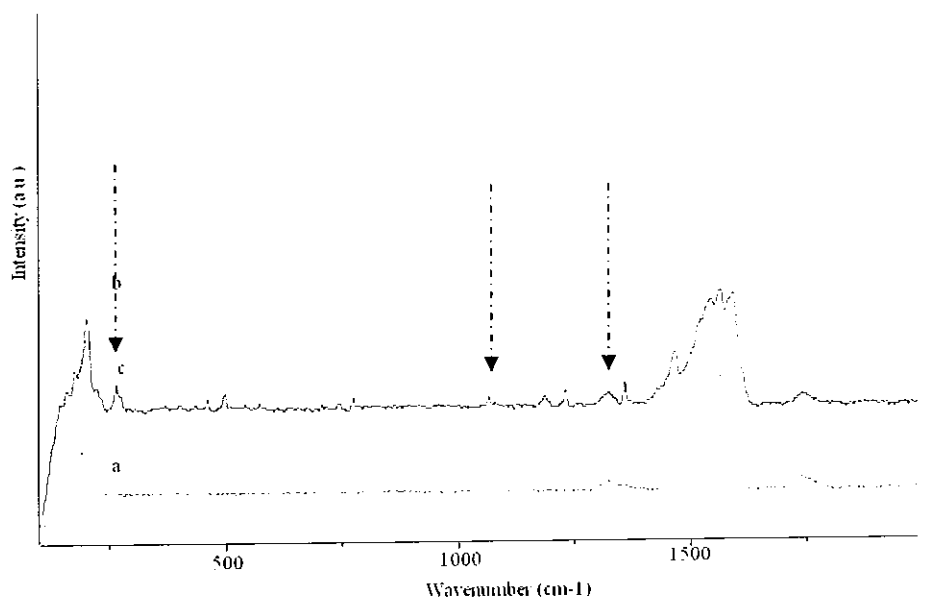

Figure 5.9 Raman spectra of (a) the untreated LV-SWNT, (b) the pristine anthracene powder and (c) the composite sample at 3 x 10^{-3} M as a 1:1 w/w ratio of anthracene/SWNT at laser excitation 632.8 nm.

Summary

The PAH molecules anthracene and *p*-terphenyl have been shown to enhance the solubility of SWNTs in toluene and purify the LV-SWNT sample *via* what is proposed to be a π-π interaction between the PAH molecules and LV-SWNT. The interaction between the two components allowed the LV-SWNT to be solubilised while the amorphous carbon and catalyst particles precipitated out. The composite solutions were found to be stable for prolonged periods of time with no indications of LV-SWNT settling observed in over five years. Spectroscopic investigations such as fluorescence and Raman point toward a mapping of the PAHs onto the LV-SWNT surface. Fluorescence spectroscopy indicated that an interaction occurred due to quenching in the PAH fluorescence on the addition of LV-SWNT to the solution. In addition, evidence that *p*-terphenyl molecules were mapping onto the LV-SWNT surface was provided from the red shift observed, attributable to a change in the torsion angle from 25° to 0°. This notion of an interaction occurring was further supported by Raman spectroscopic studies which showed the Raman of a composite spectrum contained unique vibrational modes. Washing the composite sample with excess toluene resulted in a Raman spectrum similar to that of the untreated LV-SWNT spectrum. The Raman spectrum of the washed composite provided clear evidence that the PAHs are interacting with the SWNTs and not any of the unwanted side products in the untreated LV-SWNT sample therefore the PAHs can be used to purify untreated samples of SWNTs. Chapter 6 follows on from Chapter 5 by investigating whether structurally selective interactions take place between the PAHs and SWNTs as well as the notion that the PAH molecules debundle the SWNTs on interaction *via* spectroscopic methods. A model is used to determine the concentration range where aggregated and isolated PAHs and SWNTs interact with microscopic techniques used to support spectroscopic results.

REFERENCES

Bahr, J.L., Mickelson, E.T., Bronikowski, J., Smalley, R.E., Tour, J.M., (2001), "Dissolution of small diameter single walled carbon nanotubes in organic solvents", *Chem. Comm.*, 193 - 194.

Branca, C., Corasaro, C., Frusteri, F., Magazu, V., Mangione, A., Migliardo, F., Wanderlingh, U., (2004), "Structural and vibrational properties of carbon nanotubes by TEM and infrared spectroscopy", *Diamond and Related Materials,* 13, 1249 - 1253.

Chen, J., Hamon, M.A., Hu, H., Chen, Y., Rao, A.M., Eklund ,P.C., Haddon, R.C., (1998), "Solution properties of single-walled carbon nanotubes", *Science*, 282, 95 - 98.

Cote, M., Haynes, P.D., Molteni, C., (2001), "Boron Nitride polymers: Building blocks for organic electronic devices", *Phys. Rev. B.*, 63, 125207-1-125207-4.

Cote, M., (2003), "Electronic properties of polymers", *Physics in Canada*, 59, 1-15.

Dalton, A.B., (1999), "Morphological influences on the excited state dynamics of conjugated polymers", PhD thesis, Trinity College, Dublin, Ireland.

Dalton, A.B., Blau, W.B., Chambers, G., Coleman, J.N., Henderson, K., Lefrant, S., McCarthy, B., Stephan, C., Byrne, H.J., (2001), "A functional conjugated polymer to process, purify and selectively interact with single walled carbon nanotubes", *Synth. Metals*, 121, 1217 - 1218.

Dalton, A.B., Stephens, C., Coleman, J.N., McCarthy, B., Ajayan, P.M., Lefrant, S., Bernier, P., Blau, W.B., Byrne, H.J., (2000), "Interaction of a semiconjugated organic polymer with single-wall nanotubes", *J. Phys. Chem. B.*, 104, 10012 - 10016.

Duesberg, G.S., Blau, W., Byrne, H.J., Muster, J., Burghard, M., Roth, S., (1999), "Chromatography of carbon nanotubes", *Synth. Metals*, 103, 2484 - 2485.

Hedderman, T.G., Keogh, S.M., Chambers, G., Byrne H.J., (2004), "Solubilisation of SWNT with organic dye molecules", *J. Phys. Chem B.*, 108, 18860 - 18865.

Henderson, K., Kretsch, K.P., Drury, A., Maier, S., Davey; A.P., Blau W., Byrne, H.J., (2000), "Correlation of molecular vibrational structure with luminescent quantum yields", Proceedings of ICEL2, Sheffield, *Synth. Metals*, 111, 559 – 561.

Jorio, A., Souza Filho, A.G., Dresselhaus, G., Dresselhaus, M.S., Swan, A.K., Unlu, M.S., Goldberg, B.B., Pimenta, M.A., Hafner, J.H., Lieber, C.M., Saito, R., (2002), "G-band resonant Raman study of 62 isolated single-wall carbon nanotubes", *Phy. Rev. B.*, 65, 155412-1 – 155412-9.

Keogh, S.M., Hedderman, T.G., Gregan, E., Farrell, G., Chambers, G., Byrne, H.J., (2004), "Spectroscopic analysis of single-walled carbon nanotubes and semiconjugated polymer composites", *J. Phys. Chem. B.*, 108, 6233 – 6241.

Kuzmany, H., Plank, W., Hulman, M., Kramberger, Ch., Gruneis, A., Pichler, Th., Peterlik, H., Kataura, H., Achiba, Y., (2001), "Determination of SWCNT diameters from the Raman response of the radial breathing mode", *Eur. Phys. J. B.*, 22, 307 - 320.

Niyogi, S., Hu, H., Hamon, M.A., Bhowmik, P., Zhao, B., Rozenzhak, S.M. Chen, J., Itkis, M.E., Meier, M.S., Haddon, R.C., (2001), "Chromatographic purification of soluble single-walled carbon nanotubes", *J. Am. Chem. Soc.*, 123, 733 - 734.

Rao, A.M., Richter, E., Bandow, S., Chase, B., Eklund, P.C., Williams, K.A., Fang, S., Subbaswamy, K.R, Menon, M., Thess, A., Smalley, R.E., Dresselhaus, G., Dresselhaus, M.S., (1997), "Diameter-selective Raman scattering from vibrational modes in carbon nanotubes", *Science*, 275, 187 - 191.

CHAPTER 6 - A STUDY OF THE INTERACTION OF SWNT WITH *P*-TERPHENYL AND ANTHRACENE

6.1 Introduction

When SWNTs are produced they are almost always in the form of bundles (Dresselhaus *et al.*, 2001; Nikolaev *et al.*, 1999; Thess *et al.*, 1996). It has been shown that the properties of the bundles are inferior to those of individual SWNTs (Cadek *et al.*, 2004; Coleman *et al.*, 2004.; Strong *et al.*, 2003.; Thess *et al.*, 1996; Tomenak *et al.*, 2000). For many application purposes it is necessary to have access to isolated SWNTs where particular electronic characteristic may be routinely selected. Organic molecules such as PAHs have been shown to solubilise SWNTs but the degree of debundling has not been demonstrated. The aim of this study is to probe the interactions between PAHs and SWNTs and investigate the debundling of SWNTs through spectroscopic methods such as fluorescence and Raman (Hedderman *et al.*, 2006). This chapter will also explore the potential of selective interaction between the PAHs and SWNTs through fluorescence concentration dependent studies and Raman. Chapter 2 discussed and depicted the three possible structures that can exist within a sample of SWNTs, armchair, zigzag and chiral. The proposal of this work is that if the PAHs were to exhibit structural selectivity, anthracene and *p*-terphenyl would preferentially map to armchair and zigzag SWNTs respectively.

6.2 Sample Preparation

Solutions in toluene in the range of ~4.5 x 10^{-12} and ~2.5 x 10^{-3} M for *p*-terphenyl and ~1.0 x 10^{-8} and ~3.0 x 10^{-3} M for anthracene were prepared. LV-SWNT gifted from Rice University (Tubes@rice, Houston, TX) were added to all PAH solutions in a 1:1 by weight ratio (w/w) SWNT/PAH except where specified. Both the PAHs and composite solutions were characterised using fluorescence (Perkin Elmer LS55) and Raman spectroscopy (Instruments SA LabRam 1B). AFM (Asylum MFP-3D) was used to image SWNTs from

the composite solutions. As described in Chapter 4 the dynamic tapping method was used with the appropriate tips which were NSC 36/ No AL and had a spring constant of 5 N/M (see www.spmtips.com).To reduce the error incurred by the large tip size with respect to the smaller SWNTs the same tip was used to measure all LV-SWNT samples to prevent variation in the estimated SWNT width.

All PAH and composite solutions were sonicated using a sonic tip (ultrasonic processor VCX, 750 Watts) for 30 s and allowed to settle for 24 hours, after which the supernatant liquid from the composite samples was carefully withdrawn. The suspensions were then allowed to settle for a further 24 hours before being characterised by the various spectroscopic methods mentioned above. The precipitate was found to be relatively rich in SWNTs therefore as described in Chapter 5 the dispersion concentrations quoted are as prepared. For Raman measurements at 632.8 and 514.5 nm and AFM imaging, the samples were dispersed on an activated silicon surface and this involved covering the surface in a layer of 3-aminopropyl tri-ethoxysilane (APTES) for 10 minutes followed by rinsing with deionised water and then drying at room temperature. The activated surface was then immersed in the composite solution for approximately three weeks and once removed from the solution the surface was rinsed with deionised water and allowed to dry at room temperature before being characterised. The purpose of activating the silicon surface was to prevent aggregation of the SWNTs as previous dropcasting methods on an inactive surface has shown. Aggregation is prevented as a result of the interaction between the SWNTs and alkylamine chain. The alkylamine chains act like 'sticky fingers' and interact with the SWNTs in solution and fix them to the activated surface.

6.3 Results and Discussion

Fluorescence Spectroscopy

To gain a better understanding of the behaviour of the PAHs and their interaction with SWNTs the fluorescence behaviour over a broad range of concentrations in toluene was probed. Two sets of samples were prepared, one set contained just the PAHs and the second

set contained similar concentrations of the PAH/LV-SWNT at a 1:1 w/w ratio. Comparing the fluorescence of the PAHs in the absence and presence of LV-SWNT yields information on the effect concentration has on the behaviour of the PAHs, for example the concentration range where isolated and aggregated PAHs exist. The study also reveals the effect the LV-SWNT exerts on the PAHs.

The fluorescence of *p*-terphenyl in the absence (filled black circles) and presence of LV-SWNT (filled grey squares) is depicted in Figure 6.1 within the concentration range of ~2.5 x 10^{-9} and ~2.5 x 10^{-3} M. With respect to *p*-terphenyl (filled black circles) the concentration dependence of the fluorescence fits well to a linear increase between ~2.5 x 10^{-9} and ~4 x 10^{-6} M denoted by the black solid line (note the plot is depicted in a linear/log axes format). Within a concentration range of ~4 x 10^{-6} to ~2.5 x 10^{-3} M the fluorescence of *p*-terphenyl deviates from linearity and this deviation is evident both at the spectral maximum and on the red side of the spectrum, indicating that it is not due to re-absorption. Therefore the deviation is attributed to the formation of aggregates of *p*-terphenyl which causes quenching of the fluorescence.

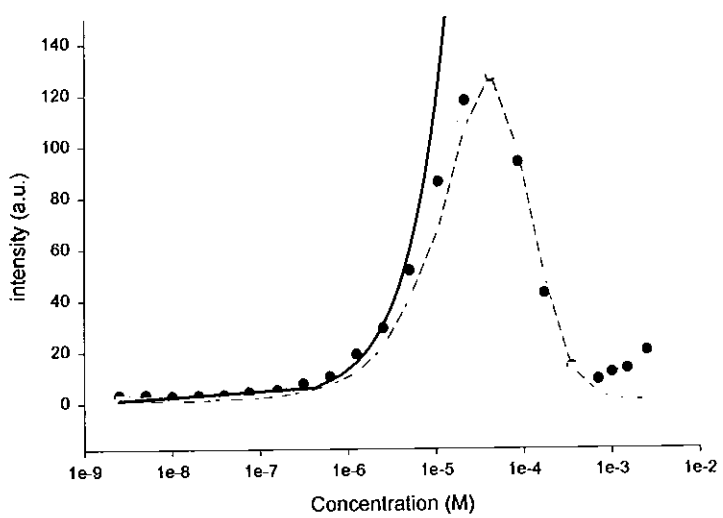

Figure 6.1 Fluorescence of *p*-terphenyl in the absence (filled black circles) and presence of LV-SWNT (filled grey squares) as a function of concentration on a linear/log axis. The solid black line represents a linear fit to the data. Deviation from the fit is as a result of aggregation of the PAH molecules.

Upon the addition of LV-SWNT (filled grey squares) to the *p*-terphenyl solutions at a 1:1 w/w ratio, the composite fluorescence trend appears similar to that of the *p*-terphenyl discussed in the previous paragraph, within the concentration range of ~2.5 x 10^{-9} and ~2 x 10^{-5} M. Between a concentration of ~4 x 10^{-5} M and 2 x 10^{-4} M the composite fluorescence deviates from linearity and relative to the fluorescence of *p*-terphenyl the composite fluorescence is now in excess. The additional fluorescent intensity observed is explained by the de-stacking of the *p*-terphenyl aggregates as the fluorescence data suggests that the presence of SWNTs interferes with and hinders the aggregation process of *p*-terphenyl. This affect on aggregation indicates that *p*-terphenyl preferentially interacts with LV-SWNT and suggests that the binding energy of *p*-terphenyl/LV-SWNT is greater than the binding energy between *p*-terphenyl/*p*-terphenyl. This suggestion is not unreasonable since theoretical binding energy calculations and thermal desorption studies discussed later in this chapter for graphitic structures and PAHs show that the PAH/graphite interactions are more favourable than the PAH/PAH interactions (Chakarova and Schroder, 2005; Lee *et al.*, 2005; Zacharia *et al.*, 2004).

The fluorescence of anthracene in the absence (filled black circles) and presence of LV-SWNT (filled grey squares) is depicted in Figure 6.2. The profile is similar to that of *p*-terphenyl in Figure 6.1. An interesting point to note is that the concentration for the aggregation of anthracene is greater than the concentration for the aggregation of *p*-terphenyl, Figure 6.1. Theoretical calculations report that as the number of carbons in the PAH increases the binding energy also increases and this is expressed *via* fluorescence spectroscopy by the formation of aggregates at lower concentrations (Chakarova and Schroder, 2005; Lee *et al.*, 2005; Zacharia *et al.*, 2004). In the previous paragraph it was discussed how LV-SWNT interfered with aggregation of *p*-terphenyl and how the additional fluorescence of the *p*-terphenyl in the composite sample indicated this. However with regards to anthracene this region is not as distinct. Evidence of where the interference process begins can be seen in the region of ~1 x 10^{-4} M marked by the additional fluorescence of the anthracene in the composite solution compared to fluorescence of anthracene at a similar concentration but otherwise quenching of the composite solutions is observed. This result may be indicative of the fact that once the anthracene aggregates are

dispersed by the LV-SWNT the free anthracene molecules interact with the surrounding LV-SWNT hence quenching would be observed whereas it appears that *p*-terphenyl preferentially remain free in solution. The length of the two molecules is considered in order to explain this observation. The molecule *p*-terphenyl is a longer molecule than anthracene, with lengths of 1.2 nm and 0.72 nm respectively along the long axis of the molecule. Therefore less *p*-terphenyl molecules compared with anthracene could map to the surface of LV-SWNT of a similar size.

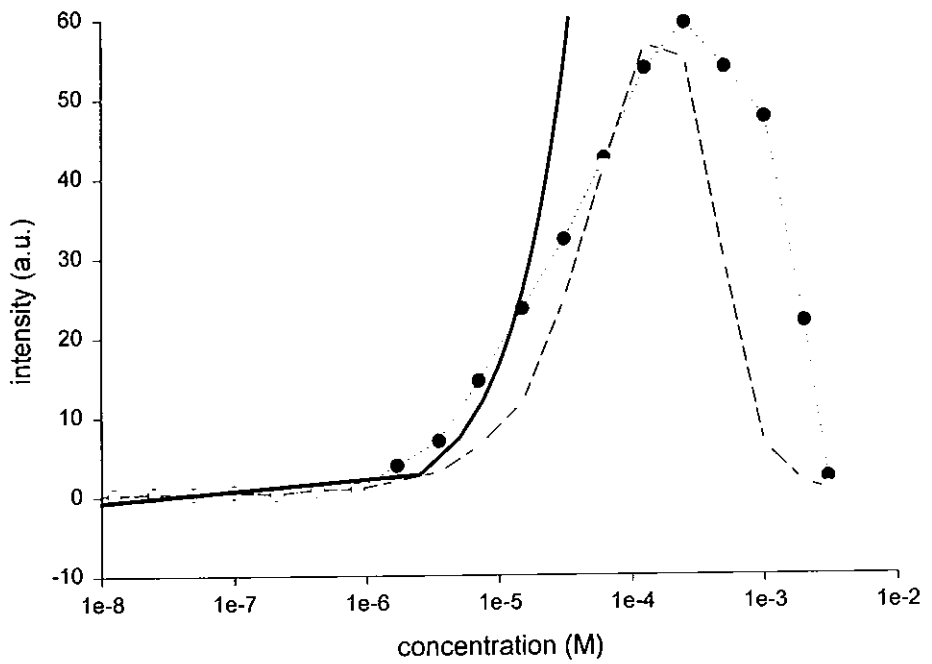

Figure 6.2 Fluorescence of anthracene in the absence (filled black circles) and presence of LV-SWNT (filled grey squares) as a function of concentration on a linear/log axis. The solid black line represents a linear fit to the data. Deviation from the fit is as a result of aggregation of the PAH molecules.

Theoretical models based on the interaction of PAH dimers and graphite have been described in the literature (Chakarova and Schroder, 2005; Lee *et al.*, 2005; Zacharia *et al.*, 2004). The binding energies for PAH dimers and PAH/graphite were calculated using

methods such as van der Waals density functional, Hartree-Fock and Redhead to name a few. The structure of a SWNT is that of a curved single layer of graphite and these structures are commonly found in bundles (Chapter 2). The quasi crystalline arrangements of close packed SWNTs, like graphite, are held together by a long range van der Waals interaction and with both graphite and SWNTs possessing similar structural properties it is reasonable to expect similar degrees of interaction between both structures with the PAHs. As previously stated, an increase in the carbon number of PAHs increases the binding energy between PAHs, with larger PAHs having similar interlayer distances and binding energies comparable to graphite (Chakarova and Schroder, 2005; Lee *et al.*, 2005; Zacharia *et al.*, 2004). The binding energy between a PAHs and graphite are predicted to be larger than the binding energy of the corresponding PAH dimer. For example the binding energy of benzene and naphthalene on a graphite surface were calculated to be 0.5 eV and 0.9 eV respectively (Chakarova and Schroder, 2005). The cohesive energy is determined by thermal desorption measurements of PAHs on the graphite surface, and reveals a binding energy of 52 +/- 5 meV per carbon atom with a contribution of 27 meV per hydrogen (Zacharia *et al.*, 2004). The binding energies for the PAH dimers were estimated to be 0.1 eV, 0.17 eV and 0.25 eV for benzene, naphthalene and anthracene respectively (subject to stacking arrangement) (Chakarova and Schroder, 2005). With the available theoretical and experimental data it is reasonable to say that the SWNT/PAH binding energy is greater than the PAH/PAH binding energy as indicated in Figures 6.1 and 6.2.

To summarise, the data from Figures 6.1 and 6.2 indicate the concentration range where aggregated and isolated PAHs exist as well as providing evidence that the interactions between the LV-SWNT and PAHs is stronger and more favourable than that between the PAH molecules. To continue, the next study investigates the concentration range where bundled and debundled LV-SWNT may be found.

The following study employs a model constructed by Coleman *et al.* (2004). The model is based on the adsorption/desorption equilibrium of SWNTs and a fluorescent organic molecule as a function of concentration as a result of the quenching of the fluorescence of the molecule when bound to the SWNT (which is deemed to have zero fluorescence when

bound). The ratio of the maximum fluorescence intensity of the composite sample, that contains bound and unbound fluorescent organic molecules, and the maximum fluorescence of the organic molecular solution, comprised solely of unbound fluorescent organic molecules, is plotted as a function of concentration. The model presented is for low concentrations and when the system is in equilibrium the adsorption rate equals the desorption rate. The adsorption rate was calculated theoretically; representing a SWNT (or bundle) as a cylinder and assuming that any molecule that reaches the SWNT adsorbs *via* van der Waals interactions. The desorption rate was shown to follow first order kinetics and was calculated as a function of the number of bound molecules per unit volume, the volume of solution occupied by one SWNT. As the fraction of free fluorescent molecules changes over the concentration range studied, a relationship is derived whereby the change in the fraction of free fluorescent organic molecules could be described by a characteristic concentration C_0 and SWNT concentration C_{NT}. Determination of the characteristic concentration allows the indirect measurement of the fluorescent organic molecule/SWNT binding energy and an elucidation of the binding scheme can be achieved.

Equation 6.1 represents the equilibrium at which the adsorption rate equals the desorption rate, where N_F is the number of free molecules, N_B is the number of bound molecules, Fl_{comp} is the fluorescence of the composite and Fl_{mol} is the fluorescence of the fluorescent organic molecule which gives the fraction of free organic molecules in solution. The model is derived for 1:1 w/w ratios and so for all concentrations the partial SWNT concentration, C_{NT}, equals the partial molecular concentration, C_m.

$$N_F/(N_F + N_B) = 1/(1 + C_{NT}/C_0) = Fl_{comp}/Fl_{mol} \qquad \text{Equation 6.1}$$

The study by Coleman *et al.*, (2004), demonstrated that the model was well behaved in 1:1 w/w ratio up to concentrations of 1 x 10^{-7} kg/m^3 in the case of the polymer composites of SWNTs and a single value for the characteristic concentration (C_0) of 2.2 x 10^{-5} kg/m^3 was obtained (Coleman *et al.*, 2004). A binding energy of 1.1 eV per molecule of poly [*m*-

phenylenevinylene-*co*-(1,5-dioctyl-2,6-naphthlene vinylene)] (p*m*NV) was calculated with deviation from the ideal behaviour resulting from changes in the SWNT size i.e. the bundle size, and as a result the model could elucidate the concentration range where the polymer interacted with debundled SWNTs and bundled SWNTs of varying diameter.

C_0 is an important term as it contains much of the information about the dynamics of the system as shown in Equation 6.2. Parameters such as the binding energy (E_B) and the SWNT bundle surface area (A_{bun}) describe the delicate nature of the system. It indicates that the C_0 value is sensitive to such things as the viscosity of the solvent and the size of the PAH which are accounted for in the diffusion (D) term. The varying SWNT bundle mass (ρ_{bun}) and surface area A_{bun} are recognised as factors that will affect the position of the C_0 curve and this in turn is expressed in the E_B because the two parameters are closely related. Other parameters within the equation are υ which represents a pre-exponential factor and describes desorption of organic molecules from graphitic surfaces whereas f, the space integral describes the probability of the organic molecule reaching the SWNT bundle and adsorbing to it.

$$C_0 = \pi^2 \upsilon \rho_{bun} A_{bun} e^{-E_B/kT} /(48Df) \qquad \text{Equation 6.2}$$

The model developed by Coleman *et al.*, (2004) was adapted for this research and the data from Figures 6.1 and 6.2 were used and Equation 6.1 was applied resulting in a plot of the fraction of free PAHs as a function of concentration as shown in Figures 6.3 and 6.6.

Proceeding from left to right across Figure 6.3, from approximately ~4 x 10^{-12} to ~6 x 10^{-9} M the fluorescence of the fraction of free p-terphenyl decreases steadily with increasing concentration, the PAHs and LV-SWNT exist in dynamic equilibrium with bound PAHs and LV-SWNT. The data within this concentration range fits well to the solid line which is a plot of Equation 6.1, resulting in a C_0 value of ~4 x 10^{-10} M. This value indicates that below ~4 x 10^{-10} M in toluene isolated p-terphenyl molecules are interacting with

debundled LV-SWNT of a constant surface area. Deviation from the fit indicates that one or more of the parameters are changing and the change is attributed to an increase in the SWNT bundle surface area (Coleman *et al.*, 2004). The concentration at which deviation from the fit occurs is observed at approximately ~6 x 10^{-9} M. Within the concentration range of ~6 x 10^{-9} to ~2.5 x 10^{-5} M, isolated *p*-terphenyl molecules are interacting with SWNTs of increasing surface area. From a concentration of approximately 2.5 x 10^{-5} M upwards, the fluorescence of the fraction of free *p*-terphenyl decreases due to the interaction between bundles of LV-SWNT and aggregated *p*-terphenyl.

An important point to mention is that in the low concentration range the fluorescence is found to exceed 1.0 and this is assumed to be the result of a background effect due to the SWNT.

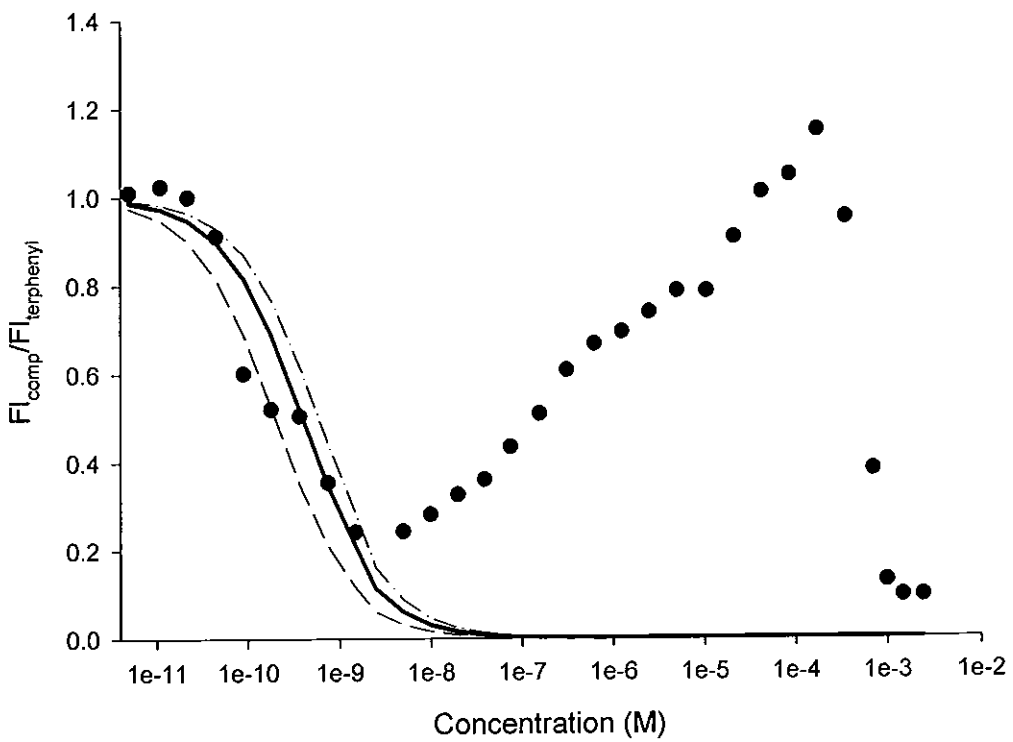

Figure 6.3 Graph of the fraction of unbound *p*-terphenyl as a function of concentration. The solid line is a fit to Equation 6.1. The black solid line gives a C_0 value of ~4 x 10^{-10} M and the best fit to the data. To the left of the solid line, the dashed line gives a C_0 value of ~2 x 10^{-10} M and to the right of the solid line the dashed dotted line gives a C_0 value of ~6 x 10^{-10} M.

As previously stated, C_0 contains a large amount of information with regards to the chemical system. Data found to fit the calculated C_0 value indicates that the parameters within the system are all constant. Figure 6.4 shows the calculated C_0 values for all concentrations for the case of *p*-terphenyl. C_0 is seen to have an approximately constant value of 2 x 10^{-9} M up to a concentration of 2 x 10^{-9} M, whereupon it increases steadily with concentration up to a value of 4 x 10^{-2} M for a concentration of 3 x 10^{-3} M. Variation of C_0 is attributed to an increase in the LV-SWNT bundle surface area and AFM of the SWNTs from composite solutions of varying concentrations was employed to investigate the LV-SWNT bundle surface area. Figure 6.4 superimposes the AFM bundle size results on the C_0 plot and it is well correlated indicating that indeed the deviation from the model is due to varying SWNT bundle size.

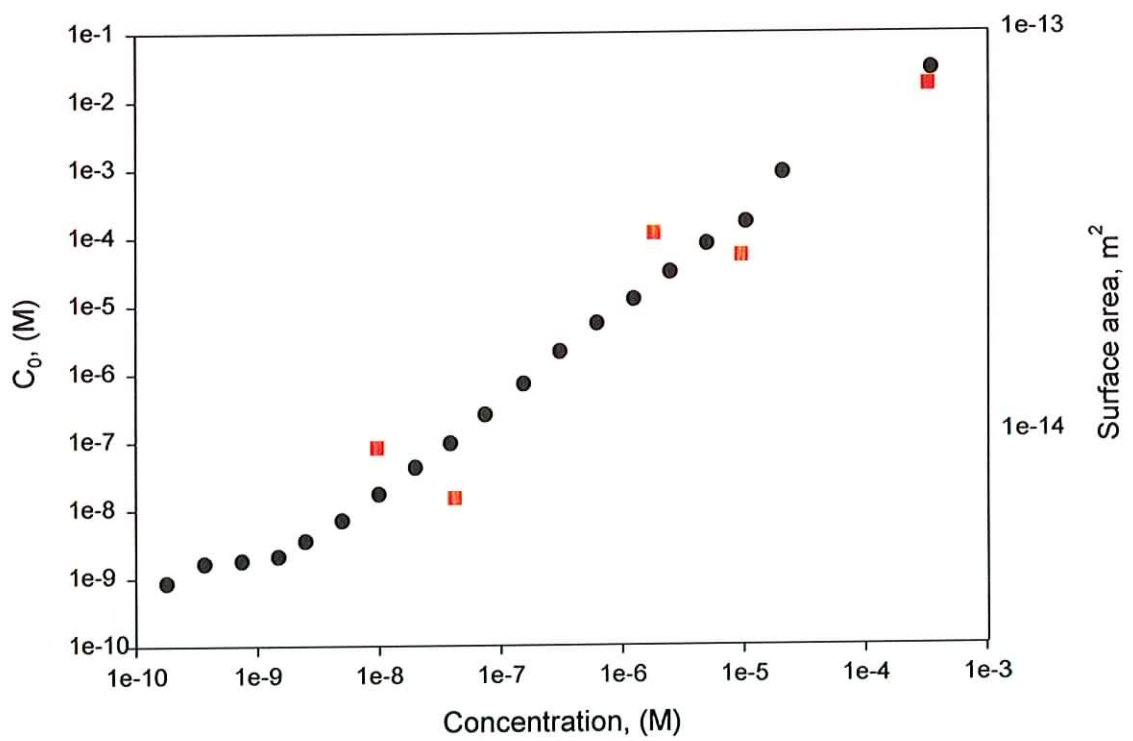

Figure 6.4 C_0 values (black circles) as a function of concentration and AFM study (red squares) results for the changing bundle size of LV-SWNT surface area as a result of the changing concentration in the presence of *p*-terphenyl where the ratio of SWNT/*p*-terphenyl is at a 1:1 w/w ratio.

Figure 6.5 (a) and (b) depict AFM images of the untreated LV-SWNT and composite sample of *p*-terphenyl/LV-SWNT at 1 x 10^{-8} M respectively. Comparing both images it is evident the bundle surface area of the LV-SWNT has decreased on average from 3.7 x 10^{-13} m^2 to 9.6 x 10^{-15} m^2 on going from Figure 6.5 (a) to Figure 6.5 (b). The surface area of the SWNTs was calculated using the surface area of an elongated box given the shape of the bundle from the dimensions taken from AFM data. Table 6.1 lists the average dimensions of the untreated LV-SWNT and the *p*-terphenyl and anthracene composites at the stated concentrations.

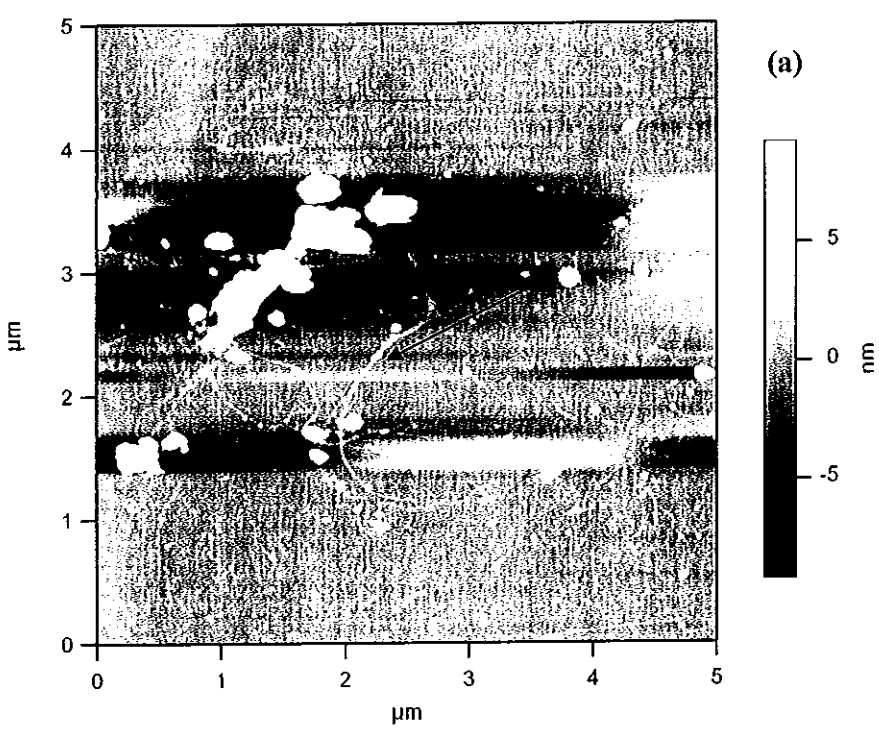

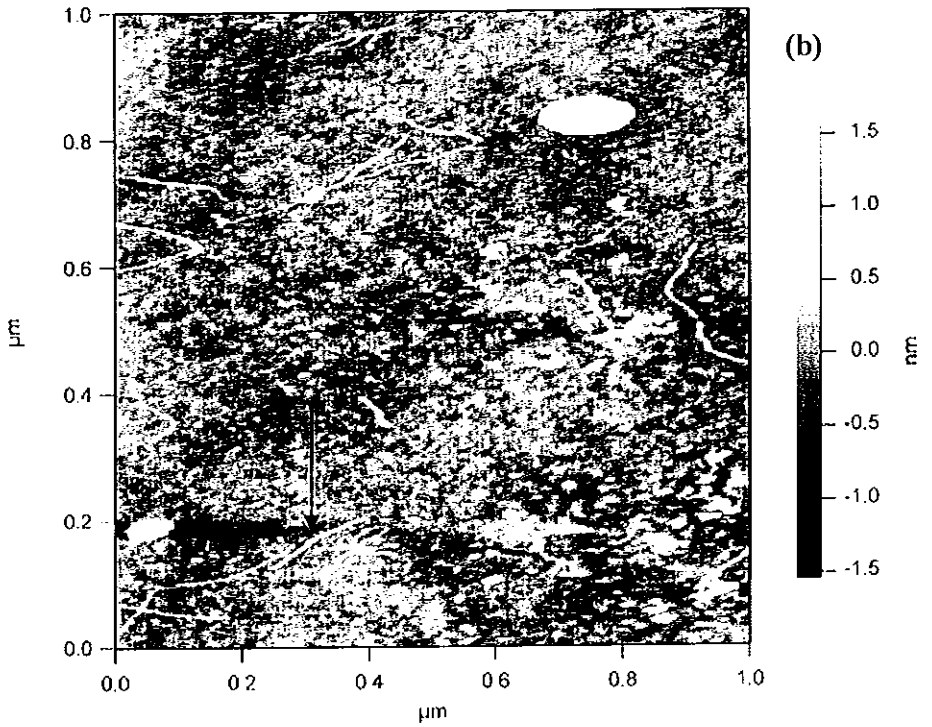

Figure 6.5 AFM of (a) untreated LV-SWNT and (b) 1 x 10^{-8} M of *p*-terphenyl/LV-SWNT. The string like features represent SWNTs (as indicated by the markers) and are between 3-6 nm in height and 5 µm in length for the untreated SWNTs sample and 0.6-1.2 nm in height and 400 nm for the composite sample.

Table 6.1 Observed AFM dimensions of LV-SWNT in their untreated state, at 1 x 10^{-8} M for *p*-terphenyl composite at a 1:1 w/w ratio and at 1 x 10^{-6} M for anthracene composite at a 1:1 w/w ratio. Note that all dimensions are averaged.

SWNT Sample	length	width	height
Untreated LV-SWNT	5,000 nm	33 nm	4 nm
1 x 10^{-8} M LV-SWNT/*p*-ter	400 nm	11 nm	1 nm
1 x 10^{-6} M LV-SWNT/ant	400 nm	23 nm	1.2 nm

A similar study modeling the interaction of LV-SWNT with the fluorescent organic molecule, anthracene was conducted and results are depicted in Figure 6.6. Proceeding from left to right across Figure 6.6, from approximately ~1 x 10^{-9} to ~3.5 x 10^{-6} M the fluorescence of the fraction of free anthracene decreases steadily with increasing concentration, the free PAHs and LV-SWNT exist in dynamic equilibrium with bound PAHs and LV-SWNT. The data in this concentration region fits well to the solid line which is a plot of Equation 6.1 resulting in a C_0 value of ~2 x 10^{-6} M. As was the case for *p*-terphenyl in Figure 6.3, isolated anthracene is interacting with debundled LV-SWNT below the value of approximately ~2 x 10^{-6} M. Deviation from the fit is attributed to the change in the LV-SWNT bundle surface area. It is worth mentioning that the C_0 value is considerably higher compared to the value obtained for the *p*-terphenyl of 4 x 10^{-10} M in Figure 6.3. From this result it may be interpreted that anthracene in comparison to *p*-terphenyl is more prolific at dispersing SWNT bundles due to the rigid, planar structure of anthracene which may allow a relatively easy intercalation between bundles and once there it can act as a nanospacer and disperse the bundled SWNT. In the case of *p*-terphenyl, its natural structure is non planar and its three phenyl rings are rotated with respect to each other. Therefore, it may be argued that it is more difficult for *p*-terphenyl to penetrate the SWNT bundle and disperse the SWNT within the bundle (Cote *et al.*, 2001).

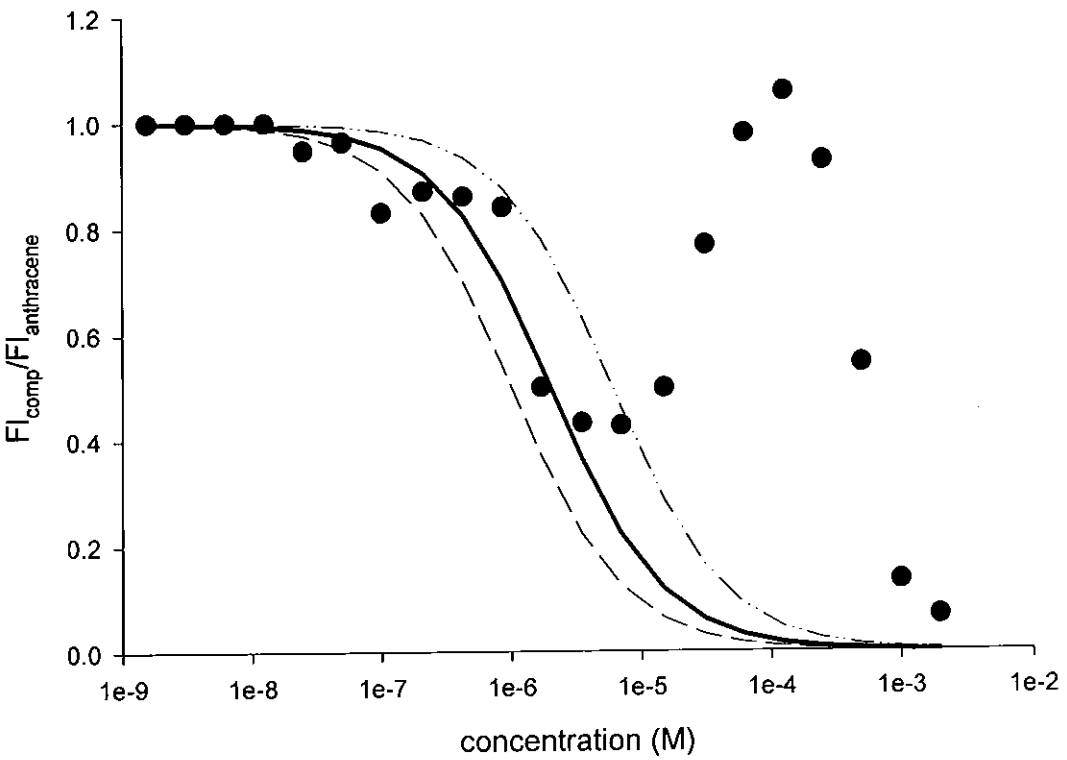

Figure 6.6 Graph showing the fraction of unbound anthracene as a function of concentration. The solid line is a fit to Equation 6.1. The black solid line gives a C_0 value of ~2 x 10^{-6} M and the best fit to the data. To the left of the solid line, the dashed line gives a C_0 value of ~1 x 10^{-6} M and to the right of the solid line the dashed dotted line gives a C_0 value of ~6 x 10^{-6} M.

A similar study which gave similar outcomes to that depicted in Figure 6.4 was conducted for anthracene. A graph depicting the C_0 as a function of concentration as well as the AFM results showing a decrease in bundle size is given Figure 6.7. It shows the calculated C_0 values for all concentrations for the case of anthracene. C_0 is seen to have an approximately constant value of 2 x 10^{-6} M up to a concentration of 1 x 10^{-6} M, whereupon it increases steadily with concentration up to a value of 4 x 10^{-3} M for a concentration of 1 x 10^{-4} M. Variation of C_0 is attributed to an increase in the LV-SWNT bundle surface area and AFM of the SWNT from composite solutions of varying concentrations is employed to investigate the LV-SWNT bundle surface area. Figure 6.7 superimposes the AFM bundle size results on the C_0 plot and it is well correlated with Figure 6.6 indicating that indeed the

deviation from the model is due to varying SWNT bundle size and also that the C_0 parameters cease to change dramatically below 1 x 10^{-6} M. The bundle surface area has changed from 3.7 x 10^{-13} m^2 for the untreated sample to 1.9 x 10^{-14} m^2 for a concentration of 1 x 10^{-6} M for anthracene with SWNTs present at a 1:1 w/w ratio.

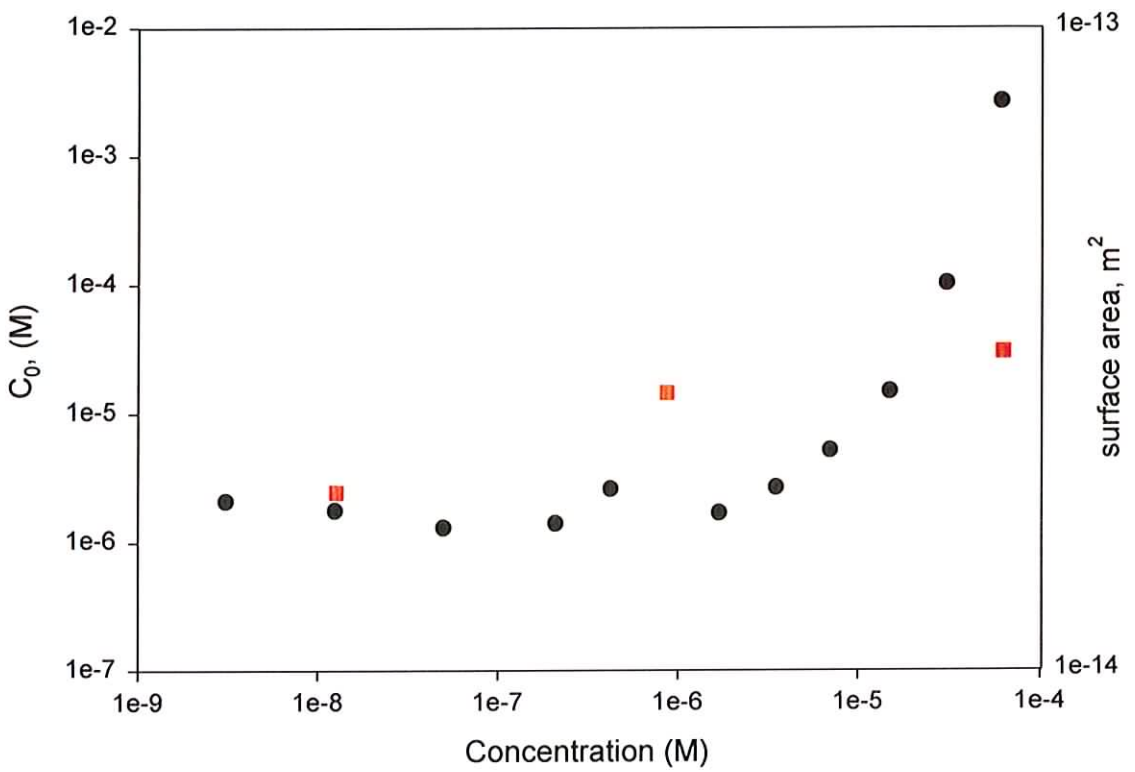

Figure 6.7 C_0 values (black circles) as a function of concentration and AFM study results (red squares) for the changing bundle size of LV-SWNT as a result of the changing concentration in the presence of anthracene where the ratio of SWNT/anthracene is at a 1: 1 w/w ratio.

Table 6.2 Calculated parameters for Equation 6.2. The references indicate the sources of the equations used to calculate the values and in the case of υ and *f* the values were taken directly from the literature.

Parameters	Values	Source of equations and data
υ	10^{18} Hz	(Zacharia *et al.*, 2004)
D *p*-terphenyl	7.6 x 10^{-10} m^2/s	(See Appendix A, Table 1)
D anthracene	1.2 x 10^{-9} m^2/s	(See Appendix A, Table 1)
ρ_{bun}	1.33 x 10^3 kg/m^3	(See Appendix A, Table 2)
f	800	(Coleman *et al.*, 2004)
A_{bun} for *p*-terphenyl	9.6 x 10^{-15} m^2	(Table 6.1)
A_{bun} for anthracene	1.9 x 10^{-14} m^2	(Table 6.1)

Using Equation 6.2 and the C_0 values from Figures 6.3 and 6.6 the binding energies for both anthracene and *p*-terphenyl to debundled SWNTs were calculated. It is noted that C_0 was proportional to the inverse exponent of E_B and the point of deviation of the model from the data appears inversely related to the binding energy, with the polymer characterised by Coleman *et al.*, (2004), following this trend. The C_0 value for *p*-terphenyl was calculated to be 4 x 10^{-10} M and that for anthracene to be 2 x 10^{-6} M. These values along with those in Table 6.2 were inserted into Equation 6.2 and the resulting binding energies were calculated to be 1.1 and 0.9 eV for *p*-terphenyl/SWNT and anthracene/SWNT respectively. A true comparison of results obtained for the anthracene and *p*-terphenyl composites in this study to the polymer p*m*NV by Coleman *et al.*, (2004), cannot be made as different systems are involved. The system studied by Coleman *et al.*, (2004), was comprised of chloroform, HiPco SWNTs and p*m*NV and the systems studied here comprised of toluene, LV-SWNT and small organic molecules. Different systems will affect the C_0 value and consequently the E_B. However from the results it may be deduced that *p*-terphenyl binds more tightly to the LV-SWNT compared to anthracene and is less effective in intercalating and dispersing the LV-SWNT. Using the values quoted by Chakarova and Schoder (2005) of 52 +/-5 meV

per carbon atom and 27 meV per hydrogen atom the binding energy of anthracene and *p*-terphenyl to graphite was calculated to be 1.0 eV and 1.3 eV respectively, a difference of 0.2 eV between both models. These values are in good agreement with those obtained from the model.

While obtaining the data for Figure 6.1 it was noted that the fluorescence emission maximum of *p*-terphenyl on interaction with LV-SWNT showed the red-shift described in Chapter 5 for concentrations greater than ~3 x 10^{-5} M and this is depicted in Figure 6.8. However no fluorescence red-shift of *p*-terphenyl in the absence of LV-SWNT was observed at the concentrations probed in Figure 6.1 (Hedderman *et al.*, 2004). AFM data shows that the SWNT bundle size increases with increasing concentration therefore it was considered that perhaps the change in the fluorescence red-shift of *p*-terphenyl was related to the change in the SWNT bundle size. This research question was explored both theoretically and experimentally (Meehan *et al.*, 1980; Zacharia *et al.*, 2004). The interactions of PAHs with graphite have been theoretically modelled by Zacharia *et al.* (2004) and Meehan *et al.*, (1980). It was calculated that a graphene sheet with a coverage of less than one monolayer of PAHs (PAH having less than five rings), have a parallel orientation with the graphene surface. Coverage, approaching one monolayer or greater sees the PAHs adapt an orientation with the molecular planes perpendicular (or tilted) to the surface of the graphene sheet so as to satisfy the steric and entropic constraints. These calculations were verified by spectroscopic methods such as Nuclear Magnetic Resonance (NMR) and thermal desorption spectroscopy (Meehan *et al.*, 1980; Zacharia *et al.*, 2004). In this study a parallel orientation of *p*-terphenyl would be expressed by a red-shift in an emission spectrum due to planarisation whereas a perpendicular orientation would not require planarisation and thus would result in a negligible red-shift (Cote *et al.*, 2001; Hedderman *et al.*, 2004). It is proposed therefore that, as the bundle size of the LV-SWNT decreases with decreasing concentration, the coverage of *p*-terphenyl on the surface of the bundle increases until there is sufficient coverage to trigger a change in orientation of the PAHs. This alteration in orientation is expressed by a decrease in fluorescence red-shift with decreasing concentration as depicted in Figure 6.8.

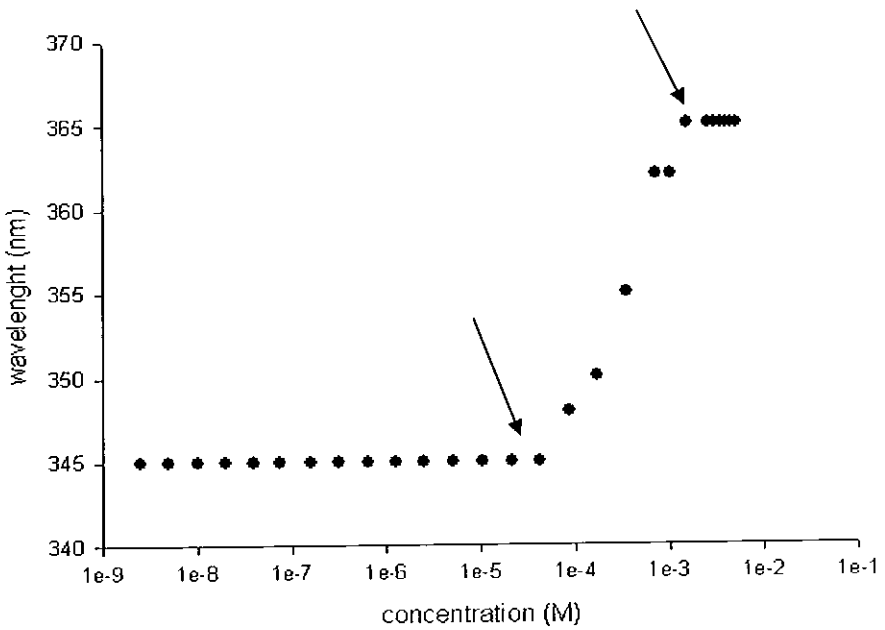

Figure 6.8 Fluorescence red-shift of the emission maximum of *p*-terphenyl as a function of concentration in the presence of LV-SWNT at a 1:1 w/w ratio.The markers indicate the concentration range where the fluorescence emission maxium of *p*-terphenyl in the composite sample increases as a function of concentration.

To further explore and support the evidence that the fluorescence red-shift of *p*-terphenyl is related to the bundle surface area of SWNTs the following experiment was conducted. Using the information from Figure 6.8 the SWNT bundle size at a concentration of 1.5 x 10^{-3} M and 1.5 x 10^{-5} M for *p*-terphenyl in toluene of with SWNT present at a 1:1 w/w ratio were measured *via* AFM. The concentrations were chosen because as indicated by the markers in Figure 6.8 no fluorescence red-shift in the emission maxium of *p*-terphenyl was detected at a concentration of 1.5 x 10^{-5} M for *p*-terphenyl in the composite sample (with SWNT present at a 1:1 w/w ratio to *p*-terphenyl) and a red-shift in the fluorescence emission maximum of *p*-terphenyl from 345 nm to 365 nm was observed in the composite sample at a concentration of 1.5 x 10^{-3} M for *p*-terphenyl. The mass of SWNTs present in the composite samples were 3.5 x 10^{-2} mg and 3.5 mg for a concentration of 1.5 x 10^{-5} M and 1.5 x 10^{-3} M respectively. AFM studies estimated the SWNT bundle surface area to be

6.2×10^{-14} m^2 when a mass of 3.5 mg of LV-SWNT was added to a 10 ml solution of *p*-terphenyl in toluene and 2.5×10^{-14} m^2 when a mass of 3.5×10^{-2} mg was added to 10ml solution of *p*-terphenyl in toluene at a 1:1 w/w ratio.

Two sets of *p*-terphenyl solutions in toluene with concentrations between ~2.5×10^{-6} and ~2.5×10^{-3} M were prepared. To the first set of solutions a mass of 3.5 mg LV-SWNT was added. To the second set of solutions a mass of 3.5×10^{-2} mg LV-SWNT was added. In both cases the mass of SWNT is approximately constant at the specified weights while the concentration of *p*-terphenyl varies. Figure 6.9 depicts the results of the interaction between LV-SWNT of a certain bundle surface area and *p*-terphenyl as a function of concentration. The fluorescence of *p*-terphenyl, where the average SWNT bundle surface area was calculated to be 6.2×10^{-14} m^2 (filled circles), is observed to red-shift at all concentrations, suggesting a parallel orientation of the PAH. For the second set of soultions (clear circles) where the average SWNT bundle surface area was 2.5×10^{-14} m^2 no fluorescence red-shift of *p*-terphenyl was observed suggesting a perpendicular orientation on interaction. The experiment concludes that LV-SWNT surface area can play a role in the orientation of *p*-terphenyl.

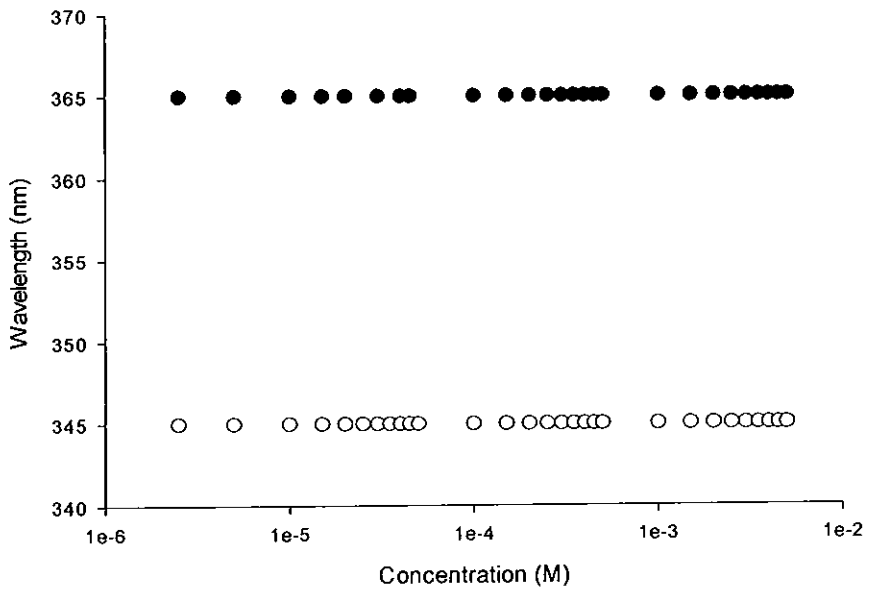

Figure 6.9 Fluorescence red-shift of *p*-terphenyl as a function of concentration in the presence of 3.5 mg of LV - SWNT with an average bundle size 6.2 x 10^{-14} m^2 (black circles) and 3.5 x 10^{-2} mg of LV-SWNT with an average bundle size of 2.5 x 10^{-14} m^2 (clear circles).

Raman Spectroscopy

Raman spectroscopy is used as a tool to further explore the effect of the changing bundle size by probing the RBMs as this frequency region is related to the diameter of SWNTs (Chapter 4). Previous papers report that the debundling of SWNTs is expressed by a change in the RBM profile such as an increase in the frequency. Although a shift in frequency of the RBMs may be interpreted as the debundling of the SWNTs, profile changes are also dependent on the local environment of the SWNTs and the resonant conditions (Duesberg *et al.*, 2000; Fantini *et al.*, 2004; Keogh *et al.*, 2004; Rao *et al.*, 2001). Indeed the resonant conditions have been shown to be dependent on the environment and can be influenced by binding and potentially the nanotube substrate environment (Fantini *et al.*, 2004). Thus binding and substrate may also affect changes in the profile through shifting of the frequencies or the disappearance of features due to changing resonance conditions. This study investigates the effect of the change in the SWNT bundle size as a result of the interaction with the PAHs, anthracene and *p*-terphenyl. The SWNT RBM frequencies are

also probed after the PAHs are removed from the SWNTs to investigate the affect the PAHs exert on the SWNTs and any potential structural selectivity.

Presented in Figure 6.10 (a) are the RBM spectra for untreated LV-SWNT, the *p*-terphenyl composite and the anthracene composite. Figure 6.10 (b) depicts the untreated LV- SWNT and the washed *p*-terphenyl and anthracene composite at a laser excitation of 632.8 nm. The concentrations under investigation in Figure 6.10 are 2.5 x 10^{-3} M for *p*-terphenyl and 3.0 x 10^{-3} M for anthracene with LV-SWNT present in a 1:1 w/w ratio. It is clear from Figure 6.10, (a) that the untreated LV-SWNT sample shows a dominant feature at 191 cm^{-1} with indications of further features at 165 and 215 cm^{-1} and this profile is consistent with the resonance of larger diameter metallic SWNTs (Duesberg *et al.*, 1999; Kataura, *et al.*, 1999; Pimenta *et al.*, 1998a). Comparing the profiles of the anthracene and *p*-terphenyl composite spectra to the untreated LV-SWNT spectrum, it is evident that the overall profile is similar but that the dominant feature originating at 191 cm^{-1} is up-shifted by ~6 cm^{-1} to 197 cm^{-1}.

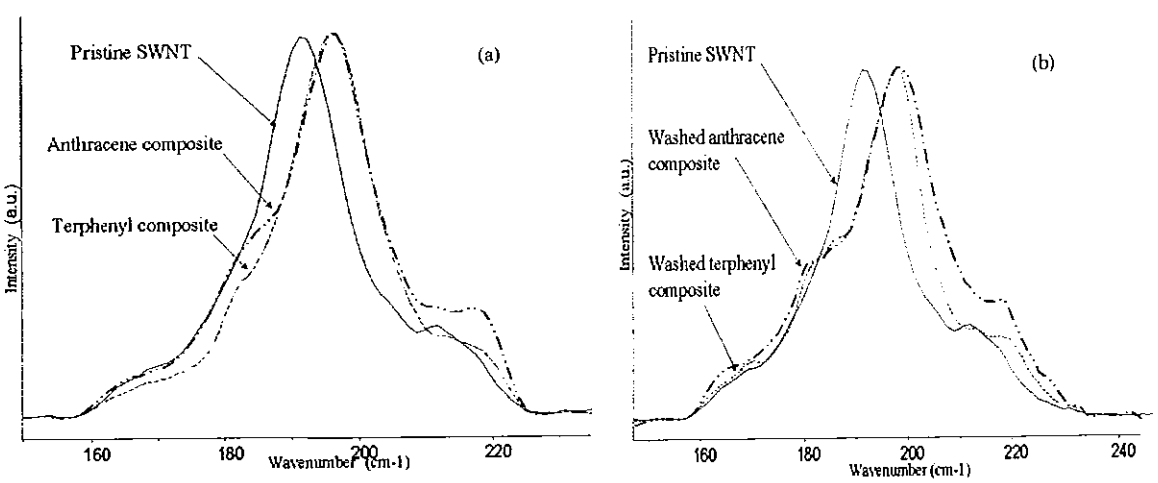

Figure 6.10 Raman spectra showing the RBMs of untreated LV-SWNT and the composite RBMs at 3 x 10^{-3} M anthracene/LV-SWNT and 2.5 x 10^{-3} M *p*-terphenyl/LV-SWNT at a 1:1 ratio w/w PAH/SWNTat laser excitation line 632.8 nm.

The features originating at 165 cm^{-1} and 215 cm^{-1} become relatively more pronounced in both the anthracene and *p*-terphenyl composite spectra. The spectra indicate that anthracene solubilises on the whole, medium diameter LV-SWNT as well as a few smaller and larger diameter LV-SWNT. Compared to the anthracene composite, *p*-terphenyl leans more towards the solubilisation of medium and a fewer larger and smaller diameter LV-SWNT, with the loss of the smaller diameter tubes.

Figure 6.10 (b) shows the untreated LV-SWNT and the washed anthracene and *p*-terphenyl composite RBM. The profiles in Figure 6.10 (b) are similar to that discussed for Figure 6.10, (a) except the profiles of the composite spectra have up-shifted further. Comparing the washed composites with the untreated LV-SWNT sample, a total up-shift of ~8 cm^{-1} is observed for both washed composite samples compared with the untreated LV-SWNT. This is a further shift of 2 cm^{-1} from the composites in Figure 6.10 (a). However an up-shift of 2 cm^{-1} is quite small and thus is not considered significant enough to be attributed to a change in the local environment of the LV-SWNT. What is significant however is the fact that once the PAHs are removed the RBMs do not return to that of the untreated LV-SWNT and also the profile of the washed composites remains unchanged from that of the composite. Studies conducted by Keogh *et al.*, (2004) where the composite spectra of SWNT and P*m*PV are investigated show that when the polymer interacts with the SWNTs the RBMs up-shift but when the polymer is removed the RBMs return to that of the untreated SWNT sample and the profile of the composite RBMs compared to the washed SWNTs differ. Such a result is attributed to the change in the local environment of the SWNTs such as the damping effect exerted by polymer on the SWNTs upon interaction. When the SWNTs are washed the damping effect of the polymer is removed and the RBMs returns to that of the untreated SWNTs with similar profiles. With regards to the PAHs the profile of the RBMs does not change when the PAHs are removed from the LV-SWNT. This indicates that unlike the large P*m*PV polymer molecule the small PAH molecules do not exert a damping effect on the LV-SWNT thus no change in the RBM profile is observed on removal of the PAHs. Infact from Chapter 5 it is evident that the reverse occurs. The composite spectra in Figures 5.6 and 5.7 indicate that it is mainly the PAH Raman modes that are damped on

interaction. The consistent nature of the RBMs in the composite and washed state may be attributed to the selective nature of the PAH molecules.

Although selectivity is hinted at in Figure 6.10, no attempt is made to assign the diameter or chirality of the LV-SWNT. From the fluorescence concentration dependence studies discussed above and the profile of the RBMs (broad profile) the concentration range probed in Figure 6.10 is that of bundled LV-SWNT and aggregated PAHs therefore making it difficult to assign specific diameters.

At 514.5 nm, the incident light is predominantly resonant with non-metallic SWNTs in the untreated SWNT material (Pimenta *et al.*, 1998b). In Figure 6.11 (a) and Figure 6.11 (b), the RBM region is dominated by a feature at 184 cm^{-1} for the untreated LV-SWNT spectrum, with evidence of further features on both sides. A point to note is that the RBM spectra at 514.5 nm do not up-shift to the same extent as they do at 632.8 nm and that the profiles are not as well resolved. In Figure 6.11 (a) the anthracene and *p*-terphenyl composite spectra are up-shifted by ~4 and ~2 cm^{-1}, respectively and the composite profiles are dominated by the feature originating from 184 cm^{-1}. In the case of the anthracene composite, the feature originating from 205 cm^{-1} no longer dominates the spectrum to the extent it did in the untreated LV-SWNT sample therefore there is a loss of small diameter LV-SWNT in the anthracene composite meaning that large and medium LV-SWNT are solubilised by anthracene. The profile of the *p*-terphenyl composite is similar to that of anthracene, but with the additional loss of the feature at ~165 cm^{-1}, the larger diameter LV-SWNT. This result may indicate an increased selectivity by *p*-terphenyl. In Figure 6.11 (b) the washed composite samples upshift by a further ~2 cm^{-1}compared with the composite samples in Figure 6.11 (a).

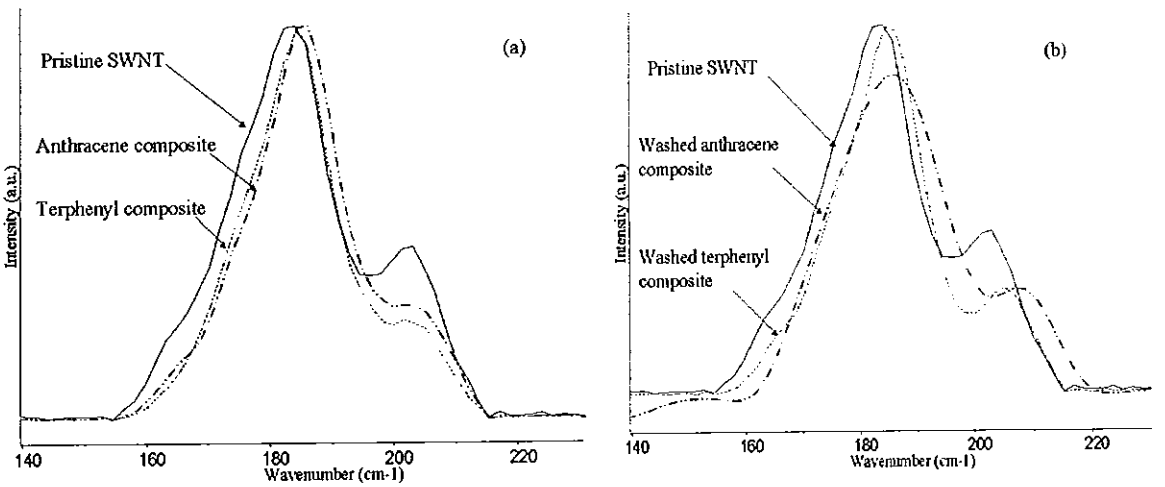

Figure 6.11 Raman spectra showing the RBMs of untreated LV-SWNT and the composite RBMs at 3 x 10^{-3} M anthracene/LV-SWNT and 2.5 x 10^{-3} M *p*-terphenyl/LV-SWNT at a 1:1 w/w ratio PAH/SWNTat laser excitation line 514.5 nm.

Spectroscopic techniques such as fluorescence and Raman and microscopic techniques such as AFM support the proposal that the LV-SWNT bundle size decreases with decreasing concentration. The fraction of free PAH fluorescence models in Figures 6.3 and 6.6 gave an indication as to the concentration range where debundled and bundled LV-SWNT existed. To investigate the selectivity of the PAHs the concentration region where debundled LV-SWNT exist is probed and Equation 4.5 which relates the RBM frequency to the diameter of the SWNTs is employed. After the diameter is determined the structure of the SWNTs are assigned according to models previously published and the selective nature of the PAHs are probed (Jorio *et al.*, 2001, Rols *et al.*, 2000).

Figures 6.12 to 6.15 continue the work from Figures 6.10 and 6.11 and investigate the debundling of SWNTs down to concentrations where fully debundled LV-SWNT exist. The effect of debundling on the RBM frequency and G-line is examined and discussed. Figure 6.12(a) shows the RBM Raman spectrum of untreated LV-SWNT, Figure 6.12 (b) shows the anthracene composite spectrum at 1 x 10^{-6} M, Figure 6.12 (c) shows the anthracene composite spectrum at 1 x 10^{-7} M and Figure 6.12 (d) shows the anthracene

composite spectrum at 1 x 10^{-8} M at laser excitation 632.8 nm. It is important to note that some of the modes observed in Figures 6.12 and 6.14 are due to the activated silicon substrate such as those at 300, 521 and 963 cm^{-1}, the anthracene molecule at 150, 286, 400 cm^{-1} and the APTES at 180 cm^{-1}. To clarify the areas of interest in Figures 6.12 and 6.14 the appropriate modes have been shaded. In Figure 6.12 (a) the central positioning of the RBMs for the untreated SWNTs is ~198 cm^{-1} and subsequently it is found that as the concentration decreases in the composite samples the RBMs up-shift and appear to separate. In Figure 6.12 (b) at 10^{-6} M three distinct RBMs are present, at 198, 225 and 230 $cm^{-1}$and in Figure 6.12 (c) at 10^{-7} M three RBMs are clearly visible, at 198, 235 and 254 cm^{-1}. Comparing Figure 6.12 (b) and (c) the feature at 198 cm^{-1} is less intense when the concentration is decreased and the features at 225 and 230 cm^{-1} in Figure 6.12 (b) have both up-shifted by 15 cm^{-1} and their intensity has increased. In Figure 6.12 (d) at 10^{-8} M three RBMs are again present at 198, 235 and 250 cm^{-1}. Comparing Figure 6.12 (c) and (d) it is evident that there is no further up-shift and RBM are in the same region as they were at in Figure 6.12 (c) at 1 x 10^{-7} M. This may indicate that the LV-SWNT are completely dispersed leaving only debundled SWNT and this result correlates with the plot of the fraction of free anthracene in Figure 6.6. The up-shift observed is very significant and adds further support to the proposal that LV-SWNT debundle with decreasing concentration. From Figure 6.12 it would appear that the LV-SWNT are completely dispersed at ~1 x 10^{-7} M (Figure 6.12 (c)) as the LV-SWNT cease to up-shift further and also it would appear that once dispersed the anthracene molecules interact with SWNTs of specific diameter range. The up-shift is calculated to be 62 cm^{-1} in total on going from the untreated LV-SWNT sample in Figure 6.12 (a) to the 1 x 10^{-7} M composite sample in Figure 6.12 (c).

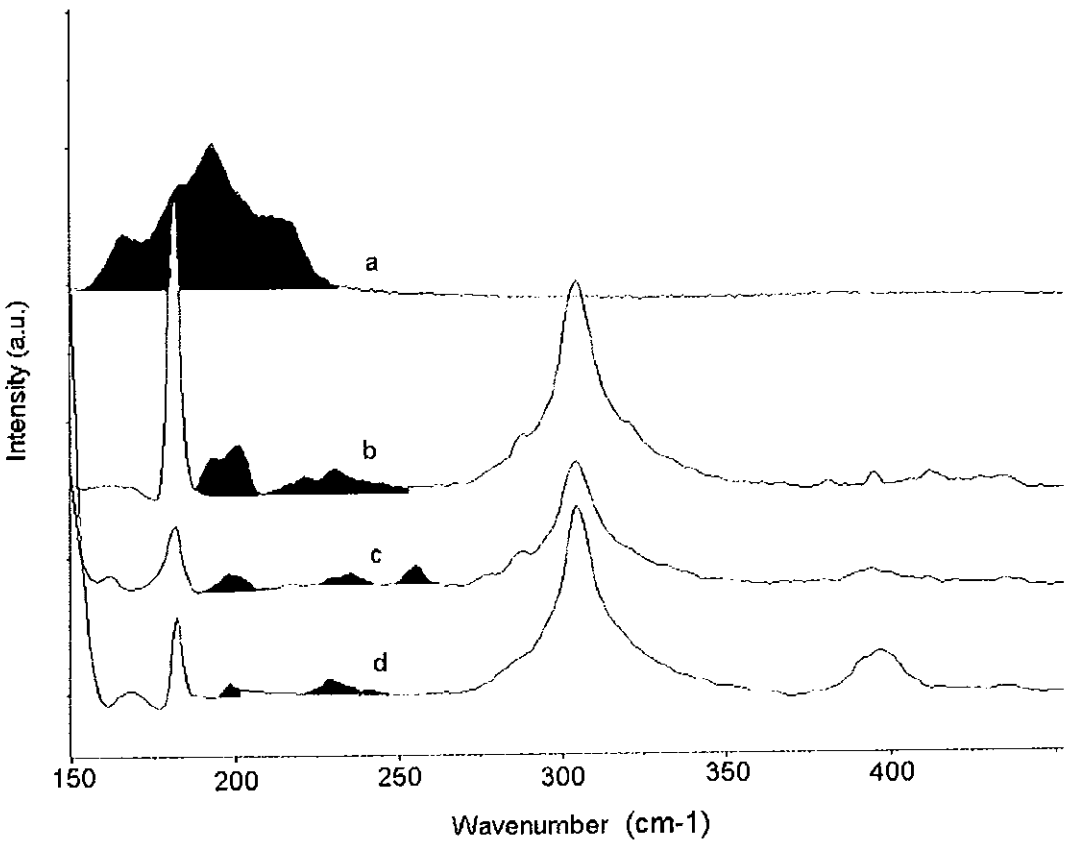

Figure 6.12 Raman spectra showing the RBMs at 632.8 nm, of (a) untreated LV-SWNT, (b) anthracene composite spectrum of LV-SWNT and anthracene at a 1:1 w/w ratio at 1 x 10^{-6} M, (c) 1 x 10^{-7} M, and (d) 1 x 10^{-8} M.

Comparing Figure 6.13 (a) with Figure 6.13 (b)-(d), the characteristic SWNT mode at 1570 cm^{-1}, the G-line, shows an up-shift from 1570 cm^{-1} to 1592 cm^{-1} on going from the untreated LV-SWNT sample to the composite sample at 1 x 10^{-7} M in Figure 6.13 (c) of the composite sample. The initial G-line profile of Figure 6.13 (a) has changed from metallic in nature to a more narrow and sharp peak characteristic of semiconducting SWNTs (Bachilo *et al.*, 2002; Yu and Brus, 2001). It is worth noting that both metallic and semiconducting G-lines are observed for anthracene composite samples at concentrations as low as 1 x 10^{-5} M and below this concentration only narrow sharp G-lines with weak intensities relative to the RBMs is observed. Typically for bundled SWNTs the intensities of the G-line relative to the RBMs are more intense. However, once dispersed the relative intensities become

inverted (Duesberg *et al.*, 1999). The enhanced intensity of the RBMs at the lower concentrations is attributed to the release of strain (or damping) imposed by bundling of SWNTs and various authors have also observed and reported similar findings (Bachilo *et al.*, 2002; Keogh *et al.*, 2004; Pfeiffer *et al.*, 2003).

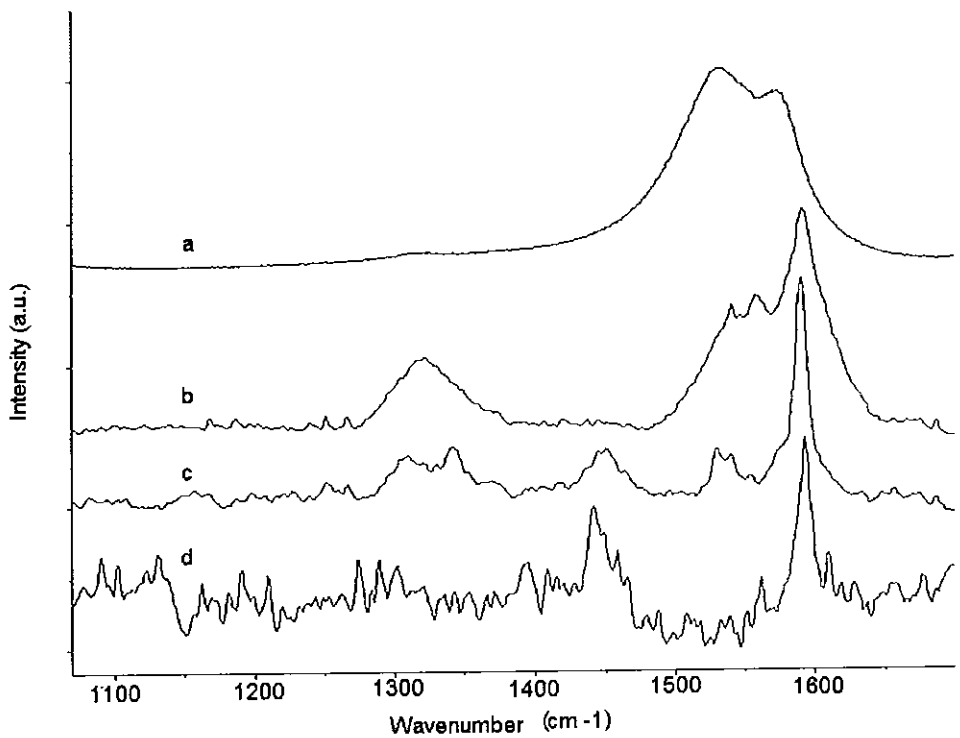

Figure 6.13 Raman spectra showing the G-line at 632.8 nm for (a) untreated LV-SWNT, (b) composite spectrum of LV-SWNT and anthracene at a 1:1 w/w ratio at 1 x 10^{-6} M, (c) 1 x 10^{-7} M, and (d) 1 x 10^{-8} M.

Similar behaviour was observed for the *p*-terphenyl composite samples ranging from 1 x 10^{-6} M to 1 x 10^{-9} M, as shown in Figures 6.14 and 6.15. The composite spectrum at 1 x 10^{-6} M in Figure 6.14 (b) depicts RBMs at 200, 250 and 260 cm^{-1}. The RBMs at 1 x 10^{-7} M in Figure 6.14 (c) are at 210, 250 and 260 cm^{-1}. At 1 x 10^{-9} M in Figure 6.14 (d) the RBMs further up-shift to 335 and 360 cm^{-1}. The observation of RBMs at such high frequencies of 335 and 360 cm^{-1} is not uncommon and authors such as Kulovecz *et al.*, observed RBMs with wavenumbers within this region (Kukovecz *et al.*, 2002). The total up-shift calculated

from the untreated SWNT material in Figure 6.14 (a) to 1 x 10^{-9} M in Figure 6.14 (d) in the *p*-terphenyl composite material is 168 cm $^{-1}$.

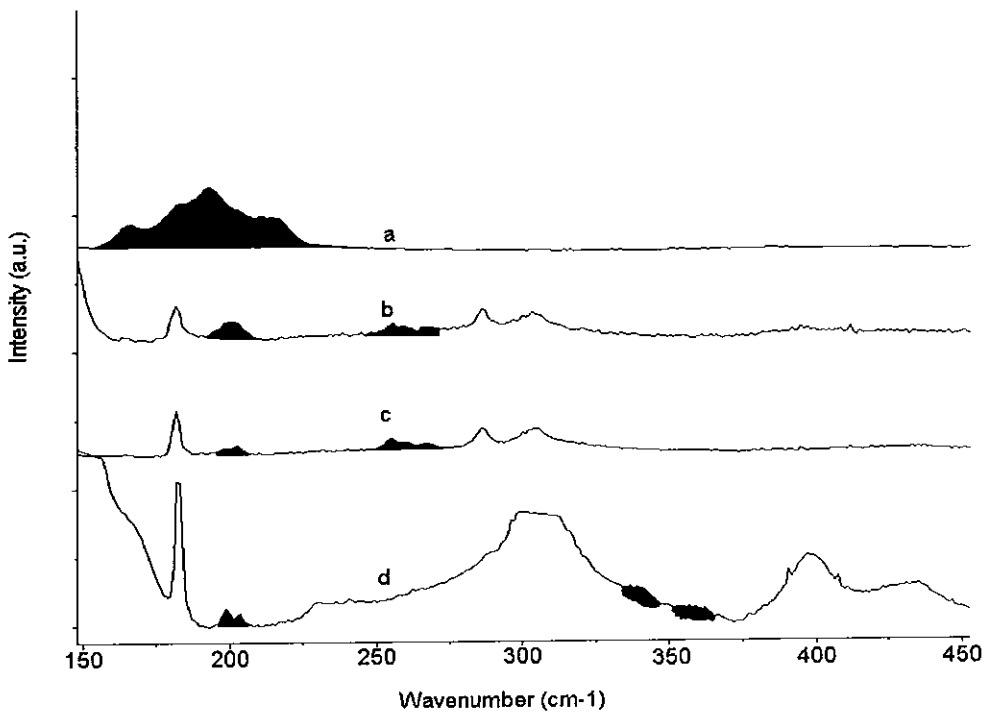

Figure 6.14 Raman spectra of the RBMs at 632.8 nm of (a) untreated LV-SWNT, (b) composite spectrum of LV-SWNT and *p*-terphenyl at a 1:1w/w ratio 1 x 10^{-6} M, (c) 1 x 10^{-7} M, and (d) 1 x 10^{-9} M.

Figure 6.15 below shows the G-line for untreated SWNT (Figure 6.15 (a)) and *p*-terphenyl composite samples (Figure 6.15 (b)-(d)). As with Figure 6.13 the G-line up-shifts with decreasing concentration and the modes once again become narrow and sharp. Papers reviewed show isolated SWNTs with narrow sharp G-lines with weaker intensities relative to the RBMs and the up-shift of the G-line with decreasing concentration (Duesberg *et al.*, 1999; Jorio *et al.*, 2001; Roa *et al.*, 2001). Work conducted by Roa *et al.*, (2001), show that Lorenztian line shape analysis of bundled SWNTs have a least four narrow sub-bands while isolated SWNTs resulted in a single narrow mode. Such observations provoke the question of whether the Breit-Wigner-Fano (BWF) line shape observed for what is reported to be

metallic SWNTs is a feature of SWNT bundles only and adding support to this is the fact that the G-line up-shifts with decreasing concentration indicating that the bundle imposes a strain on the G-line. It is interesting to note that although many authors have observed such a change in the G-line there is little comment with regards to the significant change of profile.

Comparing the debundled LV-SWNT solubilised by *p*-terphenyl and anthracene it would appear that the PAH molecules exhibit a degree of selectivity. Anthracene preferentially solubilises larger SWNTs compared to *p*-terphenyl based on the accepted relationship of RBM frequency and diameter given in Equation 4.5 (Chapter 4). The following paragraph describes how the diameter of the debundled LV-SWNT are elucidated and how the physical properties of the selected SWNTs are determined.

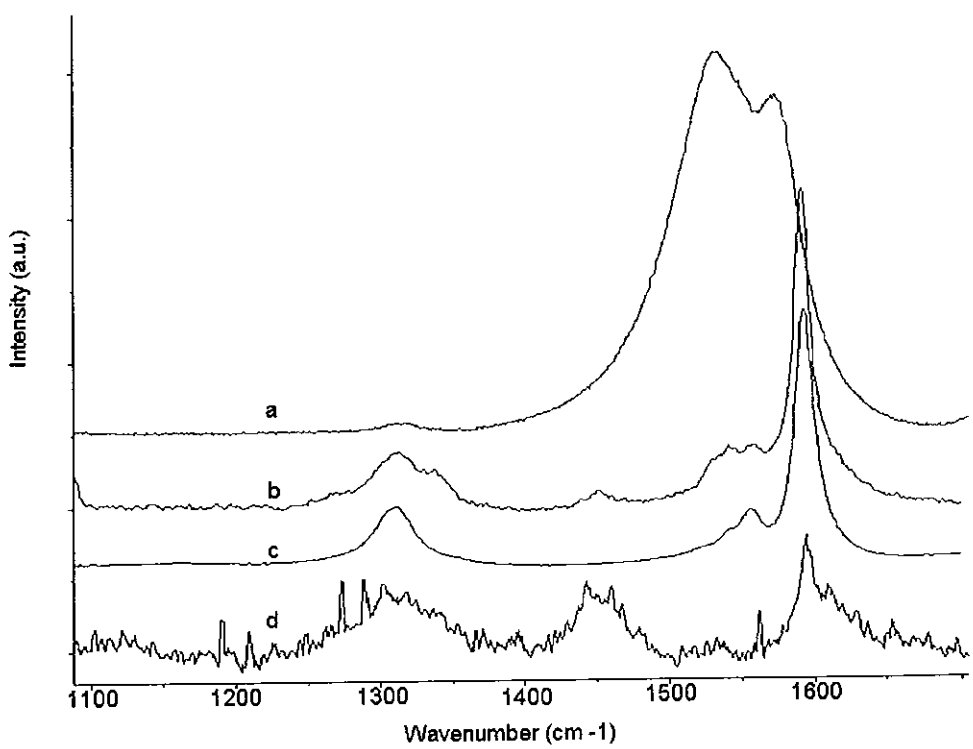

Figure 6.15 Raman spectra of the G-line at 632.8 nm for (a) untreated LV-SWNT, (b) composite spectrum of LV-SWNT and *p*-terphenyl at a 1:1 w/w ratio at 1 x 10^{-6} M, (c) 1 x 10^{-7} M, and (d) 1 x 10^{-9} M.

It is well documented that the RBM frequency is related to the SWNT diameter and chirality but the formula to elucidate this is still under debate (Bachilo *et al.*, 2002; Jorio *et al.*, 2001; Keogh *et al.*, 2004; Pfeiffer *et al.*, 2003; Rols *et al.*, 2000). The models of Jorio *et al.*, (2001) and Rols *et al.*, (2000) were used in this research to determine the diameters of the LV-SWNT. For the anthracene composite at a concentration of ~1 x 10^{-7} M the RBM frequency (υ_{RBM}) of 198, 235 and 254 cm $^{-1}$ gave diameters of 1.26, 1.06 and 0.98 nm respectively in accordance with the model derived by Jorio *et al's.*, (2001). The diameters were estimated at 1.21, 1.02, 0.95 nm respectively for the model derived by Rols *et al.*, (2000). For the *p*-terphenyl composite at a concentration of ~1 x 10^{-9} M treatment using the model derived by Jorio *et al.*, (2001) relates the υ_{RBM} of 198, 338 and 360 cm^{-1} to diameters of 1.26, 0.74 and 0.69 nm respectively. According to Rols *et al.*, (2000) the diameters are 1.21, 0.71 and 0.67 nm respectively. Comparing the resulting diameters from the two models it would appear that there is a difference in the range of 0.05 – 0.02 nm. The difference in the diameters estimated by both models only becomes significant to this research if the diameters conflict with the physical properties assigned but no such disagreement occurs (Jorio *et al.*, 2001). As discussed in Chapter 4 the model of Jorio *et al.*, (2001) is unique in that it was based on the study of isolated SWNTs unlike other models contrived from the study of bundled SWNTs (Jorio *et al.*, 2001; Wang *et al.*, 2001). Therefore it is more accurate to assign SWNT properties with the model derived by Jorio *et al.*, (2001) as opposed to the latter model by Bandow *et al.*, (1998) and Rols *et al.*, (2000).

The results indicate that anthracene interacts with metallic SWNTs whereas *p*-terphenyl interacts mainly with semiconducting SWNTs. The model indicates that the value 1.2 nm for *p*-terphenyl is metallic and therefore its structure is possibly (12,6) chiral or (9,9) armchair (Rols *et al.*, 2000; Wang *et al.*, 2001). For the values below 1 nm it reported that SWNTs are semiconducting and that implies that the structure of the LV-SWNT are either zigzag of chiral. In the case of anthracene the diameters are approximately 1 – 1.2 nm where only metallic SWNTs are resonant therefore at ~1.2 nm the structure is either (12,6) chiral or (9,9) armchair. At ~1 nm the structure is (9,6) chiral and at ~0.97 the structure is either (10,4), chiral or (12,0) zigzag. Unfortunately current models are not sophisticated enough to determine a single (n,m) value thereby revealing the structure of the SWNTs.

However the results are significant in that they indicate selective interaction of the PAH molecules with debundled SWNTs. It was previously proposed that the PAH molecules anthracene and *p*-terphenyl may potentially interact with specific SWNTs due to their differing backbone structure (Chapter 1). Anthracene was proposed to map onto metallic SWNTs and *p*-terphenyl to mainly semiconducting SWNTs and results presented in this chapter support this proposal (Hedderman *et al.*, 2006).

Summary

The PAH molecules, anthracene and *p*-terphenyl have been shown not only to solubilise, and purify a sample of LV-SWNT but also debundle with strong indications of selective interaction. The spectroscopic investigations such as fluorescence and Raman point towards a mapping of the PAHs onto the LV-SWNT surface with fluorescence concentration dependence studies indicating concentration ranges where aggregates of SWNTs and PAHs as well as debundled LV-SWNT and PAHs interact. It was also found that the concentration range where LV-SWNT bundles disperse is not constant but is a three way system dependent on the solvent used and the method by which the SWNTs are produced and the molecule used to disperse the SWNTs. These factors must be taken into account if direct comparison of different systems is to be considered. Binding energies for both composite samples were obtained and found to be 1.1 and 0.9 eV for *p*-terphenyl and anthracene respectively. Such a result indicates that *p*-terphenyl binds more tightly to the LV-SWNT surface than anthracene but anthracene is more prolific at dispersing LV-SWNT bundles.

Quenching in the fluorescence of the PAH molecules on introduction of LV-SWNT points towards interaction and the resulting changes in the degree of the fluorescence red-shift of *p*-terphenyl gave insight as to the orientation of the PAHs as a result of the influence of the LV-SWNT bundle size on interaction.

Raman spectroscopy showed composite spectra with the characteristic SWNT modes such as the RBMs and the G-line up-shifted in frequency on comparing the untreated LV-SWNT

material to the composite material. The up-shift of the composite RBMs in relation to the untreated LV-SWNT sample was indicative of debundling with decreasing concentration and this was supported by AFM studies. Examination of the Raman RBMs and the fluorescence of the free PAHs indicate that the results from both spectroscopic methods correlate when determining the region at which fully dispersed LV-SWNT and PAHs are interacting. Results show that anthracene disperses LV-SWNT at $\sim 10^{-7}$ M and *p*-terphenyl at $\sim 10^{-9}$ M. Raman studies were then used to probe for selective interaction of the PAHs with LV-SWNT in the concentration range where dispersed LV-SWNT and PAHs existed. It was found that anthracene preferentially interacted with metallic LV-SWNT whereas *p*-terphenyl preferentially interacted with mainly semiconducting LV-SWNT hence providing evidence of selective interaction. Therefore it may be deduced that the PAH molecules solubilise, purify and debundle LV-SWNT as initially proposed with strong indications of selective interaction.

REFERENCES

Bachilo, S.M., Strano, M.S., Kittrell, C., Hauge, R.H., Smalley, R.E., Weisman, R.B., (2002), "Structure-assigned optical spectra of single-walled carbon nanotubes", *Science*, 298 2361 - 2366 .

Bandow, S., Asaka, S., Saito, Y., Rao, A.M., Grigorian, L., Richter, E., Eklund, P.C., (1998), "Effect of the growth temperature distribution and chirality of single – wall carbon nanotubes", *Phys Rev. Lett.*, 80, 3779 - 3782.

Baughman, R.H., Zakhidov, A.A., (2002), "Carbon nanotubes - the route toward applications", *Science*, 297, 787 - 792.

Cadek, M., Coleman, J.N., Ryan, K.P., Nicolosi, V., (2004), "Reinforcement of polymers with carbon nanotubes: the role of nanotube surface area", *Nanoletters*, 4, 353 - 357.

Chakarova, S., Schroder, E., (2005), "van der Waals interactions of polycyclic aromatic hydrocarbon dimers", *J.Chem. Phys.*, 122, 054102-1 – 054102-5.

Coleman, J.N., Maier, S., Fleming, A., O'Flaherty, S., Minett, A., Ferreira, M.S., Hutzler, S., Blau, W.J., (2004), "Binding kinetics and SWNT bundle dissociation in low concentration polymer-nanotube dispersions", *J. Phsy. Chem. B.,* 108, 3446 - 3450.

Coleman, J.N., Dalton, A.B., Munoz, E., Collins, S., Kim, B.G., Razal, J., Selvidge, M., Vieiro, G., Baughman, R.H., Blau, W.J., (2003), "Improving the mechanical properties of single-walled carbon nanotube sheets by intercalation of polymeric adhesives", *App. Phys, Letts.,* 82, 1682-1684.

Cote, M., Haynes, P.D., Molteni, C., (2001), "Boron nitride polymers: building blocks for organic electronic devices", *Phys. Rev. B.,* 63, 125207-1-125207-4.

Dresselhaus, M.S., Dresselhaus, G., Avouris, Ph., (2001), *Carbon Nanotubes: Synthesis, Structure, Properties and Applications*, Springer-Verlag, Berlin Heidelberg.

Duesberg, G.S., Blau, W.J., Byrne, H.J., Muster, J., Burghard, M., Roth, S., (1999), "Experimental observation of individual single-wall nanotube species by Raman microscopy", *Chem. Phys. Lett.*, 310, 8 - 14.

Duesberg G.S., Loa I., Burghard M., Syassen K., Roth S., (2000), "Polarised Raman spectroscopy on isolated single-wall carbon nanotubes", *Phys. Rev. Lett.*, 85, 5436 - 5439.

Fantini, C., Jorio, A., Souza, M., Strano, M.S., Dresselhaus, M.S., Pimenta, M.A., (2004), "Optical transition energies for carbon nanotubes from resonant Raman spectroscopy: environment and temperature effects", *Phys. Rev. Lett.*, 93, 147406-1 – 147406-4.

Hamada, N., Sawada, S, Oshiyama, S., (1992), "New one-dimensional conductors: graphitic microtubules", *Phys. Rev. Lett.*, 68, 1579 - 1581.

Hedderman, T.G., Keogh, S.M., Chambers, G., Byrne H.J., (2004), "Solubilisation of SWNT with organic dye molecules", *J. Phys. Chem B.*, 108, 18860 - 18865.

Hedderman, T.G., Keogh, S.M., Chambers, G., Byrne H.J., (2006), "In-depth study into the interaction of single walled carbon nanotubes with anthracene and *p*-terphenyl", *J. Phys. Chem. B.*, 110, 3895-3901.

Javey, A., Guo, J., Farmer, D.B., Wang, Q., Yenilmez, E., Gordon, R.G., Lundstrom, M., Dai, H., (2004), "Self-aligned ballistic molecular transistors and electrically parallel nanotube arrays", *Nanoletters*, 4, 1319-1322.

Jorio, A., Saito, R., Hafner, J.H., Lieber, C.M., Hunter, M., McClure, T., Dresselhaus, G., Dresselhaus, M.S., (2001), "Structural (n,m) determination of isolated single-wall carbon nanotubes by resonant Raman scattering", *Phys. Rev. Lett.*, 86, 1118 - 1121.

Kataura H., Kumazawa Y., Maniwa Y., Umezu I., Suzuki S., Ohtsuka Y., Achiba Y., (1999), "Optical properties of single – wall carbon nanotubes", *Synth. Metals*, 103, 2555 - 2558.

Keogh S.M., Hedderman T.G., Gregan E., Farrell G., Chambers G., Byrne H.J., (2004), "Spectroscopic analysis of single-walled carbon nanotubes and semiconjugated polymer composites", *J. Phys. Chem. B.*, 108, 6233 – 6241.

Keogh S.M., Maguire A., Hedderman T.G., Gregan E., Farrell G., Dalton A.B., McCarthy B., Chambers G., Byrne H.J., (2002), "Physical interactions between HiPco SWNT and semiconducting polymers", *Proceedings of SPIE,* 4876, 723 - 731.

Kukovecz, A., Kramberger, Ch., Georgakilas, V., Prato, M., Kuzmany, H., (2002), "A detailed Raman study on thin single-wall carbon nanotubes prepared by the HiPco process", *The Eur. Phy. Journ. B.*, 28, 223 - 230.

Kurti, J., Kuzmany, H., Burger, B., Hulman, M., Winter, J., Kresse, G., (1999), "Resonance Raman investigation of single walled carbon nanotubes", *Synth. Metals*, 103, 2508 - 2509.

Kuzmany, H., Plank, W., Hulman, M., Kramberger, Ch., Gruneis, A., Pichler, Th., Peterlik, H., Kataura., H., Achiba, Y., (2001), "Determination of SWCNT diameters from the Raman response of the radial breathing mode", *Eur. Phys. J. B.*, 22, 307 - 320.

Lee, N.K., Kim, S.K., (2005), "*Ab initio*-based intermolecular carbon-carbon pair potential for polycylic aromatic hydrocarbon clusters", *J. Chem. Phys.*, 122, 031102-1 – 031102-4.

Mc Euen, P.L., (2000), "Single walled carbon nanotubes": *Physics World*, 13, 31 - 36.

Meehan, P., Rayment, T., Thomas, R.K., (1980), "Neutron diffraction from benzene adsorbed on graphite", *J. Chem. Soc., Faraday I*, 76, 2011-2015.

Nikolaev, P., Bronikowski, M.J., Bradley, R.K., Rohmund, F., Colbert, D.T., Smith, K.A., Smalley, R.E., (1999), "Gas-phase catalytic growth of single walled carbon nanotubes from carbon monoxide", *Chem. Phys. Lett.*, 313, 91-97.

Pfeiffer, R., Kuzmany, H., Kramberger, Ch., Schaman, Ch., Pichler, T., Kataura, H., Achiba, Y., Kurti, J., Zolyomi, V., (2003), "Unusual high degree of unperturbed environment in the interior of single-wall carbon nanotubes", *Phys. Rev. Lett.*, 90, 225501-1 – 225501-4.

(a) Pimenta M.A., Marucci A., Empedocles S.A., Bawendi M.G., Hanlon E.B., Roa A.M., Eklund P.C. Smalley R.E., Dresselhaus G., Dresselhaus M.S., (1998), "Raman modes of metallic carbon nanotubes", *Phys. Rev. B.*, 58, R16016 – R16019.

(b) Pimenta M.A., Marucci A., Empedocles S.A., Brown S.D.M., Mathews M.J., Roa A.M., Eklund P.C. Smalley R.E., Dresselhaus G., Dresselhaus M.S., (1998), "Resonant Raman effect in single-wall carbon nanotubes", *J. Mater. Res.*, 13, 2396 - 2404.

Rao A.M., Chen J., Richter E., Sclecht U., Eklund P.C., Haddon R.C., Venkateswaran U.D., Kwon Y.K., Tomanek D., (2001), "Effect of van der Waals interactions on the Raman modes in single walled carbon nanotubes", *Phys. Rev . Lett.*, 86, 3895 – 3898.

Rao, A.M., E. Richter, E., Bandow, S., Chase, B., Eklund, P.C., Williams, K.A., Fang, S., Subbaswamy, K.R., Menon, M., Thess, A., Smalley, R.E., Dresselhaus, G., Dresselhaus, M.S., (1997), "Diameter selective Raman scattering from vibrational modes in carbon nanotubes", *Science*, 275, 187 - 191.

Rols, S., Righi, A., Alvarvez, L., Anglaret, E., Almairac, R., Journet, C., Bernier, P., Sauvajol, J.L., Benito, A.M., Maser, W.K., Munoz, E., Martinez, M.T., de la Fuente, G.F., Girard, A., Ameline, J.C., (2000), "Diameter distribution of single walled carbon nanotubes in nanobundles", *The Euro. Phys. Journ. B.*, 18, 201 – 205.

Strong, K.L., Anderson, D.P., Lafdi, K., Kuhn, J.N., (2003), "Purification process for single-wall carbon nanotubes", *Carbon*, 41, 1477 - 1488.

Thess, A., Lee, R., Nikolaev, P., Dai, H., Petit, P., Robert, J., Xu, C., Lee, Y.H., Kim, S.G., Rinzler, A.G., Colbert, D.T., Scuseria, G.E., Tomanek, D., Fisher, J.E., Smalley, R.E., (1996), "Crystalline bundles of metallic carbon nanotubes", *Science*, 273 483 - 487.

Tomanek, D., Enbody R.J., *Science and application of Nanotubes*, (2000), Kluwer Academic Publishers/Plenum Publishers, New York, 300-302.

Walzer, K., Sternberg, M., Hietschold, M., (1998), "Formation and characterization of coronene monolayers on HOPG (0001) and MoS_2 (0001): A combined STM/STS and tight binding study", *Surface Science*, 415, 376 - 382.

Wang Y.F., Cao, X.W., Hu, S.F., Liu, Y.Y., Lan, G.X., (2001), "Graphical method for assigning Raman peaks of radial breathing modes of single-wall carbon nanotubes", *Chem. Phys. Lett.*, 336, 47 - 52.

Yu, Z., Brus, L., (2001), "Rayleigh and Raman scattering from individual carbon nanotubes", *J. Phys. Chem. B.*, 105, 1123 - 1134.

Zacharia, R., Ulbricht, H., Hertel, T., (2004), "Interlayer cohesive energy of graphite from thermal desorption of polyaromatic hydrocarbons", *Phy. Rev. B.*, 69, 155406-1 – 155406-7.

Zhang M., Yudasaka M., Koshio A., Jabs C., Ichihashi T., Iijima S., (2002), "Structure of single-wall carbon nanotubes purified and cut using polymer", *App. Phys. A.*, 74,7-10.

CHAPTER 7 – THE INTERACTION AND DEBUNDLING OF SWNT PRODUCED BY DIFFERENT METHODS IN THE PRESENCE OF *P*-TERPHENYL

7.1 Introduction

Obtaining pure, isolated SWNTs of specific structures in large quantities is problematic. There is currently no information in the literature on a production or processing method which is capable of achieving such specifications. The hydrocarbon, *p*-terphenyl, has shown potential in this area with respect to LV-SWNT (Chapters 5 and 6). The hydrocarbon was shown to purify and debundle SWNTs with strong evidence of selectivity. In this study the interaction between and the ability of *p*-terphenyl to debundle SWNTs produced by different methods is investigated with SWNTs produced by the high pressure carbon monoxide disproportionation (HiPco) and arc-discharge probed. The outcomes are compared to the results obtained for laser vapourisation SWNTs which are presented in Chapters 5 and 6. It is well established that SWNTs produced by different methods contain SWNTs with different bundle sizes and degrees of purity (Journet *et al.*, 1997; Nikolaev *et al.*, 1999; Thess *et al.*, 1996). Therefore the study will allow a greater understanding as to the interaction between and the ability of *p*-terphenyl to debundle SWNTs of different compositions i.e. initial purity and bundle size. This study will look at the interaction that occurs between SWNTs with *p*-terphenyl with the interaction charaterised *via* concentration dependent fluorescence spectroscopic studies. Atomic force microscopy (AFM) is used to image and measure the surface profile of the SWNT at similar concentration thereby allowing the extent of SWNT debundling to be estimated. The results from this study will assist in the quest for a standardised processing and purification protocol.

7.2 Sample Preparation

Solutions in the range of ~4.5 x 10^{-12} to ~2.5 x 10^{-3} M for *p*-terphenyl in toluene were prepared. HiPco SWNT (H-SWNT) purchased from Carbon Nanotechnologies Incorporated (CNI) (http://www.cnanotech.com) and arc-discharge SWNT (AD-SWNT)

gifted from Montpellier University (now, http://www.nanoledge.com) were added to all *p*-terphenyl solutions in a 1:1 w/w ratio SWNT/PAH. Both solutions containing *p*-terphenyl and the composite samples were sonicated using an ultra sonic tip (ultrasonic processor VCX, 750 Watts) for 30 s and allowed to settle for 24 hours after which the supernatant liquid from the composite solutions was carefully withdrawn. The composite solutions were then allowed to settle for a further 24 hours before being characterised by fluorescence spectroscopy (Perkin Elmer LS55) and imaged *via* AFM (Asylum MFP-3D). The precipitate of the composite solutions was found to be relatively rich in SWNTs so solubility of the SWNTs is only partial however, concentrations are quoted as prepared. For AFM studies the composite samples were dispersed on an activated silicon surface and the silicon wafer was activated as described in Chapter 6, section 6.2.

7.3 Results and Discussion

Chapter 5 reports how *p*-terphenyl purified a sample of untreated LV-SWNT *via* a $\pi - \pi$ interaction as shown by Raman studies. Before investigating the extent of interaction and debundling of SWNTs produced by different methods as a result of the interaction of *p*-terphenyl, solubility effects of the toluene solvent are first explored. Samples of mass 5.6 mg of AD-SWNT and H-SWNT are added to toluene and are observed to precipitate out in less than 24 hours as was the case for LV-SWNT (Chapter 5). *p*-Terphenyl is then added to both solutions at a 1:1 w/w ratio giving a concentration of 2.5 x 10^{-3} M for *p*-terphenyl, which results in the enhanced solubility of the SWNTs in both cases. However, differences are observed in the appearance of the composite solution of the AD-SWNT and H-SWNT compared with LV-SWNT as depicted in Figure 7.1. It is evident that at similar concentrations the degree of solubility of the different SWNT types varies. While the LV-SWNT solution has a dark brown translucent aspect (c), both the H-SWNT (a) and AD-SWNT (b) composite samples is visibly clear at a concentration of 2.5 x 10^{-3} M for *p*-terphenyl.

(a) (b) (c)

Figure 7.1 The composite solution at 2.5 x 10^{-3} M for *p*-terphenyl with SWNT present at a 1:1 w/w ratio. (a) depicts a composite solution containing H-SWNT, (b) contains a composite solution with AD-SWNT and (c) contains the composite solution containing LV-SWNT.

In Chapter 6 a fluorescence concentration dependence study was conducted for both the PAH molecules and the composite samples containing LV-SWNT. The study yielded information with regards to the concentration range where isolated and aggregated PAH molecules existed and also the effect the SWNTs exerted over the aggregation process of the PAH molecules. A similar study is conducted where H-SWNT and AD-SWNT are used and results are compared with the LV-SWNT study. It is anticipated that such a study may provide answers to the observations described in Figure 7.1.

Figure 7.2 depicts the fluorescence of *p*-terphenyl in the absence (filled black circles) and presence (filled grey squares) of AD-SWNT within a concentrations range of ~2.5 x 10^{-9} and ~2.5 x 10^{-3} M. As is the case in Chapter 6 the plot is a linear/log axis and the solid

black line denotes linear behaviour. The *p*-terphenyl (filled black circles) fluorescence fits well to a linear increase between ~2.5 x 10^{-9} and ~3 x 10^{-6} M. From a concentration of ~3 x 10^{-6} to ~2.5 x 10^{-3} M the fluorescence deviates from linearity and is considerably quenched due to aggregation as described in Chapter 6.

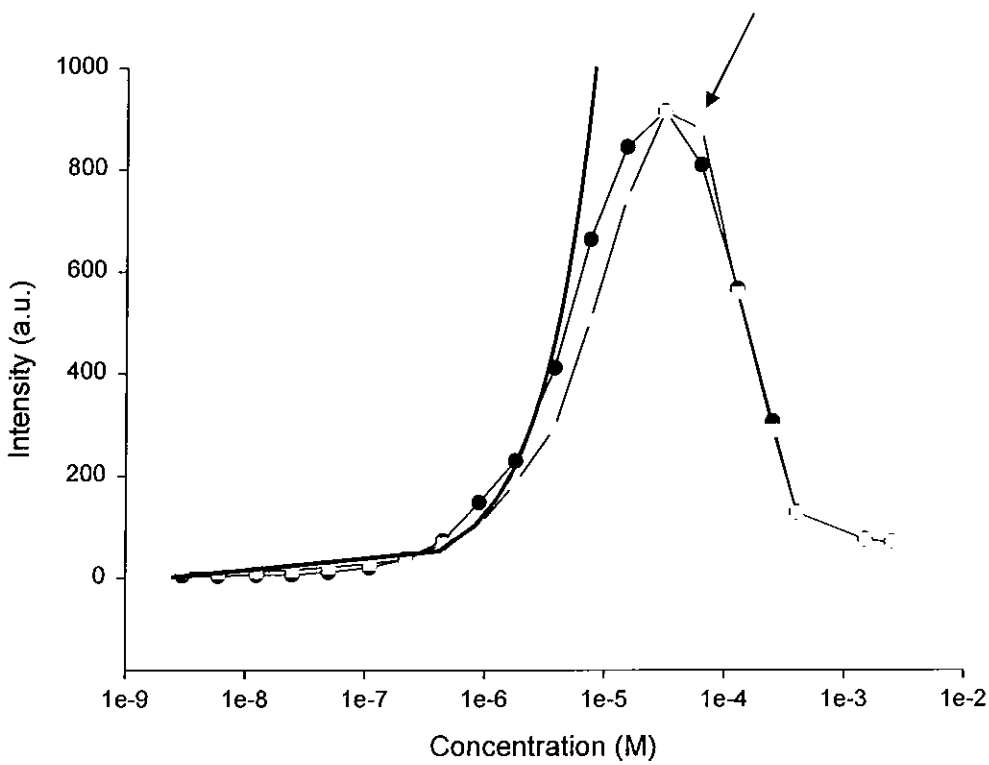

Figure 7.2 Fluorescence of *p*-terphenyl in the absence (filled black circles) and presence (filled grey squares) of AD-SWNT on a linear/log axis. The solid line denotes a linear fit.

Upon the addition of AD-SWNT (filled grey squares) the fluorescence trend appears similar to that discussed above. Within a concentration range of ~2.5 x 10^{-9} and ~3 x 10^{-6} M the fluorescence is again linear but quenched relative to *p*-terphenyl as a result of the $\pi - \pi$ interaction between the the PAH molecules and the SWNTs. Within the concentration range of ~3 x 10^{-6} and ~2.5 x 10^{-3} M the fluorescence deviates from linearity as was the case for *p*-terphenyl alone within a similar concentration range. At a concentration of 1 x 10^{-4} M the fluorescence is now in excess relative to *p*-terphenyl and that is attributed to the

de-stacking of *p*-terphenyl aggregates as the presence of AD-SWNT interferes with the aggregation process as indicated by the marker in Figure 7.2 (refer to Chapter 6).

Similar fluorescence results for *p*-terphenyl were observed when using H-SWNT as depicted in Figure 7.3. Figure 7.3 depicts the fluorescence of *p*-terphenyl in the absence (filled black circles) and presence (filled grey squares) of H-SWNT within a concentrations range of ~2.5 x 10^{-9} and ~2.5 x 10^{-3} M in toluene. However what is most noticeable in Figure 7.3 is that no excess fluorescence of p-terphenyl on interaction with H-SWNT was observed as indicated by the marker, in contrast to both AD-SWNT and LV-SWNT (Figures 6.1 and 7.2).

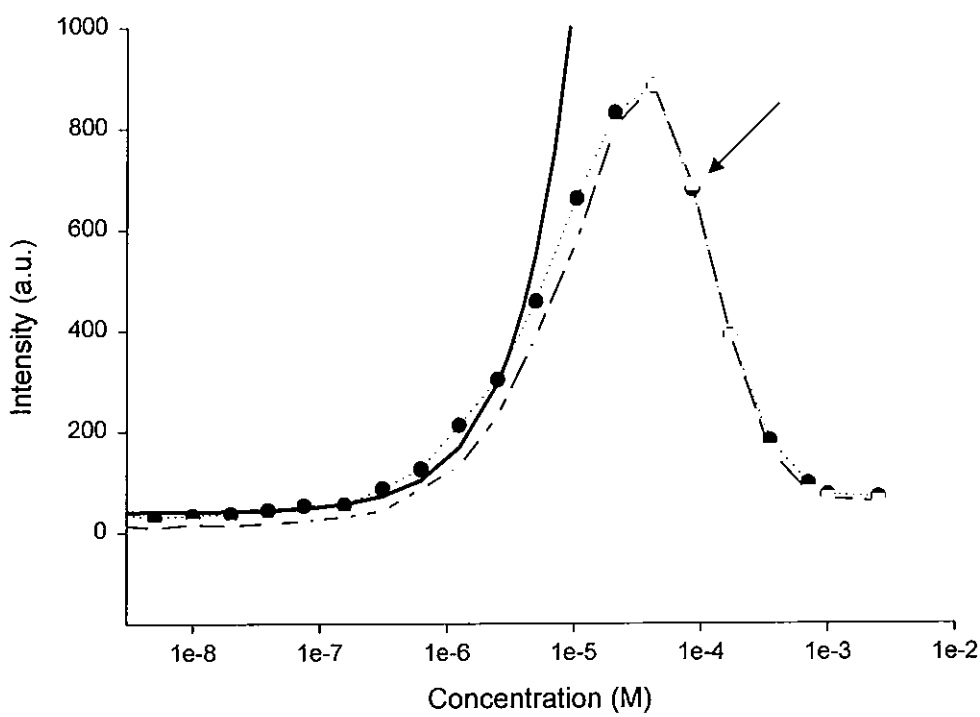

Figure 7.3 Fluorescence of *p*-terphenyl in the absence (filled black circles) and presence (filled grey squares) of H-SWNT as a function of concentration on a linear/log axis. The solid line denotes a linear fit.

The studies in Figurse 6.1, 7.2 and 7.3 reveal the concentration range where *p*-terphenyl exists as isolated and aggregated molecules. The studies also reveals that the presence of SWNT hinders the aggregation of *p*-terphenyl molecules and this is expressed by the excess emission of *p*-terphenyl in the composite solutions containing LV-SWNT and AD-SWNT compared to the fluorescence of *p*-terphenyl alone. Results show that LV-SWNT are better at preventing the aggregation of *p*-terphenyl than AD-SWNT and H-SWNT and this is shown by fluorescence studies where the excess fluorescence of *p*-terphenyl is experienced and is greater in the presence of LV-SWNT than either of the other two SWNT types. The interference of the aggregation of *p*-terphenyl by the presence of SWNT shows that the hydrocarbon preferentially interacts with the SWNT as opposed to itself. Such a result is not surprising as theoretical and experimental studies described in Chapter 6 discuss the favourable interaction between the hydrocarbon molecules and graphitic surfaces. To decifer as to why both LV-SWNT and AD-SWNT hinder the aggregation process of *p*-terphenyl while H-SWNT do not, the composition of each of the SWNT samples was examined. Table 7.1 lists the parameters of the SWNTs present in each sample.

Table 7.1 Composition of SWNT as reported by literature (Journet *et al.*, 1997; Nikolaev *et al.*, 1999; Thess *et al.*, 1996).

	diameter distribution	average	no. of tubes per bundle		purity
LV- SWNT	broad	1.4 nm	100-500	tubes	85%
AD- SWNT	broad	1.4 nm	20-40	tubes	70%
H- SWNT	narrow	1.1 nm	20-40	tubes	90%

Examination of the composition of each of the tube samples along with results from Figures 6.1. 7.1 to7.3 show that large bundles of SWNT along with a large tube diameters are preferable for the interaction and solublisation of SWNT by *p*-terphenyl in toluene at a 1:1 ratio *p*-terphenyl/SWNT. Figure 7.1 indicates that the large bundle size of LV-SWNT is favourable for a high degree of interaction with *p*-terphenyl. The fluorescence

concentration dependence study of *p*-terphenyl in Figures 6.1, 7.2 and 7.3 indicate that larger diameter SWNTs are preferable for a good degree of interaction with *p*-terphenyl which is depicted by the excess fluorescence of *p*-terphenyl in the composite samples of AD-SWNT and LV-SWNT compared to *p*-terphenyl alone at a similar concentration. H-SWNT which is stated to have a smaller diameter distribution between 0.7 -1.2 nm does not exert the same effect over the *p*-terphenyl molecules.

It was noted that the general trend of the fluorescence concentration dependence study is similar for all three SWNT types in Figures 6.1, 7.2 and 7.3. However the degree of quenching in the fluorescence of *p*-terphenyl and the emission maximum varies with SWNT type. At a concentration of 2.5 x 10^{-3} M for the LV-SWNT composite the emission maximum was observed to be 365 nm (Figure 5.4) yet at similar concentrations for the AD-SWNT and H-SWNT the emission maximum is 345 nm as depicted in Figure 7.4 (a) and (b) respectively.

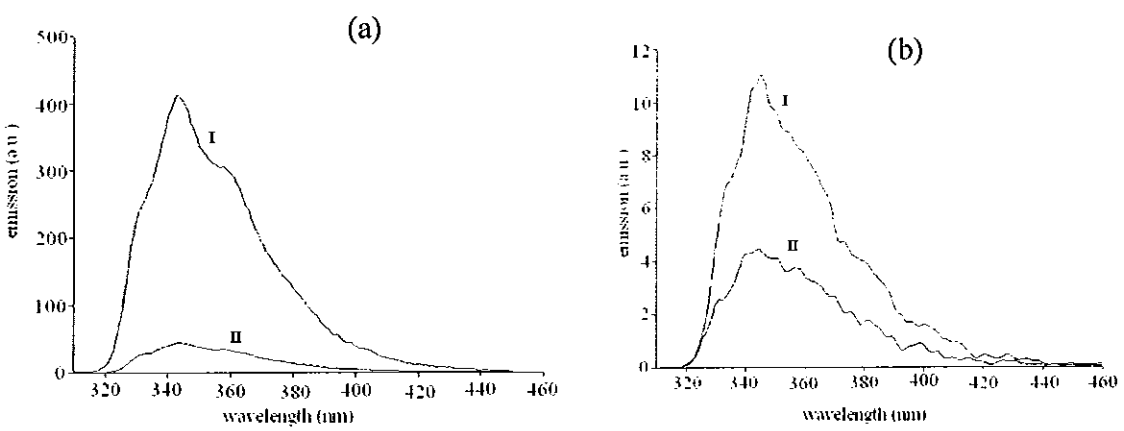

Figure 7.4 Graph (a) and (b) represent the fluorescence of *p*-terphenyl in the absence (I) and presence (II) of AD-SWNT and H-SWNT at a concentration of 2.5 x 10^{-3} M in toluene respectively. The spectra labelled (II) emphasises the fluorescence emission maximum as a result of the interaction with different SWNT types.

Both the degree of fluorescence quenching and the variation in the fluorescence emission maximum of *p*-terphenyl may be attributed to the bundle size of the SWNTs in question. Results from Chapter 6 gave strong indications that indicate that quenching is subject to the SWNT surface area that the hydrocarbon interacts with. As discussed in Chapter 6, the fluorescence emission maximum is sensitive to the SWNT bundle surface area. Depending on the bundle size and hydrocarbon concentration the molecules will interact *via* face-face interaction when there is sufficient space or T-shape interaction when crowding of the hydrocarbons occurs on the SWNT bundle surface area (Meehan *et al.*, 1980; Zacharia *et al.*, 2004). If this is the case the results suggest that LV-SWNT should have the largest bundles of the three SWNT samples. AFM studies are conducted to verify this claim. The dimensions obtained from AFM studies are listed in Table 7.2.

Table 7.2 Observed dimensions of the different SWNT types in their as produced state *via* AFM measurements.

SWNT Sample	average length	average width	average height
AD-SWNT	1,000 nm	19 nm	1.5 nm
H-SWNT	800 nm	15 nm	1.25 nm
LV-SWNT	5,000 nm	33 nm	4 nm

Table 7.2 reveals that the bundle size of LV-SWNT is 3.7×10^{-13} m^2 and H-SWNT and AD-SWNT are 2.6×10^{-14} m^2 and 4.1×10^{-14} m^2 respectively. The formula to calculate the surface area is that for the surface area of an elongated box based on the geometry of the results obtained from AFM studies. From these results it is clear that LV-SWNT have the largest bundles of the three SWNT samples thereby confirming the interpretation of results discussed above. Because LV-SWNT have a much larger bundle size than either the H-

SWNT or AD-SWNT this further supports evidence which indicates that *p*-terphenyl exhibits a greater interation with larger SWNT bundles. LV-SWNT have very large bundles compared to the other two SWNT samples and therefore a greater degree of interaction can take place between the PAH and SWNT surface. A high degree of interaction between the two components leads to a high degree of solubility with respect to the SWNTs and this high degree of interaction is visibly evident in the LV-SWNT composite sample in Figure 7.1. The H-SWNT and AD-SWNT, being of a much smaller bundle size, do not experience the same degree of interaction with the PAHs and this is expressed by a reduced degree of solubility (Figure 7.1 (a) and (b)). Such a result also provides evidence as to why the fluorescence quenching is less for H-SWNT and AD-SWNT compared with LV-SWNT.

A model to investigate the debundling of LV-SWNT is described in Chapter 6. The same model is used in this study to monitor and compare the rate and extent of the debundling of both the H-SWNT and AD-SWNT. The theory behind this model may be found in Chapter 6 and it is worth reiterating that the model is based on the interaction of a fluorescent organic molecule with SWNT at a 1:1 w/w ratio.

Adapting the model to this study and applying Equation 6.1 to Figure 7.5 depicted below, a plot of the fraction of free *p*-terphenyl as a function of concentration was achieved as a result of the interaction with H-SWNT. Proceeding from left to right across Figure 7.5, from approximately ~1 x 10^{-11} to ~1 x 10^{-8} M the fluorescence of the fraction of free *p*-terphenyl decreases steadily with increasing concentration, the free, isolated PAHs and H-SWNT exist in dynamic equilibrium with bound PAHs and H-SWNT. The data within this concentration range fits well to the solid line which is a plot of Equation 6.1, resulting in a C_0 value of ~1 x 10^{-8} M. This value indicates that below ~1 x 10^{-8} M *p*-terphenyl molecules are interacting with H-SWNT where the surface area of the SWNTs is constant. Deviation from the fit at approximately ~2 x 10^{-8} M is attributed to an increase in the SWNT bundle surface area as demonstrated for LV-SWNT composites in Chapter 6 (Coleman *et al.*, 2004). Within the concentration range of ~2 x 10^{-8} to ~2.5 x 10^{-5} M isolated *p*-terphenyl molecules are interacting with SWNT of increasing surface area. From a concentration of

approximately 2.5 x 10^{-5} M up-wards, the fluorescence of the fraction of free *p*-terphenyl decreases due to the interaction between bundles of H-SWNT and aggregated *p*-terphenyl.

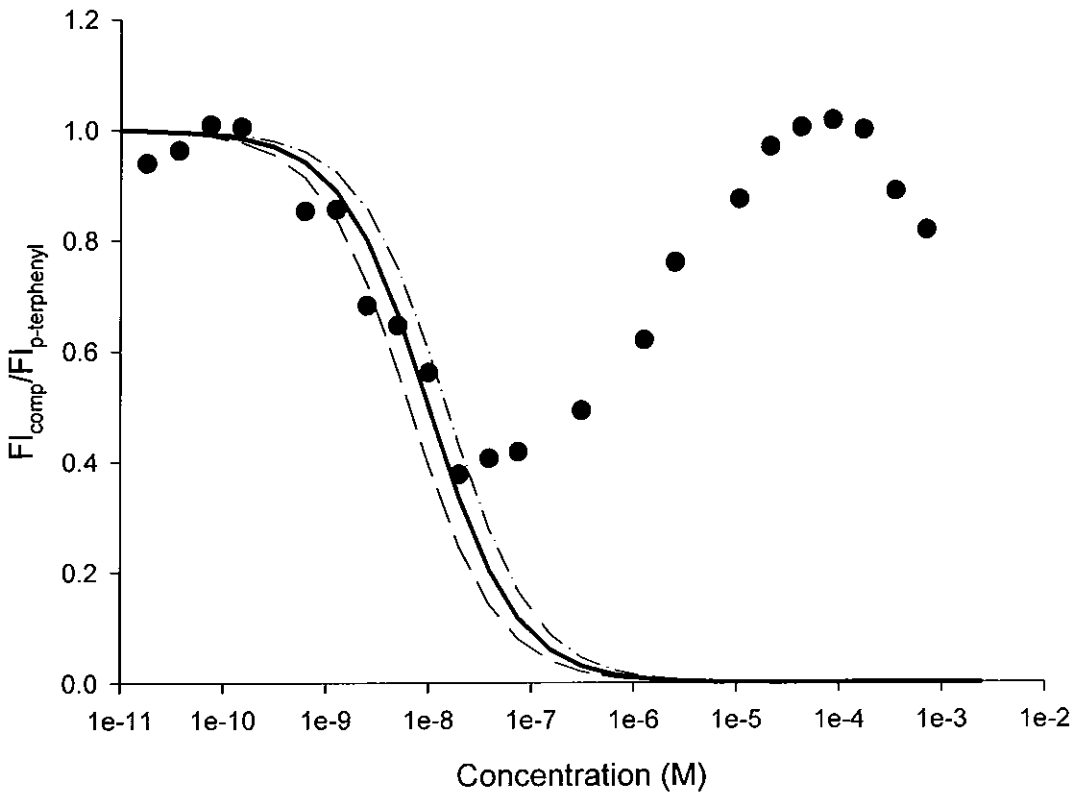

Figure 7.5 Graph of the fraction of free *p*-terphenyl as a function of concentration. The solid line is a fit to Equation 6.1 for H-SWNT. The black solid line gives a C_0 value of ~1 x 10^{-8} M and the best fit to the data. To the left of the solid line, the dashed line gives a C_0 value of ~6.5 x 10^{-9} M and to the right of the solid line the dashed dotted line gives a C_0 value of ~2.5 x 10^{-8} M.

AFM studies presented in Figure 7.6 confirm what the model predicts in that the bundle size of the H-SWNT decreases with concentration. The AFM measurements of the untreated H-SWNT and the composite samples at ~1 x 10^{-8} M result in an estimated bundle size of 2.6 x 10^{-14} m^2 to 1.5 x 10^{-14} m^2 for both sample respectively. In accordance to the fit of the data the C_0 indicates that the extent of debundling occurs to an estimated value of 1.5 x 10^{-14} m^2 and the H-SWNT then cease to debundle further.

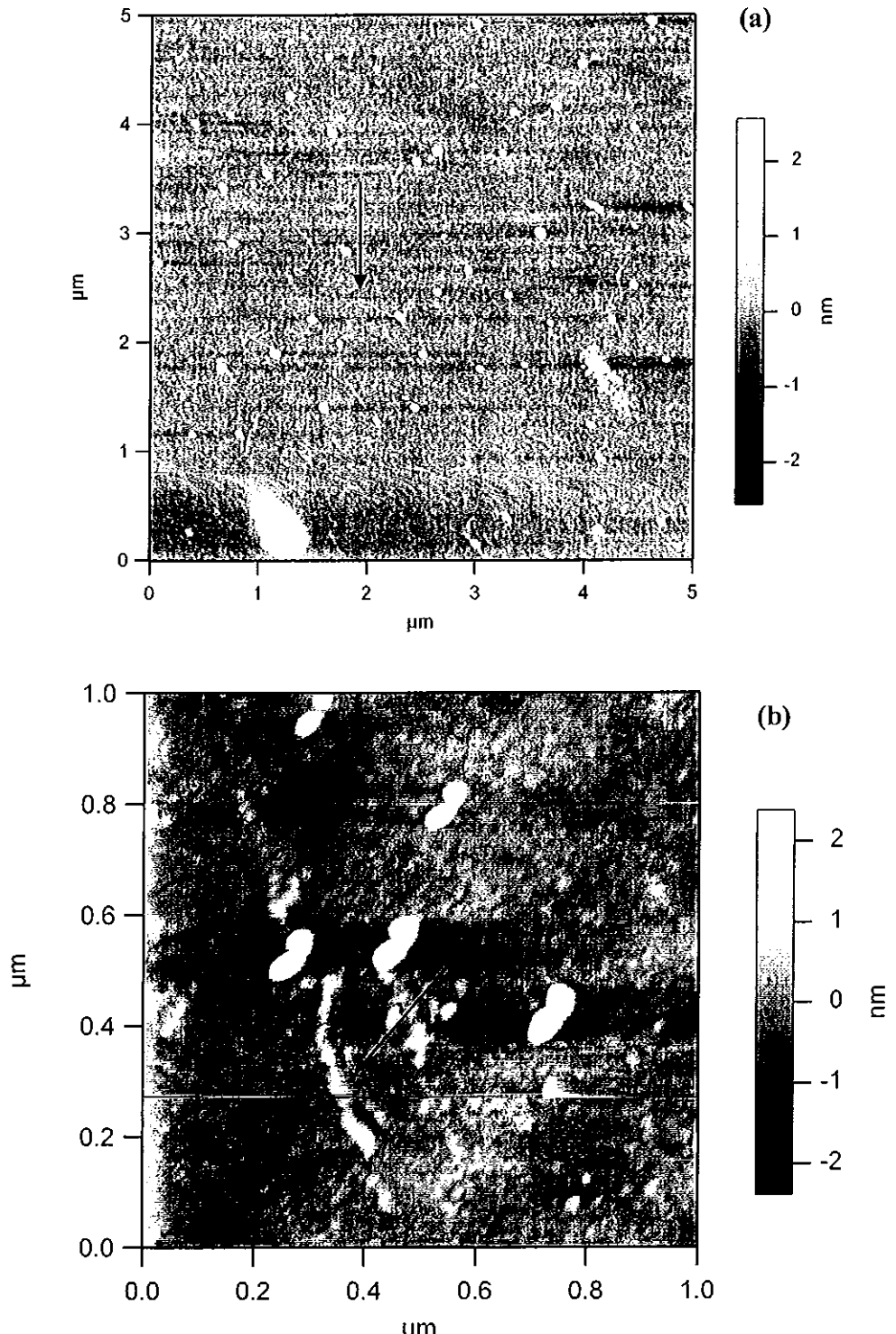

Figure 7.6 AFM of (a) untreated sample of H–SWNT and the composite (b) ~1 x 10^{-8} M of *p*-terphenyl/H-SWNT in toluene. The string-like features represent SWNT as indicated by the markers with a bundle surface area of approximately 2.6 x 10^{-14} m^2 for the untreated H-SWNT and 1.5 x 10^{-14} m^2 for the composite sample.

Similar studies were conducted using AD-SWNT and the results are presented in Figure 7.7. The most striking feature of the model with respect to Figure 7.7 is that no value for C_0 is found to produce a good fit to the data in contrast to Figures 7.5 and 6.3. To further investigate this result, AFM studies were conducted in order to observe the SWNT within the low concentration range.

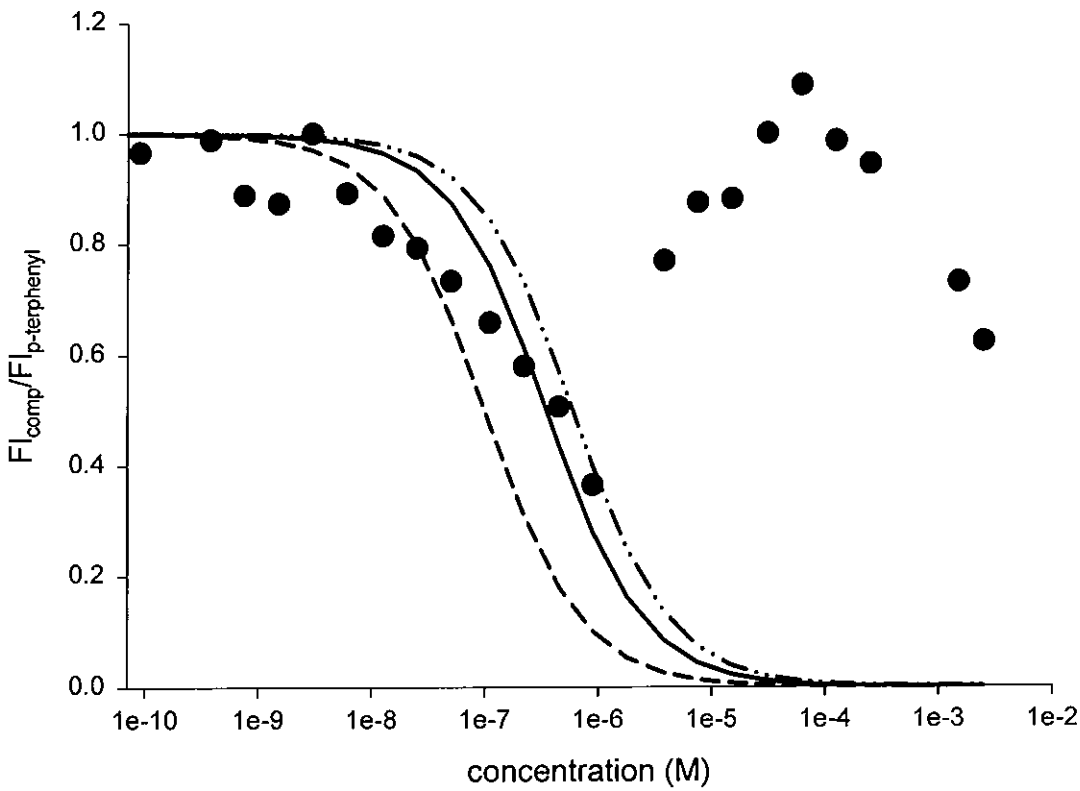

Figure 7.7 Fraction of free *p*-terphenyl as a function of concentration. The solid line is a fit to Equation 6.1 for AD-SWNT. The black solid line gives a C_0 value of ~3.5 x 10^{-7} M and the best fit to the data. To the left of the solid line, the dashed line gives a C_0 value of ~1 x 10^{-7} M and to the right of the solid line the dashed dotted line gives a C_0 value of ~6 x 10^{-7} M.

AFM was conducted on the composite sample at approximately ~1 x 10^{-8} M (Figure 7.8). The results estimate a surface area of 2.4 x 10^{-14} m^2 for the composite at 1 x 10^{-8} M compared to 4.1 x 10^{-14} m^2 for the untreated AD-SWNT.

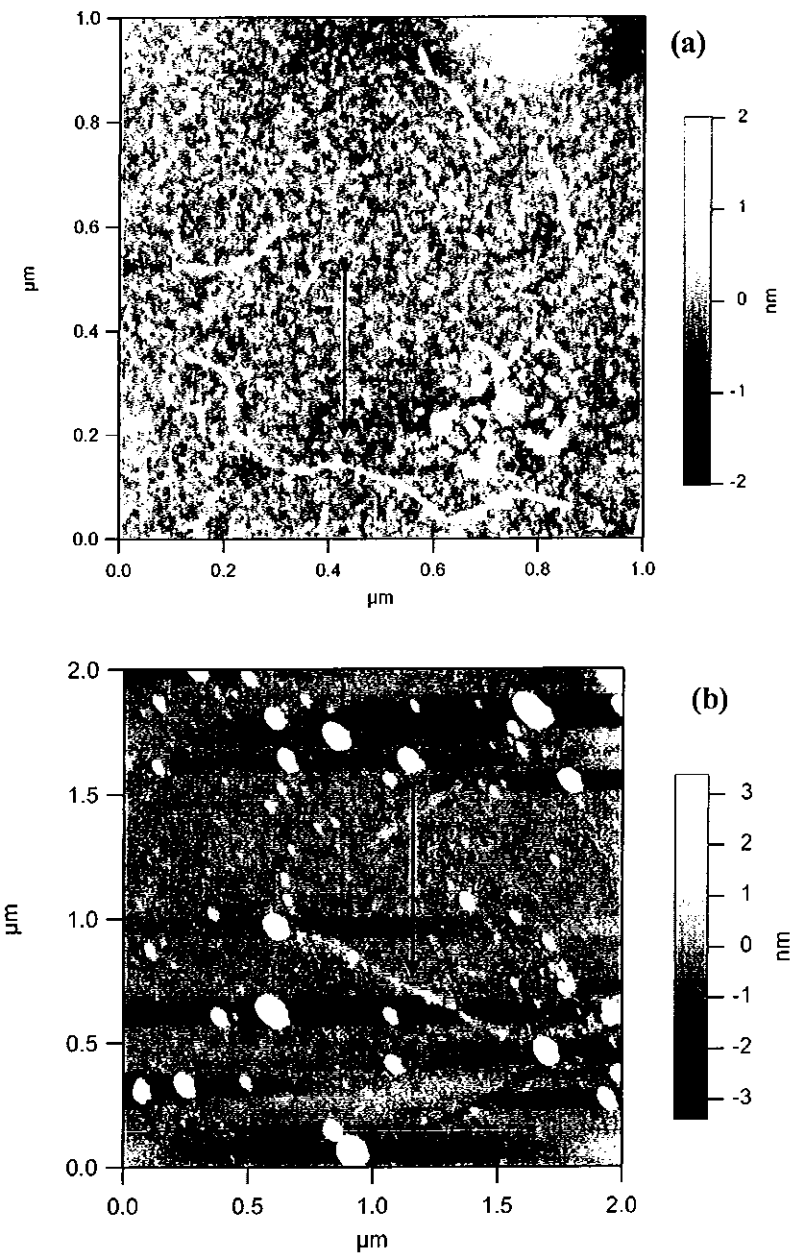

Figure 7.8 AFM of (a) untreated sample of AD-SWNT and the composite (b) 1 x 10^{-8} M of p-terphenyl/AD-SWNT in toluene. The string-like images are the SWNT as indicated by the markers. The bundle surface area is approximately 4.1 x 10^{-14} m^2 for the untreated AD-SWNT and 2.4 x 10^{-14} m^2 for the composite sample at 1 x 10^{-8} M.

The AFM data for the three different SWNT types is compiled in Table 7.3. The initial bundle size and the bundle size at 1 x 10^{-8} M for all three SWNT types are tabulated. These results can then be compared to that of an isolated SWNT which is calculated using the area of an open cylinder as quoted by Coleman et al., (2004) from which the study was adapted, in order to compare the extent of debundling.

Table 7.3 Calculated bundles sizes for SWNTs in their initial state and the composites at 1 x 10^{-8} M *p*-terphenyl/SWNT in toluene. The bundle sizes were calculated using the surface area of an elongated box due to the parameters resulting from AFM studies. The area of an isolated SWNT using the area of a cylinder ($2\pi rl$ as used by Coleman *et al.*, 2004) was calculated in order to compare the degree of debundling of the SWNT samples.

SWNT sample	Initial bundle size	Bundle size at 1 x 10^{-8} M *p*-terphenyl/SWNT	Isolated SWNT
LV-SWNT	3.7 x 10^{-13} m^2	9.6 x 10^{-15} m^2	1.8 x 10^{-15} m^2
H-SWNT	2.6 x 10^{-14} m^2	1.5 x 10^{-14} m^2	1.5 x 10^{-15} m^2
AD-SWNT	4.1 x 10^{-14} m^2	2.4 x 10^{-14} m^2	2.2 x 10^{-15} m^2

A comparison between the bundle sizes at 1 x 10^{-8} M and the estimated area of an isolated SWNT indicate that LV-SWNT disperse to the greatest degree and given the error incurred measuring the width of the SWNT at 1 x 10^{-8} M as a result of the apex radius of the AFM tip at 10 nm it may be suggested that LV-SWNT are fully disperse. It is suggested by the Table 7.3 that both H-SWNT and AD-SWNT remain bundled to some degree even at the very low concentrations with H-SWNT being more dispersed than AD-SWNT.

An overlay of the data for the fraction of free *p*-terphenyl as a function of concentration as a result of the interaction with different SWNT types is given in Figure 7.9. This graph highlights the degree of debundling of the different SWNT types as a function of concentration.

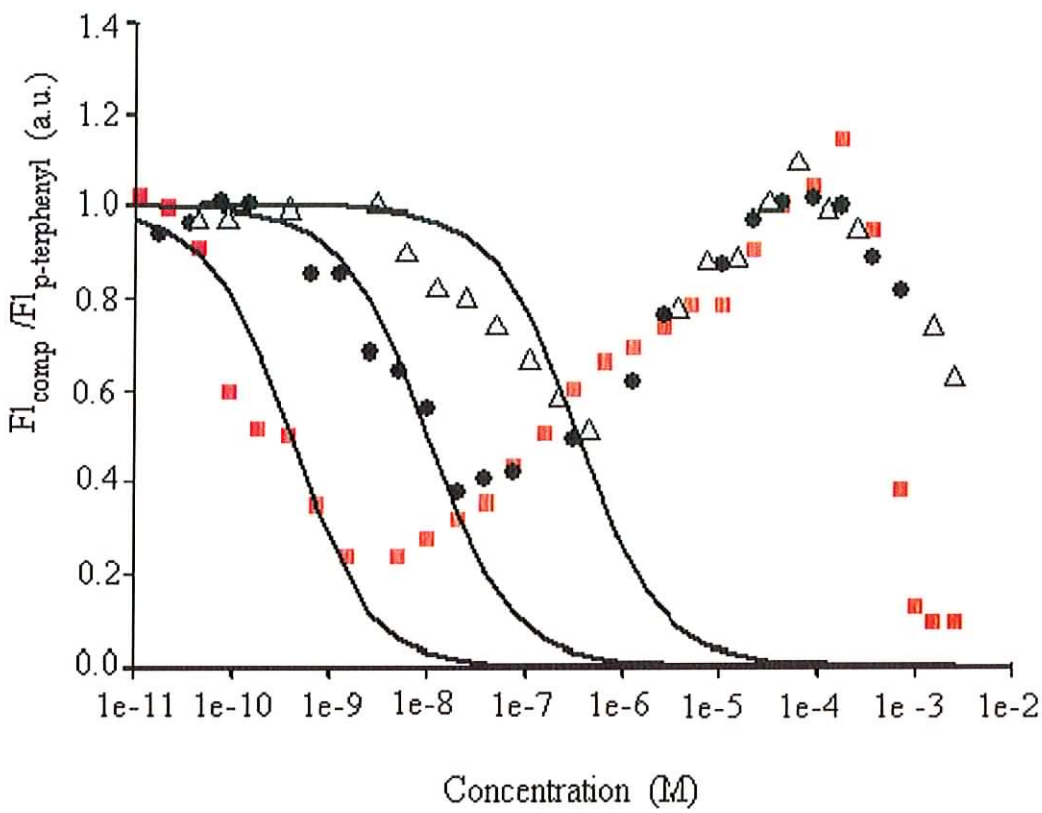

Figure 7.9 Graph of the fraction of free *p*-terphenyl on the interaction with the different SWNT types as a function of concentration. The red squares represent a plot of the fraction of free *p*-terphenyl on interaction with LV-SWNT as a function of concentration. The black circles and grey triangles represent a plot of the fraction of free *p*-terphenyl on interaction with H-SWNT and AD-SWNT as a function of concentration respectively. The solid lines are fits to Equation 6.1 for the different samples. The black solid lines give C_0 values of 4×10^{-10} M, ~1×10^{-8} M, 3.5×10^{-7} M, for LV-SWNT, H-SWNT and AD-SWNT respectively and the best fits to each set of data.

Figure 7.9 suggests that from a concentration of approximately 1 x 10^{-4} M with decreasing concentration the rate of debundling of the SWNTs is approximately equal for all types. Deviation occurs first for the AD-SWNT at a concentration of approximately 3.5 x 10^{-7} M. The poor fit of the model to the subsequent data indicates that no single C_0 value exists and thus that some degree of further debundling occurs in the range of 10^{-7} – 10^{-8} M. Both H-SWNT and LV-SWNT continue to debundle at an almost equal rate until H-SWNT ceases debundling at approximately 2 x 10^{-8} M. The LV-SWNT continue to debundle down to a concentration of approximately 2 x 10^{-9} M. It is interesting to note that as the degree of debundling increases so too does the degree of quenching suggesting that the two are linked. The fluorescence minimum of *p*-terphenyl varies in both concentration and degree of quenching on interaction with different SWNT types. The difference in the fluorescence quenching profiles of the three samples gives a clear indication that the effectiveness of *p*-terphenyl in dispersing the SWNTs varies.

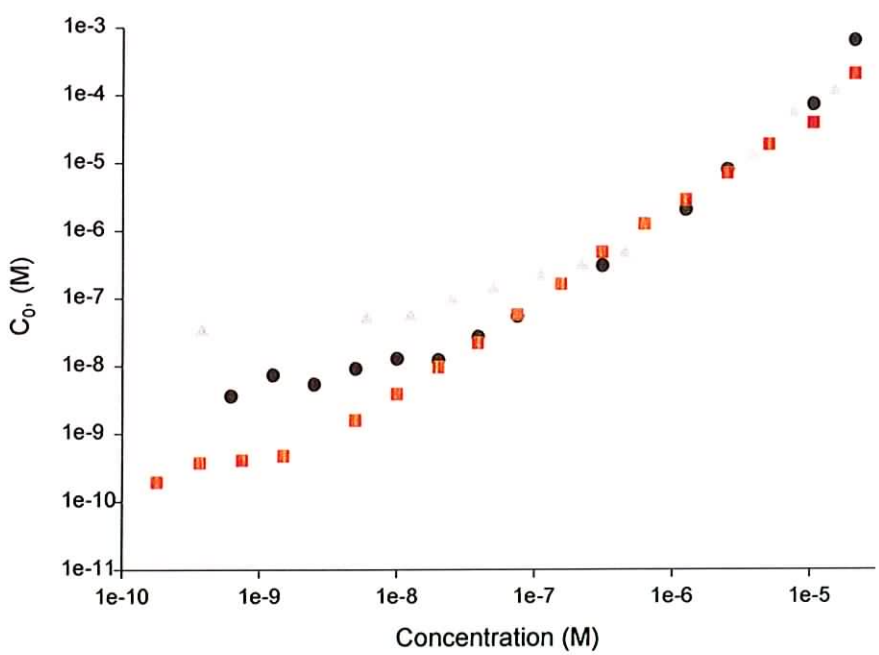

Figure 7.10 C_0 as a function of concentration. The red squares represent a plot of the C_0 for *p*-terphenyl on interaction with LV-SWNT as a function of concentration. The black circles and grey triangles represent a plot of the C_0 for *p*-terphenyl on interaction with H-SWNT and AD-SWNT respectively as a function of concentration.

A plot of the C_0 as a function of concentration for the three different SWNT types is depicted in Figure 7.10. The graph adds support to the results in Figure 7.9 in that it clearly displays the concentration at which the parameters within Equation 6.2 cease to change. Figure 7.11 shows an overlay of the bundle size of the different SWNT as a function of concentration as measured by AFM. Both Figure 7.11 and Table 7.3 confirm that LV-SWNT debundle to the greatest extent suggesting that the LV-SWNT are isolated. The C_0 value for H-SWNT and AD-SWNT was found to increase with increasing concentration indicating that the extent of debundling decreases with increasing concentration and AFM studies presented in Figure 7.11 confirm that both H-SWNT and AD-SWNT are bundled in the low concentration range with H-SWNT more dispersed than AD-SWNT.

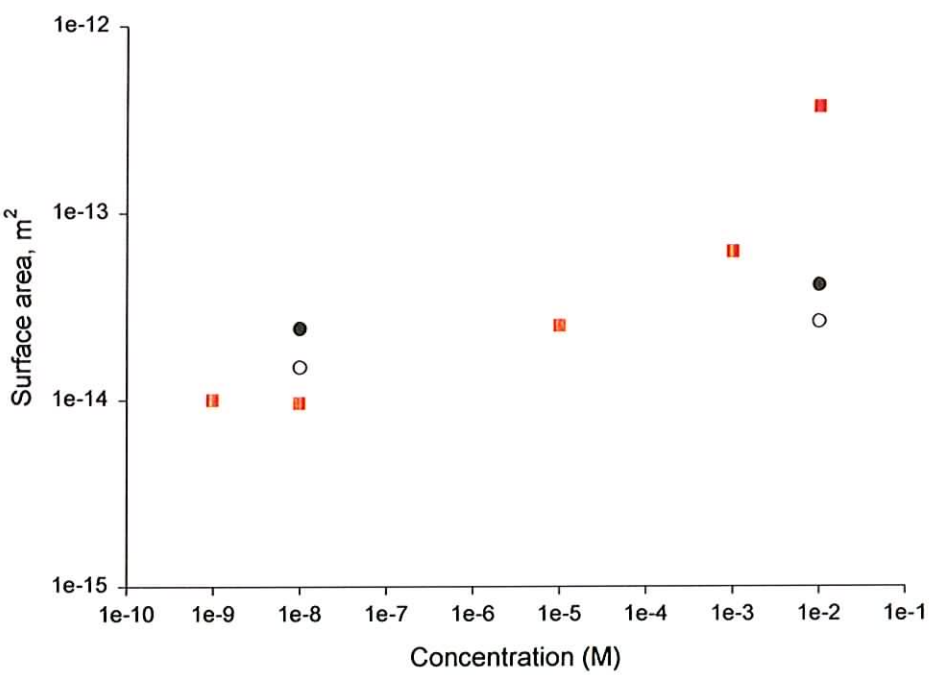

Figure 7.11 AFM data of SWNT surface area as a function of concentration. The red squares display the LV-SWNT data. The black circles and the clear circles display the AD-SWNT and H-SWNT data respectively.

These finding are attributed to the bundle size and purity of the SWNT sample as this has an impact on the assumption of a 1:1 ratio by mass of SWNT to *p*-terphenyl on which the model is based. A variation in the ratio will affect the position of the C_0 value and as the ratio of *p*-terphenyl increases the C_0 value moves to higher concentrations. However, differences of purity of 90 % and 70 % would not account for variations of effective concentrations by 2 orders of magnitude (Journet *et al.*, 1997; Nikolaev *et al.*, 1999; Thess *et al.*, 1996).

The extent of SWNT debundling in the presence of p-tephenyl at a 1:1 w/w ratio is related to the initial bundle size of the SWNT material. Results show that larger bundles with a broad diameter range (LV-SWNT) interact more strongly with (measure of the degree of fluorescence quenching of *p*-terphenyl, Figure 9) and disperse to a greater extent (Figures 9 – 11) whereas smaller SWNT bundles (AD-SWNT and H-SWNT) are more tightly bound and in the case of AD-SWNT (Figure 7, Figure 10) do not disperse at a constant rate. Smaller bundles are often more tightly bound than larger ones (Kai *et al.*, 2005; Strong *et al.*, 2003). The fact that H-SWNT disperse to a greater degree than AD-SWNT may result from the initial purity of the SWNT sample as this has an impact on the assumption of a 1:1 w/w ratio of SWNT *p*-terphenyl on which the model is based. A variation in the weight ratio will affect the position of the C_0 value and as the ratio of *p*-terphenyl compared to SWNT increases the C_0 value moves to higher concentrations. However, differences of purity of 90 % (H-SWNT) and 70 % (AD-SWNT) would not account for variations of effective concentrations by 2 orders of magnitude so this area requires further research (Chiang et al., 2001; Colomer et al., 2001; Nikolaev et al., 1999).

Summary

This chapter investigated the interaction of and debundling of SWNTs produced by different methods in the presence of the molecule *p*-terphenyl in toluene. The study showed that under similar conditions that the degree of interaction of SWNT with *p*-terphenyl was favoured by large bundles of SWNT with a broad diameter distribution where the average diameter of the SWNT was 1.4 nm. The extent of debundling was found to be related to bundle size with larger bundles dispersing to a greater extent than smaller bundles.

However differences in the extent of debundling were noted for SWNT of similar bundle size and the difference were attributed to the degree of purity of the SWNT sample as this would effect the assumption of the 1:1 w/w ratio of SWNT/p-terphenyl in toluene and shift the C_0 value to higher concentrations. However more work is needed in this area to verify this.

REFERENCES

Chiang, I.W., Brinson, B.E., Huang, A.Y., Willis, P.A., Bronikowski, M.J., Margrave, J.L., Smalley, R.E., Hauge, R.H., (2001), "Purification and characterisation of single-wall carbon nanotubes (SWNT) obtained from gas-phase decomposition of CO (HiPco process)", *J. Phys. Chem. B.*, 105, 8297-8301.

Coleman, J.N., Maier, S., Fleming, A.,O'Flaherty, S., Minett, A., Ferreira, M.S., Hutzler, S., Blau, W.J., (2004), "Binding kinetics and SWNT bundle dissiociation in low concentration polymer-nanotube dispersions", *J. Phy. Chem. B.*, 108, 3446 - 3450.

Colomer, J.F., Benoit, J.M., Stephan, C., Lefrant, S., Van Tendeloo, G., Nagy, J.B., (2001), "Characterisation of single-wall carbon nanotubes produces by CCVD method", *Chem. Phys. Lett.*, 345, 11-17.

Journet, C., Maser, W.K., Bernier, P., Loiseau, A., Lamy de la Chapelle, M., Lefrant, S., Deniard, P., Lee, R., Fischer, J.E., (1997), "Large-scale production of single-walled carbon nanotubes by the electric arc technique", *Nature*, 388, 756 - 758 .

Kai, S., Curran, S., Xu, H., Rogelj, S., Jiang, Y., Dewald, J., Pietrass T., (2005), "Single-Walled Carbon Nanotube Purification, Pelletization, and Surfactant-Assisted Dispersion: A Combined TEM and Resonant Micro-Raman Spectroscopy Study", *J. Phys. Chem. B,* 109, 4455-4463.

Meehan, P., Rayment, T., Thomas, R.K., (1980), "Neutron diffraction from benzene adsorbed on graphite", *J. Chem. Soc., Faraday I*, 76, 2011-2015.

Nikolaev, P., Bronikowski, M.J., Kelley Bradley, R., Rohmund, F., Colbert D.T., Smith, K.A., Smalley, R.E., (1999), "Gas-phase catalytic growth of single-walled carbon nanotubes from carbon monoxide", *Chem. Phys. Letts.*, 313, 91- 97.

Strong, K.L., Anderson, D.P., Lafdi, K., Kuhn, J.N., (2003), "Purification process for single-wall carbon nanotubes", *Carbon*, 41, 1477 - 1488.

Thess, A., Lee, R., Nikolaev, P., Dai, H., Petit, P., Robert, J., Xu, C., Lee, Y.H., Kim, S.G., Rinzler, A.G., Colbert, D.T., Scuseria, G.E., Tomanek, D., Fisher, J.E., Smalley, R.E., (1996), "Crystalline bundles of metallic carbon nanotubes", *Science,* 273, 483 - 487.

Zacharia, R., Ulbricht, H., Hertel, T., (2004), "Interlayer cohesive energy of graphite from theraml desorption of polyaromatic hydrocarbons", *Phy. Rev. B.*, 69, 155406-1 – 155406-7.

CHAPTER 8 – CONCLUSIONS

8.1 Summary of Findings

The aims of the thesis were seven fold:

- To enhance the solubility of SWNTs.
- To purify an untreated sample of SWNTs that contains many side products.
- To gain a greater understanding of the interaction between PAHs and SWNTs.
- To debundle and disperse SWNTs.
- To select SWNTs of a specific structure based on the structures of the PAHs.
- To observe and compare the interaction of PAHs with SWNTs produced by different methods.
- To elucidate factors that may disrupt universal behaviour between different SWNT samples.

Chapter 5 presented results which showed that the PAH molecules anthracene and *p*-terphenyl purify and enhance the solubility of LV-SWNT in toluene *via* π-π interaction between the two components. SWNTs show a poor level of solubility in toluene and precipitate out within a matter of hours and therefore the solvent is a good indicator as to any enhanced solubility due to the presence of the PAHs. Upon the introduction of PAHs to a solution of LV-SWNT in toluene the solubility of the SWNTs is greatly enhanced and the LV-SWNT are finely dispersed with the composite solutions stable for prolonged periods of time (now greater than five years) with no indications of the LV-SWNT settling observed. The PAHs draw the LV-SWNT into solution and allow the precipitation of the side products such as the amorphous carbon and metal catalyst particles. Spectroscopic investigations such as fluorescence and Raman point toward a mapping of the PAHs onto the LV-SWNT surface. Fluorescence spectroscopy indicates that an interaction occurs between the two components by the quenching in the PAH fluorescence. This result is further supported by Raman spectroscopic studies. Within the composite spectrum there are modes from the PAHs and LV-SWNT present but also a number of unique vibrational modes. The washing of the composite sample with excess toluene results in a Raman

spectrum similar to the untreated LV-SWNT spectrum. The Raman spectrum of the washed composite provides clear evidence that the PAH are interacting with the LV-SWNT and not any of the side products present therefore it may be concluded that the PAH purify untreated samples of SWNT as well as enhance there solubility.

Literature information is scarce with regards to the nature of the interaction that takes place between organic molecules and SWNTs. The research presented in Chapter 6 investigates the interactions that take place between the PAHs and SWNTs as well as the proposal that the interaction results in the debundling of the SWNTs *via* spectroscopic methods. A model is used to determine the concentration range where aggregated and dispersed PAHs and SWNTs interact and microscopic techniques are used to support spectroscopic results.

Fluorescence concentration dependence studies clearly indicate concentration ranges where aggregates of SWNTs and PAHs as well as dispersed LV-SWNT and PAHs interact. The fluorescence studies show that at the higher concentration range the presence of SWNTs hinders the PAH aggregation and it was also observed that the PAHs debundled the SWNTs. This indicates that the interaction between the PAHs and SWNTs is more favourable than the interaction between the PAHs molecules. Quenching in the fluorescence and the resulting changes in the degree of the fluorescence red-shift of *p*-terphenyl gave insight as to the orientation of the PAH and it is found that the orientation is influenced by the PAH concentration and the SWNT bundle size at the time of interaction.

The model by Coleman *et al.*, (2004), is used to determine the concentration range where bundled and dispersed LV-SWNT exist. However, where a ternary system is concerned the model is sensitive to the solvent used and the method by which the SWNT are produced as well as the molecules used to disperse the SWNTs. These factors must be taken into account if direct comparison of different systems is to be considered. Binding energies for both composite samples were obtained and found to be 1.1 and 0.9 eV for *p*-terphenyl and anthracene composite samples respectively. Such a result indicates that *p*-terphenyl binds more tightly to the LV-SWNT surface than anthracene but anthracene is more prolific at dispersing LV-SWNT bundles.

Raman spectroscopy shows the composite spectra with the characteristic SWNT modes such as the RBMs and the G-line up-shifted in frequency on going from the untreated LV-SWNT material to the composite material. The up-shift of the composite RBMs compared to the untreated LV-SWNT sample is indicative of debundling with decreasing concentration and this is supported by AFM studies. Examination of the Raman RBMs and the fluorescence concentration dependence study of the PAHs indicate that the results from both spectroscopic methods correlate when determining the region at which fully dispersed LV-SWNT and PAHs are interacting. Results show that anthracene disperses LV-SWNT at $\sim 10^{-7}$ M and *p*-terphenyl at $\sim 10^{-9}$ M. Raman studies were then used to probe for selective interaction of the PAHs with LV-SWNT in the concentration range where dispersed LV-SWNT and PAHs exist. It is found that anthracene preferentially interacts with metallic LV-SWNT whereas *p*-terphenyl preferentially interacts with mainly semiconducting LV-SWNT hence providing evidence of selective interaction. However due to the lack of sophistication of the current models available it was not possible to clarify the extent of selectivity any further and therefore deduce if indeed the PAHs had interacted with SWNT of a specific structure but selective interaction was strongly indicated. Therefore it may be deduced that the PAH molecules solubilise, purify and debundle LV-SWNT with strong indications of selective interaction as initially proposed.

Finally the study presented in Chapter 7 investigates the potential of using PAH molecules to process a variety of SWNTs. The study elucidates a number of similarities as well as contrasting features with regards to the interaction between *p*-terphenyl and SWNT produced by different methods. Firstly *p*-terphenyl enhances the solubility and debundles SWNTs in toluene irrespective of the SWNT sample used. However the extent and degree of debundling varies from SWNT sample to sample. When investigated spectroscopically, the spectral changes of the *p*-terphenyl fluorescence on interaction with the different types of SWNTs indicates a non universal behaviour. Differences in the quenching in the fluorescence of *p*-terphenyl and variations in the emission maximum of *p*-terphenyl are observed on interaction of *p*-terphenyl with the different SWNT samples at similar concentrations. The variation in the degree of fluorescence quenching is believed to be related to the ratio of *p*-terphenyl/SWNT and the initial SWNT bundle size. Both fluorescence and AFM studies revealed that LV-SWNT fully disperse, with partial

debundling observed for H-SWNT and AD-SWNT debundled least of the three samples. It is well established that SWNTs produced by different methods contain SWNTs with differing bundle sizes and degrees of purity and this is an important consideration in the quest for a standardised processing and purification protocol.

8.2 Future Work

To further the research presented in this thesis a number of suggestion are made below. Additional research such as the study of the composites under different conditions would further the knowledge of the behaviour of SWNTs and PAHs.

- Adjusting the ratios of the SWNTs and PAHs.

  The main focus of the research presented in this thesis was at a 1:1 ratio by weight for PAH/SWNT. By adjusting the ratios, the interaction between the PAHs and SWNTs may be maximised and from that the viability of up scaling the method for use as a standard purification technique may be considered and tested.

- Investigate the role of the solvent in the PAH/SWNT system.

  Toluene was the only solvent used throughout this thesis. Although toluene is known for its poor affinity for the retention of SWNTs its contribution was not considered in the composite systems with all changes being attributed to the interaction between the PAHs and SWNTs. The investigation of different solvent systems may shed light as to the role of the solvent with regards to the interaction of the PAHs and SWNTs and also any debundling effects the solvent may exert on the PAHs and SWNTs.

- The use of longer PAHs molecules

  The interaction of the molecules anthracene and *p*-terphenyl containing three phenyl rings, from the constrained and unconstrained PAHs catagories respectively, with SWNT were investigated. Similarities and differences are observed with respect to their interaction with SWNT. To continue this research and to build a profile of the behaviour of the PAHs with SWNTs, longer PAH chains need to be investigated.

Increasing the PAH chain length may effect a number of properties such as the structural selectivity of SWNTs, the degree of interaction, rate of debundling and strength of interaction. Figure 8.1 proposes the interaction between tetracene and *p*-quaterphenyl with SWNTs. It may be seen that the diagram proposes that the PAHs may display structural selectivity with the structure of tetracene being similar to that of an armchair SWNTs and of *p*-quaterphenyl being similar to a zigzag SWNTs.

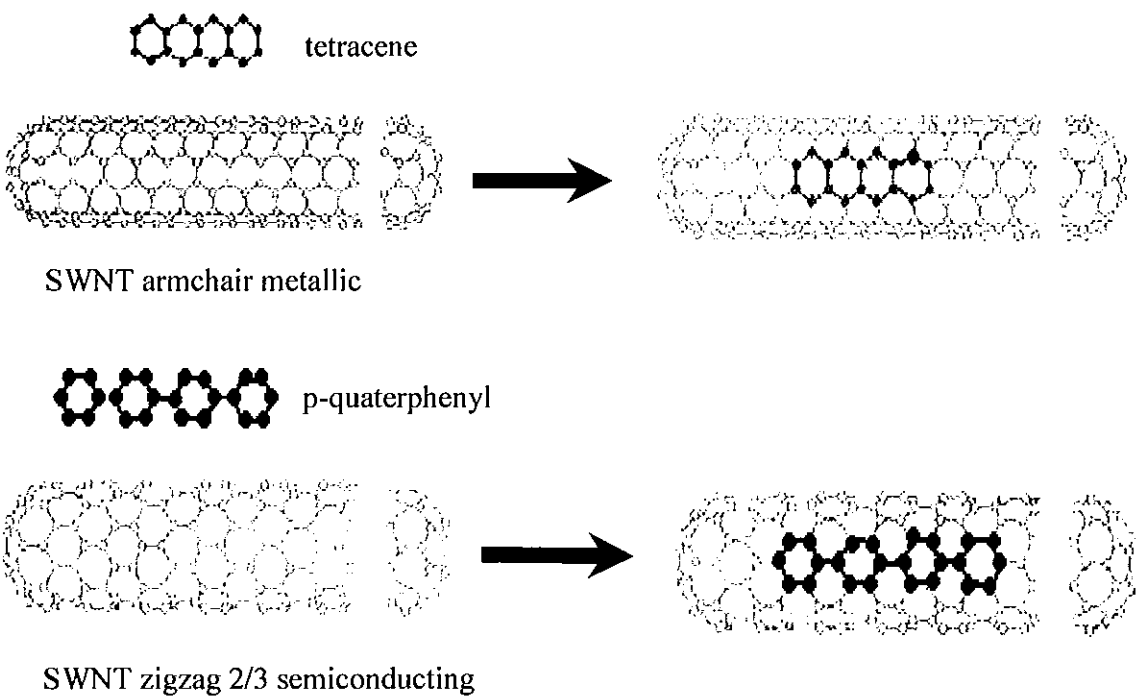

Figure 8.1 Proposed interaction between tetracene and *p*-quaterphenyl with armchair and zigzag SWNT respectively.

APPENDICES

APPENDIX A

Calculated parameters for the determination of C_0 values for LV-SWNT

$$C_0 = \pi^2 \upsilon \rho_{bun} A_{bun} e^{-E_B / kT} / (48Df) \qquad \text{Equation 6.2}$$

Table 1 Calculated parameters for LV-SWNT composites for Equation 6.2, where D = kt/6πηa. Where η is the viscosity of the solvent and *a* is the radius of the long axis of the PAH.

Parameters	p-terphenyl/LV-SWNT	anthracene/LV-SWNT
C_0	9.2×10^{-8} kg/m^3	3.6×10^{-4} kg/m^3
d	1.3 nm	1.3 nm
l	300 nm	400 nm
υ	10^{18} Hz	10^{18} Hz
π	3.14	3.14
A_{bun}	1.0×10^{-14} m^2	2.3×10^{-14} m^2
f	800	800
ρ_{bun}	1.33×10^3 kg/m^3	1.33×10^3 kg/m^3
D	7.6×10^{-10} m^2/s	4.6×10^{-10} m^2/s
t	298K	298K
η	0.5×10^{-3} sPa	0.5×10^{-3} sPa
a	5.74×10^{-10} m	3.6×10^{-10} m

Calculated parameters for the determination of ρ_{bun} values

$\rho_{bun} = 8\pi DM_c/[3a_{c\text{-}c}(D+d)]$ Equation 9.1

Table 2 Calculated parameters for LV-SWNT, H-SWNT and AD-SWNT for Equation 9.1.

Parameters	LV-SWNT	H-SWNT	AD-SWNT
D	1.3×10^{-7} cm	9×10^{-8} cm	1.3×10^{-7} cm
d	3.4×10^{-8} cm	3.4×10^{-8} cm	3.4×10^{-8} cm
Mc	2×10^{-23} g	2×10^{-23} g	2×10^{-23} g
$a_{c\text{-}c}$	1.42×10^{-8} cm	1.42×10^{-8} cm	1.42×10^{-8} cm

Calculated parameters for the determination of C_0 values for H-SWNT and AD-SWNT

Table 3 Calculated parameters for H-SWNT and AD-SWNT *p*-terphenyl composites for Equation 6.2. where D = kt/6πηa.

Parameters	*p*-terphenyl/H-SWNT	*p*-terphenyl/AD-SWNT
C_0	2.3×10^{-6} kg/m^3	8.1×10^{-5} kg/m^3
d	0.9 nm	1.3 nm
l	750 nm	1000 nm
υ	10^{18} Hz	10^{18} Hz
π	3.14	3.14
A_{bun}	2.1×10^{-15} m^2	2.4×10^{-14} m^2
f	800	800
ρ_{bun}	1.6×10^3 kg/m^3	1.33×10^3 kg/m^3
D	7.6×10^{-10} m^2/s	7.6×10^{-10} m^2/s
t	298K	298K
η	0.5×10^{-3} sPa	0.5×10^{-3} sPa
a	5.74×10^{-10} m	5.74×10^{-10} m

APPENDIX B

Transmission Electron Miicroscopy of AD- SWNT

Figure 1 depicts the TEM images of AD-SWNT, with the long bundle-like images representing the SWNT bundles and the dark amorphous structures representing the metal catalyst particles and amorphous carbon within the sample. It is clear from the image that the untreated SWNT samples exist in bundles and the bundle sizes were estimated on average to be approximately 30 nm.

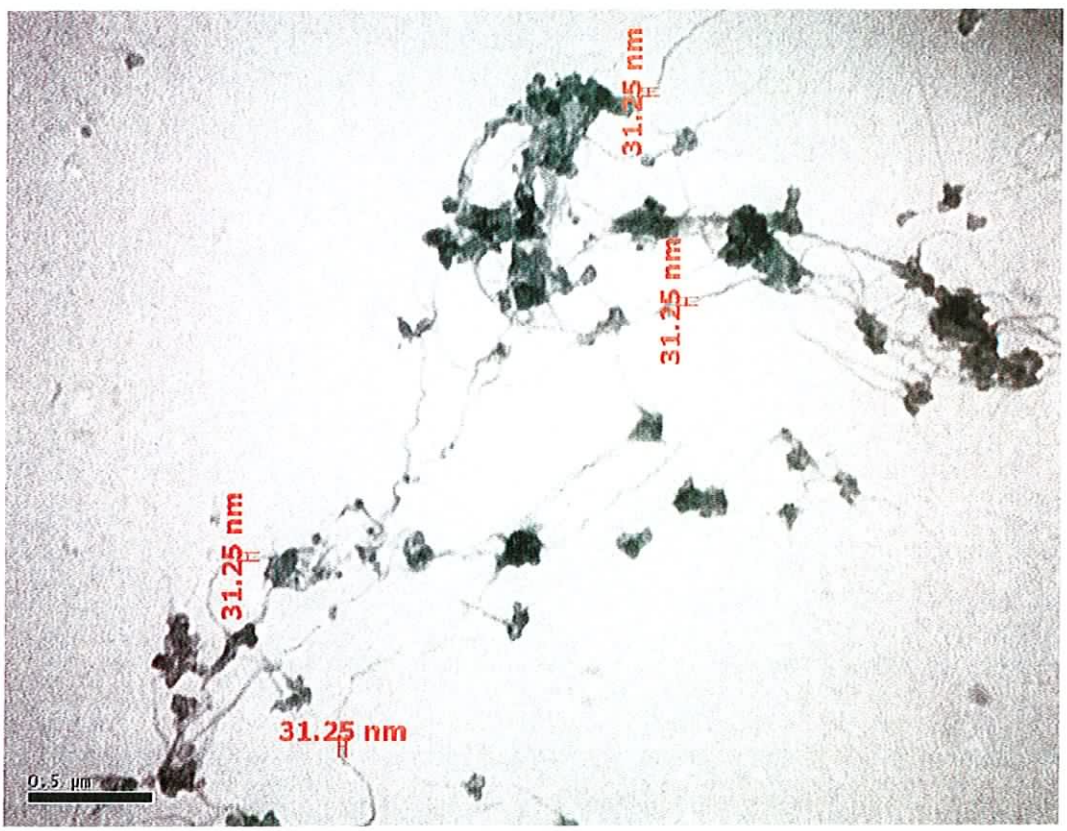

Figure 1 TEM images of untreated arc discharge SWNT at a magnification of 40,000X. The bundle-like structures represent the SWNT bundles and the amorphous structures represent the metal catalyst particles and amorphous carbon.

Raman Spectra of the PAHs, SWNTs and Composite Samples

Raman spectroscopy of AD-SWNT bundles was concucted. The purpose of this was to investigate if new modes were present in the composite spectrum compared to that of the untreated AD-SWNT and pristine PAHs as was observed for the composite spectra of LV-SWNT.

Figure 2 compares the Raman spectra of the untreated AD-SWNT (Figure 2 (a)), pristine *p*-terphenyl powder (Figure 2 (b)), and a composite sample derived from a 1:1 w/w ratio of SWNT/*p*-terphenyl for a 2.5 x 10^{-3} M solution (Figure 2 (c)) taken at a laser excitation of 514.5 nm. The composite spectrum in Figure 2 (c) is in some ways a combination of the untreated LV-SWNT and the PAH material but unique modes not accounted for in either the LV-SWNT or the PAH spectra are also present. The new modes are indicated by the markers in Figure 2. Therefore the composite spectrum maybe considered to be a unique compound.

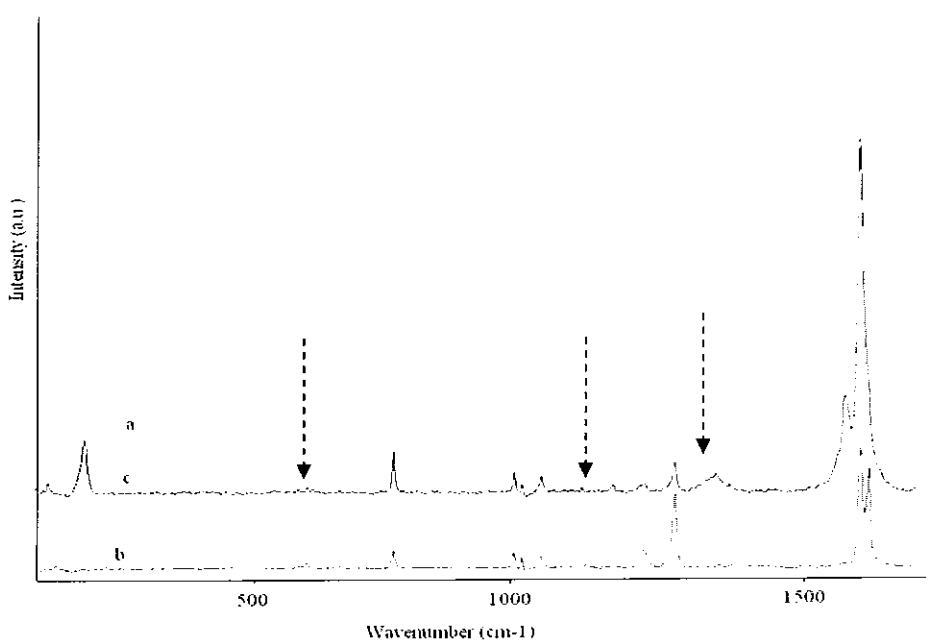

Figure 2 Raman spectra of (a) the untreated AD-SWNT, (b) the pristine *p*-terphenyl powder and (c) the composite sample at 2.5 x 10^{-3} M a 1:1 w/w ratio of *p*-terphenyl/SWNT at laser excitation 514.5 nm.

Figure 3 compares the Raman spectra of the untreated AD-SWNT (Figure 3 (a)), pristine *p*-terphenyl powder (Figure 3 (b)), and a composite sample derived from a 1:1 w/w ratio of SWNT/*p*-terphenyl for a 2.5 x 10^{-3} M solution (Figure 3 (c)) taken at a laser excitation of 632.8 nm. The composite spectrum in Figure 3 (c) shows little or no sign of any PAH modes prehaps because these modes are damped on interaction or it may be a result of the laser line used as similar observations were made with regards to LV-SWNT at laser excitation line 632.8 nm (see Chapter 5). What is interesting about spectrum (c) is that the RBMs have up-shifted and the profile of both the RBMs and G-line has changed. An up-shift is indicative of a change in the local environment and may result from selective interaction. However more research is required to verify selectivity.

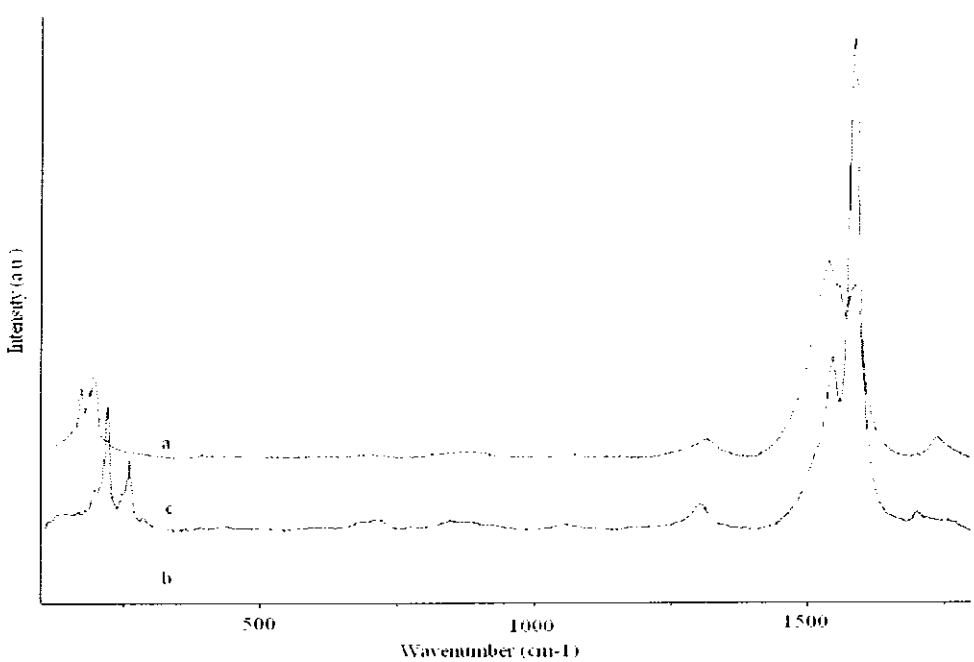

Figure 3 Raman spectra of (a) the untreated AD-SWNT, (b) the pristine *p*-terphenyl powder and (c) the composite sample at 2.5 x 10^{-3} M a 1:1 w/w ratio of *p*-terphenyl/SWNT at laser excitation 632.8 nm.

Figure 4 compares the Raman spectra of the untreated AD-SWNT (Figure 4 (a)), pristine anthracene powder (Figure 4 (b)), and a composite sample derived from a 1:1 w/w ratio of SWNT/anthracene for a 3 x 10^{-3} M solution (Figure 4 (c)) taken at a laser excitation of 632.8 nm. As is the case with Figure 3, the composite spectrum in Figure 4 (c) shows no PAH modes and no up-shift is observed for the RBMs although the profile is different compared to spectrum (a). To add to this the profile of the G-line has altered slightly but still remains broad which is characteristic of metallic behaviour.

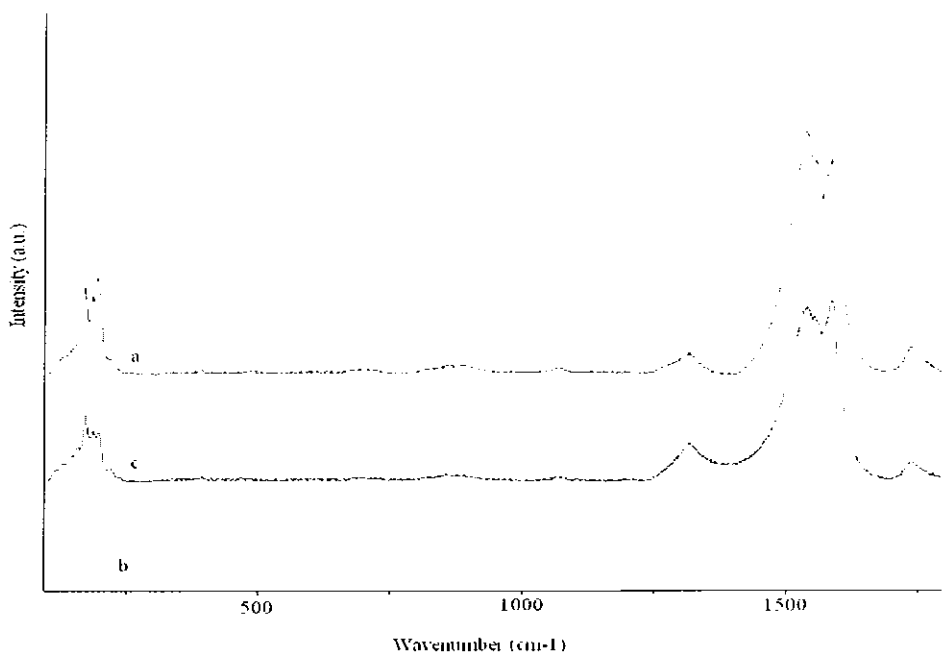

Figure 5 Raman spectra of (a) the untreated AD-SWNT, (b) the pristine anthracene powder and (c) the composite sample at 2 x 10^{-3} M a 1:1 w/w ratio of anthracene/SWNT at laser excitation 632.8 nm.

APPENDIX C

Transmission Electron Miicroscopy of HiPco SWNT

Figures 1 and 2 depict the TEM images of H-SWNT, with the long bundle-like images representing the SWNT bundles and the dark amorphous structures representing the iron catalyst particles within the sample. It is clear from the image that the untreated SWNT samples exist in bundles and the bundle sizes were estimated on average to be approximately 30 nm. Figure 2 in particular shows the presence of the iron particles and these are represented by the circular objects adhered to the SWNT bundles.

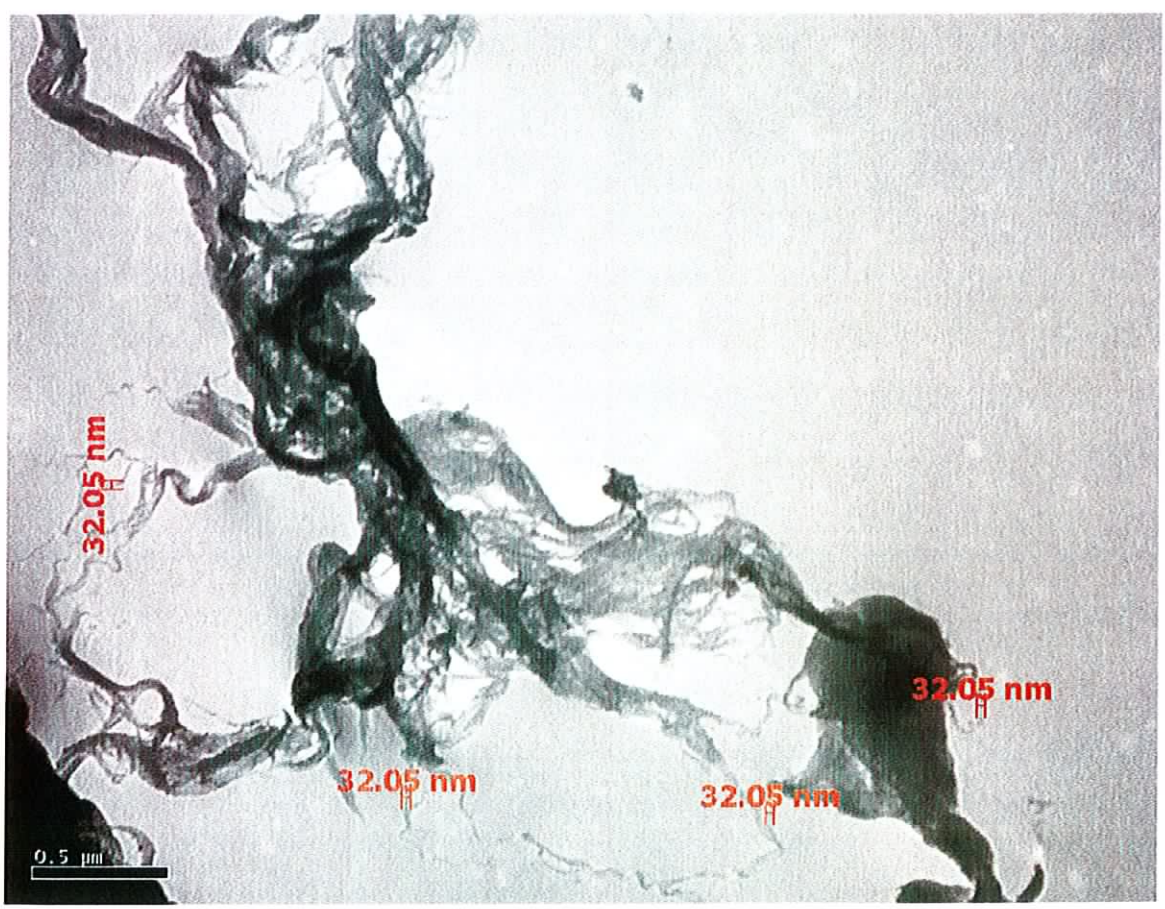

Figure 1 TEM images of untreated HiPco SWNT at a magnification of 80,000X. The bundle-like structures represent the SWNT bundles and the amorphous structures represent the iron catalytst particles.

Figure 2 TEM images of untreated H–SWNT at a magnification of 100,000X. The bundle-like structures represent the SWNT bundles and the circular structures represent the iron catalyst particles.

Raman Spectra of the PAHs, SWNTs and Composite Samples

Raman spectroscopy of AD-SWNT bundles was concucted. The purpose of this was to investigate if new modes were present in the composite spectrum compared to that of the untreated AD-SWNT and pristine PAHs as was observed for the composite spectra of LV-SWNT.

Figure 3 compares the Raman spectra of the untreated H-SWNT (Figure 3 (a)), pristine anthracene powder (Figure 3 (b)), and a composite sample derived from a 1:1 w/w ratio of SWNT/anthracene at a concentration of 3×10^{-3} M (Figure 3 (c)) taken at a laser excitation of 632.8 nm. The composite spectrum in Figure 3 (c) shows little or no sign of any PAH modes prehaps because these modes are damped on interaction or it may be a result of the laser line used as similar observations were made with regards to LV-SWNT at laser excitation line 632.8 nm (see Chapter 5). What is interesting about spectrum (c) is that the RBMs have up-shifted and the profile has changed. An up-shift is indicative of a change in the local environment and may result from selective interaction. However more research is required to verify selectivity.

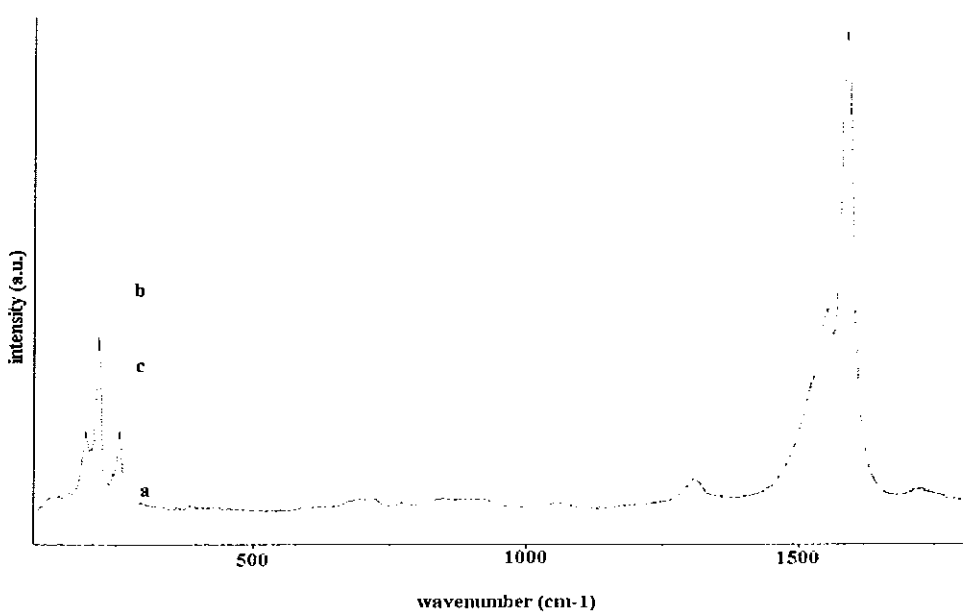

Figure 3 Raman spectra of (a) the untreated H-SWNT, (b) the pristine anthracene powder and (c) the composite sample at 2×10^{-3} M a 1:1 w/w ratio of anthracene/SWNT at laser excitation 632.8 nm.

Figure 4 compares the Raman spectra of the untreated H-SWNT (Figure 4 (a)), pristine *p*-terphenyl powder (Figure 4 (b)), and a composite sample derived from a 1:1 w/w ratio of SWNT/*p*-terphenyl at a concentration of 2.5 x 10^{-3} M (Figure 4 (c)) taken at a laser excitation of 632.8 nm. The composite spectrum in Figure 4 (c) shows little or no sign of any PAH modes prehaps because these modes are damped on interaction or it may be a result of the laser line used as similar observations were made with regards to LV-SWNT at laser excitation line 632.8 nm (see Chapter 5). What is interesting about spectrum (c) is that the RBMs have up-shifted. An up shift is indicative of a change in the local environment and may result from selective interaction. However more research is required to verify selectivity.

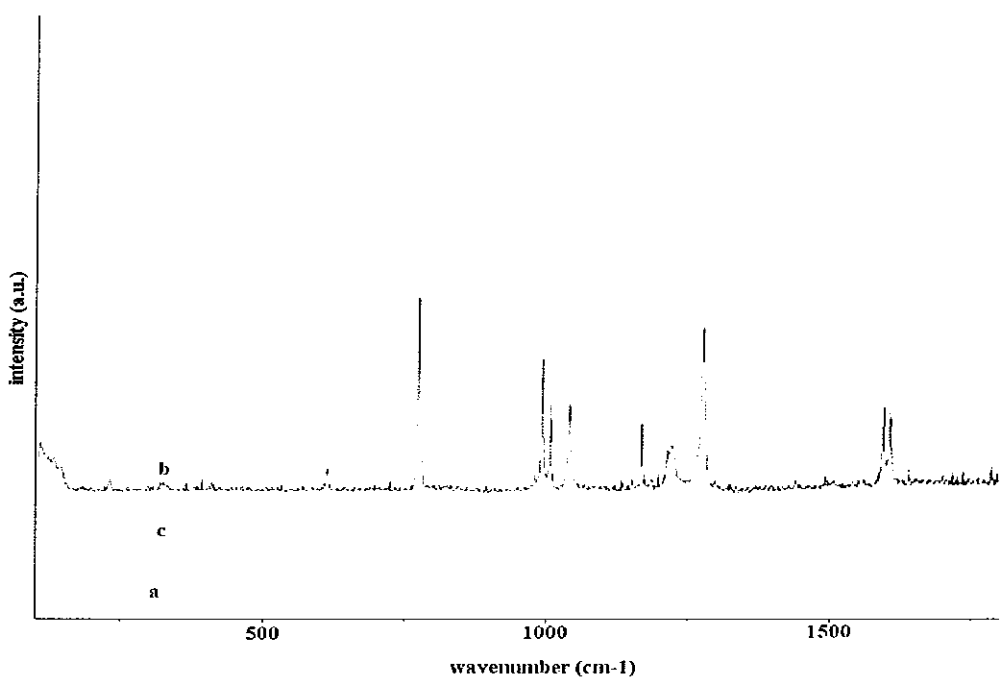

Figure 4 Raman spectra of (a) the untreated H-SWNT, (b) the pristine *p*-terphenyl powder and (c) the composite sample at 1.5 x 10^{-3} M a 1:1 w/w ratio of *p*-terphenyl/SWNT at laser excitation 632.8 nm

Publications

Refereed Journals

Hedderman, T.G., Keogh, S.M., Chambers, G., Byrne H.J., (2006), "The investigation of hydrocarbons to universally process SWNT", *J. Phys. Chem. B.*, submitted August 2006.

Hedderman, T.G., Keogh, S.M., Chambers, G., Byrne H.J., (2006), "In-depth study into the interaction of single walled carbon nanotubes with anthracene and *p*-terphenyl", *J. Phys. Chem. B.*, 110, 3895-3901.

Hedderman, T.G., Keogh, S.M., Chambers, G., Byrne H.J., (2004), "Solubilisation of SWNT with organic dye molecules", *J. Phys. Chem. B.*, 108, 18860-18865.

Keogh S.M., Hedderman T.G., Gregan E., Farrell G., Lynch, P., Chambers G., Lyng, F.M., Byrne H.J., (2006), "Fluorescence concentration studies of HiPco SWNT", *J. Phys. Chem. B.*, in press.

Keogh S.M., Hedderman T.G., Ruther, M.G., Lyng. F.M., Gregan E., Farrell G., Chambers G., Byrne H.J., (2005), "Temperature- induced nucleation of poly(*p*-phenylene vinylene-*co*-2,5-dioctyloxy-*m*-phenylene vinylene) crystallization by HiPco SWNT", *J. Phys. Chem. B.*, 109, 5600–5607.

Keogh S.M., Hedderman T.G., Gregan E., Farrell G., Chambers G., Byrne H.J., (2004), "Spectroscopic analysis of single-walled carbon nanotubes and semiconjugated polymer composites", *J. Phys. Chem. B.*, 108, 6233–6241.

Gregan, E., Keogh, S.M., Maguire, A., Hedderman, T.G., O'Neill, L., Chambers G., Byrne, H.J., (2004), "Purification and isolation of SWNT", *Carbon*, 42, 1031-1035.

Conference Proceedings

Hedderman, T.G., O'Neill, L., Maguire, A., Keogh, S.M., Gregan, E., McCarthy, B., Dalton, A.B., Chambers, G., Byrne, H.J., (2005), "Spectroscopic analysis of the interaction of SWNT with simple organic molecules", *Proceedings of Opto Ireland, The International Society for Optical Engineering, Society of Photographic Instrumentation Engineers (SPIE)*, 5826, 12-24.

Hedderman T.G., O'Neill, L., Maguire, A., Keogh, S.M., Gregan, E., Chambers, G., Byrne, H.J., (2003), "Interaction of SWNT with simple dye molecules", *Proceedings of the International Winterschool of the Electronic Properties of Novel Materials (IWEPNM)*, 685, 261-264.

Hedderman, T.G., O'Neill, L., Maguire, A., Keogh, S.M., Gregan, E., McCarthy, B., Dalton, A.B., Chambers, G., Byrne, H.J., (2002), "The use of single walled carbon nanotubes as templates for organic molecules", *Proceedings of the International Winterschool of the Electronic Properties of Novel Materials (IWEPNM),* 633, 610-613.

Hedderman, T.G., O'Neill, L., Maguire, A., Keogh, S.M., Gregan, E., McCarthy, B., Dalton, A.B., Chambers, G., Byrne, H.J., (2002), "Single walled carbon nanotubes as templates for organic molecules", *Proceedings of Opto Ireland, The International Society for Optical Engineering, Society of Photographic Instrumentation Engineers (SPIE)*, 4876, 696-703.

Keogh, S.M., Maguire, A., Hedderman, T.G., Gregan, E., Chambers, G., Byrne, H.J., (2005), "Fluorescence concentration studies of HiPco SWNT and semi-conjugated polymers", *Proceedings of Opto Ireland, The International Society for Optical Engineering, Society of Photographic Instrumentation Engineers (SPIE)*, 5826, 67-74.

Keogh, S.M., Hedderman, T.G., Farrell, G.F., Ruether, M., Gregan, E., McNamara, M., Chambers, G., Byrne, H.J., (2005), "Temperature dependent studies of HiPco SWNT and polymer composites", *International Conference of Synthetic Metals (ICSM),* 154, 197-207.

Keogh, S.M., Maguire, A., Hedderman, T.G., Gregan, E., Chambers, G., Byrne, H.J., (2003), "Physical interaction between HiPco SWNT's and semi-conjugated polymers", *Proceedings of the International Winterschool of the Electronic Properties of Novel Materials (IWEPNM)*, 685, 265-268.

Keogh, S.M., Maguire, A., Hedderman, T.G., Gregan, E., Chambers, G., Byrne, H.J., (2002), "Physical interaction between HiPco SWNT's and Semi-conjugated polymers", *Proceedings of Opto Ireland, The International Society for Optical Engineering, Society of Photographic Instrumentation Engineers (SPIE)*, 4876, 723-731.

Keogh, S.M., Maguire, A., Hedderman, T.G., Gregan, E., McCarthy, B., Dalton, A.B., Chambers, G., Byrne, H.J., (2002), "Physical interaction between HiPco SWNT's and semi-conjugated polymers", *Proceedings of the International Winterschool of the Electronic Properties of Novel Materials (IWEPNM)*, 633, 570-573.

Gregan, E., Keogh, S.M., Hedderman, T.G., Chambers, G., Byrne, H.J., (2005), "Use of Raman in the investigation of debundling of single walled carbon nanotubes", *Proceedings of Opto Ireland, The International Society for Optical Engineering, Society of Photographic Instrumentation Engineers (SPIE)*, 5826, 56-66.

Gregan, E., Keogh, S.M., Hedderman, T.G., Chambers, G., Byrne, H.J., (2002), "Stokes/anti-Stokes Raman spectroscopy of HiPco single walled carbon nanotubes", *Proceedings of Opto Ireland, The International Society for Optical Engineering, Society of Photographic Instrumentation Engineers (SPIE)*, 4876, 1149-1157.

Gregan, E., Keogh, S.M., Hedderman, T.G., McCarthy, B., Farrell, G., Chambers, G., Byrne, H.J., (2002), "Stokes/anti-Stokes Raman spectroscopy of HiPco single walled carbon nanotubes", *Proceedings of the International Winterschool of the Electronic Properties of Novel Materials (IWEPNM)*, 633, 294-297.

Oral presentations

"Spectroscopic analysis of the interaction of polycyclic aromatic hydrocarbons with SWNT", *International Conference of Synthetic Metals (ICSM),* Trinity College, Dublin, July 2006.

"Spectroscopic analysis of the interaction of SWNT with simple organic molecules", *Opto Ireland, Society of Photographic Instrumentation Engineers (SPIE)* conference, Royal Dublin Society, Dublin, April 2005.

Poster presentations

"The analysis of the interaction of SWNT with terphenyl" *International Conference of Synthetic Metals (ICSM)*, Trinity College, Dublin, July 2006.

"Carbon nanotubes as templates for organic molecules", *International Winterschool of the Electronic Properties of Novel Materials (IWEPNM),* Kirchberg, Austria, March, 2003.

"Single walled carbon nanotubes as templates for organic molecules", *Opto Ireland, Society of Photographic Instrumentation Engineers (SPIE)* conference, Galway, September 2002.

"Carbon nanotubes as templates for organic molecules", *International Winterschool of the Electronic Properties of Novel Materials (IWEPNM),* Kirchberg, Austria, March, 2002.